MOLECULAR GENETIC CHARACTERIZATION OF ATAXIC MOVEMENT DISORDERS IN MOUSE AND HUMAN

A thesis presented in partial fulfillment of the requirements for
the degree of Doctor of Philosophy to the University College London

by Joyce Catharina Hendrika van de Leemput

Department of Neurodegenerative Disease,
Institute of Neurology, University College London (UK)

in partnership with

Laboratory of Neurogenetics,
National Institute on Aging, National Institutes of Health (USA)

Declaration on origin of work described herein

I, Joyce Catharina Hendrika van de Leemput, confirm that the work presented in this thesis is my own. Where information has been derived from other sources, every effort has been made to indicate this clearly in the thesis, with due reference to literature and acknowledgement of collaborative research and discussion.

Part of the work described herein has been published in scientific journals

van de Leemput J., Chandran J., Knight M. A., Holtzclaw L. A., Scholz S., Cookson M. R., Houlden H., Gwinn-Hardy K., Fung H. C., Lin X., Hernandez D., Simon-Sanchez J., Wood N. W., Giunti P., Rafferty I., Hardy J., Storey E., Gardner R. J., Forrest S. M., Fisher E. M., Russell J. T., Cai H., and Singleton A. B. (2007) Deletion at ITPR1 underlies ataxia in mice and spinocerebellar ataxia 15 in humans. *PLoS Genet* **3,** e108.

Knight M. A., Hernandez D., Diede S. J., Dauwerse H. G., Rafferty I., **van de Leemput J.**, Forrest S. M., Gardner R. J., Storey E., van Ommen G. J., Tapscott S. J., Fischbeck K. H., and Singleton A. B. (2008) A duplication at chromosome 11q12.2-11q12.3 is associated with spinocerebellar ataxia type 20. *Hum Mol Genet* **17,** 3847-3853.

van de Leemput J., Wavrant-De Vrièze F., Rafferty I., Bras J. M., Fisher E. M. C., Hardy J., Singleton A. B., and Houlden H. (2009) Sequencing analysis of *ITPR1* in and autosomal dominant spinocerebellar ataxia type III (ADCA III) cohort. *Submitted*

IF AT FIRST THE IDEA IS NOT ABSURD, THEN THERE IS NO HOPE FOR IT.

-- ALBERT EINSTEIN

ABSTRACT

Deletion at *ITPR1* underlies a young onset autosomal recessive ataxia in mice and a late onset autosomal dominant ataxia (SCA15) in humans.

Data presented show the utility of investigating spontaneous mouse mutations in understanding human disease. Through linkage and sequence analysis a novel mutation in the gene encoding inositol 1,4,5-triphosphate receptor type 1 was identified to underlie a severe movement disorder in mice. The 18bp in frame deletion in *Itpr1* exon 36 was shown to be allelic to that of another model, *opisthotonos* (Lane 1972). The *Itpr1*$^{\Delta 18}$ mutation leads to a decreased to almost total lack in the normally high level of ITPR1 expression in cerebellar Purkinje cells. In addition, high density genome wide SNP genotype data in humans showed a *SUMF1-ITPR1* deletion to segregate with spinocerebellar ataxia 15 (SCA15), a late-onset autosomal dominant disorder, which was previously mapped to the genomic region containing *ITPR1*; however, no causal mutations had been identified (Knight et al. 2003). With this deletion not observed in a control population, decreased ITPR1 protein levels in individuals carrying the deletion, and subsequent identification of similar deletions in additional spinocerebellar ataxia families, the data provide compelling evidence that heterozygous deletion in *ITPR1* underlies SCA15. As demonstrated, high density genome wide SNP analysis can facilitate rapid detection of structural genomic mutations that may underlie disease when standard sequencing approaches are insufficient. The data suggest genetic alterations at *ITPR1* underlie approximately over 1% of autosomal dominant SCA type III (ADCA III) cases for which currently no genetic cause has been identified. Data described herein add weight to a role for aberrant intracellular Ca^{2+} signaling in Purkinje cells in the pathogenesis of spinocerebellar ataxia.

ACKNOWLEDGEMENT

Many thanks go out to my supervisors. John Hardy, (quote, with a smile) ‘no worries… you are a pain in the ass.’ Thank you for having faith in me. Andy Singleton, (quote) ‘luck is where preparation meets opportunity.’ Thank you for teaching me to believe in my own research, especially when the odds seemed against us. Lizzy Fisher, (quote), ‘buy an enormous packet of biscuits, some nice coffee and give yourself a couple of days just to think.’ Thank you for great advice and keeping me sane during thesis writing.

Of course a thank you to all the people that very willingly shared their expertise with me and so much more. The LNG gang, who taught me more then they will ever realize. With special thanks to the illumina team, who adopted me and shared their cookies and tree-climbing-crab stories. I will always remain ‘a friend of illumina’. Sonja thank you so much for everything; for having me as your roommate, for joining in a refusal to understand American logic, running an a.s.a.p. experiment on the weekend, or going for a coffee whenever one was needed most. Also many thanks to Jayanth without whom there wouldn’t have been a project to begin with, to Melanie (from upstairs) for taking an interest in my research and enabling the project to become a great story, to Lynne (Russell lab) for always having the door open for experimental advise or a wee chat, and to Henry Houlden (UCL), the Huw Morris lab and the Brice lab for sharing their samples.

Many, many, many thanks to my family and friends, don’t know how I would have been able to accomplish this without your support. Pappa, mamma en pusje, zonder jullie had ik dit niet kunnen doen. Dankjewel dat jullie er voor mij zijn elke stap die ik zet, de hoogte en de diepte punten, en bij elk avontuur dat ik onderneem, zelfs als ze een oceaan ver weg zijn. Ik hou van jullie. To all the people I met along the way and may call my friends; you all left your mark in great memories and wisdom (without always realizing it) and each in your own way helped me in the right direction. Thank you for that. Gerdi, Bob, Karin, Esther, Ian, Dena, Sonja, Sarah, Georgia, Parastoo & Pardis & Parviz, Hoon, GM & mrs Roberts & M smittie & the KS family, the cabin-trip-gang, Elena & Steve, Karine & Ted.

Thank you. It has been an amazing journey.
May the odyssey continue.

TABLE OF CONTENTS

FIGURES

TABLES

SUPLEMENTARY MATERIAL

CD-rom (attached to the back cover of this thesis)

Suplementary video - Severe movement disorder in mice

ABBREVIATIONS

GENERAL

A	adenine (nucleotide)
A, a	affected
aa	amino acid
ABI	Applied Biosystems
aCHG	array-based comparative genomic hybridization
ADCA(s)	autosomal dominant cerebellar ataxia(s)
ADP	adenosine diphosphate
aff	affected
ALS	amyotrophic lateral sclerosis
AM	ante meridiem
amp	ampere
ARPKD	autosomal recessive polycystic kidney disease
ATP	adenosine triphosphate
AUS1	Australian kindred, original SCA15 kindred (Storey et al. 2001)
BACC2, nucleon	nucleon blood and cultured cells 2
BCA	bicinchoninic acid
BLAST	basic local alignment search tool
blastn	nucleotide-nucleotide BLAST
B-ME	beta-mercapto ethanol
bp	base pairs
BSA	bovine serum albumin
c=(A*e)/b	Beer-Lambert's law: c, nucleic acid concentration in ng/µl; A, absorbance in AU (absorbance units); e, wavelength-dependent extinction coefficient in ng-cm/µl; b, path length in cm
°C	degrees Celsius
C	cytosine (nucleotide)
C, c	control
c.	cDNA sequence
$[Ca^{2+}]_i$	intracellular calcium concentration
CA	cerebellar atrophy
CA1	cornu ammonis 1
$(CAG)_{exp}$	polyglutamine expansion
cAMP	cyclic adenosine monophosphate

CAPS	N-cyclohexyl-3-aminopropanesulfonic acid
CCPPRB	Comité Consultatif de Protection des Personnes dans la Recherche Biomédicale
cDNA	copy deoxyribonucleic acid
cGMP	cyclic guanosine monophosphate
chr	chromosome
chrom alum	chromium (III) potassium sulfate dodecahydrate
CICR	calcium-induced calcium release
CI	cytoplasmic inclusion
CLP	continental lab products
cm	centimeter
cM	centimorgan
CMCT	central motor conduction time
CNS	central nervous system
CNV(s)	copy number variation(s)
Ct	cycle threshold
CT	computed tomography
C-terminus	carboxyl (-COOH) terminal end
D-28K	28 kiloDalton
DABCO	1,4-diazobicyclo-[2.2.2]-octane
DAG	diacylglycerol
dbSNP	database single nucleotide polymorphism, NCBI entrez SNP
Dec.	December
dG	free energy
dG temp.	free energy temperature
DHPLC	denaturing high performance liquid chromatography
DIC (objective)	differential interference contrast
DMD	Duchenne muscular dystrophy
DMSO	dimethyl sulfoxide
DNA	deoxyribonucleic acid
DNS	diffuse nuclear staining
DRPLA	dentatorubral-pallidoluysian atrophy
DSBs	double strand breaks
dsDNA	double strand deoxyribonucleic acid
EA2	episodic ataxia type 2
EBV	Epstein-Barr virus
EDTA	ethylenediaminetetraacetic acid
EMPReSS	European Mouse Phenotyping Resource of Standardised Screens

ENU	*N*-ethyl *N*-nitrosourea
ER	endoplasmic reticulum
ES cell(s)	embryonic stem cell(s)
et al.	*et alibi*
EUMORPHIA	European Union Mouse Research for Public Health and Industrial Applications
exp	expanded
F	female
F_x	filial generation, generation x following the parental generation
F primer, fwd.	forward primer
FAM	carboxy-fluorescein
FHM	familial hemiplegic migraine
freq.	frequency
fwd, F primer	forward primer
G=H-TS	G calculation: G, energy; H, enthalpy; S, entropy; T, dG temperature; dG, free energy
g	gram
G	guanine (nucleotide)
g.	genomic DNA sequence
x*g*	times gravity (centrifugal force)
geno__	prefix, related to genome
GII	glial intranuclear inclusion
Glu	glutamate
Golgi App.	Golgi apparatus
GT	genotype
GTP	guanosine triphosphate
HD	Huntington's disease
het	heterozygote
HEX	hexachloro-fluorescein
hg	human genome assembly
Hi-Di formamide	highly deionized formamide
HMW	high molecular weight
ho	hot-foot
HUGE database	Human Unidentified Gene-Encoded database
HUGO	Human Genome Organization
Hz	hertz

ID	identification
IgG (H+L)	immunoglobulin G (heavy polypeptide chain + light polypeptide chain)
IHC	immunohistochemistry
IHGSC	International Human Genome Sequencing Consortium
IMR	Induced Mutant Research
IMRC	International Mouse Resource Consortium
inHg	inches of mercury (unit for pressure)
IoN	Institute of Neurology
IP3	inositol 1,4,5-triphosphate
[IP3]	inositol 1,4,5-triphosphate concentration
IVS	intronic variants
JAX, TJL	The Jackson Laboratory
kb	kilo base pairs
kD	kiloDalton
kg	kilogram
KOMP	Knockout Mouse Project
l	liter
L	ladder (DNA size and/or weight standard)
laser	light amplification by stimulated emission of radiation
Lc	Lurcher
LCLs	lymphocyte cell lines
LCR(s)	low copy repeat(s)
LCSN	Laboratory of Cellular and Synaptic Neurophysiology
LDS	lithium dodecyl sulfate
LINE	long interspersed nuclear element
LNG	Laboratory of Neurogenetics
LNO	nonlinear optical (crystal, laser)
LOD	logarithm of odds
LREC	local research and ethics committee
LSM	laser scanning microscope
LTD	long-term depression
LTR	long terminal repeat
M	male
M	molar (mole of solute per liter of solution)
M	marker (protein size and/or weight standard)
M, Mb	mega base pairs

max	maximum
Mb, M	mega base pairs
MD	Maryland
mg	milligram
MGB	3'-minor groove binder
MGI	Mouse Genome Informatics
milliQ	water obtained from a Millipore water purification system
min	minimum
MJD	Machado-Joseph disease
ml	milliliter
MLINK	multi-locus linkage analysis
mm	millimeter
mM, mMol	millimolar
mMol, mM	millimolar
MMRRC	mutant mouse regional resource centers
MOPS	3-(N-morpholino)propanesulfonic acid
MRI	magnetic resonance imaging
mRNA	messenger ribonucleic acid
MSD	multiple sulfatase deficiency
mut	mutated allele
Myr	million years
n	number of subjects, samples
N	normal
n/a	not available
NA (objective)	numerical aperture
NAHR	non-allelic homologous recombination
NC	no template control
NCBI	National Center for Biotechnology Information
nclf	neuronal ceroid lipofuscinosis
neo	*neomycin*
NF-160, NF-M	neurofilament, medium polypeptide
NF-M, NF-160	neurofilament, medium polypeptide
ng	nanogram
NHEJ	non-homologous end joining
NHNN	National Hospital for Neurology and Neurosurgery
NHS	National Health Service
NIA	National Institute on Aging
NICHD	National Institute on Child Health and Development
NIH	National Institutes of Health

NII	neuronal intranuclear inclusion
NINDS	National Institute of Neurological Disorders and Stroke
nm	nanometer
NMDA	N-methyl-D-aspartic acid
nmol	nanomolar
no.	number
NP-40	nonyl phenoxylpolyethoxylethanol
NPCA	non-progressive congenital ataxia
NSA	NeuroScience Associates
nt	nucleotide
NT_	RefSeq accession number of contig assembly produced by NCBI
N-terminus	amine (-NH_2) terminal end
OLAW	Office of Laboratory Animal Welfare
OMIM	Online Mendelian Inheritance in Man
OPCA	olivopontocerebellar atrophy
opt	*opisthotonos*
p	*p*-value (probability measure in statistics)
P	phosphorylation site
p.	protein sequence
P9, 10, 14, 15	postnatal day 9, 10, 14, 15
PBS	phosphate buffered saline
pcd	Purkinje cell degeneration
PCR	polymerase chain reaction
PCR, A	annealing
PCR, AE	annealing and extension
PCR, D	denaturation
PCR, Di	initial denaturation
PCR, E	extension
PCR, Ef	final extension
PC tube	polycarbonate tube
pH	power of hydrogen
Pi	inorganic phosphate
PM	post meridiem
PMCT	peripheral motor conduction time
pMol	picomolar
PNP	peripheral neuropathy
polyQ	polyglutamine
PVDF membrane	polyvinylidene fluoride membrane

QA	quisqualate
R primer, rev.	reverse primer
rcf.	relative centrifugal force
refSNP	reference single nucleotide polymorphism
rep__	prefix, referring to repeat
rev, R primer	reverse primer
RFLP(s)	restriction fragment length polymorphism(s)
RIKEN	Rikagaku Kenkyusho
RIPA buffer	radio immuno precipitation assay buffer
RNA	ribonucleic acid
RNAi	ribonucleic acid interference
rpm	revolutions per minute
rs.no., rs#	reference number
RT	room temperature (21-25 degrees Celsius)
RT-PCR	reverse transcriptase - polymerase chain reaction
SI, SII, SIII	splicing region I, II, III
salt con.	salt concentration
SCA(s)	spinocerebellar ataxia(s)
SD	standard deviation
SDS	sodium dodecyl sulfate
SDS-page	sodium dodecyl sulfate – polyacrylamide gel electrophoresis
sg	staggerer
SHIRPA	SmithKline Beecham, Harwell, Imperial College School of Medicine, Royal London Hospital, Phenotype, Assessment
SINE	short interspersed nuclear element
SNP(s)	sinlge nucleotide polymorphism(s)
spdh	synpolydactyly homolog
SSR(s)	simple sequence repeat(s)
STS	sequence tagged sites
sq f	forward primer sequence
sq r	reverse primer sequence
T	thymine (nucleotide)
TBE buffer	tris-borate-EDTA
TBS buffer	tris-buffered saline
TBS-PI	tris-buffered saline - protease inhibitor
TBS-SDS	tris-buffered saline - sodium dodecyl sulfate
TBS-T, TBS-Tx100	tris-buffered saline - triton (tween-20)

TE buffer	tris-EDTA buffer
temp.	temperature
tg	tottering
TGS buffer	tris-glycine-SDS
TJL, JAX	The Jackson Laboratory
tk	thymidine kinase
Tm	melting point
Tm dif.	difference between the primers of a pair
TNES buffer	tris-NaCl-EDTA-SDS buffer
tRNA	transfer ribonucleic acid
µg	microgram
µl	microliter
µm	micrometer
µM	micromolar
U	unaffected
U	uracil (nucleotide)
Ub	ubiquitin
UCL	University College London
UCSC	University of California Santa Cruz
UK	United Kingdom
UPR	unfolded protein response
USA	United States of America
UTR(s)	untranslated region(s)
UV	ultraviolet
V	volt
v.	version
VIC	2'-chloro-7'-phenyl-1,4-dichloro-6-carboxy-fluorescein
vLINCL	variant late infantile neuronal ceroid lipofuscinosis
VOR	vestibule-ocular reflex
(v/v)	volume:volume ratio
VWR	Van Waters and Rogers
wks	weeks
wt	wild type, wild type allele
(w/v)	weight:volume ratio
y, yrs.	years of age
yrs, y.	years of age

GENES AND/OR PROTEINS

4.1N	4.1N protein
483344P13Rik	RIKEN cDNA 4833447P13 gene
Agtpbp1	ATP/GTP binding protein 1
AMPA, AMPAR	α-amino-3-hydroxy-5-methyl-4-isoxazole propionate receptor
ARL10C, Arl10c	ADP-ribosylation factor-like 10C
ATN1, Atn1	atrophin 1
ATXN1, Atxn1	ataxin 1
ATXN2, Atxn2	ataxin 2
ATXN3, Atxn3	ataxin 3
ATXN7	ataxin 7
Atxn8	ataxin 8
ATXN8OS	ataxin 8, opposite strand
ATXN10	ataxin 10
BHLHB2, Bhlhb2	basic helix-loop-helix domain containing, class B2
CA	carbonic anhydrase
CACNA1A, Cacna1a	Ca(v)2.1 voltage-dependent calcium channel, P/Q type, subunit alpha-1A
Calb1	calbindin D28K
Calb2	calretinin
CaM	calmodulin, calcium modulating protein
CaMKII	calcium/calmodulin-dependent protein kinase II
CARP	carbonic anhydrase-related protein
Ca(v)2.1, CACNA1A, Cacna1a	voltage-dependent calcium channel, P/Q type, subunit alpha-1A
CBP	CREB (cAMP response element binding) binding protein
CHL1	cell adhesion molecule with homology to L1CAM
Cln6	ceroid-lipofuscinosis, neuronal 6
CNTN4, Cntn4	contactin 4
CNTN6	contactin 6
CRBN, Crbn	cereblon
CREB	cAMP response element binding
CytC	cytochrome C
DAGLA	diacyl glycerol lipase, subunit a, alpha
DJ1	Park7, Parkinson disease (autosomal recessive, early onset) 7

EAAT4, SLC1A6	solute carrier family 1 (high affinity aspartate/glutamate transporter), member 6
EDEM1, Edem1	ER degradation enhancer, mannosidase alpha-like 1
FGF14	fibroblast growth factor 14
FKBP12	FK506-binding protein (12kDa)
FLJ	Japanese database Full-Length human cDNA clone
G*β*/Rack1	G*β* homologue receptor for activated C kinase-1
Girk2, Kcnj6	potassium inwardly-rectifying channel, J6
GPCRs	G-protein-coupled receptors
Grid2	glutamate receptor, ionotropic, delta 2
GRM7	glutamate receptor, metabotropic 7
HB	hemoglobin, beta, delta
Hoxd13	homeo box D13
IL5RA, Il5ra	interleukin 5 receptor, alpha
IP3R, ITPR, P400	inositol 1,4,5-triphosphate receptor
IP3R1, ITPR1, Itpr1	inositol 1,4,5-triphosphate receptor, type 1
ITPR(s), IP3R, P400	inositol 1,4,5-triphosphate receptor(s)
ITPR1, Itpr1, IP3R1	inositol 1,4,5-triphosphate receptor, type 1
KCNC3	voltage-gated potassium channel, type C, *Shaw*-related subfamily
Kcnj6, Girk2	potassium inwardly-rectifying channel, J6
KIAA	human novel large (>4kb) cDNA identified in the HUGE protein database
KLHL1, Klhl1	Kelch-like 1
L1CAM	L1 gene family of neural Cell Adhesion Molecules
LOC	hypothetical protein in which orthologs have not yet been determined
LOC384471	similar to RIKEN cDNA 2410080P20
LOC434075	similar to ZGC:56193
LOC435913	similar to 40S ribosomal protein S8
LOC545871	similar to DEAD (Asp-Glu-Ala-Asp) box polypeptide 18
LRRN1, Lrrn1	leucine rich repeat protein 1, neuronal
NMDA, NMDAR	N-methyl-D-aspartate receptor
Nna1	nuclear ATP/GTP-binding protein
nr	nervous

P400, IP3R, ITPR	inositol 1,4,5-triphosphate receptor
PKA	protein kinase A
PKC	protein kinase C
PKG	protein kinase G
PLC	phospholipase C
PLEKHG4	puratrophin-1 (Purkinje cell atrophy associated protein-1)
PMCA	plasma membrane calcium ATPase
PP2A	protein phosphates 2A
PPP2R2B	protein phosphatase 2, regulatory subunit b, beta
PRKCG	protein kinase C, gamma
Reln	reelin
ROCs	receptor-operated channels
Rora	RAR-related orphan receptor alpha
RYR, RyR(s)	ryanodine receptor(s)
SERCA	sarco-endoplasmatic reticulum calcium ATPase
SET domain	Su(var)3-9, Enhancer-of-zeste, Trithorax (Su(var), suppressor of variation)
SETMAR, Setmar	SET domain and mariner transposase fusion gene
SLC1A6, EAAT4	solute carrier family 1 (high affinity aspartate/glutamate transporter), member 6
SPTBN2	spectrin, beta, norerythrocytic, 2
SUMF1, Sumf1	sulfatase modifying factor 1
$TAF_{II}130$	TAF4 RNA polymerase II; TBP-associated factor, 135kDa
TBP	TATA box-binding protein
TrkB	neurotrophic tyrosine kinase receptor, type 2
TRNT1, Trnt1	tRNA nucleotidyl transferase, CCA-adding, 1
TTBK1	tau tubulin kinase 1
TTBK2	tau tubulin kinase 2
VOCCs	voltage-operated calcium channels

AMINO ACIDS

A, Ala	alanine
Ala, A	alanine
Arg, R	arginine
Asn, N	asparagine
Asp, D	aspartic acid
C, Cys	cysteine
Cys, C	cysteine
D, Asp	aspartic acid
E, Glu	glutamic acid
F, Phe	phenylalanine
G, Gly	glycine
Gln, Q	glutamine
Glu, E	glutamic acid
Gly, G	glycine
H, His	histidine
His, H	histidine
I, Ile	isoleucine
Ile, I	isoleucine
K, Lys	lysine
L, Leu	leucine
Leu, L	leucine
Lys, K	lysine
M, Met	methionine
Met, M	methionine
N, Asn	asparagine

P, Pro	proline
Phe, F	phenylalanine
Pro, P	proline
Q, Gln	glutamine
R, Arg	arginine
S, Ser	serine
Ser, S	serine
T, Thr	threonine
Thr, T	threonine
Trp, W	tryptophan
Tyr, Y	tyrosine
V, Val	valine
Val, V	valine
W, Trp	tryptophan
Y, Tyr	tyrosine

MISCELANEOUS

’	minutes
’’	seconds

CHAPTER 1 INTRODUCTION

1.1 SPINOCEREBELLAR ATAXIA (SCA)

Autosomal dominant cerebellar ataxias (ADCAs) are hereditary progressive neurodegenerative disorders, also known as spinocerebellar ataxias (SCAs). They form a complex group of neurological disorders characterized by cerebellar ataxia of gait and limbs variably associated with ophthalmoplegia, pyramidal and extrapyramidal signs, dementia, pigmentary retinopathy and peripheral neuropathy (Zoghbi 2000). Phenotypic heterogeneity leads to ataxias being some of the most poorly understood neurological disorders. The finding that expansion of polyglutamine repeats underlies pathogenic mechanisms of different SCA subtypes initially provided an explanation for many of the clinical phenomena such as anticipation and the variable severity observed even within one family (Orr et al. 1993). However, subsequent identification of additional ataxia genes has resulted in renewed confusion due to their apparent lack of a common pathogenic mechanism: a calcium channel (*CACNA1A*) is mutated in SCA6, implicating altered calcium homeostasis (Zhuchenko et al. 1997), a member of the tau tubulin kinase family (*TTBK2*) is mutated in SCA11 indicating phosphorylation dysfunction (Houlden et al. 2007), and fibroblast growth factor (*FGF14*) is mutated in SCA27 suggesting possible involvement of synaptic plasticity in SCA pathogenesis (van Swieten et al. 2003). Identification of additional ataxia genes would aid in elucidating the pathogenesis of SCAs, important cellular pathways, and development of potential therapies. Currently there is no treatment for spinocerebellar ataxias, except for supportive care such as physical and speech therapy (H Houlden (IoN/UCL, NHNN), personal communication).

1.1.1 Phenotypic characteristics

1.1.1.1 Epidemiology

Prevalence studies of autosomal dominant ataxias are rare, and those published disagree in their estimates. Differences between the studies are due to focus on a specific SCA locus or gene, inclusion of all hereditary ataxias (dominant and recessive variants) or geographically limited measurements. Epidemiological studies conducted in different European regions found prevalence estimates of dominant inherited ataxias of less than 6/100,000, mostly ranging from 0.3 to 2.0 per 100,000 inhabitants (Koeppen et al. 1977;Schoenberg 1978;Brignolio et al. 1986;Polo et al. 1991;Leone et al. 1995;Silva et al. 1997;van de Warrenburg et al. 2002). As more SCA genes are identified, the prevalence of autosomal dominant ataxia is expected to be higher than previously anticipated and to lie in the range of other neurological disorders such as sporadic amyotrophic lateral sclerosis (6.2/100,000) (Traynor et al. 1999) and inherited Huntington's disease (6.4/100,000) (Morrison et al. 1995).

1.1.1.2 Diagnosis and pathology

Autosomal dominant SCAs are a group of neurodegenerative diseases, clinically and genetically heterogeneous, characterized by progressive cerebellar ataxia of gait and limbs, variably associated with ophthalmoplegia, pyramidal and extrapyramidal signs, dementia, pigmentary and peripheral neuropathy. Disease onset is usually between 30 and 50 years of age, although early onset (in childhood) and onset in later decades (after 60 years) have been reported. The prognosis is variable depending on the underlying cause of the SCA subtype (Duenas et al. 2006). In 1983, Harding proposed a classification of the SCAs based on clinical symptoms and distinguished three types of autosomal dominant cerebellar ataxias; ADCA I, ADCA II and ADCA III (table 1.1).

ataxic disorders of unknown etiology
autosomal dominant cerebellar ataxia, type
I. ophthalmoplegia/ optic atrophy/ dementia/ extrapyramidal features
II. pigmentary retinopathy ±ophthalmoplegia/ extrapyramidal features
III. 'pure' autosomal dominant cerebellar ataxia of later onset
other progressive dominant disorders
periodic autosomal dominant cerebellar ataxia

Table 1.1. Classification of ADCAs by Harding (1983)

Clinical features and classification of autosomal dominant late onset cerebellar ataxias of unknown etiology (Harding 1983).

ADCA type I (Harding 1993), in early disease stages most frequently presents as a progressive ataxia of gait with limb involvement and is invariably associated with dysarthria of mixed cerebellar and pseudobulbar type. Additional symptoms have been described, including supranuclear ophthalmoplegia with lid retraction, nuclear and intranuclear eye movement abnormalities, optic atrophy in some patients (usually not associated with visual loss), clinically significant cognitive impairment in about one-third of patients, extrapyramidal signs such as parkinsonism, chorea and dystonia, and peripheral neuropathy presenting as distal wasting and fasciculation of face and tongue but not always clinically evident, loss of proprioception and vibration sense, and pyramidal weakness. The clinical features in this group of ataxias are caused by a combination of degeneration of the cerebellum, basal ganglia, cerebral cortex, optic nerve, pontomedullary systems, spinal tracts or peripheral nerves. Disease onset ranges from 15 to 65 years, usually in the third or fourth decades of life. The majority of patients lose the ability to walk within 20 years of onset and life expectancy is shortened due to disability and bulbar dysfunction. An early onset usually predicts a rapidly progressive disability.

ADCA type II (Harding 1993) is clinically distinct from ADCA type I because of the presence of pigmentary retinopathy. Pigmentary retinal degeneration predominantly affects the macula leading to blindness and occasionally extends to the peripheral fundus. Visual failure may precede ataxic symptoms by several years. Additional clinical features include supranuclear ophthalmoplegia in about half of patients, cognitive impairment, extrapyramidal features, pyramidal signs in legs together with loss of position and vibration sense. Disease onset ranges between 15 and 25 years, early childhood onset predicting a rapidly progressive course. Most patients lose ability to walk within 15 years after onset. At autopsy, the majority of ADCA II cases show olivopontocerebellar atrophy as well as degeneration in spinal cord and basal ganglia.

ADCA type III (Harding 1993) is a relatively ‘pure’ cerebellar syndrome where the degenerative process is limited to the cerebellum, although some affected individuals may also manifest mild pyramidal signs and autopsy of one case showed cerebellar cortical atrophy with loss of cells in the dentate nuclei. Disease onset is generally late adulthood, over 50 years of age.

Other types of autosomal dominant late onset cerebellar ataxia are rare (Harding 1993): May-White syndrome of deafness, characterized by late onset cerebellar ataxia,

myoclonus and peripheral neuropathy; dominantly inherited ataxia associated with essential tremor, parkinsonism, peripheral neuropathy, cataracts, deafness and deposition of cerebrovascular amyloid; Gerstmann-Straussler syndrome with prominent ataxia in the early phase of disease with dementia usually more prominent at later stages. Autosomal dominant periodic ataxia (Harding 1993) is characterized by childhood or adolescent onset of episodes of ataxia, dysarthria, vertigo and nystagmus. Duration of the attacks varies from a few hours to several weeks and attacks tend to be more severe in childhood. Nystagmus and mild cerebellar signs often persist in between the attacks.

The classification of autosomal dominant ataxias by Harding has remained the standard for scientists and clinicians in prioritizing genetic testing in SCA families; see table 1.2 for Harding based categorization of all SCA subtypes currently assigned by the HUGO Gene Nomenclature Committee (HUGO, Human Genome Organization; http://www.genenames.org).

Table 1.2. Autosomal dominant ataxias categorized based on classification by Harding (1983)
Data are based on tables published in Schols et al. (2004) and Duenas et al. (2006), and have been supplemented with findings described in Hellenbroich et al. (2006) (SCA4); Knight et al. (2004) (SCA20); Verbeek et al. (2004) (SCA23); Yu et al. (2005) (SCA26); Mariotti et al. (2008) (SCA28). Currently, autosomal dominant ataxias comprise 26 SCAs and DRPLA. SCA9 and 24 have not been annotated; SCA15 and 16 have both been attributed to deletion in *ITPR1* (van de Leemput et al. 2007;Iwaki et al. 2008); SCA19 and 22 share disease locus and a highly similar phenotype (Verbeek et al. 2002;Chung et al. 2003;Chung and Soong 2004;Schelhaas et al. 2004).
*age at onset, mean (range) in years; ADCA, autosomal dominant cerebellar ataxia; SCA, spinocerebellar ataxia; CT, computed tomography; MRI, magnetic resonance imaging; PNP, peripheral neuropathy; PMCT, peripheral motor conduction time; CMCT, central motor conduction time; OPCA, olivopontocerebellar atrophy; MJD, Machado-Joseph disease; CA, cerebellar atrophy; DRPLA, dentatorubral-pallidoluysian atrophy. **(table 1.2, *on next page*)**

(table 1.2, *continued from previous page*)

ADCA I

phenotype. *cerebellar ataxia with ophthalmoplegia, pyramidal signs, extrapyramidal signs, cognitive impairment, and/or peripheral neuropathy*

neuropathology. *cerebellar atrophy with degeneration of basal ganglia, cerebral cortex, optic nerve, pontomedullary systems, spinal tracts, and/or peripheral nerves*

subtype	***age at onset, yrs.****	***phenotype***	***CT/ MRI findings***
SCA1	37 (4-74)	ataxia, dysarthria, nystagmus, slow saccades, ophthalmoplegia, spasticity, PNP, executive dysfunction; increase in PMCT and CMCT	OPCA
SCA2	32 (1-65)	ataxia, dysarthria, slow saccades, hyporeflexia, titubation, dementia, (rarely) parkinsonism	OPCA + spinal atrophy, some cortical atrophy
SCA3 (MJD)	36 (5-70)	ataxia, dysarthria, nystagmus, lid retraction, diplopia, faciolingual fasciculation, dystonia, parkinsonism, restless legs, temperature discrimination; onset <35 years with ataxia + spasticity, onset >45 years with ataxia + PNP	OPCA (mild), 4th ventricle enlarged
SCA4	? (19-72)	ataxia, dysarthria, sensory axonal neuropathy, pyramidal signs	CA + brainstem atrophy
SCA8	40 (1-73)	ataxia, dysarthria, nystagmus, tremor	CA
SCA10	36 (26-45)	ataxia, dysarthria, nystagmus, epilepsy	CA
SCA12	35 (8-55)	ataxia, nystagmus, tremor, bradykinesia, hyperreflexia	CA + cerebral atrophy
SCA13	childhood (<1-45)	ataxia, dysarthria, nystagmus, hyperreflexia, mental + motor retardation, slow progression	OPCA
SCA17	33 (6-48)	ataxia, dysarthria, nystagmus with dementia, slow saccades or epilepsy, hyperreflexia, akinesia, dystonia, chorea, psychosis, mutism	CA, some; general atrophy
SCA18	15 (12-25)	ataxia, dysarthria, nystagmus, sensory-motor axonal neuropathy, Babinski sign	CA
SCA19	34 (11-45)	mild ataxia, dysarthria, nystagmus, cognitive impairment, myoclonus, tremor, hyporeflexia, hyperreflexia	CA, some; cerebral atrophy
SCA20	47 (19-64)	ataxia, dysarthria, (mild/moderate) dysphonia, ballistic overshoot, bradykinesia, palatal (some + lips) tremor	dentate calcification + panCA (in most)
SCA21	18 (7-30)	ataxia, dysarthria, akinesia, rigidity, postural and rest tremor, hyporeflexia, cognitive impairment	CA
SCA22	? (10-46)	ataxia, dysarthria, nystagmus, slow progression, hyporeflexia	CA
SCA23	50 (43-56)	'pure' ataxia, dysarthria, (mild) disturbance oculomotor control, hyperreflexia (Babinski sign in some), slow progression	CA
SCA25	? (1-39)	ataxia, dysarthria, nystagmus, sensory neuropathy	CA
SCA27	34 (27-40)	ataxia, dysarthria, nystagmus, tremor, psychiatric episodes	CA
SCA28	20 (12-36)	ataxia, dysarthria, hyperreflexia (Babinski sign in some), nystagmus, ophthalmoparesis; juvenile onset, slow progression	CA (superior vermis)
DRPLA	30 (0-62)	ataxia, onset <20 years with myoclonus, epilepsy; onset >20 years with choreoathetosis, dementia, psychosis	OPCA, cerebral white-matter lesions

ADCA II

phenotype. *cerebellar ataxia with pigmentary retinopathy*

neuropathology. *cerebellar atrophy with pigmentary retinal degeneration*

subtype	***age at onset, yrs.****	***phenotype***	***CT/MRI findings***
SCA7	35 (0-70)	ataxia, dysarthria, visual loss owing to pigmentary retinopathy, slow saccades, pyramidal signs	OPCA

ADCA III

phenotype. *'pure' cerebellar ataxia*

neuropathology. *cerebellar atrophy*

subtype	***age at onset, yrs.****	***phenotype***	***CT/MRI findings***
SCA5	30 (10-68)	'pure' ataxia, dysarthria, normal life expectancy; early onset, bulbar signs	CA
SCA6	52 (30-71)	'pure' ataxia, dysarthria, nystagmus, normal life expectancy, (commonly) diplopia, (rare and mild) PNP, pyramidal signs negative family history owing to late onset	CA
SCA11	25 (25-43)	'pure' ataxia, dysarthria, nystagmus, normal life expectancy, (rarely) hyperreflexia	CA
SCA14	27 (12-42)	ataxia (slow progression) ± head tremor or myoclonus (early onset)	CA (vermis)
SCA15	26 (10-50)	'pure' ataxia, dysarthria, nystagmus, normal life expectancy; some patients with hyperreflexia	CA (vermis)
SCA16	40 (20-66)	'pure' ataxia, dysarthria, nystagmus, normal life expectancy; some patients with head tremor	CA
SCA26	42 (26-60)	'pure' ataxia, dysarthria, nystagmus, dysmetric saccades	CA

Table 1.3. Autosomal dominant ataxias; genetics and molecular pathways implicated

The autosomal dominant ataxias comprise 26 SCA subtypes and DRPLA (SCA9 and 24 have not been annotated). **a.** Japanese SCA4 was initially assigned to SCA4 due to phenotypic similarities and linkage assigned to the same locus, however, no *puratrophin-1* mutations have been found in the original SCA4 families (Hellenbroich et al. 2008) implicating Japanese SCA to be of a different subtype. **b.** Some controversy exists around the pathogenic mechanism of SCA8, recent findings suggesting a dual pathogenic mechanism (Moseley et al. 2000;Nemes et al. 2000;Worth et al. 2000;Stevanin et al. 2000;Aromolaran et al. 2007). **c.** SCA15 and 16 have both been attributed to deletion in *ITPR1* (van de Leemput et al. 2007;Iwaki et al. 2008), and therefore can now be regarded as the same condition (SCA15) (Gardner 2008). **d.** SCA19 and 22 share disease locus and a highly similar phenotype suggesting they might share an underlying genetic cause (Verbeek et al. 2002;Chung et al. 2003;Chung and Soong 2004;Schelhaas et al. 2004). **e.** SCA20 locus was assigned to 11p11.2-q13.2. In a recent paper Knight and colleagues (2008) described duplication at 11q12.2-12.3 in SCA20 patients, narrowing the linkage region, and speculated the disease causing gene within the duplicated segment to be *DAGLA* (*diacylglycerol lipase, alpha*). Additional families or experimental data are critical to confirm these findings. **f.** Defined loci for SCA18 and 29 are based on data provided by the HUGO Gene Nomenclature Committee (HUGO, Human Genome Organization; http://www.genenames.org) as no published linkage studies were available. A paper by Devos et al. (2001) does provide a phenotypical description of the SCA18 family. SCA, spinocerebellar ataxia; $(---)_n$, expanded repeat; MJD, Machado-Joseph disease; UTR, untranslated region; n/a, not available; DRPLA, dentatorubral-pallidoluysian atrophy. **(table 1.3, *on next page*)**

(table 1.3, *continued from previous page*)

SCA	locus	Gene	mutation	gene/protein-name	function/ process	reference
SCA1	6p23	*ATXN1*	$(CAG)_n$	*ataxin 1*	*unknown*	Orr et al. (1993)
SCA2	12q23-24.1	*ATXN2*	$(CAG)_n$	*ataxin 2*	*unknown*	Pulst et al. (1996), Sanpei et al. (1996), Imbert et al. (1996)
SCA3 (MJD)	14q21	*ATXN3*	$(CAG)_n$	*ataxin 3*	*unknown*	Kawaguchi et al. (1994), Haberhausen et al. (1995)
SCA4[a]	16q22.1					Flanigan et al. (1996), Hellenbroich et al. (2008)
Japanese SCA4[a]	16q22.1	*PLEKHG4*	substitution 5'UTR	*puratrophin-1* (Purkinje cell atrophy associated protein-1)	*unknown*	Ishikawa et al. (2005), Ohata et al. (2006)
SCA5	11q13.2	*SPTBN2*	deletion, missense	*spectrin, beta, nonerythrocytic, 2*	glutamate signaling	Ikeda et al. (2006)
SCA6	19p13	*CACNA1A*	$(CAG)_n$	*voltage-dependent calcium channel, P/Q type, subunit alpha-1A*	calcium homeostasis	Zhuchenko et al. (1997)
SCA7	3p21.1-p12	*ATXN7*	$(CAG)_n$	*Ataxin 7*	*unknown*	David et al. (1997)
SCA8[b]	13q21	*ATXN8OS*	$(CTG)_n$ 3'UTR	*ataxin 8, opposite strand (non-protein coding); Kelch-like 1* (*KLHL1*)	organization actin cytoskeleton	Koob et al. (1999), Chen et al. (2008)
SCA10	22q13	*ATXN10*	$(ATTCT)_n$ intron	*ataxin10*	*unknown*	Matsuura et al. (2000)
SCA11	15q15.2	*TTBK2*	frameshift premature stop	*tau tubulin kinase 2*	microtubule assembly, stability cytoskeleton	Houlden et al. (2007)
SCA12	5q32	*PPP2R2B*	$(CAG)_n$ 5'UTR	*protein phosphatase 2, regulatory subunit b, beta*	cell-cycle progression, tau phosphorylation, apoptosis	Holmes et al. (1999)
SCA13	19q13.33	*KCNC3*	missense	*voltage-gated potassium channel, type C*, *Shaw*-related subfamily	neuronal signaling	Waters et al. (2006)
SCA14	19q13.4	*PRKCG*	missense	*protein kinase C, gamma*	cellular signaling, cell proliferation and differentiation	Chen et al. (2003)
SCA15[c]	3p26.1	*ITPR1*	deletion	*inositol 1,4,5-triphosphate receptor, type 1*	calcium homeostasis	van de Leemput et al. (2007)
SCA16[c]	3p26.1	*ITPR1*	deletion	*inositol 1,4,5-triphosphate receptor, type 1*	calcium homeostasis	Iwaki et al. (2008)
SCA17	6q27	*TBP*	$(CAG)_n$	*TATA box-binding protein*	gene transcription	Nakamura et al. (2001)
SCA18[f]	7q22-q32					Devos et al. (2001), *n/a*
SCA19[d]	1p21-q21					Verbeek et al. (2002), Schelhaas et al. (2004)
SCA20[e]	11p11.2-q13.3					Knight et al. (2004)
	11q12.2-q12.3	*DAGLA*	duplication	*diacylglycerol lipase, subunit a, alpha*	*synaptic transmitter release*	Knight et al. (2008)
SCA21	7p21.3-p15.1					Vuillaume et al. (2002)
SCA22[d]	1p21-q23					Chung et al. (2003), Chung and Soong (2004)
SCA23	20p13-12.3					Verbeek et al. (2004)
SCA25	2p21-p15					Stevanin et al. (2004)
SCA26	19p13.3					Yu et al. (2005)
SCA27	13q34	*FGF14*	missense	*fibroblast growth factor 14*	axonal function, synaptosomal function, or neurotransmission	van Swieten et al. (2003)
SCA28	18p11.22-q11.2					Cagnoli et al. (2006)
SCA29[f]	3p26					*n/a*
DRPLA	12p	*ATN1*	$(CAG)_n$	*atrophin 1*	*unknown*	Koide et al. (1994), Nagafuchi et al. (1994a;1994b)

1.1.2 Pathogenesis of spinocerebellar ataxias

The molecular and cellular events that underlie cerebellar atrophy and degeneration of additional brain regions in spinocerebellar ataxia are still poorly understood. Although numerous ataxia genes have been identified in the past decade, their apparent lack of a common pathogenic mechanism has caused confusion. Initially, expansion of unstable repeats were found to underlie SCA pathogenesis, however in recent years conventional mutations, non-repeat mutations, have been identified in several SCA subtypes (table 1.3); for example missense mutation in FGF14 in SCA27 (van Swieten et al. 2003), deletion of 2 bases in *TTBK2* underlying SCA11 (Houlden et al. 2007), deletions ranging from several exons to the entire *ITPR1* gene in SCA15 and SCA16 (van de Leemput et al. 2007;Hara et al. 2008;Iwaki et al. 2008) and linkage in SCA20 to a duplication on chromosome 11 comprising several genes (Knight et al. 2008). Genes implicated in SCA etiology have been shown to be involved in regulation of phosphorylation, protein aggregation and clearance, neuronal signaling pathways, and calcium homeostasis (figures 1.1, 1.2).

1.1.2.1 Expansion of unstable repeats

Polyglutamine repeats represent the most common pathogenic mechanism found to underlie autosomal dominant inherited ataxia, accounting for more that 50% of affected families worldwide (Schols et al. 2004). To date, ten spinocerebellar ataxias have been attributed to a CAG-repeat expansion in the coded region of a gene; SCA1, 2, 3 (also know as Machado-Joseph disease), 6, 7, 17 and DRPLA (dentatorubral-pallidoluysian atrophy). The function of the affected protein is only known for two of these; the α1A-subunit of a P/Q-type calcium channel (CACNA1A) in SCA6 (Zhuchenko et al. 1997), and the TATA-box binding protein (TBP) in SCA17 (Nakamura et al. 2001). The polyglutamine (polyQ) repeat expansions form the major common characteristic of affected proteins, suggesting pathogenesis is directly linked to the expanded polyglutamine stretch. The mechanism by which these polyQ-proteins cause neurodegeneration is still unknown. Studies of extended polyglutamine repeats in other diseases, such as Huntington's disease (HD), have shown expanded stretches of polyglutamine lead to abnormal protein configuration (β-sheet structures) resulting in formation and deposition of fibrillar aggregates in the nucleus (Perutz 1996). Similar pathological inclusions have been shown in the nucleus of spinocerebellar ataxias 1, 3, 7 and 17, whereas in SCA2 inclusions have been found both in the nucleus and cytoplasm, and in SCA6 inclusion bodies have been shown exclusively in the cytoplasm (Schols et al. 2004). These polyglutamine repeat fragments have been

suggested to sequester other proteins into the aggregates, to block cell vesicle trafficking, to inhibit proper proteasome function, and to lure chaperones away from the rest of the cell by toxic titration (Truant et al. 2008). Early studies defined mutant aggregates as static, misfolded, precipitated proteins that rendered cell clearance machinery, such as the ubiquitin-dependent proteasome system and autophagy, inadequate. Recent studies however, have shown some of the polyglutamine expanded proteins in inclusion bodies exchange back to the soluble phase, others appear static and sequester soluble protein, whereas some move between inclusions (Truant et al. 2008). These findings suggest a much more dynamic system in which a polyglutamine expansion effect on protein function would not necessarily be universal for all proteins. Aggregation seems to occur through formation of a reservoir of soluble intermediates, whose population and stability increases with polyglutamine length. Increasing evidence indicates the soluble oligomers to be the toxic species and not the protein in aggregates, with protein context defining toxicity possibly through interaction with other proteins and small molecules. A more detailed discussion on polyglutamine toxicity in neurodegenerative disease can be found in a review by Truant et al. (2008). An alternative, or possibly complementary explanation would be that the continual presence of mutant polyglutamine protein overloads the cellular pathways for protein quality control. This results in accumulation of polyglutamine aggregates as well as other misfolded proteins thereby disturbing global protein homeostasis, eventually leading to neural cell death (Gidalevitz et al. 2006).

Unstable repeat expansions found in SCA8, 10 and 12, fall outside the protein coding region of the respective disease genes: SCA8 has been identified as being partly caused by a CTG repeat expansion in the untranslated, endogenous antisense RNA that overlaps the *Kelch-like 1* (*KLHL1*) gene (Koob et al. 1999;Chen et al. 2008); an expansion of a pentanucleotide (ATTCT) repeat in intron 9 of *ATXN10* has been identified in SCA10 (Matsuura et al. 2000); expansion of a CAG trinucleotide repeat in the 5'UTR of *PPP2R2B*, encoding the beta regulatory subunit of protein phosphatase 2, is associated with SCA12 (Holmes et al. 1999). It remains unclear how these non-coding repeats cause neurodegeneration. One explanation could be a dominant toxic mechanism occurring at the RNA level similar to that shown in myotonic dystrophy in which expanded RNA repeats sequester RNA-binding proteins, leading to aberrant RNA splicing (Osborne and Thornton 2006;Soong and Paulson 2007). However, no evidence has been found to support this theory in SCA8, 10 or 12. Alternatively, neurodegeneration might be caused by gene specific effects. The *SCA8* transcript has

been proposed to act as an antisense regulator for *KLHL1* (*kelch-like 1*) based on the genomic organisation of both genes (Chen et al. 2008), and the absence of extended open reading frames or significant homology to known genes. The trinucleotide (CTG) repeat expansion would then abolish *KLHL1* regulation, indeed over-expression of the *SCA8* gene region in mice induced motor deficits, generalized wasting and premature death (Yamada et al. 2008). The SCA12 polyglutamine repeat expansion is located in the 5'UTR of *PPP2R2B* (protein phosphatase 2, regulatory subunit beta), a regulator of protein phosphatase PP2A activity for specific substrates including vimentin and tau, both linked to neuronal cell death (Holmes et al. 1999).

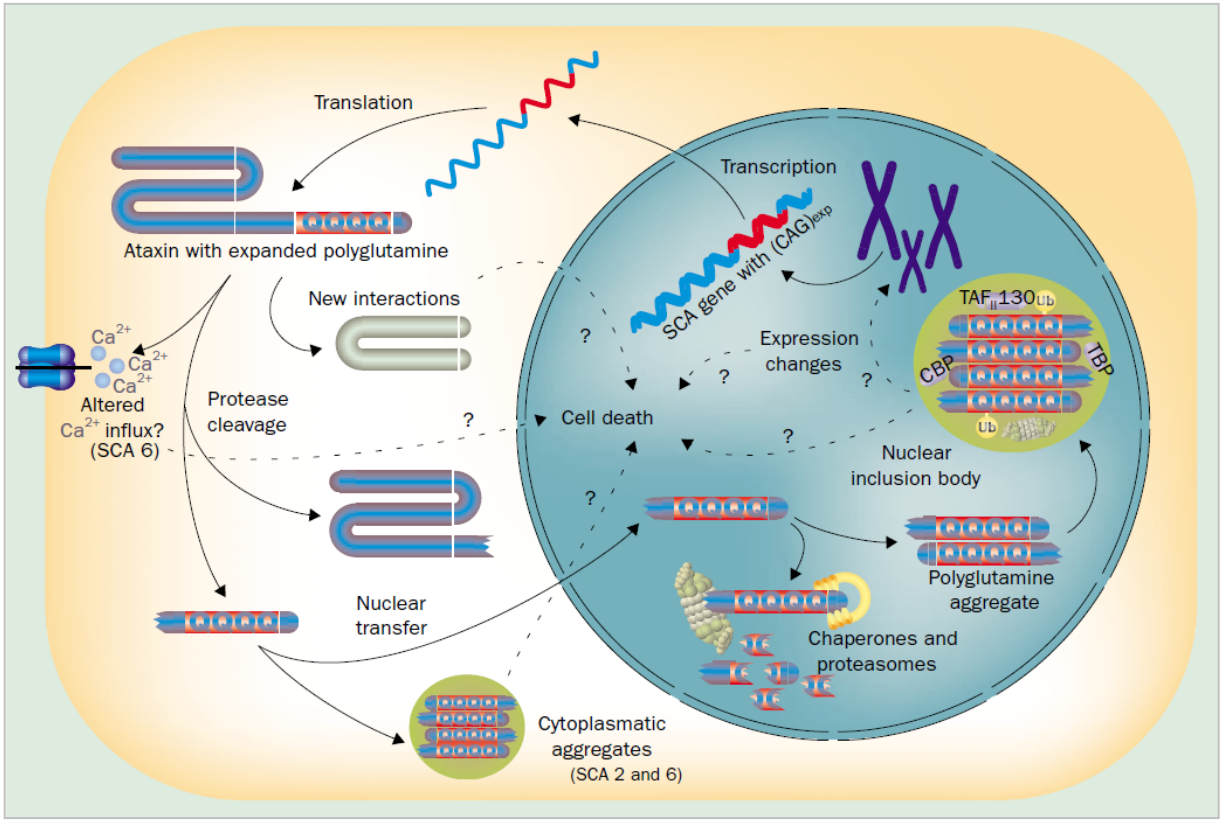

Figure 1.1. Molecular mechanisms of neurodegeneration in SCAs caused by polyglutamine expansion

Polyglutamine aggregates form in the nucleus and/or cytoplasm. Chaperones and proteasomes are recruted to refold or dispose polyglutamine containing fragments in order to prevent further aggregation. Small aggregates sequester other proteins and protein complexes including ubiquitin, proteasomes, chaperones and transcription factors thereby forming nuclear inclusion bodies. Ca^{2+}, calcium ions; $(CAG)_{exp}$, polyglutamine expansion; $TAF_{II}130$, TBP-associated factor (135kDa); Ub, ubiquitin; CBP, CREB (cAMP response element binding) binding protein; TBP, TATA box-binding protein. Reproduced from Schols et al. (2004).

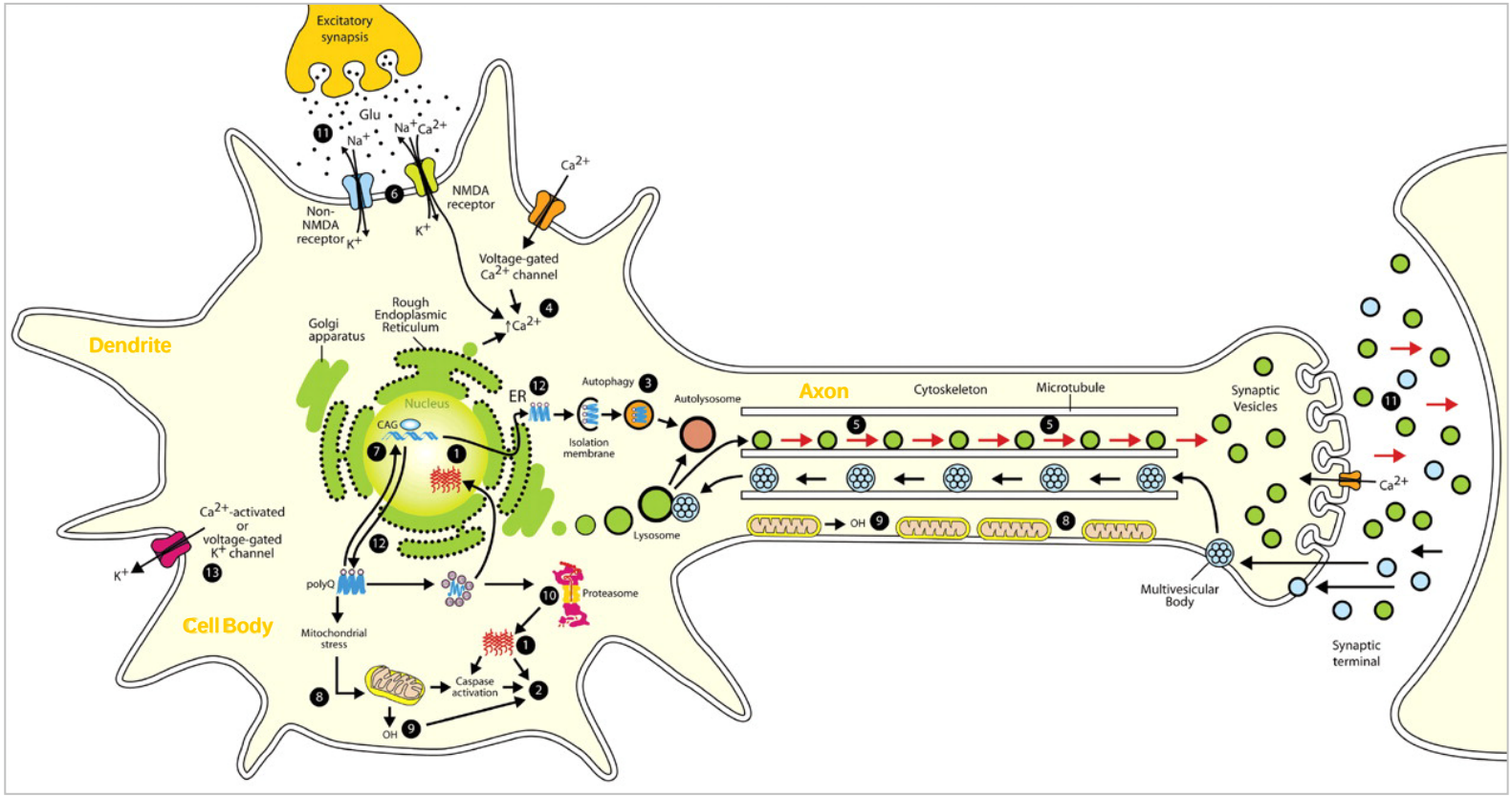

Figure 1.2. Molecular mechanisms of neurodegeneration in SCAs caused by conventional mutations

1, aggregation; 2, apoptosis; 3, autophagy; 4, Ca^{2+} homeostasis alterations; 5, disruption of axonal transport and vesicle trafficking; 6, excitotoxicity; 7, interference with gene transcription; 8, mitochondrial impairment; 9, oxidative stress; 10, alterations of proteasome degradation; 11, synaptic dysfunction; 12, unfolded protein response (UPR); 13, potassium channel dysfunction. Ca^{2+}, calcium ions; ER, endoplasmic reticulum; Glu, glutamate; K^+, potassium ions; Na^+, sodium ions; NMDA, N-methyl-D-aspartic acid; OH, hydroxyl radical; Q, glutamine; Ub, ubiquitin. Adapted from Duenas et al. (2006).

1.1.2.2 Neuronal signalling dysfunction

Several spinocerebellar ataxias have been attributed to disruption of neuronal signalling. Mutations in the *fibroblast growth factor* (*FGF)14* gene underlie SCA27 pathogenesis. FGF14 has been shown to play a role in regulating synaptic plasticity by controlling mobilization, trafficking or docking of synaptic vesicles to presynaptic active zones (Soong and Paulson 2007). SCA5 is caused by mutations in the *spectrin* gene. Spectrin is a cytoskeletal component and has been associated with Golgi and vesicle membranes and shown to bind dynactin, suggesting a possible role in transport. Another function of β-spectrin is stabilization of membrane proteins, such as the Purkinje cell-specific glutamate transporter EAAT4 (Ikeda et al. 2006). The *Kelch-like 1* (*KLHL1*) gene has been implicated in SCA8 pathology. KLHL1 protein has been suggested to function as an actin-organizing protein thereby modulating neurite outgrowth, dynamic properties of dendritic spines and neuronal proteins essential for postsynaptic function (Soong and Paulson 2007). A single nucleotide substitution in the 5'UTR of the *puratrophin-1/ PLEKHG4* (*Purkinje cell atrophy associated protein-1*) gene has been described to underlie Japanese SCA4. *Puratrophin-1* protein has been suggested to play a role in intracellular signalling and actin dynamics at the Golgi apparatus (Duenas et al. 2006). Mutations in the *KCNC3* gene, encoding a voltage-gated potassium channel (Kv3.3), have been shown to cause SCA13. Mutations have a dominant-negative effect on the electrophysiological properties of the potassium channel, slowing channel closing and thereby changing the output characteristics of fast-spiking cerebellar neurons, in which KCNC channels confer capacity for high-frequency firing (Waters et al. 2006).

1.1.2.3 Altered calcium homeostasis

Alteration of calcium homeostasis plays a central role in apoptosis, and Ca^{2+} overload or perturbation of intracellular Ca^{2+} compartmentalization has long been recognized to be potentially cytotoxic (Orrenius et al. 2003). Purkinje cell degeneration in SCA6 has been associated with polyglutamine expansions in the *CACNA1A* gene, encoding a major pore forming subunit of the Ca(v)2.1 voltage-dependent P/Q-type calcium channel (Zhuchenko et al. 1997). P/Q-type calcium channels have been shown to be highly expressed in granule cells and Purkinje cells of the cerebellar cortex, and have been suggested to play a major role in synaptic transmission (Ishikawa et al. 1999). Moreover, KLHL1, the actin-organizing protein associated with SCA8, has been shown to interact with and modulate voltage-gated calcium channels, in particular the alpha (1A) subunit of P/Q-type channels (Aromolaran et al. 2007). Recently, SCA15 and

SCA16 have been attributed to deletions in the *ITPR1* (*inositol 1,4,5-triphosphate receptor, type 1*) gene (van de Leemput et al. 2007;Iwaki et al. 2008) (chapter 4). *ITPR1* encodes an IP3(inositol 1,4,5-triphosphate)-gated calcium-release channel located in the endoplasmic reticulum membrane, thereby controlling Ca^{2+} release from the major cellular calcium store and playing a critical role in maintaining intracellular calcium homeostasis. Interestingly, mutations in PRKCG have been identified in SCA14 pathology. PKC (protein kinase C) is another major player in the IP3-pathway (Chen et al. 2003). And PPP2R2B, implicated in SCA12, has been shown to interact with PKC (Price and Mumby 1999). These data suggest an important role for aberrant calcium homeostasis in the pathogenesis of ataxia.

1.1.2.4 Dysregulation of phosphorylation

Findings of mutations in several proteins with phosphatase or kinase activity imply a role for dysregulation of phosphorylation in SCA etiology. An expanded polyglutamine repeat in the 5'UTR of *PPP2R2B* has been identified in SCA12. *PPP2R2B* encodes a brain specific subunit (B) of a protein serine/threonine phosphatase that regulates phosphorylation in a large number of cellular processes, including modulation of cell cycle progression, tau phosphorylation and apoptosis (Holmes et al. 1999). Mutations in *tau tubulin kinase 2* (*TTBK2*, SCA11) and *protein kinase Cγ* (*PRKCG*, SCA14) have been shown to underlie SCA pathogenesis. TTBK2 is a casein kinase with tau and tubulin among possible substrates, raising the possibility of a disease pathway similar to another tau kinase, TTBK1, that has been implicated in Alzheimer's disease and tangle formation (Houlden et al. 2007). PKCγ is a serine/threonine kinase that mediates second messenger signalling pathways involved in multiple cellular processes, including the IP3 (inositol 1,4,5-triphosphate) calcium-sensitive signalling pathway (Chen et al. 2003).

1.1.2.5 Transcriptional dysregulation

SCA17 is caused by a mutation in the gene encoding *TATA box-binding protein* (*TBP*), an important general transcription initiation factor (Nakamura et al. 2001). Data supporting a role for transcriptional dysregulation in SCA etiology have also come from study of the other polyglutamine repeat expansion ataxias. Neuronal inclusions have been shown to contain transcription factors and co-activators, in addition to the other cellular components like chaperones, ubiquitin protein tags and proteasomes (Everett and Wood 2004). Polyglutamine protein sequestering of transcription factors, as well as impaired transcription factor functioning due to interaction with polyQ-proteins,

could possibly cause transcriptional shutdown and subsequent neuronal degeneration (Soong and Paulson 2007).

1.2 HUMAN MOLECULAR GENETICS

1.2.1 Linkage mapping and disease gene identification

In the early 1900s, Bateson and Punnett were studying inheritance in the sweet pea. Based on the observation that some genes did not segregate independently at meiosis they proposed a more dynamic use of the Mendelian inheritance laws, thereby describing gene linkage for the first time and paving the way for eventual mapping of phenotypic characteristics to a specific chromosomal location. Linkage mapping within families with a proven heritable phenotype is a widely used approach to identify disease genes. Defining the phenotype is essential as this allows assignation of disease status, unaffected or affected, to each member of the family. A detailed pedigree chart is drawn that includes phenotypic information such as disease status and age at onset, to allow deduction of inheritance mode of the trait (dominant or recessive, autosomal or sex-chromosomal) as well as an estimation of disease penetrance and detection of a possible mechanism of anticipation.

Originally markers used for linkage were detectable phenotypes derived from coding DNA sequences, like the flower color of the sweet pea in inheritance studies by Bateson and Punnett. Currently single nucleotide polymorphisms (SNPs), microsatellites and to a lesser extend restriction fragment length polymorphisms (RFLPs) are used (Human Genome Project; http://www.ornl.gov/sci/techresources/Human_Genome/home.shtml). These genetic variations are more abundant in non-coding regions although they occur in coding genomic sequences as well. SNPs occur every 100 to 500 bases, making up about 90% of all human genetic variation (Sachidanandam et al. 2001). Microsatellites are simple sequence repeats (SSRs) of 1-6 basepairs, repeated 10 to 100 times. Trimers and pentamers are found 500-1000bp/Mb, whereas di-, tetra- and hexanucleotide repeats occur 2000-3000bp/Mb. Tri- and hexanucleotide repeats appear more abundant in exons, the other repeat sequences are more abundant in non-coding regions (Subramanian et al. 2003). RFLPs are genetic variations that result in formation or alteration of a restriction site which can be detected by enzymatic digestion followed by DNA electrophoresis. Most RFLP markers are co-dominant (both alleles in the heterozygous sample will be detected) and highly locus specific (Young and Tanksley 1989). Genotype data from genome wide linkage markers and pedigree data are combined to generate estimates of the recombination frequency (θ); the frequency of chromosomal crossover between two loci during meiosis, a 1%

recombination frequency being equal to 1cM (centimorgan). Next, LOD (logarithm of odds) scores are calculated for each recombination frequency estimate using the following function;

$$\text{LOD} = Z = \log 10 \frac{(1-\theta)^{NR} \times \theta^{R}}{0.5^{(NR+R)}}$$

NR, number of non-recombinant offspring; R number of recombinant offspring; nominator gives probability of birth sequence with a given linkage value; denominator give probability of birth sequence with no linkage, 0.5 signifies a 50% chance of recombination in completely segregated genes.

LOD scores greater than 3.0 are considered evidence for linkage, indicating the likelihood of observing the given pedigree in absence of linkage is less than 1 in 1000. A LOD score of less than -2.0 is considered evidence to exclude linkage. With completion of the Human Genome Project, data on the physical position of markers used to define linkage are publicly available (NCBI map viewer, http://www.ncbi.nih.gov/mapview; UCSC genome browser, http://genome.ucsc.edu; Ensembl, http://www.ensembl.org). The number of candidate genes and unknown transcripts found within the critical region, depends on the physical size of the mapped linkage region, which is determined by marker density and sample size, and on the transcript density of the chromosomal region, for example telomeric and centromeric regions tend to be gene poor (Lander et al. 2001). Subsequently, candidate genes are prioritized based on literature and database searches, those homologous to a gene linked to the phenotype or with functional data from available cell or animal models, or with data on associated pathways and gene expression related to the phenotype are considered priority candidates. DNA sequencing is used to identify the actual mutation in the disease causing gene. Identification of additional families with the same mutant gene, as well as functional studies are essential to confirm pathogenicity of the candidate gene. The positional gene discovery approach has been proven an effective method for identifying disease genes in an unbiased manner, without prior knowledge, as has been shown in Huntington's disease (The Huntington's Disease Collaborative Research Group 1993), cystic fibrosis (Riordan et al. 1989), breast cancer (Miki et al. 1994;Wooster et al. 1995), and many other disorders.

1.2.2 High density genome wide SNP genotyping

Recent technical advances enabling high density genome wide SNP genotyping have not only increased the power of linkage studies (high throughput, high SNP density, genome wide), but also provided a platform for genome wide association studies, even applicable to complex diseases (Craddock et al. 2008). Moreover, Log R ratio, a surrogate for copy number, and B allele frequency metrics can be derived from genome wide SNP genotype data using specialized software, making it possible to study structural genomic changes such as deletion, duplication and inversion as well as study of haplotypes, copy number variations (CNVs), and homozygosity and autozygosity traits in large populations (Simon-Sanchez et al. 2007;Camargos et al. 2008;Jakobsson et al. 2008).

1.3 MOUSE MOLECULAR GENETICS

1.3.1 Why mice?

Humans and mice are separated by approximately 90Myr (million years) of evolution (Bininda-Emonds et al. (2007); figure 1.3); therefore many physiological, anatomical and metabolic parallels are found as well as a high similarity at the level of the genome. For virtually every gene locus in the human genome a syntenic region can readily be identified in the mouse. Approximately 90% of the mouse and human genomes can be partitioned into regions of conserved synteny, constituting about 350 segments, their sizes ranging from 300kb to 65Mb (Guenet 2005). Mutation analysis remains one of the most informative experimental approaches to study gene function. Because of the human-mouse synteny, the application of reverse genetics, induction of genetic mutations in mice to gain insight in gene function by studying phenotypic effects, has been proven very successful in providing insight in human disease processes and identifying their genetic cause (Baker et al. 2005;Fillon and Kahle 2005). Exploitation of this principle is evident in the numerous ENU (*N*-ethyl *N*-nitrosourea, an alkylating agent that induces point mutations) (Acevedo-Arozena et al. 2008) and targeted mutagenesis programs around the world. To date, the international mouse resource consortium, IMRC, comprises approximately 8,700 mouse strains as well as more than 15,000 ES cell lines (JT Eppig (IMR/TJL), personal communication).

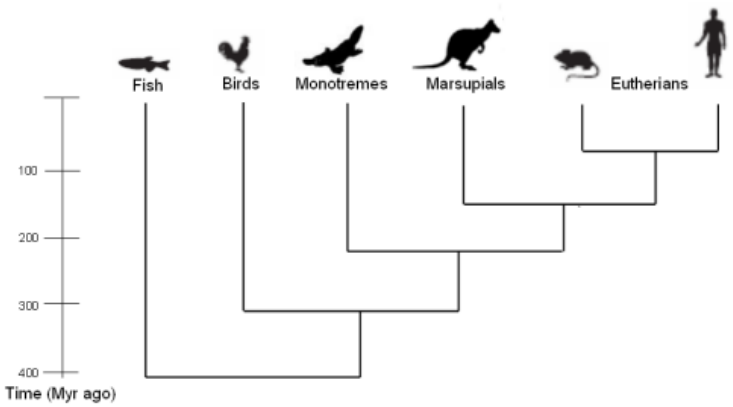

Figure 1.3. Phylogenetic tree of vertebrate species

Mammals are divided into three groups; Monotremata, Marsupialia and Eutheria. Eutherian animals diverged approximately 150 million years (Myr) ago from the marsupial mammals, which in turn diverged from the egg-laying monotremes approximately 165 Myr ago. Rodentia and primates, both part of the Eutheria, separated about 90 Myr ago (Bininda-Emonds et al. 2007). Reproduced from Welcome Trust Sanger Institute (http://www.sanger.ac.uk/PostGenomics/epicomp).

In addition, spontaneous mutations continue to provide valuable models of human disease and fundamental research systems for understanding mammalian biology. Numerous examples have been described in the literature of spontaneous mouse models that have lead to the identification of novel gene mutations underlying human disorders; tottering *Cacna1a*^{tg} episodic ataxia type 2 (Fletcher et al. 1996), *spdh* mouse *Hoxd13*^{spdh} syndactyly type II (Johnson et al. 1998), *nclf* mouse *Cln6*^{nclf} variant late infantile neuronal ceroid lipofuscinosis (vLINCL) (Gao et al. 2002;Wheeler et al. 2002), or provided potential models for human inherited disorders with unknown genetic cause; Purkinje cell degeneration (*pcd*) mouse *Nna1* (Wang and Morgan 2007), hot-foot *Grid2*^{ho} ataxic model (Lalouette et al. 1998;Lalonde and Strazielle 2007).

1.3.2 Mouse genetics

1.3.2.1 Forward genetics, a phenotype driven approach

Positional gene discovery in mice is in essence identical to the positional cloning approach used in humans, however more power in linkage analysis can be achieved through breeding strategies, by generating an increased family size and back crosses to narrow down the region of linkage. This phenotype driven approach in mice is also known as forward genetics (figure 1.4). Similar to human studies, definition of phenotype and generation of a detailed pedigree chart are fundamental in mouse genetics.

Identification of a spontaneous mutation in mice is dependent on careful observation of breeding colonies to detect any deviating phenotypes. Naturally occurring mutation rates are estimated at 10^{-5} to 10^{-7} events per gene per generation (Balling 2001). Several techniques have been developed to increase the mutation rates in mice up to 10-fold or more by inducing random mutations, these include treatment with chemicals like ENU (point mutations), exposure to gamma radiation (deletions) and genetic engineering of DNA insertions (insertional knockouts). In both spontaneous and randomly induced mutations, genetic transmission and propagation of the trait needs to be confirmed before linkage mapping strategies can be applied. To determine mode of inheritance, a phenotypic abnormal mouse is crossed to a wild type mouse. Affected F_1 progeny suggest dominant or X-linked inheritance, a recessive character will reappear in approximately one fourth of the F_2 progeny, whereas a semi-dominant gene will produce an intermediate phenotype in the F_1 progeny and both intermediate and original phenotypes in the F_2 generation. Once the pattern of inheritance has been established, positional candidate gene cloning can be applied to map the genetic cause. Genome wide linkage localizes the disease gene to a chromosomal location, which subsequently can be fine mapped using additional polymorphic markers or by crossing the affected line to a different inbred strain. The F_1 generation of this cross allows fine mapping of a dominant trait. Intercross of the F_1 mice results in an F_2 generation that allows fine mapping of a recessive trait. In both cases, mapping is carried out by linking the phenotype to a haplotype based on strain variation. Next, genome databases are searched for known and predicted genes in the critical region and candidate genes are prioritized based on available literature. Sequence analysis and functional studies enable identification and confirm pathogenicity of the candidate gene. A paper by Xie et al. (2007) describes application of a forward genetic screen leading to identification of the gene underlying the *Wobbly* mutant. The *Wobbly*

phenotype is characterized by ataxia and shows cerebellar atrophy with focal reduction of the molecular layer. The founder *Wobbly* mouse was detected in an ENU mutagenesis dominant behavioral screen. Positional cloning revealed a missense mutation in *CACNA1A*, which encodes a P/Q-type calcium channel implicated in several human neurological disorders (Ophoff et al. 1996;Zhuchenko et al. 1997).

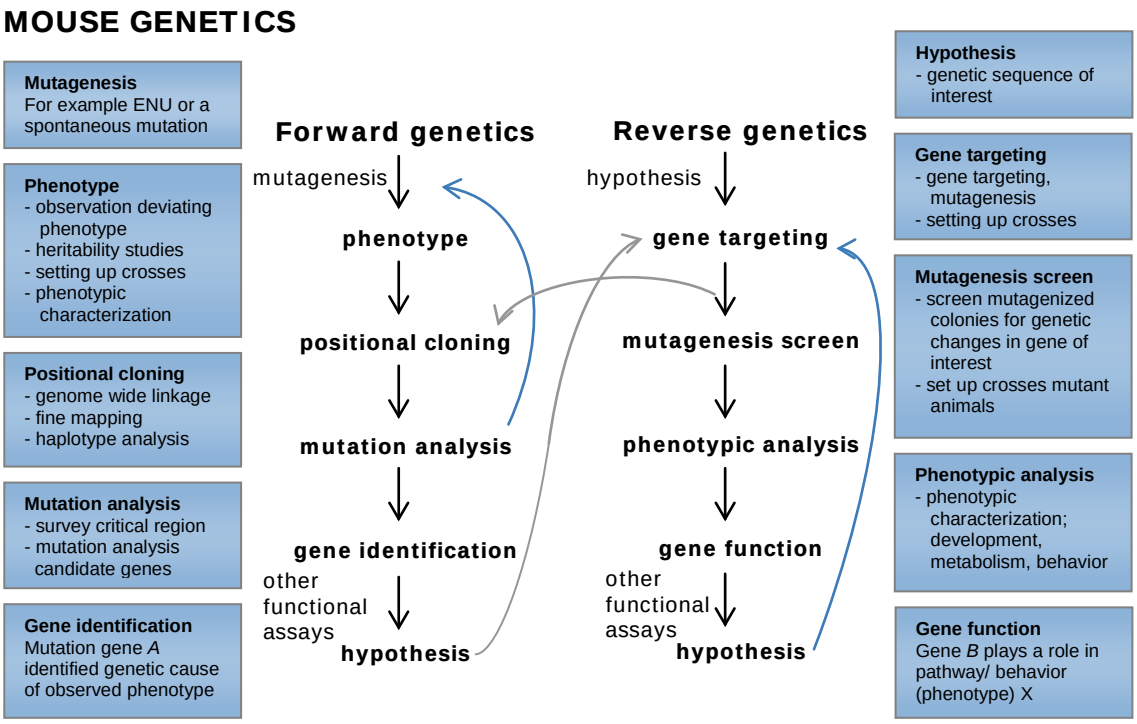

Figure 1.4. Mouse genetics; forward genetics, reverse genetics

Forward genetics, or positional gene discovery, is a phenotype driven approach using genetics to identify the underlying genetic cause (genetic characterization) of the observed phenotype. Reverse genetics, on the other hand, is a genotype driven approach based on a hypothesis that is tested by observing the effects (phenotypic characterization) of targeted gene modification. ENU, *N*-ethyl *N*-nitrosourea.

1.3.2.2 Reverse genetics, a genotype driven approach

In reverse genetics, the functional study of a gene starts with a specific genetic sequence rather than a deviating phenotype (figure 1.4). Using various methodologies the genetic sequence of interest can be changed and its effect on the development or behavior of the mouse analyzed. Gene silencing for example, can be accomplished using RNA interference (RNAi). RNAi allows for a relatively rapid screening of loss of function phenotypes by creating a knockdown of gene function without altering the DNA. Gene targeting on the other hand, generates null alleles (knockouts), thereby permanently removing all gene function. Gene targeting can also be used to identify amino residues essential for protein function by inducing codon changes or to study the role of gene promoter regions by creating alterations in regulatory domains. Generation of transgenic mice by overexpressing wild type or mutant genes provides another way to interfere at the genetic level in order to study gene function. In addition, mutagenized populations similar to those in forward genetic screens can be used to study the effect of random deletions (gamma radiation), insertions (insertional knockouts) and point mutations (application of chemicals like ENU). The mutagenized mouse colonies are screened for changes in the genetic sequence under study using standard molecular techniques like polymerase chain reaction (PCR) and sequence analysis. Mutant animals thus identified are subsequently tested for phenotypic abnormalities in development, metabolism, behavior (for example open field, modified SHIRPA (SmithKline Beecham, Harwell, Imperial College School of Medicine, Royal London Hospital, Phenotype, Assessment) protocol), or motor coordination (for example suspended wire, rotarod) (based on the EMPReSS database developed by the EUMORPHIA consortium; http://empress.har.mrc.ac.uk; http://www.eumorphia.org).

Reverse genetics combined with the complete human and mouse genome sequences provides the means to study every gene known (Copeland et al. 1993;Lander et al. 2001;Venter et al. 2001). In addition to gene function, entire gene families and associated pathways can be studied using the mouse as a model organism for human disease or studying fundamental biological hypothesis. An elegant example of the application of reverse genetics has been described in a paper by Bergami and colleagues (2008) where an inducible mouse line (Cre-lox) was used to study the role of TrkB (neurotrophic tyrosine kinase receptor, type 2) signaling specifically in adult neurogenesis. Finding that specific lack of TrkB signaling in recently generated neurons leads to a remarkable increase in anxiety-like behavior in mice carrying the

mutation, these data add weight to a role for adult neurogenesis in regulating mood related behavior.

1.3.2.3 Reverse-forward genetics, a combined approach

To study gene function in disease pathogenesis, cellular pathways or for development of potential therapies, mutation analysis remains one of the most informative experimental approaches. Both forward and reverse genetic approaches eventually lead to new hypothesis, and each approach can be extended by generating more mutants either through mutagenesis to create new phenotypes or through gene targeting (figure 1.4). Reverse genetics provides an important complement to forward genetics as currently for most genes no mutant models are available. Which is the main reason, the Knockout Mouse Project (KOMP), a trans-National Institutes of Health (NIH) initiative, aims to generate a comprehensive and public resource comprised of mice containing a null mutation in every gene in the mouse genome (http://www.knockoutmouse.org) (Austin et al. 2004).

The pronuclear microinjection technique has been widely used in reverse genetic approaches to express exogenous genes in mice to develop transgenic models for human disease. However, in some mice the exogenously added DNA integrated into a host chromosome and becomes a stably heritable genetic trait (Rijkers et al. 1994). Integration of the transgene into the host genome leads to a disruption in the structure of the chromosomal DNA at the integration site and causes a special class of mutations referred to as insertional mutations (Woychik and Alagramam 1998). It has been proposed that about 5-10% of transgenic mice harbor transgene induced chromosomal alterations, such as transgene insertions, deletions or translocations (Meisler 1992;Rijkers et al. 1994;Woychik and Alagramam 1998). Integration of the transgene most often occurs at only one or a limited number of sites in the genome of the transgenic founder animal, with each site potentially harboring anywhere from one to hundreds of copies of the microinjected fragment typically in a head-to-tail configurations. Although multilocus disruption has also been described; this is caused by alterations in the gross structure of the chromosome near the transgene integration site, resulting in multiple gene inactivation events or multiple integrations of the transgene, often noticeable by segregation of the affected chromosomes in successive generations (Rijkers et al. 1994;Woychik and Alagramam 1998). In targeted mutagenesis random integration of the transgene-construct similar to insertional mutations in microinjection experiments have been found, in some cases leading to

non-specific mutagenic effects in the genome resulting in unexpected phenotypes, for example the *TgN737Rpw* transgenic mouse line as a model for autosomal recessive polycystic kidney disease (ARPKD) in humans (Woychik and Alagramam 1998). Any tags to the transgene might aid in identification of the mutation at the molecular level. However, often positional gene discovery/ forward genetic approaches are required to characterize the insertional mutation. The mechanism underlying these chromosomal structural changes caused by non-specific mutagenic effects, remain unknown.

Table 1.4. Mouse models of cerebellar dysfunction and degeneration

Table comprises spontaneous and induced mouse mutations modeling human spinocerebellar ataxias as well as a selection of mouse models with unknown human cognate variant that are characterized by ataxia, impaired motor dysfunction and neuronal atrophy. *Locus information (chromosome, strand, genome coordinates) was obtained from the MGI database (Mouse Genome Informatics, The Jackson Laboratory; http://www.informatics.jax.org/) and data were based on NCBI build 37; Mb, mega base pairs; n/a, not available; SCA, spinocerebellar ataxia; MJD, Machado-Joseph disease; EA2, episodic ataxia type 2; FHM, familial hemiplegic migraine; DRPLA, dentatorubral-pallidoluysian atrophy; ENU, *N*-ethyl *N*-nitrosourea; NII, neuronal intranuclear inclusion; CI, cytoplasmic inclusion; GII, glial intranuclear inclusion; DNS, diffuse nuclear staining. **(table 1.4, *on next page*)**

mouse	gene	gene name	locus*	mutation		phenotype		human disorder	references
SCA1	*Atxn1*	ataxin-1	13 (-) 45.7-46.1Mb	$(CAG)_{82}$, $(CAG)_{145}$	transgene, Purkinje cell specific	ataxia, wasting, cognitive deficits	Purkinje cell loss; NII (Purkinje cell/ widespread)	SCA1	Burright et al. (1995), Yamada et al. (2008)
SCA2	*Atxn2*	ataxin-2	5 (+) 122.2-122.3Mb	$(CAG)_{58}$, $(CAG)_{75}$	transgene, Purkinje cell specific	impaired motor function	Purkinje cell loss; CI	SCA2	Yamada et al. (2008)
SCA3, MJD	*Atxn3*	ataxin-3	12 (-) 103.2-103.2Mb	$(CAG)_{64\text{-}84}$, $(CAG)_{71}$, $(CAG)_{70,148}$	transgene (Purkinje cell specific/ endogenous promoter/ prion promoter)	ataxia, impaired motor function/ hypotonia, sensory loss, premature death/ tremor, reduced motor and exploratory activity	loss of pontine nuclei, dentate nucleus, Purkinje cells; NII (affected regions/ widespread)	SCA3, MJD	Yamada et al. (2008)
tottering, leaner, Wobbly, Ca(v)2.1 knockout	*Cacna1a*	voltage-dependent P/Q type calcium channel, alpha 1A subunit	8 (+) 86.9-87.2Mb	missense, knockout	spontaneous, ENU, targeted knockout	epilepsy, ataxia/ premature death	cerebellar atrophy	SCA6 (EA2, FHM)	Doyle et al. (1997), Xie et al. (2007)
SCA7	*Atxn7*	ataxin-7	14 (+) 14.9-14.9Mb	$(CAG)_{92}$, $(CAG)_{266}$	transgene (prion promoter)	retinal degeneration, ataxia, premature death	retinal loss; NII (widespread)/ GII	SCA7	Yamada et al. (2008)
DRPLA	*Atn1*	atrophin-1	6 (-) 124.7-124.7Mb	$(CAG)_{65}$, $(CAG)_{129}$	transgene (prion promoter)	ataxia, tremor, seizures, premature death/ myoclonus	DNS (widespread), NII (some regions/ widespread)/ CI, GII	DRPLA	Yamada et al. (2008)
SCA8	*Klhl1 (Atxn8)*	ataxin-8, kelch-like 1 (Drosophila)	14 (-) 96.5-96.9Mb	$(CTG)_{116}$	transgene (endogenous promoter)	impaired motor function, generalized wasting, premature death	NII	SCA8	Yamada et al. (2008)

(table 1.4, *continued on next page*)

(table 1.4, *continued from previous page*)

mouse	gene	gene name	locus*	mutation		phenotype		human disorder	references
tm1Tno, opisthotonos, m1Asb	*Itpr1*	inositol 1,4,5-triphosphate receptor, type 1	6 (+) 108.2-108.5Mb	knockout, deletion	targeted knock out, spontaneous	ataxia, impaired motor function, premature death		SCA15, SCA16	Matsumoto et al. (1996), Ogura et al. (2001), Street et al. (1997), van de Leemput et al. (2007)
Lurcher, hot-foot	*Grid2*	glutamate receptor, ionotropic, delta 2	6 (+) 63.2-64.6Mb	gain of malfunction, deletion	spontaneous	ataxia, impaired motor function, premature death	Purkinje cell loss, granule cell loss (deep nuclei)/ granule-Purkinje synaptic loss	*unknown*	Lalonde and Strazielle (2007)
staggerer	*Rora*	RAR-related orphan receptor alpha	9 (+) 68.5-69.2Mb	deletion	spontaneous	ataxia, impaired motor function	Purkinje cell loss, granule cell loss	*unknown*	Lalonde and Strazielle (2007)
Purkinje cell degeneration	*Agtpbp1*	ATP/GTP binding protein 1	13 (-) 59.6-59.7Mb	deletion	spontaneous	impaired motor function	Purkinje cell loss, granule cell loss	*unknown*	Lalonde and Strazielle (2007)
nervous	*nr*	*unknown*	8 *n/a*	*unknown*	spontaneous	ataxia, agitation, impaired motor function	Purkinje cell loss (granule cell loss)	*unknown*	Lalonde and Strazielle (2007)
reeler	*Reln*	reelin	5 (-) 21.4-21.9Mb	deletion, frameshift	spontaneous	ataxia, impaired motor function	Purkinje cell loss, granule cell loss	*unknown*	Lalonde and Strazielle (2007)
weaver	*Girk2 (Kcnj6)*	potassium inwardly-rectifying channel, J6	16 (-) 95.0-95.2Mb	gain of malfunction	spontaneous	ataxia, impaired motor function	granule cell loss, Purkinje cell loss	*unknown*	Lalonde and Strazielle (2007)

1.3.3 Mouse models of ataxic movement disorders

Identification of the genetic cause in several spinocerebellar ataxias has led to the generation of mouse models by targeted mutagenesis. In addition, spontaneous mutation models exist that present with ataxia, deficits in motor coordination and cerebellar atrophy. Mouse models of ataxic disorders include models for the human polyglutamine spinocerebellar ataxias, spinocerebellar ataxias caused by conventional mutations, and models for which a congenic human variant of the disorder is yet unknown (table 1.4; for review, see Lalonde and Strazielle (2007) and Yamada et al. (2008).

1.3.3.1 Nucleotide repeat expansion models

Transgenic mouse models have been created for SCA1, 2, 3, 7 and 8, and DRPLA, as no naturally occurring repeat expansions have been described in mice. In both humans and mice, the polyglutamine disorders are characterized by ataxia and impaired motor coordination, associated with neuronal degeneration. Brains of affected ataxic animals present with misfolded protein aggregates that were shown to contain full length or truncated mutant protein and ubiquitin (Yamada et al. 2008). Aggregates are usually present in the nucleus but have also been shown in the cytoplasm of affected neurons. Similar inclusion bodies have subsequently been demonstrated in human brains affected by different polyglutamine repeat proteins, such as polyQ-ataxin 1 aggregates in SCA1 brains and polyQ-TBP containing inclusions in SCA17 brains (Schols et al. 2004;Yamada et al. 2008). Initially, these inclusions were considered toxic and the cause of neural cell death. However, findings in transgenic mice and humans have shown the pathologic changes are present beyond the distribution of neuronal atrophy, indicating neurons are affected more widely than has been recognized previously and raising the possibility that protein aggregates are not the toxic species but might even play a protective role (Yamada et al. 2008). Interestingly, polyglutamine repeat expansions that cause ataxia in humans are by themselves not sufficient for creating the conditions characteristic of each disease in mice, suggesting protein context plays an important role in toxicity (Yamada et al. 2008).

Studies in mice overexpressing mutant protein have shown the aberrant protein has to enter the nucleus to cause cellular dysfunction; the nuclear localization signal and protein modification by interaction with other proteins have been implicated in this process (Yamada et al. 2008). Although some differences between mouse and human pathology in atrophy distribution and cell types affected remain, data obtained have

provided evidence that clinical onset is not clearly associated with neuronal cell death but depends on intranuclear accumulation of mutant protein in neurons. It has been hypothesized that soluble mutant proteins might bind other proteins, for example those essential in maintaining cell function, rendering them dysfunctional or sequestering them into aggregates, thereby disturbing global protein homeostasis, eventually leading to cell death (Gidalevitz et al. 2006).

1.3.3.2 Conventional mutation models

Spontaneous mutation mouse models with an ataxic phenotype for which no cognate disorder in humans has currently been identified, have aided in gaining insight into the processes underlying cerebellar disorders. Behavioral studies and motor coordination tasks requiring balance and equilibrium (stationary beam, suspended wire, vertical grid, and rotarod tests) establish the extent of motor dysfunction in the different mouse mutants. The underlying genetic mutations have been identified in most ataxic models (table 1.4). Interestingly, findings in these conventional mutation models indicate underlying cellular disease processes are remarkably similar to those in polyglutamine expansion models. Both have demonstrated there is no clear correlation between phenotype (onset and severity of symptoms) and cell atrophy. Striking examples are *Lurcher* mice (*Grid2*^{Lc}) that despite a total absence of Purkinje cells perform better on motor coordination tasks than *hot-foot* (*Grid2*$^{ho\text{-}Nancy}$) or *staggerer* (*Rora*^{sg}), two other spontaneous cerebellar mutants (Lalonde and Strazielle 2007). Neurochemistry and pathology studies in the conventional mutation models have shown higher metabolic activity in cerebellum and related structures (deep cerebellar and vestibular nuclei, primary relays of the cerebellar cortex, and direct afferent or efferent cerebellar pathways), indicating Purkinje cell atrophy and subsequent loss of Purkinje cell inhibitory functions results in cell hyperexcitability that might be the cause of ataxia and diminished motor function (Lalonde and Strazielle 2007).

Other mouse models have provided further evidence of a role for aberrant calcium homeostasis in the etiology of ataxic disorders. Mice carrying a spontaneous mutation or induced knockout of *Itpr1* (*inositol 1,4,5-triphosphate receptor, type 1*), an IP3 gated intracellular calcium channel highly expressed in Purkinje cells, displayed a rapidly progressive, severe ataxic phenotype in the absence of neuronal atrophy (Matsumoto et al. 1996;Street et al. 1997). Targeted *Calb1* (*calbindin D28K*) and *Calb2* (*calretinin*) null mutants of the corresponding cytoplasmic calcium binding proteins with high Purkinje cell expression levels, resulted in impaired motor coordination despite

absence of ataxia (Lalonde and Strazielle 2007). Study of current and additional mouse models of cerebellar movement disorders will aid to elucidate the pathogenic mechanism underlying spinocerebellar ataxias, essential for the identification of novel pharmacological targets and approaches. The ataxic mouse mutants would provide a useful source of potential models to test therapeutic efficacy.

1.4 THESIS AIM AND OUTLINE

This thesis tells the scientific story that began with a probable spontaneous mutation in a mouse resulting in a severe ataxic movement disorder that, through a combination of classical and novel molecular genetic techniques, led to discovery of the genetic cause underlying spinocerebellar ataxia type 15 in humans.

Chapter 2 describes the experimental approaches taken and the molecular and genetic techniques used to obtain the data that form the foundation of this thesis.

Chapter 3 introduces the spontaneous mouse mutant and describes the use of forward genetics; from the phenotypic observations and genome wide linkage making use of the variations in genetic background of the mouse strains, to identification of the genetic cause and subsequent protein data to confirm pathogenicity.

Chapter 4 starts with an overview of spinocerebellar ataxia (SCA) 15 data previously gathered by Knight et al. (2003). Discusses why *ITPR1* was reinvestigated as a cause for SCA15 after having been previously ruled out. Before describing current findings, including how high density genome wide SNP genotyping data enabled identification of the genetic cause for SCA15 where a classical sequencing approach was insufficient. Concluding with protein data providing further evidence of disease gene pathogenicity.

Chapter 5 considers findings and conclusions from the results chapters (3, 4) in a broader context. Implications of the findings are explored and recommendations for future work discussed.

CHAPTER 2 MATERIALS AND METHODS

2.1 MATERIALS

2.1.1 Reagents and prepared solutions

Molecular grade water (Cellgro) was used in most applications, when water from a Millipore water purification system (milliQ) or deionized water was used this has been indicated. Room temperature denotes a temperature between 21-25 degrees Celsius.

Reagents

Agarose (GPG/LE)	American Bioanalytical
Agarose (SeaKem ME)	Cambrex
Antibody, Alexa Fluor 488 goat anti-mouse IgG (H+L)	Invitrogen
Antibody, Alexa Fluor 555 goat anti-rabbit IgG (H+L)	Invitrogen
Antibody, donkey anti-mouse IgG (H+L)	Jackson ImmunoResearch
Antibody, donkey anti-rabbit IgG (H+L)	Jackson ImmunoResearch
Antibody, mouse anti-(β-actin), monoclonal	Sigma
Antibody, mouse anti-calbindin D-28K	Sigma
Antibody, mouse anti-neurofilament 160, monoclonal	Sigma
Antibody, rabbit anti-IP3R1, polyclonal	Chemicon
Antibody-peptide, rabbit anti-IP3R1 antibody	Chemicon
Antigen preserve solution	NeuroScience Associates
BCA (bicinchoninic acid) protein assay	Pierce
Beta-mercapto ethanol (B-ME)	American Bioanalytical
BigDye terminator v3.1; ready reaction mix	Applied Biosystems
BigDye terminator v1.1, v3.1; 5x sequencing buffer	Applied Biosystems
Biomax XAR film	Kodak
Blood and Cell Culture DNA midi kit (Genomic-tip 100/G)	Qiagen
Bromophenol blue sodium salt, 10x	Sigma
CAPS (N-cyclohexyl-3-aminopropanesulfonic acid)	Sigma
Chrom alum *(chromium (III) potassium sulfate dodecahydrate)*	Sigma
Criterion 4-20% tris-HCl gel (precast)	Biorad
DABCO (1,4-diazobicyclo-[2.2.2]-octane)	Sigma

Direct-PCR lysis reagent, 102-T	Viagen
DMSO (dimethyl sulfoxide)	Sigma
ECL plus western blotting detection system	Amersham Biosciences
EDTA (ethylenediaminetetraacetic acid)	Sigma
EDTA (ethylenediaminetetraacetic acid) (0.5M, pH8.0)	KD Medical
Ethanol, ultrapure	American Bioanalytical
Ethidium bromide solution	American Bioanalytical
FastStart PCR mastermix	Roche
Gelatin from porcine skin, type A	Sigma
GeneRuler 100bp DNA ladder plus	Fermentas
GeneRuler DNA ladder mix	Fermentas
Glycerol (density 1.257-1.263g/ml), ultrapure	Invitrogen
Hi-Di formamide	Applied Biosystems
HiMark pre-stained HMW protein standard	Invitrogen
Infinium HumanHap610-Quad SNP genotyping assay	Illumina
Infinium HumanHap550 SNP genotyping assay	Illumina
Isopropanol, ultrapure	American Bioanalytical
LIZ genescan	Applied Biosystems
Magnesium solution	Qiagen
Methanol	American Bioanalytical
MOPS (3-(N-morpholino)propanesulfonic acid), 20x	Invitrogen
Mowiol	Calbiochem
Non-fat dry milk, instant (Carnation)	Nestle
Normal bovine serum albumin (BSA) *probumin universal grade K*	Celliance
Normal goat serum	Gibco
NP-40 (nonyl phenoxylpolyethoxylethanol) (10%)	BioVision
NuPage 4-12% bis-tris gel (precast; pH6.4)	Invitrogen
NuPage LDS sample preparation buffer (pH8.4), 4x *(lithium dodecyl sulfate)*	Invitrogen
NuPage reducing agent	Invitrogen
NuPage transfer buffer, 20x	Invitrogen
OrangeG sodium salt	Sigma
Paraformaldehyde (95%)	Sigma
Phosphate-buffered saline, 1x (PBS buffer)	Gibco
Precision plus protein dual color standard	Biorad

Primers, lyophilized (10nmol scale)	Operon
Probes, fluorescently labeled (HEX, FAM, VIC; 100µM)	Applied Biosystems
Protease inhibitor cocktail (solution)	Sigma
Protease inhibitor cocktail, complete mini (tablets)	Roche
Proteinase K	Qiagen, Viagen
Protein precipitation solution	Promega
PVDF membrane, Immobilon-P, 0.45µm	Millipore
SeeBlue plus 2 prestained standard, 1x	Invitrogen
Sodium chloride, NaCl (5M)	Cellgro
Sodium deoxycholate	Sigma
Sodium-dodecyl-sulfate (SDS)	Quality Biological
Sodium fluoride	Sigma
Sodiumhydroxide, NaOH (1N)	American Bioanalytical
Sodium vanadate	Sigma
Supersignal west pico chemiluminescent substrate	Pierce
TaqMan PCR mastermix (no AmpErase UNG)	Applied Biosystems
Tris (acidic, basic)	Sigma
Tris (1M, pH7.4)	KD Medical
Tris-borate-EDTA, 1x (TBE buffer)	Cellgro
Tris-buffered saline, 1x (TBS buffer, pH7.4)	American Bioanalytical
Tris-buffered saline, 1x (TBS buffer)	Biorad
Tris-EDTA, 1x (TE buffer)	Qiagen
Tris-glycine-SDS, 10x (TGS buffer)	Biorad
Tris-HCl (2M, pH6.8)	Quality Biological
Tris-HCl (1M, pH7.4)	Quality Biological
TritonX-100	Sigma
True Allele PCR premix	Applied Biosystems
Tween-20, for electrophoresis	Sigma

Prepared solutions

Agarose gel, 2%(w/v)	3g	agarose (GPG/LE)
	150ml	1xTBE buffer
	3.0µl	ethidium bromide solution (10mg/ml)
CAPS transfer buffer	10%(v/v) methanol 10%(v/v) CAPS (22.13g/l, pH11.0) in deionized water	
Gelatin-coated slide	*glass slides (Daigger; 3x1inch, 1.2mm thick) were submerged in;* 1g/l pigskin gelatin 0.5g/l chrom alum in distilled water	
Glycerol, 10%(v/v) in PBS	10%(v/v) glycerol in 1xPBS buffer	
IHC, blocking solution	10ml normal goat serum 40ml carrier solution	
IHC, carrier solution	0.3%(v/v) triton 10g/l normal BSA 1%(v/v) normal goat serum in 1xPBS buffer *pH set to 7.32 using NaOH (1M)* *purified using 0.45µM filter (Corning)*	

Mowiol-DABCO	2.4g mowiol 6g glycerol in 6ml MilliQ water *stirred overnight at room temperature to dissolve* 12ml tris (0.2M, pH6.8) *stirred and heated to 50°C for 10 minutes* *centrifuged 15 minutes at 5,000xg,* *keep supernatant* 2.5%(w/v) DABCO *under vacuum overnight prior to use*
Non-fat milk, 5%(w/v)	2.5g non-fat dry milk, instant 50ml TBS-T
OrangeG loading buffer	1%(w/v) orangeG sodium salt 30%(v/v) glycerol in molecular grade water
Paraformaldehyde, 4%(w/v)	20g paraformaldehyde in 1xPBS up to 500ml total volume *10 drops NaOH (10M) to aid paraformaldehyde to pass into solution, stirred and heated to 70°C until dissolved*
RIPA lysis buffer	50mM Tris-HCl (pH7.4) 1%(v/v) NP-40 0.25%(w/v) sodium deoxycholate 150mM NaCl 1mM EDTA (pH 8.0) 1mM sodium vanadate 1mM sodium fluoride in molecular grade water

Sample buffer *(fractionated protein extraction)*	0.25M Tris-HCl (pH6.8) 8%(w/v) SDS 30%(v/v) glycerol 0.02% bromophenol blue 10% B-ME (beta-mercapto ethanol) in molecular grade water
TBS-PI (lysis buffer)	5mM EDTA (pH7.4) 10µl/ml protease inhibitor cocktail in 1xTBS buffer (American Bioanalytical)
TBS-SDS (lysis buffer)	5%(w/v) SDS in 1xTBS buffer (American Bioanalytical)
TBS-T	0.1%(v/v) tween-20 in 1xTBS buffer (Biorad)
TBS-Tx100 (lysis buffer)	1%(v/v) tritonX-100 10µl/ml (or 1 tablet) protease inhibitor cocktail in 1xTBS buffer (American Bionanalytical)
TNES buffer	10mM Tris (pH7.4) 400mM NaCl 100mM EDTA (pH8.0) 0.6%(w/v) SDS in molecular grade water

2.1.2 Software and equipment

Software

AlphaEase FC software (version 3.2.1)	Alpha Innotech
Analyse-it for Microsoft excel, standard edition	Analyse-it software
BeadScan (version 3.5.49.29917)	Illumina
BeadStudio/ expression module (v2.3.25)	Illumina
BeadStudio/ genotyping module (v2.3.25)	Illumina
BLAST (Basic Local Alignment Search Tool)	Altschul et al. (1990)
BLAST/ blastn (nucleotide-nucleotide BLAST)	Altschul et al. (1990)
Excel 2003 (SP3)	Microsoft
Gene Runner (version 3.05)	Hastings software
Genotyper (version 3.7 NT), ABI prism	Applied Biosystems
ImageQuant (version 5.01)	Molecular Dynamics
LINKAGE/ MLINK (multi-locus linkage analysis, version 5.1)	Lathrop et al. (1984)
LSM image browser (version 3.2.0.115)	Zeiss
Nanodrop 1000 spectrophotometer software (v3.3.0)	Thermo Scientific
SDS (sequence detection system) software (version 2.2.2)	Applied Biosystems
Sequencer software (version 4.1.4)	Gene codes corporation
SoftMax Pro software (v4.0)	Molecular Devices

Equipment

3100/ 3730xl genetic analyzer platform, ABI prism	Applied Biosystems
ABI Prism 7900HT Sequence Detection System	Applied Biosystems
384-well clear optical reaction plate (Applied Biosystems)	
Agencourt AMPure magnetic beads	Beckman Coulter
Agencourt CleanSEQ magnetic beads	Beckman Coulter
Alpha imager 2200 imaging device, UV transilluminator	alpha Innotech
Balance, Scout II, SRA210 (1200x0.1g)	Ohaus
Balance, AG204 DeltaRange (d=0.1mg/1mg)	Metler Toledo
BeadStation, scanner Infinium chips	Illumina
Biomek fx liquid handling system	Beckman Coulter
Centrifuge 5414D	Eppendorf
F45-24-11 (max 13,200rpm; max 24x3.75g)	

Centrifuge 5804/5804R	Eppendorf
F45-30-11 (max 11,000rpm; max 30x3.75kg)	
A-2-DWP (max 3,700rpm; max 2x1.01kg)	
Centrifuge 5810	Eppendorf
A-2-MTP (max 4,000rpm; max 2x1.030kg), plates	
Centrifuge, evolutionRC	Sorvall
rotor SS-34 fixed angle (max rcf. 47,800xg; κ-factor 752)	
Centrifuge, optima max ultracentrifuge	Beckman Coulter
rotor MLA-130 (max rcf. at r_{max} 1,019,000xg;	
r_{max} 53.9mm; r_{min} 29.9mm; κ-factor 8.7)	
polycarbonate tubes (11x34mm; Beckman Coulter)	
Electrophoresis, powerstation 200	CLP
Electrophoresis, system (perspex gel trays)	CLP
Hybaid thermocyclers (96-well)	Thermo Scientific
Microplate reader, SpectraMax Plus	Molecular Devices
optical flat bottom 96 deep-well plate (Molecular Devices)	
Microscope, LSM510/LNO META upright two-photon confocal	Zeiss
plan-apochromat 5x/0.16 NA (Zeiss)	
plan-apochromat 63x 1.4 oil DIC (Zeiss)	
MultisScreen-$PCR_{\mu 96}$ filter plates	Millipore
Minishaker, MS1	IKA
Ruler (cm, inches)	OriGene
Sonicator; ultrasonic processor with model CV26 sonicator	Tekmar
Spectrophotometer, NanoDrop, ND-1000	Thermo Scientific
Spectrophotometer, Ultrospec 3100 pro UV/Visible	Amersham Biosciences
Western blot, power supply model 300/ 500	VWR
X-OMAT 2000A processor, automatic developer	Kodak

2.1.3 Databases

MGI (Mouse Genome Informatics, The Jackson Laboratories)

http://www.informatics.jax.org/strains_SNPs.shtml

NCBI, Entrez SNP (National Center for Biotechnology Information, Single Nucleotide Polymorphism)

http://www.ncbi.nlm.nih.gov/SNP/MouseSNP.cgi

2.1.4 Accession numbers

source, species	gene/ protein	accession number
Mus musculus		
RefSeq	*Itpr1*	NM_010585
genomic	*Itpr1*	NC_000072
Homo sapiens		
RefSeq	*CNTN4*	NM_175607
	SUMF1	NM_182760
	ITPR1	NM_001099952.1
protein	ITPR1	NP_001093422
NCBI HomoloGene		
Homo sapiens	*ITPR1*	NP_001093422.1
Canis lupus familiaris	*ITPR1*	XP_862857.1
Bos taurus	*ITPR1*	NP_777266.1
Mus musculus	*Itpr1*	NP_034715.1
Rattus norvegicus	*Itpr1*	NP_001007236.1
Gallus gallus	*ITPR1*	XP_414438.2
Danio rerio	*LOC100149388*	XP_001921194.1
Drosophila melanogaster	*Itp-r83A*	NP_730941.1
Anopheles gambiae	*AgaP_AGAP006475*	XP_316515.2

Table 2.1. Accession numbers

Sources: NCBI RefSeq, reference sequences for the genome, transcripts and proteins, http://www.ncbi.nlm.nih.gov/RefSeq; NCBI HomoloGene, gene homologs, http://www.ncbi.nlm.nih.gov/homologene.

2.2 General Methods

2.2.1. Sample integrity

To determine DNA integrity and quantity, spectral measurements were taken using a NanoDrop, ND-1000, spectrophotometer (dynamic range 2-3700ng/µl dsDNA; Thermo Scientific). Measurements were taken according to manufacturer's protocol (http://www.nanodrop.com/pdf/NanoDrop 1000-users-manual.pdf). Briefly, the spectrophotometer was blanked against sample buffer, either molecular grade water or 1xTE-buffer, then 1-1.5µl undiluted sample was pipetted onto the pedestal. Operating software was used to measure and assess DNA purity based on absorbance ratio at 260nm/280nm, accepted values 1.7-2.0, and to calculate sample concentration in ng/µl based on absorbance at 260nm and the nucleic acid extinction coefficient (50 ng-cm/µl dsDNA), according to Beer-Lambert's law (c=(A*e)/b; c, nucleic acid concentration in ng/µl; A, absorbance in AU (absorbance units); e, wavelength-dependent extinction coefficient in ng-cm/µl; b, path length in cm).

2.2.2 DNA protocols

2.2.2.1 Primer design

Transcript-specific primers (18-22 bases in length) were designed to be complementary to the sequence encoding the genomic fragment of interest. Primers were designed using Gene Runner (version 3.05; Hastings software), based on GenBank sequence information (http://www.ncbi.nlm.nih.gov/Genbank/index.html), using the settings given in table 2.2. Amplicon annealing temperature was set above 70°C to prevent possible secondary structure formation of the primers. In addition, runs of four or more identical nucleotides, especially guanine, were avoided. And the 'secondary structure analysis' function was used to see if unwanted primer-dimer and/ or hairpin formation might occur. Finally, all primers designed were tested for regions of similarity between biological sequences using the nucleotide-nucleotide BLAST (blastn) function of Basic Local Alignment Search Tool (BLAST, http://blast.ncbi.nlm.nih.gov/Blast.cgi) to ensure specificity (Altschul et al. 1990), with exception of the primers used for linkage analysis in mice which were retrieved from a paper by Lindblad-Toh et al. (2000). Oligonucleotide primers were custom synthesized on a 10nmol scale by Operon Biotechnologies. Primers were shipped lyophilized and rehydrated in molecular grade water to a stock concentration of 200pMol, based on the supplied optical density readings. Working dilutions were prepared with a concentration of 10pMol in molecular grade water.

primer parameters	
primer length (bp)	18-22
primer Tm (°C)	50.0-65.0
primer Tm dif. (°C) ≤	3.0
primer %GC	35.0-60.0
3' nucleotides	S
dG temp. (°C)	25.0
probe C (pMol)	250.0
salt con. (mMol)	50.0
3' end dG	(-9.0)-(-3.0)
3' end length (bp)	7

Table 2.2. Gene Runner parameters used for primer design PCR and sequencing applications

Gene Runner (version 3.05; Hastings software) parameters used to design primers for PCR and sequencing applications: primer length (bp), sets the upper and lower limits for primer length in base pairs (5' end additions are not included); primer Tm (°C), sets melting point upper and lower limits for primers in degrees Celsius and is calculated using the nearest-neighbor thermodynamic values method of Breslauer and colleagues, a low Tm may lead to inefficient priming whereas a high Tm may permit false priming; Tm dif. (°C) ≤, sets maximum difference in Tm's (degrees Celsius) of a primer pair; primer %GC, sets upper and lower limits percentage G (guanine) and C (cytosine) content of the primers, higher %GC results in higher primer Tm and increases likelihood of strong secondary structure and false primer (5' end additions are not included in the calculation); 3' nucleotides, sets 3' base(s) requirement to S (G or C) as a 3' G or C are more stable than an A (adenine) or T (thymine); dG temp. (°C), is required for the calculation of free energy (dG) which affects all G calculations (3' end dG, hairpin loop dG and dimer dG) as well as hairpin loop Tm, default is 25 degrees Celsius; probe C (pMol), required for primer Tm calculation, default is 250pMol; salt con. (mMol), required for primer Tm and %GC Tm, default is 50mMol, the recommended salt concentration for most PCR reactions; 3' end dG, nearest-neighbor G for the last 7 bases of the 3' end (3' end length (bp) value), and is calculated by G=H-TS (H, enthalpy; S, entropy; T, dG temp.), lower numbers being more stable; 3' end length (bp), is the number of bases from the 3' end used for the 3' end stability, default is 7 bases, it is required for 3' end dG and also used for 3' end uniqueness searches.

2.2.2.2 Polymerase chain reaction (PCR)

Polymerase chain reaction

Taqman-based PCR was performed on 96-well Hybaid thermocyclers (Thermo Scientific), each reaction contained: 10µl FastStart PCR mastermix (Roche), 1.0µl transcript-specific primers (10pMol forward, 10pMol reverse), and 1.0µl DNA (10-15ng) or molecular grade water for the no-template control. Cycle settings common to many of the PCRs in this thesis are given in table 2.3.

60-to-50												
		8 cycles			16 cycles			16 cycles				
phase	Di	D	A	E	D	A	E	D	A	E	Ef	
temp.	94°C	94°C	60°C	72°C	94°C	60°C	72°C	94°C	50°C	72°C	72°C	4°C
duration	4’	20”	20”	30”	20”	20”	1’	20”	20”	30”	5’	hold

Table 2.3. Cycle settings, PCR program 60-to-50

Phases; Di, initial denaturation; D, denaturation; A, annealing; E, extension; Ef, final extension. Temp, temperature in degrees Celsius. Duration in ’ minutes; ’’ seconds.

If the 60-to-50 program failed to meet the quality and quantity of product required for downstream processing, optimisation was achieved by using different cycle settings, for example adjusting the annealing temperature, or by adding supplements such as magnesium or DMSO. Details on cycle settings, additives and primers used are given in appendix I. PCR efficiency, primer specificity and DNA fragment sizes were determined by agarose gel electrophoresis (see paragraph 2.2.2.3). Accepted primer pairs gave no product in the no template control (NC), for sequence analysis single-band products were selected to exclude primer-dimer artefacts and multiple products.

Purification PCR products

Samples were centrifuged at 201*xg* or 233*xg* for 30-60 seconds to collect any condensation that might have formed during PCR (5810/ 5804(R) respectively; Eppendorf). PCR clean-up was accomplished using either MultiScreen-PCR$_{\mu 96}$ filter plates (Millipore) or Agencourt AMPure magnetic beads (Beckman Coulter). When Millipore filter plates were used, molecular grade water was added up to a total of 100µl and diluted PCRs transferred to the Millipore plate. The filter plate was set under vacuum until all fluid was removed, 20-25inHg. Next, 20µl molecular grade water was added to each well and the plate put on a shaker for up to 10 minutes (IKA; 63x*g*, room temperature) before transferring the purified PCR products to a clean 96-well reaction plate. Plates containing the cleaned product were further processed or stored at -20°C until further use.

A Biomek fx liquid handling system (Beckman Coulter) fully automated the Agencourt AMPure protocol. To each 12µl PCR, 27µl Agencourt AMPure was added and mixed by pipetting up and down 10 times. Samples were incubated at RT for 5 minutes to allow the PCR products (≥100bp) to bind to magnetic beads. Each plate containing the PCR/ bead-mixes was placed on a magnetic plate holder (Agencourt SPRIplate 96-ring) for 5.5 minutes to separate beads from solution. The reaction plate was left on the magnetic block throughout the rest of the procedure. The cleared solution, without beads, was aspirated from the reaction plate and discarded. To each well, 100µl 70% ethanol was added and samples were incubated at RT for 30 seconds. The ethanol was aspirated and discarded. Again, 100µl 70% ethanol was added, samples incubated for 30 seconds at RT, and the ethanol aspirated and discarded. The reaction plate was left to dry at RT for 5 minutes. To elute, 40µl molecular grade water was added to each well, mixed by pipetting and left to incubate at RT for 2 minutes. Samples were transferred to a clean 96-well reaction plate and further processed or stored at -20°C until further use.

2.2.2.3 Agarose gel electrophoresis

Two percent (w/v) agarose gels were used to determine PCR efficiency and fragment sizes, this percentage (w/v) is commonly used for fragments ranging from 100-600bp in length. Agarose (GPG/LE; American Bioanalytical) was added to 1xTBE buffer (tris, boric acid, EDTA; Cellgro), to a final concentration of 2% (w/v). The agarose-TBE mixture was melted using a commercial microwave oven (60Hz, 120amp; Panasonic, NE-1012TI) and ethidium bromide solution added to a final concentration of 0.2µg/ml (10mg/ml; American Bioanalytical). Gels were cast in perspex gel trays with appropriate combs inserted for loading of samples and marker. Gels were left at room temperature for approximately 30 minutes to solidify. PCR products were mixed with orangeG loading buffer (1%(w/v) orangeG sodium salt (Sigma), 30%(v/v) glycerol (Invitrogen), molecular grade water) to facilitate gel loading. Samples as well as 5µl size reference (GeneRuler 100bp DNA ladder plus/ DNA ladder mix; 0.1µg/µl, ready to use; Fermentas) were loaded on each sample row. Electrophoresis was carried out at 110V for approximately 30 minutes under altering amperes (powerstation 200, CLP). Following electrophoresis, gels were visualised using a UV transilluminator and images obtained with an alpha imager 2200 imaging device (alpha Innotech) using alphaEase FC software (alpha Innotech, version 3.2.1).

2.2.2.4 Sequence analysis, according to Sanger

Sequence reactions

Sequence amplification was accomplished using a Hybaid thermocycler (Thermo Scientific). Sequence reactions contained: 0.5µl BigDye terminator v3.1 (Applied Biosystems), 2.0µl 5x sequence buffer (BigDye terminator v1.1, v3.1; Applied Biosystems), 1.0µl primer (10pMol either forward or reverse, see appendix I for details), 6.5µl purified PCR product. Cycle conditions are given in table 2.4.

sequence reaction				
	25 cycles			
phase	D	A	E	
temperature	96°C	50°C	60°C	4
duration	30”	15”	3’	hold

Table 2.4. Cycle settings, sequence amplification program
Phases; D, denaturation; A, annealing; E, extension. Temperature in degrees Celsius. Duration in ’ minutes; ’’ seconds.

Purification sequence reaction products

Big dye removal was carried out using either MultiScreen-PCR$_{\mu 96}$ filter plates (Millipore) or Agencourt CleanSEQ magnetic beads (Beckman Coulter). Samples were centrifuged at 201*xg* or 233*xg* for 30-60 seconds to collect any condensation that might have formed during sequence amplification (5810/ 5804(R) respectively; Eppendorf). If Millipore filter plates were used 40µl molecular grade water was added and diluted amplification products were transferred to the Millipore plate. Filter plate was put under vacuum at 20-25inHg until all fluid was removed. Again, 40µl molecular grade water was added to samples in filter plate and washed through using vacuum, 20-25inHg until all fluid was removed. Next, samples were resuspended by adding 20µl molecular grade water to each well and the plate was put on a shaker for up to 10 minutes (IKA; 63x*g*, room temperature). Purified sequence amplification products were transferred to a clean 96-well reaction plate and processed for analysis.

A Biomek fx liquid handling system (Beckman Coulter) fully automated the Agencourt CleanSEQ protocol. To each 10µl amplification product, 10µl Agencourt CleanSEQ and 42µl 85% ethanol were added and mixed by pipetting up and down 7 times. Each plate containing the sample/ bead-mixes was placed on a magnetic plate holder (Agencourt SPRIplate 96-ring) for 3 minutes to separate beads from solution. The reaction plate was left on the magnetic block throughout the rest of the procedure. The

cleared solution, without beads, was aspirated from the reaction plate and discarded, thereby removing any excess fluorescent dye and contaminants. To each well, 100µl 85% ethanol was added and samples were incubated at RT for 30 seconds to allow the beads to resettle before continuing to the next step. The ethanol was aspirated and discarded. Again, 100µl 85% ethanol was added, samples incubated for 30 seconds at RT, and the ethanol aspirated and discarded. Reaction plate was left to dry at RT for 5 minutes. To elute, 40µl of molecular grade water was added to each well and the plate incubated at room temperature for 2 minutes. Samples were transferred to a clean 96-well reaction plate and processed for analysis.

Sequence analysis

Plates with purified sequence amplification products were analysed on an ABI prism 3100/ 3730xl genetic analyser platform (Applied Biosystems). Sequencer software (Gene Codes corporation, version 4.1.4) was used to visualize the electropherograms, both for SNP genotyping analysis (linkage application) and mutation detection.

2.3 MOUSE-RELATED METHODS

Animal experiments described in this thesis were carried out under the guidance issued by the Office of Laboratory Animal Welfare and have been registered under animal protocol number 06-038 (OLAW/ Office of Extramural Research/ National Institutes of Health, Bethesda (MD), USA), documentation can be found at http://grants.nih.gov/grants/olaw/olaw.htm.

2.3.1 Generation of transgenic mice

Generation of *DJ1 (Park7)* knockout mice and detection of the *DJ1* transgene were carried out by Jayanth Chandran, at the time a PhD student in Huaibin Cai's group at the Laboratory of Neurogenetics (NIA/NIH). *DJ1*$^{-/-}$ mice were generated as a model for early-onset familial Parkinson's disease. This work has been described in Chandran et al. (2008). The description of the generation of these transgenic mice has been included in this thesis for completion.

Generation of DJ1 knockout mice

DNA fragments spanning exons 1-7 of *DJ1* were isolated from a mouse genomic phage library (Stratagene). Targeting vectors were constructed through replacement of the second exon of *DJ1* with a neomycin resistance gene. The neomycin resistance gene was flanked by a 1.7kb EcoRI-BamH1 left arm fragment and a 5.0kb right arm consisting of a 2.2kb Nhe1-EcoRI fragment joined to a 1.7kb EcoRI-SacI fragment. Linearised targeting vector was transfected by electroporation into mouse ES cells derived from the 129x1/SvJ strain (129x1/PJ5). G418-resistant colonies were selected and screened by Southern blot for homologous recombination with 5' and 3' external probes. Positive cells were injected into C57BL/6J blastocysts to generate chimeras which were then mated with C57BL/6J wild type mice to confirm germline transmission.

2.3.2 Breeding and phenotyping protocols

2.3.2.1 Maintenance mice

Maintenance of the mouse line was carried out by J Chandran (LNG/NIA/NIH) and C Xie (LNG/NIA/NIH). The *Itpr1*$^{\Delta 18}$ mutation has been maintained on a mixed 129x1B6 (129x1/SvJ, C57BL/6J) background by intercrossing heterozygous mice, with the exception of backcross to a fourth generation C57BL/6J background (figure 2.1) carried out after linkage had mapped disease status to the 129x1/SvJ haplotype. Mice were housed in a controlled environment at the on-site animal facility (NIH, Bethesda (MD), USA), in Techniplast cages on a ventilated rack system (individually ventilated, Sealsafe; Techniplast). Before weaning, at three weeks of age, mice were housed with their littermates, and either mother or both mother and father present in the cage. Animals were kept on a 12 hour light-dark cycle (6.00AM on, 6.00PM off), and with continuous access to food pellets (NIH-07, regular chow) and water.

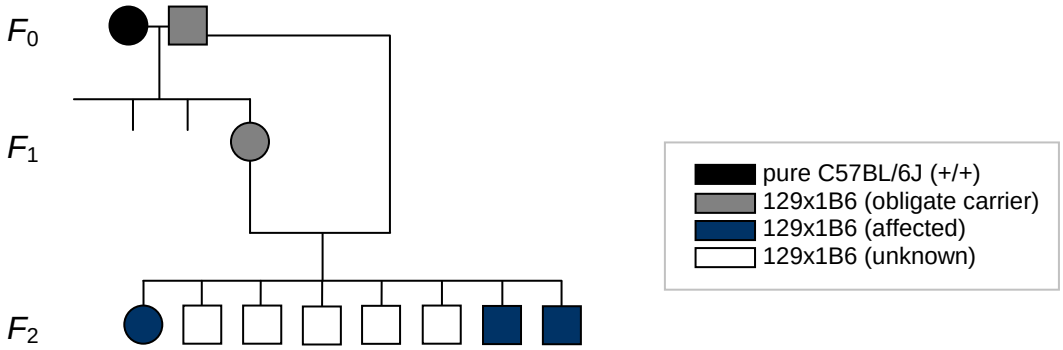

Figure 2.1. Mouse pedigree, first generation backcross

Pure C57BL/6J female, wild type (+/+) for mutation, is crossed with a known (based on previous crosses) heterozygote 129x1B6 male (obligate carrier). Unaffected F_1 females (unknown genotype) are crossed with the heterozygote 129x1B6 male (obligate carrier), if female heterozygous the phenotype will reappear in the F_2 progeny. Next, F_2 males (unknown) are backcrossed with the pure C57BL/6J female to start a next generation. F_x, filial, generation x following the parental generation; circle, female; square, male.

2.3.2.2 Genotyping Itpr1$^{\Delta 18}$mice

To genotype mice for the *Itpr1*$^{\Delta 18}$ mutation in exon 36, a multiplex PCR was designed by J Chandran (LNG/NIA/NIH). The forward primers were designed so one primer would overlap two nucleotides with the deletion site, whereas the other was shifted two nucleotides to the 5'-end thereby lying directly adjacent to the deletion site, both were combined with a single reverse primer. This multiplex PCR strategy was used to ensure both products, with and without the 18bp deletion in *Itpr1*, would amplify equally. However, as can been seen in figure 2.2, none of the primer sequences overlapped with the 18bp deletion in *Itpr1* in ataxic mice. Because the multiplex PCR design did provide a high throughput way to genotype mice for *Itpr1*$^{\Delta 18}$ it was used nonetheless. Primer details and reaction composition are given in table 2.5, amplification conditions are given in table 2.6.

108801142	CAGTCCCTTTAATACATAGCTCTTTAGGGGATAGTCAACATCTACACCAA	108801191
108801192	AGCAGACACATTCTGGAATCCAGTCCTTGACCCTTCTGGAATCCTCCCAC	108801241
108801242	TAAGATGTGGAGGGTTCCAGACAGCCTCTGTTTCTAGCCAGGCCATCTGT	108801291
108801292	GTTCTGCAGCCTTCTTCACCTCGCCTCTCTCTCTTATAGACCCGCCAGCC	108801341
108801342	TGTCTTTGTGCAACTCCTGCAAGGCGTGTTCCGAGTTTACCACTGCAACT	108801391
108801392	GGCTGATGCCGAGCCAAAAAGCCTCGGTG**GAGAGCTGCATCCGGGTG**CTC	108801441
108801442	TCTGACGTAGGTAAGGCAGCCAATCCGTCTGGATGTGGCGGGATGAAAAT	108801491
108801492	GAGTGGCCTGCTGTTTACCGAGCCGAGCCGCAGCTCTCCCAAGGAAGGAA	108801541
108801542	GCTGCAAAGCCAGACCCAGAGCCGAGCTCTTGACTCCTTGGCCTCTGTCT	108801591
108801592	TTGCCAAGCCAGCACAGTGAGAAACAGTAAATCCTTGAAAAACAAGATTC	108801641

Figure 2.2. Primer sequence locations, multiplex PCR *Itpr1*$^{\Delta 18}$ genotyping

Sequence *Itpr1*, exon 36 in blue (NM_010585), flanking genomic sequence in black (NC_000072). Deleted nucleotides *Itpr1*$^{\Delta 18}$ in bold; F1 primer sequence, grey; F2 primer sequence, black; R primer sequence, blue.

volume (µl)	reagent	details
10	FastStart PCR mastermix	(Roche)
1	primer F1 (10pMol)	GCCAGCCTGTCTTTGTGC
1	primer F2 (10pMol)	CCGCCAGCCTGTCTTTGT
1	primer R (10pMol)	TGCCTTACCTACGTCAGAGAG
1	DNA from tail/ molecular grade water (NC)	
14		

Table 2.5. Reaction composition, multiplex PCR *Itpr1*$^{\Delta 18}$ genotyping

F1, forward primer 1 (sequence, length); F2, forward primer 2 (sequence, length); R, reverse primer (sequence, length); primers, Operon Biotechnologies; NC, no template control.

***ITPR1*$^{\Delta 18}$ genotyping**						
		35 cycles				
phase	Di	D	A	E	Ef	
temperature	95°C	94°C	62°C	72°C	72°C	4°C
duration	4’	30”	30”	30”	5”	hold

Table 2.6. Amplification conditions, multiplex PCR *Itpr1*$^{\Delta 18}$ genotyping
Phases; Di, initial denaturation; D, denaturation; A, annealing; E, extension; Ef, final extension. Temperature in degrees Celsius. Duration in ’ minutes; ’’ seconds.

Agarose gel electrophoresis was used to visualize the PCR product and estimate the size of the DNA fragments. Each 14µl PCR was mixed with 3µl orangeG loading buffer, and samples as well as a size reference (GeneRuler DNA laddermix, 0.1µg/µl; Fermentas) were loaded on a 2%(w/v) agarose gel in 1xTBE with ethidium bromide (27µg/100ml). Electrophoresis for ≥2 hours at 110V with altering amperes (see paragraph 2.2.2.3) enabled size separation, fragments with and without the 18bp deletion, of the PCR amplification products (see figure 2.3).

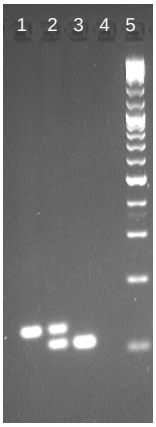

Figure 2.3. Example *Itpr1*$^{\Delta 18}$ genotype data
Example image agarose gel for *Itpr1*$^{\Delta 18}$ genotyping showing expected product sizes for each genotype. Lane 1, single band 125/127bp indicates *Itpr1*$^{wt/wt}$; lane 2, band 125/127bp and 107/109bp indicates *Itpr1*$^{wt/\Delta 18}$; lane 3, single band 107/109bp indicates *Itpr1*$^{\Delta 18/\Delta 18}$; lane 4, no template control; lane 5, GeneRuler DNA laddermix (5µl; Fermentas, 0.1µg/µl).

2.3.2.3 Phenotyping Itpr1$^{\Delta 18}$ mice

Mice were phenotypically characterized based on observation of animal development and home cage behavior. Animal development was assessed by noting developmental physical landmarks such as pinnae detachment, eye opening and fur development. In addition length (cm; ruler, OriGene), from nose to base of tail, and weight (g; balance, Ohaus Scout II (1200x0.1g), SRA210) measurements of 3 week old mice were taken. Measurements of length and weight were carried out by L Parisiadou (LNG/NIA/NIH). Length and weight data were statistically analyzed using Analyse-it for Microsoft Excel (standard edition; Analyse-it software). Observations of locomotor development included acquirement of quadruped stance (placement of limbs, trunk support/ pelvis of ground) and quadruped locomotion (hindlimb movement).

2.3.2.4 Cross-breeding Itpr1$^{\Delta 18}$ x Itpr1^{opt} mice

Female heterozygote *Itpr1$^{\Delta 18}$* mice (as determined by genotyping, see paragraph 2.3.2.2) were crossed with a male heterozygote *Itpr1^{opt}* from JAX labs (B6C3Fe-*a/a*-*Itpr1opt*/J, stock number 000019). F_1 offspring were phenotypically characterized (as described in paragraph 2.3.2.3) and findings compared to observations in homozygous *Itpr1$^{\Delta 18}$* and *opisthotonos* (*Itpr1^{opt}*) mice (Street et al. 1997). Cross-breeding was carried out by J Chandran (LNG/NIA/NIH).

2.3.3 DNA protocols

2.3.3.1 DNA preparation from mouse tail tissue

Initially the TNES buffer protocol was used for tail DNA preparation for all downstream applications, however eventually it was replaced by the direct-PCR tail method (Viagen). Collection of tail tissue was carried out by J Chandran (LNG/NIA/NIH) and C Xie (LNG/NIA/LNG).

TNES buffer protocol

Mouse tail, 0.5-1.0cm, was removed under isoflurane (gas) anaesthesia. To each tail sample, fresh or thawed for several minutes at room temperature after storage (-20°C), 500µl TNES buffer (10mM Tris (pH7.4; KD Medical), 400mM NaCl (Cellgro), 100mM EDTA (pH8.0; KD Medical), 0.6%(w/v) SDS (Quality Biological) in molecular grade water) and 10µl proteinase K (20µg/µl; Qiagen) were added. Samples were incubated overnight in a 55°C waterbath to allow complete lysis. Next day, samples were allowed to cool by incubation at room temperature for 10 minutes. Next, 300µl protein precipitation solution (Promega) was added. Samples were mixed by vortexing for 20 seconds and chilled on ice for 10 minutes, prior to centrifugation at maximum rcf. for 20 minutes (Eppendorf, centrifuge 5415D; maximum rcf. 16,100x*g*). Supernatants were transferred to clean eppendorf tubes by decanting and 500µl room temperature isopropanol was added. Samples were mixed by gentle inversion, incubated at room temperature for five minutes and centrifuged at maximum rcf. for 15 minutes (Eppendorf, centrifuge 5415D; maximum rcf. 16,100x*g*), resulting in a small pellet containing precipitated DNA. Supernatants were removed and discarded. To wash, 100µl room temperature 70% ethanol was added and mixed, and samples were centrifuged at maximum rcf. for 2 minutes (Eppendorf, centrifuge 5415D; maximum rcf. 16,100x*g*). Supernatants were carefully aspirated and discarded, and pellets air-dried for several minutes in a heating block at 65°C. Finally, DNA pellets were rehydrated in 150µl TE buffer by incubation at 55°C for 1 hour. Samples were pulse centrifuged for 7-10 seconds and stored at 4°C.

Direct-PCR tail method

Mouse tail, 0.5-1.0cm, was removed under isoflurane (gas) anaesthesia. To each sample, 250µl direct-PCR lyses reagent (102–T (tail); Viagen) and 12µl proteinase K (genomic PCR grade, 20mg/ml; Viagen) were added, or volumes adjusted according to tail length. Samples were incubated in a 55°C waterbath for 16 hours to allow complete lysis, followed by 45 minutes at 90°C (heating block) to stop enzyme activity.

Tubes were pulse centrifuged for 7-10 seconds and samples stored at 4°C.

2.3.3.2 Linkage analysis

Mice in this study came from a mixed background of C57BL/6J and 129/Sv strains. Genome wide linkage analysis was carried out by genotyping 120 fragments, containing 140 SNPs (single nucleotide polymorphisms), which were informative for strain differences between the C57BL/6J and 129/Sv mice. Fragments and corresponding primer sequences were selected from a publicly available database as described in a paper by Lindblad-Toh et al. (2000). For fine mapping additional genetic variants, SNPs and microsatellites, were selected from the Mouse Genome Informatics (MGI) database (http://www.informatics.jax.org/strains_SNPs.shtml; The Jackson Laboratory) and NCBI SNP (http://www.ncbi.nlm.nih.gov/SNP/MouseSNP.cgi; mouse build 34.1).

Genotyping single nucleotide polymorphisms (SNPs)

Single nucleotide polymorphism (SNP) genotypes were obtained by sequence analysis of the genomic fragments. DNA fragments from affected and unaffected mice were amplified and electropherograms analysed (see paragraph 2.2.2). Genotype data were collected in an excel worksheet and formatted for MLINK data entry (multi-locus linkage analysis; paragraph 2.3.3.2) (Lathrop et al. 1984).

Genotyping microsatellites

Genotypes for microsatellites were obtained using the ABI True Allele genotype system (Applied Biosystems) that allows multiplex reactions by using different fluorescent labels. A combination of Taqman probes labeled with FAM or HEX was used, for details on markers, primers and labels see appendix I. Each reaction contained: 6.0µl True Allele PCR premix (Applied Biosystems), 0.67µl primers (5pMol; for each primer pair), 1.0µl DNA, and molecular grade water up to 10µl total reaction volume. Samples were amplified using a Hybaid thermocycler (Thermo Scientific). Cycle conditions for genotype amplification are given in table 2.7.

genotyping (using microsatellites)						
		30 cycles				
phase	Di	D	A	E	Ef	
temperature	95°C	94°C	55°C	72°C	72°C	4°C
duration	12’	15”	15”	30”	10’	hold

Table 2.7. Cycle settings, microsatellite genotyping
Phases; Di, initial denaturation; D, denaturation; A, annealing; E, extension; Ef, final extension. Temperature in degrees Celsius. Duration in ’ minutes; ’’ seconds.

Following amplification, 9µl LIZ/Hi-Di (4µl LIZ genescan (Applied Biosystems) with 96µl Hi-Di formamide (Applied Biosystems) was added to 1µl product. Samples were denatured at 95°C for 5 minutes, followed by immediate incubation on ice for at least 5 minutes. Genotypes were derived from electropherograms obtained on an ABI prism 3100 genetic analyzer platform (Applied Biosystems), using genotyper software (ABI prism, version 3.7 NT) for analysis.

Genome wide linkage data analysis using MLINK

To map the location of the disease gene, linkage analysis was carried out using MLINK (multi-locus linkage analysis, version 5.1) of the computer package LINKAGE (Lathrop et al. 1984), under the assumptions of full autosomal recessive inheritance, a disease allele frequency of 0.01, full penetrance, non sex-linked, and equal frequencies of all alleles for each marker. MLINK software allowed for maximum likelihood estimation of recombination rates, calculation of LOD (logarithm of odds) score tables and analysis of genetic risks with two or more loci. MLINK data input consisted of pedigree and genotype data, combined with locus description, recombination rates and gene order information. MLINK 2-point analysis generated LOD scores by comparing each SNP, informative between C57BL/6J and 129/Sv background with disease status for linkage (Lindblad-Toh et al. 2000).

2.3.4 Protein protocols

2.3.4.1 Western blot analysis of crude protein extraction

Crude protein extraction from mouse cerebellum

Mice (33 day old littermates, 129x1B6, *n*=4) were anaesthetized using isoflurane (gas) and sacrificed by decapitation. Tissue collection was carried out by J Chandran (LNG/NIA/NIH). Brains were quickly removed and dissected in two halves along the sagittal axis. One half was snap-frozen on dry ice and stored at -80°C for future studies, the other half was kept on ice for protein analysis using western blot. Tissue was homogenized, using a glass tube and pestle on ice, in 1ml RIPA lysis buffer (50mM Tris-HCl (pH7.4; Quality Biological), 1%(v/v) NP-40 (BioVision), 0.25%(w/v) sodium deoxycholate (Sigma), 150mM NaCl (Cellgro), 1mM EDTA (pH 8.0; KD Medical), 1mM sodium vanadate (Sigma), 1mM sodium fluoride (Sigma), in molecular grade water) with 10µl protease inhibitor cocktail (Sigma). Samples were centrifuged at 100x*g* for 10 minutes at 4°C (Eppendorf 5804R, F45-30-11 rotor). Then sonicated (Tekmar; ultrasonic processor with CV26 sonicator) on ice using remote settings, approximately 10 pulses, to increase homogenization and centrifuged for 10 minutes at 100x*g* and 4°C (Eppendorf 5804R, F45-30-11 rotor). Each supernatant was collected in a clean eppendorf tube and stored at -80°C until further processing.

Western blot, crude extracted protein

Samples (aliquots) were taken from -80°C (storage) and thawed on ice. To 10µl sample, 10µl NuPage reducing agent (Invitrogen), 30µl NuPage LDS sample buffer 4x (Invitrogen) and 50µl molecular grade water were added, resulting in a 1:10 dilution of sample. Samples were heated to 70°C for 15 minutes and put on ice. Samples, 10µl each, and 10µl size reference (precision plus protein dual color standard; Biorad) (table 2.8) were loaded on a 4-12% bis-tris gel (precast gel, pH6.4, 1.5mm 10-well 37µl; Invitrogen). Gel was electrophoresed in MOPS running buffer (Invitrogen), for the inner chamber 0.5ml NuPage reducing agent (Invitrogen) was added to 200ml MOPS buffer (Invitrogen). Electrophoresis was carried out at 125-180V for approximately 2 hours.

band no.	precision plus
1	250
2	150
3	100
4	75
5	50
6	37
7	25
8	20
9	15
10	10

Table 2.8. Molecular weights precision plus protein dual color standard
Apparent molecular weight (kDa) of protein bands in precision plus protein dual color standard on a NuPAGE 4-12% bis-tris gel in MOPS (Invitrogen). Colors used correspond to visual color of band on gel or blot.

Protein was transferred to PVDF membrane (Immobilon-P, 0.45µm; Millipore) using 16V constant voltage overnight (transfer system (Biorad); power supply model 300/ 500 (VWR)), in NuPage transfer buffer (Invitrogen) with 20%(v/v) methanol. The next day, the blot was blocked using 5%(w/v) non-fat milk a high level blocker, in TBS-T (1xTBS, Biorad; 0.1%(v/v) tween-20, Sigma) a low level blocker, for 30 minutes at room temperature under gentle agitation. The blot was incubated with primary antibody diluted in 5%(w/v) non-fat milk in TBS-T (see table 2.9 for antibody specific dilutions) for 1 hour at RT in a slowly rotating 50ml tube. The membrane was washed in TBS-T for 5, 15 and 5 minutes sequentially while shaken at room temperature. Then the blot was incubated with secondary antibody diluted in 5%(w/v) non-fat milk in TBS-T (see table 2.9 for antibody specific dilutions) for 1 hour at room temperature in a slowly rotating 50ml tube. The blot was washed in TBS-T for 5, 15 and 5 minutes sequentially at room temperature under gentle shaking. For imaging, supersignal west pico chemiluminescent substrate (Pierce) was used according to manufacturer's protocol (http://www.piercenet.com/files/0636dh4.pdf). Blots were exposed to Biomax XAR film (Kodak) for visualization of signal, and developed using a Kodak X-OMAT 2000A processor (automatic developer).

antibody	dilution	manufacturer
rabbit anti-IP3R1, polyclonal (0.3mg/ml)	1:1,000	Chemicon
donkey anti-rabbit IgG (H+L) (0.8mg/ml)	1:5,000	Jackson ImmunoResearch
mouse anti-(β-actin), monoclonal	1:10,000	Sigma
mouse anti-neurofilament 160, monoclonal	1:1,000	Sigma
donkey anti-mouse IgG (H+L) (0.8mg/ml)	1:5,000	Jackson ImmunoResearch

Table 2.9. Antibodies and dilutions, western blot analysis (crude) in *Itpr1*$^{\Delta 18}$ mice

2.3.4.2 Western blot analysis of fractionated protein extraction

Fractionated protein extraction from mouse cerebellum

Mice (22 day old littermates, 129x1B6, *n*=5) were sacrificed by decapitation, brains were quickly removed and snap-frozen using liquid nitrogen and dry ice, and stored at -80°C until further processing. Tissue collection was carried out by MR Cookson (LNG/NIA/NIH). The cerebellum was dissected and minced on a cold block to keep tissue deep-frozen and thereby prevent protein degradation. Tissue samples were kept on ice throughout the procedure, except the final SDS-soluble fractions as SDS precipitates when cooled. All fractions and 10µl aliquots for the BCA protein assay were immediately stored at -80°C when obtained.

Approximately 10 volumes (ml:g), 300µl, TBS-PI were added to each sample (1xTBS (pH7.4; American Bioanalytical), 10µl/ml protease inhibitor cocktail (Sigma), 5mM EDTA (pH7.4; Sigma)). Each tissue was homogenized in TBS-PI buffer by sonication (Tekmar; ultrasonic processor with CV26 sonicator) on ice. Samples were centrifuged at 1,000x*g* for 5 minutes at 4°C to remove debris (Eppendorf 5804R, F45-30-11 rotor). Pellets, containing non-homogenized material, were discarded. Each supernatant, containing the crude homogenate, was transferred to polycarbonate tubes (11x34mm PC tube; Beckman Coulter), balanced carefully using TBS-PI buffer (AG204 DeltaRange, d=0.1mg/1mg; Metler Toledo) and centrifuged at 100,000x*g* for 60 minutes at 4°C using a Beckman Coulter optima max ultracentrifuge (rotor MLA-130 (max rcf. at r_{max} 1,019,000*xg*; r_{max} 53.9mm; r_{min} 29.9mm; κ-factor 8.7). Supernatants were retained as the TBS-soluble fraction (cytoplasmic proteins) and immediately stored at -80°C. Pellets were washed twice in 100µl 1xTBS without disturbing the pellet, and resuspended by sonication (Tekmar; ultrasonic processor with CV26 sonicator) on ice in 200µl TBS-Tx100 (1xTBS, 1%(v/v) tritonX-100 (Sigma), 10µl/ml protease inhibitor cocktail (Sigma)). Homogenates were transferred to the polycarbonate centrifuge tubes, balanced carefully using TBS-Tx100 buffer (AG204

DeltaRange, d=0.1mg/1mg; Metler Toledo) and centrifuged at 100,000x*g* for 60 minutes at 4°C using the Beckman Coulter optima max ultracentrifuge with MLA-130 rotor (Beckman Coulter). Supernatants were retained as the triton-soluble fraction (membrane-bound, soluble proteins) and immediately stored at -80°C. Pellets were carefully washed twice in 100µl 1xTBS and resuspended in approximately 5 volumes, 100µl, TBS-SDS (1xTBS, 5%(w/v) SDS (Quality Biological) by sonication at room temperature (Tekmar; ultrasonic processor with CV26 sonicator). Homogenates were retained as SDS-soluble fractions (membrane-bound, insoluble proteins) and immediately stored at -80°C.

Sample fractions were diluted 1:10 in 1xTBS (American Bioanalytical). Protein concentrations were determined using BCA protein assay (bicinchoninic acid; Pierce) carried out according to manufacturer's protocol (http://www.piercenet.com/files/1601325ProteinAssay.pdf). Standards used were 2.0, 1.5, 1.0, 0.75, 0.5, 0.25, 0.125, 0.025 mg/ml albumin in 0.9% saline and 0.05% sodium azide (Pierce), and 1xTBS as blank measurement. Samples were read at 595nm in optical flat bottom 96 deep-well plates (Molecular Devices) on a SpectraMax Plus microplate reader for colorimetric detection (Molecular Devices), using SoftMax Pro software (v4.0; Molecular Devices) to calculate protein concentrations.

Western blot, fractionated protein extraction

Samples (aliquots) were taken from -80°C storage and thawed on ice. To 10µg sample, based on BCA assay, molecular grade water was added up to 10µl total volume. Next, 5µl sample buffer (0.25M tris-HCl (pH6.8; Quality Biological), 8%(w/v) SDS (Quality Biological), 30%(v/v) glycerol (Invitrogen), 0.02%(w/v) bromophenol blue (Sigma), 10%(v/v) B-ME (beta-mercapto ethanol; American Bioanalytical) a reducing agent, in molecular grade water) was added, samples were heated to 65°C for 15 minutes and put on ice. Samples and 10µl size reference (precision plus protein dual color standard; Biorad) (table 2.8) were loaded on a 4-20% tris-HCl gel (Biorad, Criterion precast gel; 1.0mm 18-comb 30µl). Gel electrophoresis was carried out in 10xTGS running buffer (25mM tris, 192mM glycine, 0.1%(w/v) SDS, pH8.3; Biorad) at 160V for at least 2 hours.

Protein was transferred overnight to PVDF membrane (Immobilon-P, 0.45µm; Millipore) using 16V constant voltage (transfer system (Biorad); power supply model 300/ 500 (VWR)) in CAPS transfer buffer (10%(v/v) methanol, 10%(v/v) CAPS

(22.13g/l, pH11.0), in deionized water). Next day, the blot was blocked using 5%(w/v) non-fat milk a high level blocker, in TBS-T (1xTBS, Biorad; 0.1%(v/v) tween-20, Sigma) a low level blocker, for 30 minutes at room temperature under gentle agitation. The blot was incubated with primary antibody diluted in 5%(w/v) non-fat milk (see table 2.10 for antibody specific dilutions) for 1 hour at room temperature in a slowly rotating 50ml tube. Membrane was washed in TBS-T for 5, 15 and 5 minutes sequentially while shaken at room temperature. Then the blot was incubated with secondary antibody diluted in 5%(w/v) non-fat milk (see table 2.10 for antibody specific dilutions) for 1 hour at room temperature in a slowly rotating 50ml tube. Blot was washed in TBS-T for 5, 15 and 5 minutes sequentially at room temperature under gentle shaking. For imaging, supersignal west pico chemiluminescent substrate (Pierce) was used according to manufacturer's protocol (http://www.piercenet.com/files/0636dh4.pdf). Blots were exposed to Biomax XAR film (Kodak) for visualization of signal, and developed using a Kodak X-OMAT 2000A processor (automatic developer).

antibody	**dilution**	**manufacturer**
rabbit anti-IP3R1, polyclonal (0.3mg/ml)	1:1,000	Chemicon
donkey anti-rabbit IgG (H+L) (0.8mg/ml)	1:5,000	Jackson ImmunoResearch
mouse anti-(β-actin), monoclonal	1:10,000	Sigma
mouse anti-neurofilament 160, monoclonal	1:1,000	Sigma
donkey anti-mouse IgG (H+L) (0.8mg/ml)	1:5,000	Jackson ImmunoResearch

Table 2.10. Antibodies and dilutions, western blot analysis (fractionated) in *Itpr1*$^{\Delta 18}$ mice

2.3.4.3 Immunohistochemistry

Tissue preparation

Mice (three week old littermates, 129x1B6, *n*=3; wild type (*n*=1), heterozygote (*n*=1) and homozygote for *Itpr1*$^{\Delta 18}$ (*n*=1)) were perfused using 4%(w/v) paraformaldehyde (20g paraformaldehyde (Sigma), 1xPBS (Gibco) to make up a total volume of 500ml, ten drops 1M NaOH (American Bioanalytical) were added to aid the paraformaldehyde to pass into solution, the mixture was stirred and heated to 70°C until dissolved). Brains were removed and kept in 1xPBS at 4°C for several hours. Then 1xPBS was replaced with an ice cold 10%(v/v) glycerol in 1xPBS solution (15ml glycerol (Invitrogen), 1xPBS added to a total volume of 150ml), and samples were stored at 4°C for two days before being shipped to NeuroScience Associates (NSA). A wild type, heterozygote and homozygote affected mouse brain were embedded in a single gelatin block and 35µM thick sections were cryosectioned along the sagital axis using MultiBrain technology (NSA; http://www.neuroscienceassociates.com/). Embedded and sectioned tissue was stored at -20°C in the antigen preserve solution as supplied by NSA. Perfusion of animals and dissection of the brains were carried out by L Holtzclaw (LCSN/NICHD/NIH) and J Chandran (LNG/NIA/NIH).

Immunohistochemistry

Before use, sections were rinsed thoroughly in 1xPBS to eliminate any carry-over of antigen preservation solution. Then, sections were incubated in 6ml blocking solution (10ml normal goat serum (Gibco), to match host of secondary antibody, 40ml carrier solution (1xPBS, 0.3%(v/v) triton (Sigma), 10g/l normal BSA (Probumin Universal Grade (K); Celliance), 1%(v/v) normal goat serum (Gibco); pH was set to 7.4 using NaOH (1M; American Bioanalytical) and solution filtered (0.45µM; Corning) to prevent overnight growth as the solution contained a high protein concentration) for 1 hour at room temperature, under gentle shaking to prevent settling of sections on bottom of wells. Sections were transferred to a 12-well plate containing 2ml primary antibody diluted in carrier solution in each well. For peptide competition primary antibody and peptide were incubated 10:1 (10µg antibody with 1µg peptide as recommended by manufacturer (http://www.millipore.com/catalogue/item/ab5882-50ul; Chemicon) in 500µl carrier solution overnight at 4°C while rotating, prior to section incubation (see table 2.11 for antibody specific dilutions). Sections were incubated under gentle shaking at 4°C overnight (cold room).

Next day, the sections were washed in 6ml carrier solution for 5, 15 and 5 minutes sequentially, while shaken gently at room temperature. Sections were incubated in 2ml dilutions of secondary antibody in carrier solution for 1 hour at room temperature under gentle shaking (see table 2.11 for antibody specific dilutions). Sections were washed in 6ml carrier solution for 5, 15 and 5 minutes sequentially while shaken at room temperature. One section at a time was transferred to a petridish containing 1xPBS and mounted onto a gelatin-coated slide (1g/l gelatin from pigskin (Sigma), 0.5g/l chrom alum (Sigma) in distilled water; Daigger, 3x1inch, 1.2mm thick), a soft brush was used to smoothen sections. Slides were dried using a 45°C warm plate and once dry, 110µl mowiol (6g glycerol (Invitrogen), 2.4g mowiol (Calbiochem), 6ml milliQ water were combined and left at room temperature overnight, then 12ml 0.2M tris (pH6.8; Sigma) was added, solution heated to 50°C for 10 minutes and centrifuged 15 minutes at 5,000x*g* to pellet insoluble material (Evolution RC, rotor SS-34, Sorvall), and 2.5%(w/v) 1,4-diazobicyclo-[2.2.2]-octane (DABCO), an anti-bleaching agent, was added; the mowiol was left under vacuum overnight prior to use) was pipetted across each tissue section and a coverslip (Thomas Scientific, 24x40mm, #1, 0.13-0.16mm thick) positioned to cover all tissue. Slides were stored flat and dark overnight before analysis, or stored flat at 4°C in the dark long term. Images were captured using an LSM 510/LNO META upright two-photon confocal microscope (Zeiss), with plan-apochromat 5x/0.16 NA (Zeiss) and plan-apochromat 63x 1.4 oil DIC (Zeiss) objectives. Microscope parameters (pinhole, detector gain, laser power) were optimized for objective and filters used, based on the wild type section, and remained unchanged when images for heterozygous and homozygous affected sections of the same slide were taken. Images were analyzed using LSM image browser software (version 3.2.0.115; Zeiss).

antibody	**dilution**	**manufacturer**
rabbit anti-IP3R1, polyclonal (0.3mg/ml)	1:2,000	Chemicon
peptide, rabbit anti-IP3R1	1:200	Chemicon
Alexa Fluor 555 goat anti-rabbit IgG (H+L) (2mg/ml)	1:2,000	Invitrogen
mouse anti-calbindin D-28K (IgG1 6.7mg/ml)	1:6,000	Sigma
Alexa Fluor 488 goat anti-mouse IgG (H+L) (2mg/ml)	1:3,000	Invitrogen

Table 2.11. Antibodies, peptide and dilutions, immunohistochemistry in *Itpr1*$^{\Delta 18}$ mice
Dilutions used were based on specificity, signal strength and background when imaging on a Zeiss LSM 510 laser scanning microscope.

2.4 HUMAN-RELATED METHODS

2.4.1 Sample collection

Australia, SCA15 family (AUS1)

A description of the original Australian SCA15 family (AUS1) has been previously published (Storey et al. 2001;Knight et al. 2003). Melanie Knight and colleagues were kind to share their samples. Regarding sample collection, the project was approved by the Women's and Children's Hospital Human Ethics Committee (Melbourne, Australia). All participants gave their informed consent. Family members were clinically examined by a neurologist. Whole blood was collected in lithium heparin and EDTA tubes. Genomic DNA was extracted from blood leukocytes of all examined affected individuals, some apparently unaffected members, and (where possible) unaffected parents, using the Amersham Nucleon BACC2 for Blood and Cultured Cells kit (Amersham Pharmacia, Biotech).

London (England), ADCA III cohort

Henry Houlden and colleagues provided samples of familial ataxia cases collected in London (England). Ethical approval was obtained through the National Hospital for Neurology and Neurosurgery ethics committee. Patients were diagnosed at the National Hospital for Neurology and Neurosurgery based on clinical examination by a neurologist. Informed consent was given by all participants. Whole blood was collected in EDTA blood collection tubes. Genomic DNA was isolated using phenol/chloroform extraction. All samples were previously screened and found negative for SCA 1, 2, 3, 6, 7, 8, 11, 12 and 17.

Cardiff (Wales), ADCA III cohort

Samples were provided by Huw Morris at Cardiff University in Wales. Ethical approval was given by the South Wales LREC (local research and ethics committee). Patients were recruited from different sources, including hospital clinicians, general practitioners, geneticists and local health organizations. All patients sampled were examined by a clinical neurologist for diagnostic evaluation. Informed consent was obtained from all participants. Blood was collected in EDTA tubes, and DNA extracted using at the Institute of Medical Genetics using a standardized protocol (National Health Service (NHS) accredited). All samples were previously screened and found negative for SCA 1, 2, 3, 6, 7, 8, 10, 12 and 17, and DRPLA.

Paris (France), ADCA III cohort

Samples were made available by Alexis Brice's group, Fédération de Neurologie, Hôpital de la Salpêtrière (Paris, France). These samples were obtained within SPATAX, a network of European laboratories to join forces in the clinical and genetic analysis of cerebellar ataxias and spastic paraplegias (http://clinicaltrials.gov/ct2/show/NCT00140829). Ethical approval was given by the French bio-ethic committee, CCPPRB-Paris Necker (Comité Consultatif de Protection des Personnes dans la Recherche Biomédicale). Informed consent was obtained from all participants. Whole blood was collected in EDTA blood collection tubes. Phenol/chloroform extraction method was applied to extract genomic DNA.

2.4.2 DNA protocols

2.4.2.1 DNA isolation from lymphoblast cultures (SCA15)

Culture of the Epstein-Barr virus (EBV) immortalized lymphocyte cell lines from members of the original Australian SCA15 family (Storey et al. 2001) was carried out by Melanie Knight, at the time a postdoctoral fellow at the Neurogenetics Branch (National Institute of Neurological Disorders and Stroke at the National Institutes of Health, Bethesda (MD), USA). Melanie Knight also isolated the DNA from these lymphoblast cultures and ascertained DNA sample quantity and integrity.

DNA isolation from lymphoblast cell cultures was carried out using Qiagen, Blood and Cell Culture DNA midi kit according to manufacturer's protocol (Genomic-tip 100/G; http://www1.qiagen.com/literature/handbooks/literature.aspx?id=1000034). Briefly, cell pellets were thawed on ice and resuspended in 1xPBS (Gibco) to a concentration of $1x10^7$ cells/ml. Cells were lysed, nuclei pelleted, resuspended and incubated with protease at 50°C for an hour. Genomic DNA was isolated using genomic-tip filters. During this stage tubes were centrifuged at 4,000x*g*, not 5,000x*g* as the protocol states (centrifuge Eppendorf 5804(R); F45-30-11, max 11,000rpm, max 30x3.75kg). Isolated DNA was washed and resuspended in 125µl molecular grade water per $1x10^7$ cells starting material and left to dissolve overnight while shaken at room temperature.

To determine sample quantity and integrity, 1µl bromophenol blue loading dye (bromophenol blue sodium salt; Sigma) was added to 2µl isolated DNA, and samples were electrophoresed on a 1%(w/v) agarose gel (SeaKem ME agarose; Cambrex) at 60V. Optical densities (ODs) were determined for 10µl sample diluted with 490µl molecular grade water (dilution factor 50), on an Ultrospec 3100 pro UV/Visible spectrophotometer (Amersham Biosciences).

2.4.2.2 High density genome wide SNP genotyping (Illumina, Infinium 550k)

Genotyping was performed using Infinium HumanHap550 (AUS1 SCA15 family, London ADCA III cohort, Cardiff ADCA III cohort) or HumanHap610-Quad (Paris ADCA III cohort) SNP genotyping chips (Illumina) according to manufacturer's instructions (ftp://ftp.illumina.com/Infinium%20II%20documentation/Single%20Sample/ExperiencedUserCards/11280765_InfII_SingleSample_Manual_EUC.pdf; ftp://ftp.illumina.com/Infinium%20HD%20Documentation/Quad%20BeadChips/ExperiencedUserCards/Inf_HD_Super_Assay_Manual_EUC_11294817.pdf). Each chip assayed 555,352 or 373,397 unique SNPs, respectively. Briefly, 750ng (HumanHap550) or 200ng (HumanHap610-Quad) of each DNA sample was isothermally amplified in an overnight step. Amplified product was enzymatically fragmented, precipitated and resuspended. The resulting product was hybridized to a chip overnight, during which the amplified and fragmented DNA annealed to locus-specific 50-mers; each allele at each locus represented by one of two bead-types fixed to the chip. Following hybridization, allelic specificity was conferred by enzymatic extension. Products were fluorescently stained and visualization of the resulting signal and decoding of SNP position was performed using BeadStation scanner and data collection software (BeadScan, version 3.5.49.29917, Illumina). Genotypes were produced using the genotyping module of BeadStudio (v2.3.25, Illumina) and call rates generated, accepted call rates were >0.96. Log R ratios, surrogates for copy number, and B allele frequencies were visualized using the Genome viewer tool within this package. A minimum of three consecutive SNPs were required to call a homozygous deletion, and ten consecutive SNPs for a heterozygous mutation including duplication.

2.4.2.3 Gene dosage analysis

To assay for genetic dosage alterations, quantitative duplex PCR of genomic DNA samples was carried out. Primers were designed using Gene Runner (version 3.05; Hastings software), based on GenBank sequence information (http://www.ncbi.nlm.nih.gov/Genbank/index.html), similar to those used for PCR and sequence analysis (2.2.2.1). Primer pairs were designed to generate an amplicon sized <100bp to ensure equal amplification of probed region and endogenous reference (oligonucletide primers; Operon). A TaqMan MGB (3'-minor groove binder) probe for *ITPR1* exon 10 was 5' labeled with VIC (Applied Biosystems). The *hemoglobin* gene was co-amplified with *ITPR1* as an endogenous reference. The TaqMan MGB probe for *hemoglobin* was 5' labeled with FAM (Applied Biosystems). Primer and probe sequences, and reaction composition are given in table 2.12, for amplification conditions see table 2.13. Amplification and detection of fluorescence were performed in 384-well clear optical reaction plates (Applied Biosystems) on an ABI Prism 7900HT Sequence Detection System (Applied Biosystems). Each 384-well plate contained six replicates of each genomic DNA sample, including control DNA (H3332 (H3331 family, figure 4.12), III9 (AUS1 family, figure 4.1) unaffected; III5 (AUS1 family, figure 4.1), III4 (AUS1 family, figure 4.1) affected; status based on high density genome wide SNP genotype data, see 4.4.1.2 and 4.4.1.4) and a no template (NC) water control.

volume (µl)	reagent	details
10.0	Taqman mix 2x	(Applied Biosystems)
0.9	*ITPR1* primer fwd. (20pMol)	GAGAAGTTTCTCACCTGTGACG
0.9	*ITPR1* primer rev. (20pMol)	GTGGTTCTCAGGAAGACGTGC
0.9	*HB* primer fwd. (20pMol)	TGGGCAACCCTAAGGTGAAG
0.9	*HB* primer rev. (20pMol)	GTGAGCCAGGCCATCACTAAA
0.5	$ITPR1_{exon10}$ probe (10pMol)	VIC- CACAGGAAGAAGCAGCAC
0.5	*HB* probe (10pMol)	FAM-CTCATGGCAAGAAAGTGCTCGGTGC
0.4	molecular grade water	
15.0		
5.0	genomic DNA/ molecular grade water (NC)	
20.0		

Table 2.12. Reaction composition, gene dosage analysis (absolute quantification)
ITPR1, *inositol 1,4,5-triphosphate receptor, type 1*; $ITPR1_{exon10}$ amplicon, 59bp; *HB*, *hemoglobin, beta, delta*; *hemoglobin* amplicon, 68bp; fwd, forward primer (sequence); rev, reverse primer (sequence); primers, Operon Biotechnologies; probe, MGB (3'-minor groove binder) probe, Applied Biosystems; FAM, VIC, fluorescent labels; NC, no template control.

gene dosage (absolute quantification)				
			40 cycles	
phase		Di	D	AE
temperature	50°C	95°C	95°C	60°C
duration	2’	10’	15”	1’

Table 2.13. Cycle settings, gene dosage analysis (absolute quantification)
Phases; Di, initial denaturation; D, denaturation; AE, annealing and extension. Temperature in degrees Celsius. Duration in ’ minutes; ’’ seconds.

Data were analysed using SDS software (Sequence Detection System, version 2.2.2; Applied Biosystems). Outliers were removed based on visual inspection of the amplification plot for each sample (log scale), based on shape and position of each replicate amplification curve compared to the other curves of the sample. The cycle in the log phase of PCR amplification at which a significant fluorescence cycle threshold (Ct) was reached, was used to quantify each amplimer. The dosage of each amplimer relative to *hemoglobin* (ΔCt) and normalized to control DNA (average ΔCt of unaffected controls) was determined using the $2^{-\Delta\Delta Ct}$ method (Microsoft excel 2003). Accepted data showed cycle threshold values (Ct) between 23 and 30 for at least four of the six replicates (after outliers were removed), with a standard deviation (SD) ≤0.16. The $2^{-\Delta\Delta Ct}$ value was considered a heterozygous deletion between 0.4 and 0.6, normal between 0.8 and 1.2, or duplication at a value greater than or equal to 1.3. Genetic dosage alterations were only accepted after data replication in an independent experiment.

2.4.3 Protein protocols

2.4.3.1 Protein isolation from lymphoblast cultures (SCA15)

Culture of the Epstein-Barr virus (EBV) immortalized lymphocyte cell lines from members of the original Australian SCA15 family (Storey et al. 2001) was carried out by Melanie Knight, at the time a postdoctoral fellow at the Neurogenetics Branch (NINDS/NIH).

Lymphoblast cell pellets were lysed by 20 minutes incubation on ice in TBS-Tx100 (1xTBS (American Bioanalytical), 1%(v/v) tritonX-100 (Sigma), complete mini protease inhibitor cocktail tablets, 1 tablet/ml (Roche)). Each lysis-homogenate was sonicated three times for 3-4 seconds in an eppendorf tube on ice (Tekmar; ultrasonic processor with CV26 sonicator). Tubes were centrifuged at rcf. 16,100x*g* for 15 minutes at 4°C (Eppendorf 5804R, F45-30-11 rotor) and supernatant collected in fresh eppendorfs (pre-cooled on ice). Complete lysis was obtained by overnight incubation at -80°C.

Next day, undiluted protein concentrations were determined using BCA protein assay (bicinchoninic acid; Pierce) carried out according to manufacturer's protocol (http://www.piercenet.com/files/1601325ProteinAssay.pdf). Standards used were 2.0, 1.5, 1.0, 0.75, 0.5, 0.25, 0.125, 0.025 mg/ml albumin in 0.9% saline and 0.05% sodium azide (Pierce), and 1xTBS as blank measurement. Samples were read at 595nm in optical flat bottomed 96 deep-well plates (Molecular Devices) on a SpectraMax Plus microplate reader for colorimetric detection (Molecular Devices), using SoftMax Pro software (v4.0; Molecular Devices) to calculate protein concentrations. Samples were diluted based on calculated concentrations with lysis buffer (1xTBS with 1%(v/v) tween-20 and protease inhibitor) to equal 30µl of the lowest sample concentration measured based on undiluted sample.

2.4.3.2 Western blot analysis

For western blot analysis, 10µl sample buffer (8.5µl NuPage LDS sample buffer (Invitrogen), 1.5µl B-ME (beta-mercapto ethanol; American Bioanalytical), a reducing agent, was added to 30µl of each protein sample (samples were of equal protein concentration, for dilutions see paragraph 2.4.3.1). Samples were incubated at 70°C for 15 minutes and put on ice.

Samples as well as 10µl of each molecular weight standard, HiMark pre-stained HMW protein standard (Invitrogen) or SeeBlue plus 2 prestained standard (Invitrogen) (table 2.14) were loaded on a NuPAGE 4-12% bis-tris gel (NuPAGE 4-12% bis-tris 1.0, 12-well). Gel electrophoresis was carried out in MOPS buffer (Invitrogen) at 100-140V for at least 2 hours.

band no.	HiMark	SeeBlue
1	420	191
2	247	97
3	214	64
4	160	51
5	107	39
6	64	28
7	51	19
8	39	14
9	28	n/a
10		n/a

Table 2.14. Molecular weights, HiMark prestained and SeeBlue plus 2 standards
Apparent molecular weight (kDa) of protein bands in HiMark prestained and SeeBlue plus 2 standard on a NuPAGE 4-12% bis-tris gel in MOPS. Colors used correspond to visual color of band on gel or blot.

Protein was transferred to PVDF membrane (Immobilon-P, 0.45µm; Millipore) in NuPage 20x transfer buffer (Invitrogen), overnight using 20V constant voltage (transfer system (Biorad); power supply model 300/ 500 (VWR)). Next day, the blot was blocked using 5%(w/v) non-fat milk a high level blocker, in TBS-T (1xTBS (Biorad), 0.1%(v/v) tween-20 (Sigma)) a low level blocker, for 30 minutes at room temperature while gently agitating. Blot was incubated with primary antibody diluted in 5%(w/v) non-fat milk (see table 2.15 for antibody specific dilutions) for 1 hour at room temperature in a 50ml tube while slowly rotating. Membrane was washed at room temperature in TBS-T for 5, 15 and 5 minutes sequentially, while shaken. Blot was incubated with secondary antibody

diluted in 5%(w/v) non-fat milk (see table 2.15 for antibody specific dilutions) for 1 hour at room temperature in a slowly rotating 50ml tube. Blot was washed in TBS-T for 5, 15 and 5 minutes sequentially, at room temperature under gentle shaking. For imaging, ECL plus western blotting detection system (Amersham Biosciences) was used according to manufacturer's protocol (http://www6.gelifesciences.com/applic/upp00738.nsf/vLookupDoc/160135302-G350/$file/RPN2132PL_Rev_D_2006_web.pdf). Blots were exposed to Biomax XAR film (Kodak) for visualization of signal and developed using a Kodak X-OMAT 2000A processor (automatic developer).

antibody	dilution	manufacturer
rabbit anti-IP3R1, polyclonal (0.3mg/ml)	1:1000	Chemicon
donkey anti-rabbit IgG (H+L) (0.8mg/ml)	1:5000	Jackson ImmunoResearch
mouse anti-(β-actin), monoclonal (~2mg/ml)	1:10000	Sigma
donkey anti-mouse IgG (H+L) (0.8mg/ml)	1:5000	Jackson ImmunoResearch

Table 2.15. Antibodies and dilutions, western blot analysis SCA15 samples

CHAPTER 3 MOLECULAR GENETIC CHARACTERIZATION OF AN AUTOSOMAL RECESSIVE MOVEMENT DISORDER IN MICE

3.1 CHAPTER AIM

To identify the genetic cause of a severe spontaneous movement disorder in mice and characterize the disease causing gene(s).

3.2 INTRODUCTION

A spontaneous mutation resulted in an early onset movement disorder in mice. Initial observations suggested affected mice suffered from an apparently paroxysmal movement disorder, often induced by touch. The abnormal movements occurred predominantly below the cervical level and the disorder appeared progressive. A human movement disorder specialist likened the disorder to episodic intermittent ataxia or kinesiogenic paroxysmal dystonia and predicted the involvement of an ion channel mutation in the etiology (K Gwinn-Hardy (NINDS/NIH), personal communication). Affected mice presented at approximately postnatal day 14 after which the mice rapidly deteriorated, as evidenced by increased convulsion intensity and frequency, survival time without weaning was on average 4 weeks. A positional cloning approach was undertaken to identify the underlying genetic cause, findings were further characterized at the molecular level.

3.3 RESULTS

3.3.1 Origin of mice

During generation of a line of mice with knockout of the gene *DJ1* as a model for early onset familial parkinsonism, within the Laboratory of Neurogenetics (NIA/NIH, Bethesda (MD) USA), a likely spontaneous mutation resulted in an early onset severe movement disorder. *DJ1* knockout mice were expected to be hypoactive based on previous reports on different *DJ1* knockout lines (Chandran et al. 2008), in which no changes in basic motor activity had been described. And indeed the younger mice (<1 year) with targeted deletion of *DJ1* (by replacing exon 2 with a neomycin resistance gene cassette) were hypoactive and had mild gait abnormalities, however older *DJ1*$^{-/-}$ mice showed decreased body weight and grip strength and more severe gait irregularities compared to wild type littermates. No obvious pathological changes in either the nigrostriatal system or spinal motor systems and muscles were found. All offspring from *DJ1* heterozygous mating were viable, fertile and lacked obvious developmental abnormalities (Chandran et al. 2008). However, mice affected by the spontaneous disorder suffered from an apparently paroxysmal movement disorder, often induced by touch. Affected mice presented at approximately postnatal day 14 after which the mice rapidly deteriorated, noted by increased convulsion intensity and frequency, survival time without weaning was on average 4 weeks. The disorder was inherited independent of target-vector transmission as was shown using Southern blot analysis and vector specific PCR targeting the *DJ1* transgene as described in Chandran et al. (2008).

3.3.2 Mode of inheritance

Breeding experiments showed the movement disorder was inherited independently of target-vector transmission and suggested an autosomal recessive inheritance pattern with no evidence of sex bias, see (partial) initial pedigree shown in figure 3.1. Mice homozygous for the mutation were unable to reproduce, due to severity of the disorder and early death, and therefore were maintained by intercrossing heterozygotes on a 129x1B6 mixed background (129x1/SvJ, C57BL/6J strains).

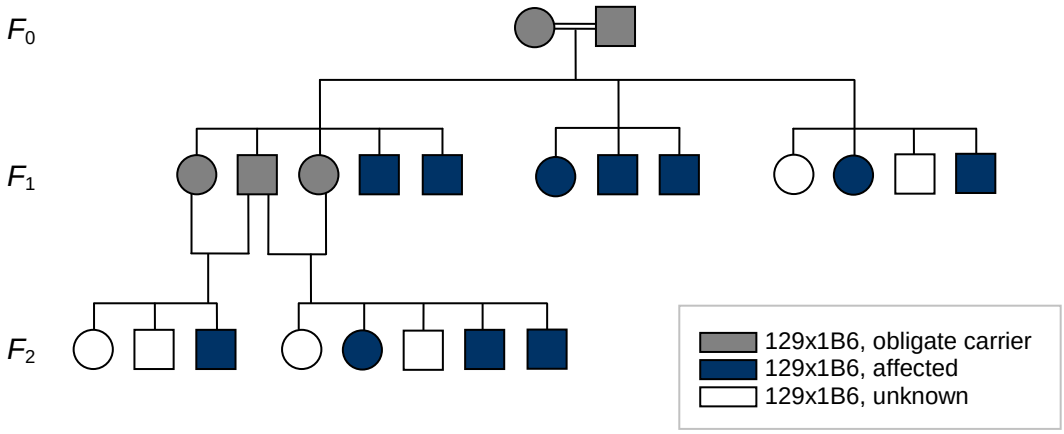

Figure 3.1. Mouse pedigree, spontaneous movement disorder

Pedigree shows an autosomal recessive inheritance pattern with no evidence of sex bias. Recessive inheritance is evident from unaffected (phenotypical indistinguishable from known wild type mice) parental mice (F_0,F_1) that gave birth to litters with affected mice (F_1, F_2 respectively) and therefore are obligate carriers of the genetic mutation. The pedigree shows no evidence of sex bias as both male and female mice were affected. Mice were maintained on a 129x1B6 mixed background (129x1/SvJ, C57BL/6J mice strains). Note this pedigree is incomplete and only shows mice included in this study. F_x, filial, generation x following the parental generation; circle, female; square, male.

3.3.3 Phenotype

Affected mice displayed developmental delay of locomotor behavior but not of physical landmarks. Age of onset was around P14, noticeable by splayed hindlimbs, after which the mice rapidly deteriorated. Phenotype was characterized by altered muscle tone, dragging of the hind limbs and apparently touch-induced seizures, marked by severe truncal, upper and lower limb contractions into unusual, twisting, seemingly painful postures (figure 3.2; supplementary video, appendix II). Progressive convulsion intensity and frequency were observed, and survival time without weaning was on average four weeks. Interestingly, heterozygote mice did not display any of the disease features.

Figure 3.2. Abnormal postures observed in affected mice

Top panels; opisthotonos-like postures. Bottom panels; spastic posture, splayed hind limbs and postural weakness (lack of quadruped stance), respectively.

Based on initial observation, affected mice appeared to be smaller then their littermates (figure 3.3; C, D). To test this observation length and weight measurements were obtained from wild type (*n*=7), heterozygote (*n*=9) and homozygote (*n*=3) affected mice at three weeks of age[1]. Measurements were taken by L Parisiadou (LNG/NIA/NIH).

[1] These measurements were taken after identification of the underlying genetic cause of the movement disorder. The genotype of each mouse was determined as to assign a wild type, heterozygote or homozygote status for the mutation. Weight and length data are discussed here instead of in chronological order to keep the flow of the chapter.

Data (appendix III) confirmed affected mice are significantly smaller, in length and weight, than their unaffected littermates. No differences were found in length and weight data between wild type and heterozygote mice (figure 3.3; A, B). These findings should be considered with a note of caution however, as the sample size is small.

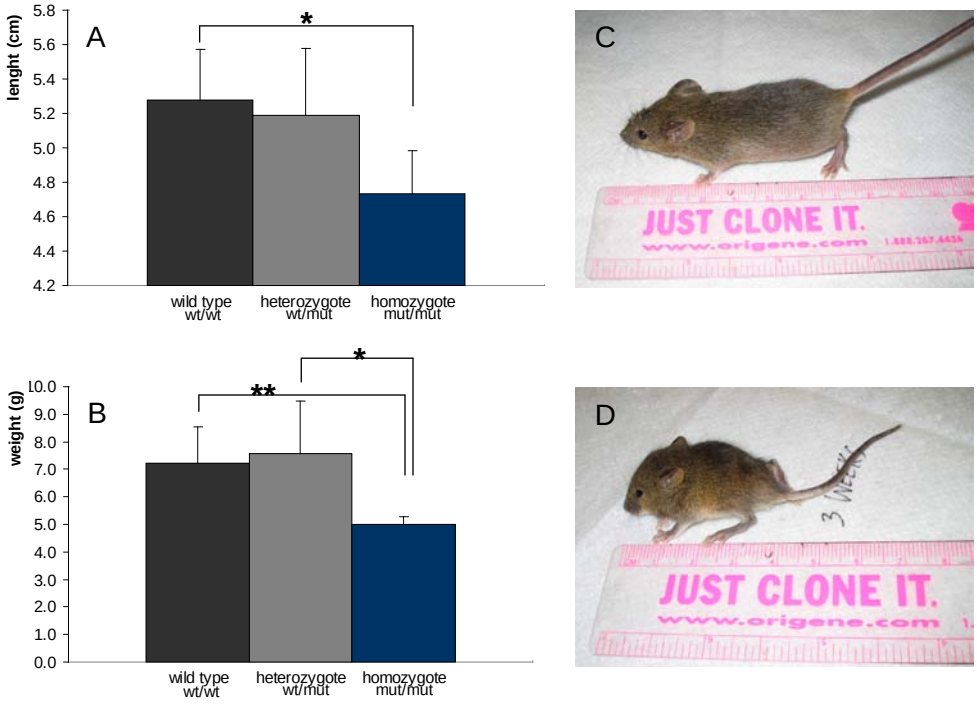

Figure 3.3. Length and weight measurements

Length (cm), nose to base of tail, and weight (g) measurements were taken from 3 week old littermates; wild type (*n*=7), heterozygote (*n*=9) or homozygote (*n*=3) for the disease causing mutation (raw data is given in appendix III). **A.** Length in centimeter (cm); average is represented by each bar, with standard deviation (SD) indicated. Homozygote mice (mut/mut) were significantly smaller in length than wild type (wt/wt) littermates, *p*=0.03. Difference in length between homozygous (mut/mut) and heterozygous (wt/mut) mice did not reach statistical significance, *p*=0.07. No difference was observed between (wt/wt) and (wt/mut) mice. (Mann-Whitney U test) **B.** Weight in gram (g); average is represented by each bar, with standard deviation (SD) indicated. Homozygote mice (mut/mut) were significantly less in weight compared to wild type (wt/wt), *p*=0.008, and heterozygote mice (wt/mut) , *p*=0.03. No difference was observed between (wt/wt) and (wt/mut) mice. (Mann-Whitney U test) **C, D.** Three week old unaffected mouse (C) and an affected littermate (D); note the small body size and abnormal body posture of the affected mouse compared to wild type.

3.3.4 Genetic mapping and characterization

3.3.4.1 Genetic background

A mutation arose spontaneously while generating transgenic *DJ1*$^{-/-}$ mice, resulting in a severe movement disorder. *DJ1* knockout mice were generated as a model for early onset familial parkinsonism using 129x1/SvJ ES cells (129x1/PJ5), containing the target construct, microinjected into blastocysts of a C57BL/6J background. Nonspecific integration of the construct was ruled out as a cause for disease using Southern blot analysis and vector specific PCR targeting of the *DJ1* transgene as described in Chandran et al. (2008).

3.3.4.2 Linkage analysis

To map the location of the disease causing mutation a crude genome wide linkage strategy was applied based on linkage to 120 fragments, each containing one or more C57BL/6J-129x1/SvJ strain specific single nucleotide polymorphisms (SNPs) (Lindblad-Toh et al. 2000). This effort entailed sequencing of 140 SNPs to obtain the genotypes for 18 mice for linkage analysis (unaffected mice, *n*=7; affected mice, *n*=11). A region of high linkage was assigned to chromosome 6, (+)105.3->146.4Mb, on the 129x1/SvJ background (see figure 3.4; appendix IV; table 3.1).

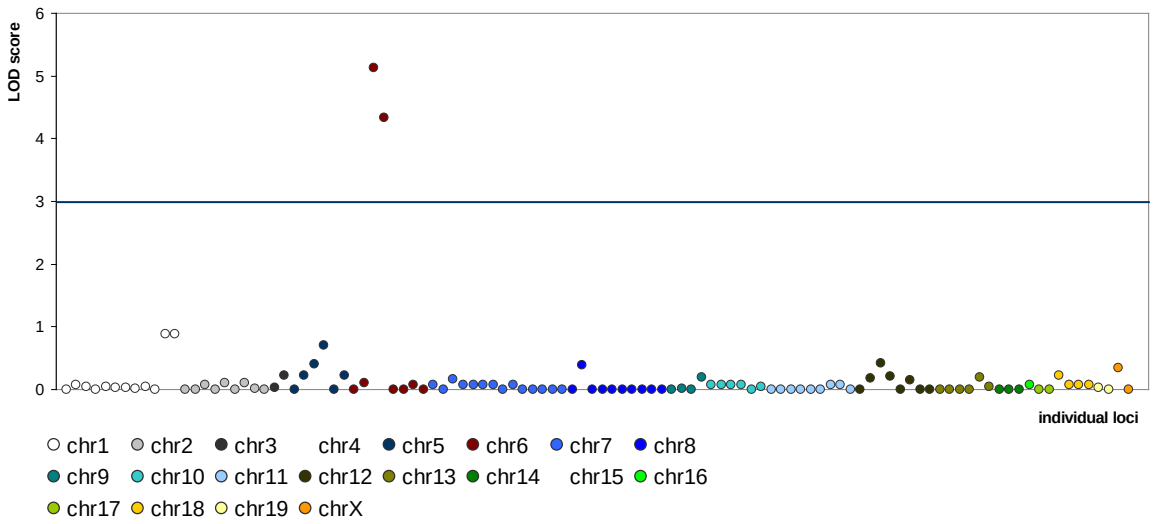

Figure 3.4. Linkage analysis plot, LOD scores for individual loci

X-axis; individual loci used for genotyping, shown in chromosomal and genomic order. Y-axis; maximum logarithm of odds (LOD) score for each locus as calculated using MLINK (multi-locus linkage analysis). LOD ≥3 considered evidence of linkage. chr, chromosome. Data given in appendix IV.

Locus	theta 0.01	theta 0.05	theta 0.10	theta 0.20	theta 0.30	theta max	max LOD score
28frh10	-11.70	-5.90	-3.50	-1.42	-0.51	0.50	0.00
84frb9	-2.92	-1.06	-0.41	0.03	0.11	0.29	0.11
85flg2	**4.88**	**5.10**	**4.78**	**3.75**	**2.49**	**0.04**	**5.13**
85flg5	**4.26**	**3.92**	**3.48**	**2.53**	**1.49**	**0.00**	**4.34**
25frb12	-11.08	-5.10	-2.80	-0.97	-0.31	0.50	0.00
27frg11	-12.86	-6.92	-4.01	-1.52	-0.49	0.50	0.00
94frg12	0.06	0.05	0.04	0.03	0.01	0.00	0.07
34fld3	-8.26	-3.61	-1.85	-0.51	-0.09	0.44	0.00

Table 3.1. LOD scores for loci on chromosome 6

LOD ≥3 considered evidence of linkage. In bold; SNPs demonstrating linkage to disease status, as measured by LOD scores≥3. Average LOD score for all SNPs across the entire genome was 0.14 ±0.46. Theta denotes recombination fraction, using MLINK (version 5.1) (Lathrop et al. 1984). LOD, logarithm of odds; max, maximum.

For finemapping, additional SNPs and microsatellites were used (NCBI database, build 34.1, www.ncbi.nlm.nih.gov/SNP/MouseSNP.cgi). SNP and microsatellite genotype data showed recombination events occurred within the initial linkage region, further delimiting the locus (figure 3.5). Recombination around marker 37.MMHAP17FRE10.seq (between markers D6Mit44 and 12.MMHAP34FLD3.seq) covered a genetic distance of approximately 14cM, estimated using the chromosome wide recombination rate for chromosome 6 of 0.45cM/Mb (Jensen-Seaman et al. 2004), and indicated this to be a likely event to have occurred over several meioses. However, a second recombination event around marker 06.MMHAP84FRB9.seq (between markers rs13478950 and rs13478951) only covered a genetic distance of approximately 0.2cM, based on the 0.45cM/Mb recombination rate for chromosome 6, and suggested this recombination to be less likely to have occurred. Marker 06.MMHAP84FRB9 was located outside the linkage block. Taken together, finemap data revealed linkage to the 129x1/SvJ background and narrowed down the region on chromosome 6 to approximately 5Mb between markers D6Mit37 (105531kb) and 44.MMHAP85FLG5.seq (110464kb) (figure 3.5).

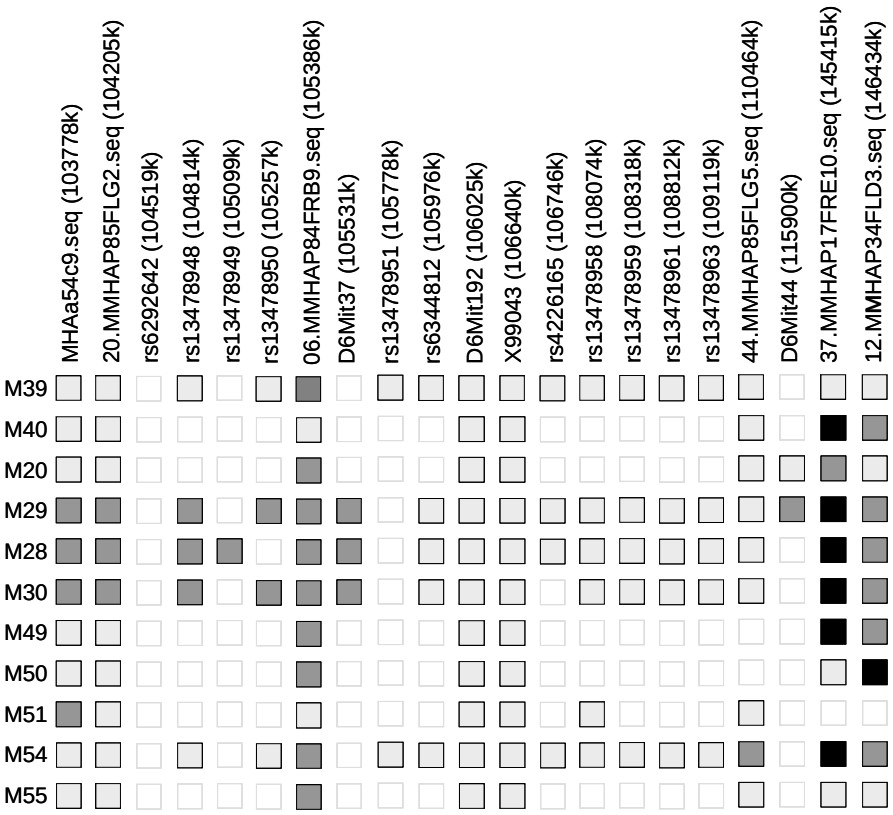

Figure 3.5. Schematic of genotyping results across mouse chromosome 6 in affected mice
Black squares are indicative of a C57BL/6J homozygous genotype; light grey squares, a 129x1/SvJ homozygous genotype; grey squares, a 129x1B6 heterozygous genotype; white squares, undetermined genotype. The critical region was determined to be between markers D6Mit37 and 44.MMHAP85FLG5. Marker locations based on mouse build 36.1.

NCBI mapviewer (mouse build 35.1) revealed this to be a gene poor region; comprising 11 genes and five unknown transcripts (figure 3.6). Genes were prioritized based on literature for information about function and associated pathways and findings from database searches for gene expression data, involvement in motoneuron pathways and/or expression in (neuro-)muscular tissue were regarded as high priority. *Lrrn1* (*leucine rich repeat protein 1, neuronal*), for example, was considered a likely candidate based on reported central nervous system expression and implication in neural development (Taguchi et al. 1996). On the contrary, *Il5ra* (*interleukin 5 receptor, alpha*) was considered an unlikely candidate as mice homozygous for disruptions in this gene displayed a generally normal phenotype with some immune system deficiencies (Mouse Genome Informatics (MGI) database, http://www.informatics.jax.org/strains_SNPs.shtml; The Jackson Laboratory).

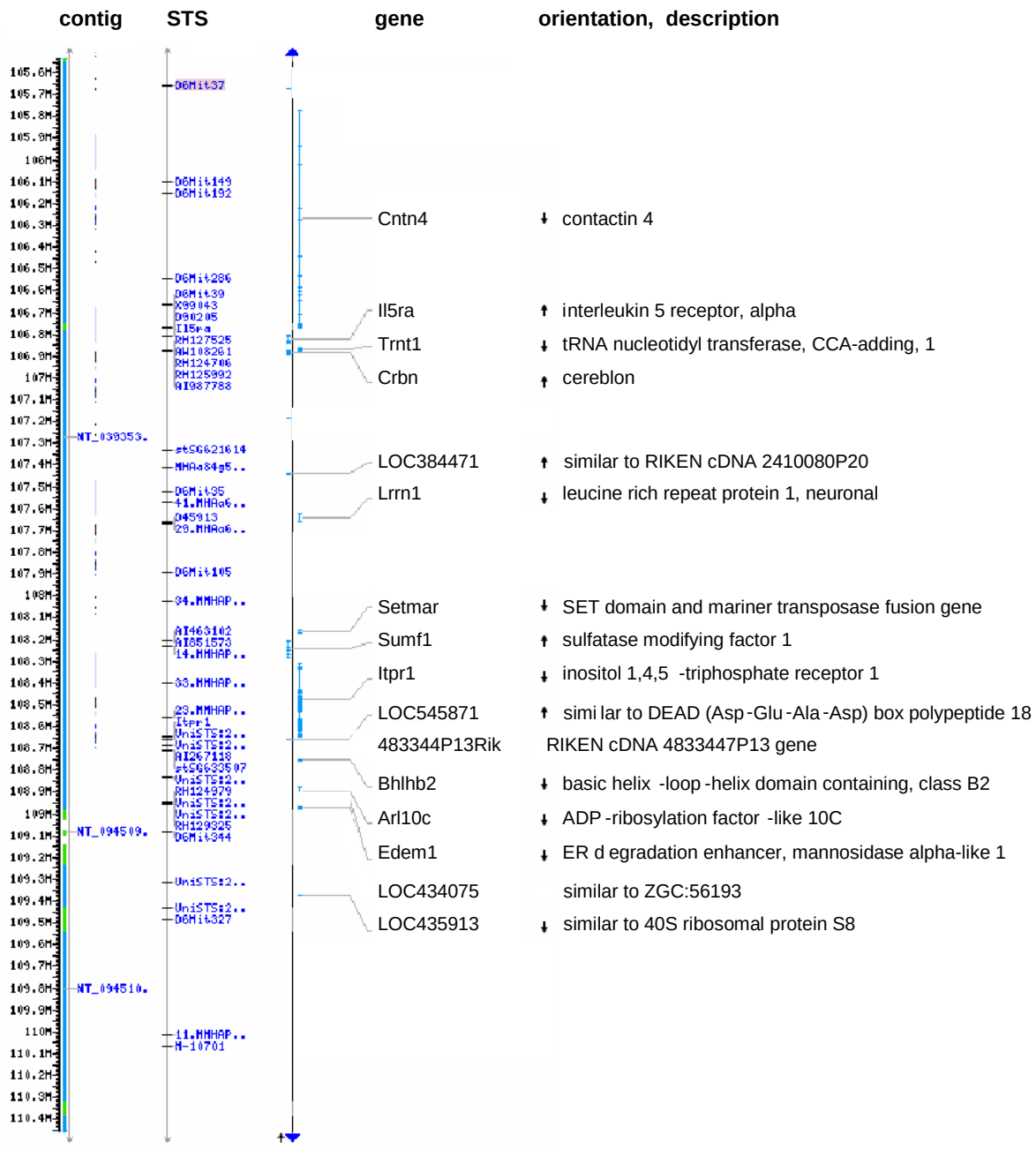

Figure 3.6. Mapview of genes comprised in the region of linkage on mouse chromosome 6 Linkage region (~5Mb) lies between markers D6Mit37 and 44.MMHAP85FLG5.seq, based on mouse build 35.1, and comprises 11 genes and five unknown transcripts (www.ncbi.nlm.nih.gov/mapview; build 34.1). STS, sequence tagged sites; NT_, RefSeq accession number of contig assembly produced by NCBI; M, mega base pairs.

3.3.4.3 Identification genetic cause

The gene with highest priority for candidacy was *Itrpr1* encoding inositol 1,4,5-triphosphate receptor type 1. The phenotype observed in the affected mice was strikingly similar to that of another model, *opisthotonos* (*opt*) which was first described in 1972 (Lane 1972) (table 3.3). The *opt* phenotype had been attributed to a homozygous in frame deletion of both exon 43 and 44 of the *Itpr1* gene (Street et al. 1997). Furthermore, the phenotype was similar, although less severe, to that described in a mouse line with targeted deletion of *Itpr1*, where ataxia was described as a prominent feature (Matsumoto et al. 1996) (table 3.3). To rule out the previously described mutation in *opt* mice as disease causing in affected mice of this study, mice were genotyped using primer pairs designed to span the full length of exon 43 and 44 as well as adjacent exon 42 and 45. The latter two were included to ensure DNA integrity. Visualisation of PCR products on an agarose gel showed all four exons were present and of expected size in affected (*n*=2) and unaffected (*n*=2) mice (figure 3.7) thereby ruling out the deletion described in *opt* mice as the cause of the movement disorder under study.

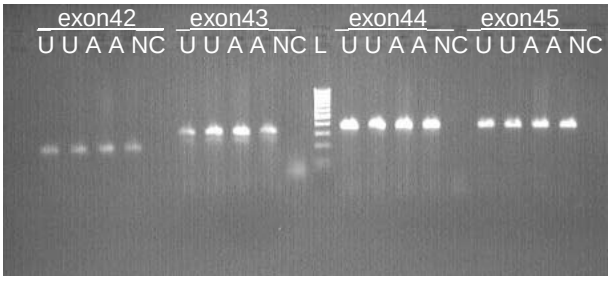

Figure 3.7. Gel image of genotype results for the *opisthotonos* (*opt*) mutation

O*pt* mouse phenotype is caused by a deletion of *Itpr1* exon 43 and 44. PCR primer pairs were designed to span the full length of exon 43 and 44, as well as, adjacent exon 42 and 45 (to ensure sample integrity). Primer sequences were as follows; exon 42, TTGTTTGTGACTGATGCTGAAG (forward), TCGTAGTTGTGTGGCTGAGG (reverse), 197bp product; exon 43, CCTGAATATCCTGTGTATGTGTG (forward), AAGCAAAAGCAGACAGCTCC (reverse), 313bp product; exon 44, GAGCATTAAAGGTTGGCACTTAG (forward), GTCTCCCTCCTGAGACCAAG (reverse), 361bp product; exon 45, CAGGCACTAATAAGCAGAATGG (forward), CCTGTTGGAACCTGGAAGC (reverse), 393bp product. PCR products were electrophoresed on a 2% agarose gel with ethidium bromide in 1xTBE. U, unaffected mouse; A, affected mouse; NC, no template control; L, GeneRuler 100bp DNA ladder plus (4µl of 0.1µg/µl; Fermentas).

As *Itpr1* could still harbor the disease causing mutation, the entire gene was sequenced for any changes segregating with disease. Initially samples from a wild type (C57BL/6J, 129x1/SvJ), a heterozygote (obligate carrier based on breeding, figure 3.1) and an affected mouse were sequenced, when a variation, possible mutation, was found additional samples from the mouse pedigree were screened. Sequencing of all 62 coding exons and intron-exon boundaries of *Itpr1* revealed a novel in frame deletion of 18bp within exon 36, resulting in a loss of six amino acids, ESCIRV (Glu-Ser-Cys-Ile-Arg-Val) (figure 3.8). The mutation was shown to segregate with the disorder based on absence of the deletion in the pure C57BL/6J and 129x1/SvJ parental strains, and findings of a wild type and a mutated copy of the gene in obligate heterozygotes (based on breeding experiments, figure 3.1) whereas all affected mice carried two mutated alleles. The affected mice have therefore been named *Itpr1*^{delta18}, and have been made publicly available at the MMRRC (mutant mouse regional resource centers; www.mmrrc.org) under strain name B6;129x1-*Itpr1*^{m1Asb} (inositol 1,4,5-triphosphate receptor 1 / mutation 1, Andrew B Singleton) or *Itpr1*^{delta18} (inositol 1,4,5-triphosphate receptor 1 / delta 18).

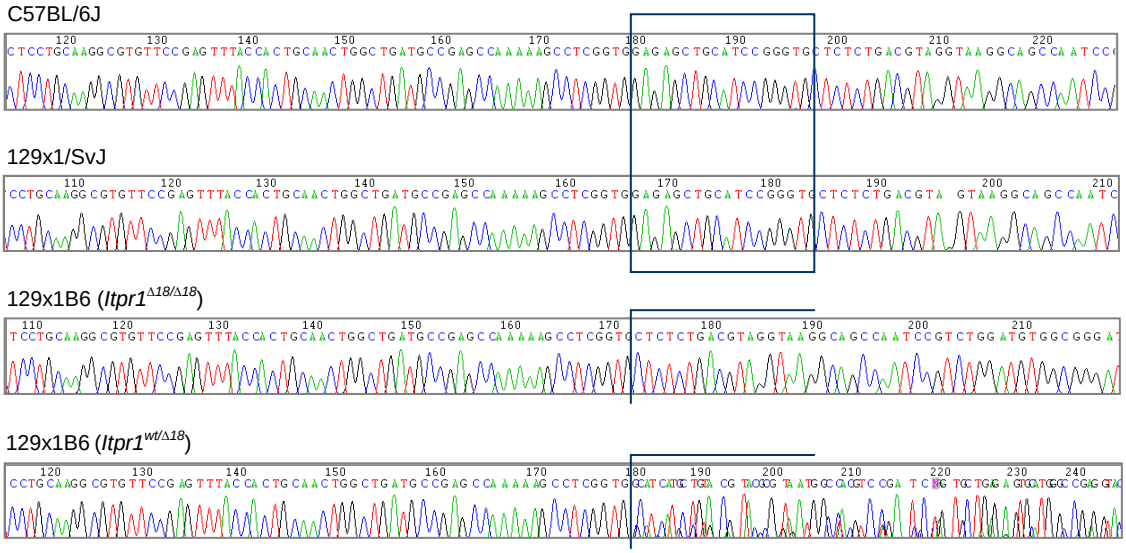

Figure 3.8. Genetic cause movement disorder in mice; 18bp in frame deletion *Itpr1*$_{exon36}$
Shown are partial sequences obtained for *Itpr1* exon 36 of a pure C57BL/6J mouse (*Itpr1*$^{wt/wt}$), a pure 129x1/SvJ mouse (*Itpr1*$^{wt/wt}$), an affected 129x1B6 mouse (*Itpr1*$^{\Delta 18/\Delta 18}$), and an unaffected 129x1B6 mouse heterozygous for the mutation (*Itpr1*$^{wt/\Delta 18}$). The deleted nucleotides are bounded by a dark blue box.

In order to rule out the deletion as a rare polymorphism, sequence data of *Itpr1* exon 36 were obtained from 24 different mouse strains; 129/ola, A, AKR, BALB, C3H, C57, CAST, CBA, DBA, FVB, Ju, MAI, MBT, MOLF, NZW, PWK, RIIIS/J, SEG, SJL, SMJ, SWR, WLA, WMP and VM. None of the strains carried the mutation (data not shown). In addition, conservation among species was determined based on protein sequence alignment using NCBI HomoloGene. The six deleted amino acids linked to the movement disorder were well conserved (table 3.2).

Mus musculus	1508	FVQLLQGVFRVYHCNWLMPSQKASV**ESCIRV**LSDVAKSRAIAIP	1551
Rattus norvegicus	1509	FVQLLQGVFRVYHCNWLMPSQKASV**ESCIRV**LSDVAKSRAIAIP	1552
Homo sapiens	1509	FVQLLQGVFRVYHCNWLMPSQKASV**ESCIRV**LSDVAKSRAIAIP	1552
Canis lupus familiaris	1516	FVQLLQGVFRVYHCNWLMPSQKASV**ESCIRV**LSDVAKSRAIAIP	1559
Bos taurus	1508	FVQLLQGVFRVYHCNWLMPSQKASV**ESCIRV**LSDVAKSRAIAIP	1551
Gallus gallus	1493	FVQLLQGVFRVYHCNWLMPSQKASV**ESCIRV**LSDVAKSRAIAIP	1536
Danio rerio	1485	FVQLLQGVFRVYHCSWLLPSQKGSV**ESCIKV**LSDVAKSRAIAIP	1528
Drosophila melanogaster	1611	FVQLLQAAHRITQCRWLSLGDRFNV**E**N**CIR**TLTESAKMRSIALP	1654
Anopheles gambiae	1557	FVKILQNSFKLTQCKGLTPSQRFNV**E**N**CIR**TLSEKAKPRGIAIP	1600

Table 3.2. Conservation deleted amino acids among species

Shown are partial amino acid sequences for ITPR1. Bold; amino acids deleted in exon 36 and linked to movement disorder in mice (ESCIRV, Glu-Ser-Cys-Ile-Arg-Val). Grey; amino acids different from *Mus musculus* sequence. Source; NCBI HomoloGene (accession numbers, see 2.1.3).

3.3.4.4 Cross-breeding opisthotonos

In order to confirm the mutation causing the movement disorder in this study lies on the same allele as the mutation for the *opisthotonos* phenotype, heterozygote *Itpr1*$^{wt/\Delta 18}$ females were crossbred with a heterozygote *opt* male B6C3Fe-*a/a*-^{Itpr1opt}/J obtained from JAX labs (http://jaxmice.jax.org/findmice/index.html). This resulted in two litters of mice with a total of 4 affected *Itpr1*$^{opt/\Delta 18}$ pups (from a total of 15) with a phenotype indistinguishable from the *Itpr1*$^{\Delta 18/\Delta 18}$ and *Itpr1*$^{opt/opt}$ mice (Street et al. 1997) (paragraph 3.3.3; table 3.3). These data not only showed unequivocally that *Itpr1* mutation underlies this movement disorder but also showed that both mutations have a similar mode of action.

	***Itpr1*$^{\Delta 18/\Delta 18}$ mouse**	***opt* mouse**	***tm1Tno* mouse**
mutation	spontaneous, deletion 18bp *Itpr1* exon 36, recessive	spontaneous, deletion exon 43-44 *Itpr1* , recessive	targeted knockout, exon1 *Itpr1* (homologous recombination; *neo, tk*)
onset	P14	P14	(P9) P15
phenotype	ataxic, loss of balance truncal torsions tonic/ tonic-clonic seizures	ataxic, loss of balance truncal torsions tonic/ tonic-clonic seizures	ataxic, loss of balance truncal torsions tonic/ tonic-clonic seizures
	smaller than littermates	smaller than littermates	smaller than littermates; body mass reduced to ~50%; overall brain size decreased ~40% in weight
	lifespan 3-4 wks	lifespan 3-4 wks	most *tm1Tno* pups die *in utero* P10; 5.5% of pups *tm1Tno* mice ; die by 3-4 wks of age
	gross anatomy cerebellum appears normal; no loss or overt morphological abnormalities of Purkinje cells	gross anatomy cerebellum appears normal; no loss or overt morphological abnormalities of Purkinje cells	gross anatomy cerebellum appears normal; no loss or overt morphological abnormalities of Purkinje cells
	heterozygotes, normal phenotype	heterozygotes, normal phenotype	heterozygotes, normal phenotype

Table 3.3. Comparison phenotype *Itpr1*$^{\Delta 18/\Delta 18}$, *opisthotonos* (*opt*) and *tm1Tno* mice

P, postnatal day; wks, weeks; *neo*, *neomycin*; *tk*, thymidine kinase. (Matsumoto et al. 1996;Street et al. 1997;van de Leemput et al. 2007)

3.3.5 Molecular characterization

3.3.5.1 ITPR1 protein expression in mouse cerebellum

Immunohistochemistry

To study the effect of the 18bp *Itpr1* deletion at the protein expression level in mouse brain, ITPR1 immunohistochemistry data were obtained from three week old littermates (129x1B6) with wild type *Itpr1*, or heterozygous or homozygous *Itpr1*$^{\Delta 18}$. Experimental control data obtained to determine antibody specificity are given in appendix V. Sagittal sections showed lower levels of ITPR1 expression in cortical and hippocampal areas, and high expression levels in cerebellum (Plan-Apochromat 5x/0.16; Carl Zeiss). Cerebellar staining was shown to be exclusive to expression in the Purkinje cells (figure 3.9; A,B,C). Immunohistochemistry for ITPR1 revealed a diminished and almost complete loss of ITPR1 protein in cerebellar Purkinje cells from mice heterozygous and homozygous for the mutation in *Itpr1* respectively, compared to wild type staining (figure 3.9; A,B,C). It should be noted, the epitope of the ITPR1 antibody used consisted of the last 20 amino acids at the C-terminal end of the protein (Swiss protein number, mouse P11881). Therefore any truncated ITPR1 protein, due to the mutation, that might be present would not have been detected with these experiments. Unfortunately, no ITPR1 antibody targeted N-terminal of the 18bp deletion was commercially available. Staining for calbindin was used to control for tissue integrity and demonstrated no overt structural changes or loss of Purkinje cells in any of the samples studied (figure 3.9; D,E,F).

Figure 3.9. Immunohistochemistry of ITPR1 protein levels in 3wk old mouse cerebellum
Immunohistochemistry of cerebellum from three week old littermates (129x1B6; *n*=3); wild type (**A, D**), mouse heterozygous for the *Itpr1* 18bp deletion (**B, E**) and mouse homozygous for the 18bp *Itpr1* deletion (**C, F**). **A, B, C.** Immunohistochemistry using polyclonal ITPR1 anti-rabbit antibody (1:2000, Chemicon; secondary antibody, Alexa Fluor 555, 1:2000, Invitrogen). ITPR1 is shown to be highly expressed in the cerebellar Purkinje cells. Immunoreactivity to ITPR1 is clearly decreased in the heterozygous and homozygous mutant mice compared to wild type. **D, E, F.** Immunohistochemistry using monoclonal calbindin anti-mouse antibody (1:6000, Sigma; secondary antibody, Alexa Fluor 488, 1:3000, Invitrogen). Tissue integrity and absence of overt structural changes is demonstrated by similar calbindin staining in *Itpr1*$^{wt/wt}$, *Itpr1*$^{wt/\Delta 18}$ and *Itpr1*$^{\Delta 18/\Delta 18}$ mice. (Plan-Apochromat 5x/0.16; Carl Zeiss) Scale bars denote 100µm. **(figure 3.9, *on next page*)**

(figure 3.9, *continued from previous page*)

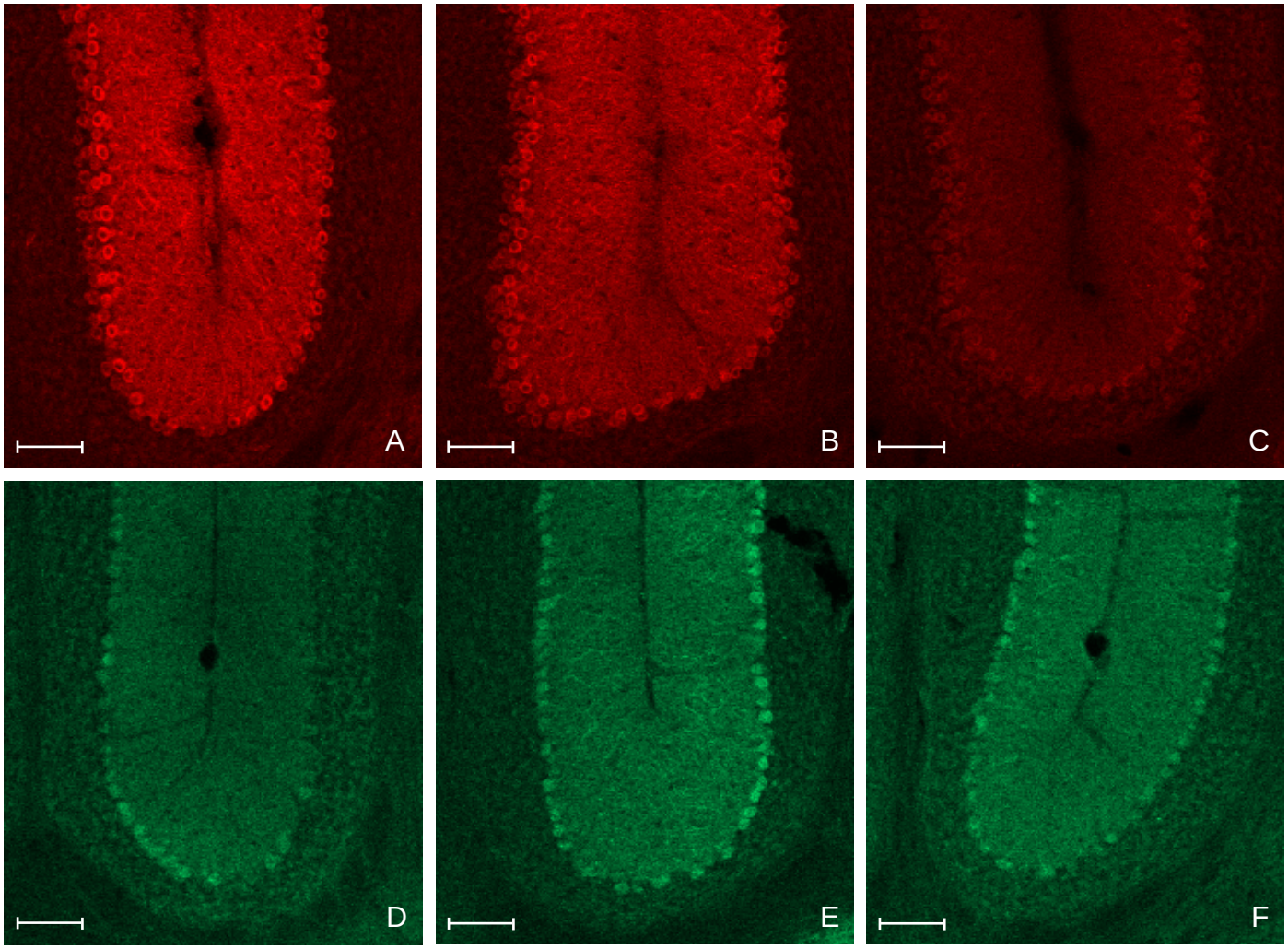

Western blot analysis

Western blot analysis for ITPR1 using whole brain RIPA buffer (1%SDS) protein extracts from 33 day old littermates (129x1B6), confirmed immunohistochemistry data by showing a decrease and almost total lack of ITPR1 protein in *Itpr1*$^{wt/\Delta 18}$ and *Itpr1*$^{\Delta 18/\Delta 18}$ mice respectively, compared to wild type (figure 3.10). Multiple bands were labeled by the ITPR1-specific antibody, one possible explanation could be the presence of alternative splice variants of type 1 inositol 1,4,5-triphosphate receptor and/ or their effect on post-translational modicification of the protein. ITPR1 has three well characterized splice sites; SI, SII, SIII (Nucifora et al. 1995) (figure 3.11). No difference was detected in amount of sample loaded as was demonstrated by equal expression of beta-actin in all samples (figure 3.10). Immunohistochemistry and western blot data corresponded with the decreased levels of ITPR1 expression described in *Itpr1*$^{opt/opt}$ and *tm1Tno* mice (Matsumoto et al. 1996;Street et al. 1997).

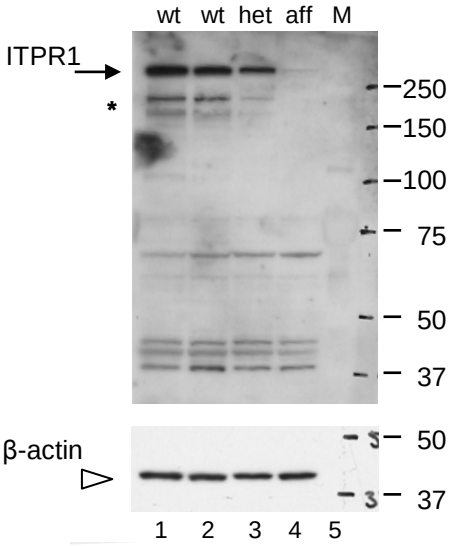

Figure 3.10. Western blot analysis of ITPR1 protein levels in mouse whole brain

Western blot performed to examine ITPR1 levels in whole brain RIPA buffer (1%SDS) protein extracts from 33 day old mice (129x1B6; *n*=4): wt, wild type, *Itpr1*$^{wt/wt}$; het, heterozygote, *Itpr1*$^{wt/\Delta 18}$; aff, affected, *Itpr1*$^{\Delta 18/\Delta 18}$. Data clearly showed a reduction of ITPR1 in brain tissue from *Itpr1*$^{wt/\Delta 18}$ mice and almost total absence of ITPR1 in *Itpr1*$^{\Delta 18/\Delta 18}$ mice. **Top panel**, shows ITPR1 levels (black arrow; ITPR1 314kD (1:1,000) polyclonal ITPR1 anti-rabbit antibody, Chemicon; secondary antibody, donkey anti-rabbit (1:5,000), Jackson ImmunoResearch). The asterisk signifies bands that might represent alternative splice variants of ITPR1. The lower bands appear to be unspecific. **Lower panel**, shows beta-actin expression levels, as a control for equal sample loading (arrow head; beta-actin 42kD (1:10,000) monoclonal mouse anti-(beta-actin) antibody, Sigma; secondary antibody, donkey anti-mouse IgG (1:5,000), Jackson ImmunoResearch). M, marker, precision plus protein dual color standard (Biorad).

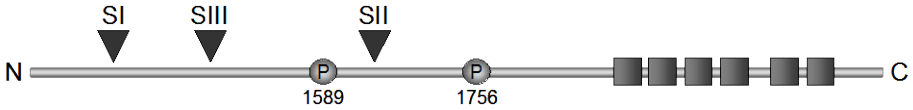

Figure 3.11. *ITPR1* alternative splice sites; SI, SII, SIII

SI splicing region is 15 amino acids long and located in the IP3 type 1-binding domain (aa318-332). SII splicing region is 40 amino acids long and located in the coupling domain between the two consensus PKA (protein kinase A) sites (aa1693-1732). SIII splicing region is nine amino acids long and located in the coupling domain (aa903-912). N, amine (-NH_2) terminus; C, carboxyl (-COOH) terminus; P, phosphorylation site; boxes, represent the membrane spanning, channel region; aa, amino acid. Adapted from Nucifora et al. (1995).

Western blot analysis of fractionated extraction of ITPR1 protein from mouse cerebellum was carried out to augment previous protein expression data by taking into account differences in extraction that might arise due to possible alterations in folding of mutant protein, as well as, focusing on cerebellar tissue as ITPR1 has been shown to be mainly expressed in Purkinje cells (Matsumoto et al. 1996) (figure 3.9). TBS fractions, containing cytoplasmic proteins, demonstrated no ITPR1 protein expression. Whereas both TBS-Tx100, membrane-bound soluble, and TBS-SDS, membrane-bound insoluble, fractions showed a similar pattern of ITPR1 expression; expression in wild type, lower expression levels in heterozygotes (*Itpr1*$^{wt/\Delta 18}$) and very low to almost non-detectable expression in *Itpr1*$^{\Delta 18/\Delta 18}$ mice (figure 3.12). Multiple bands were labeled by the ITPR1-specific antibody, one possible explanation could be the presence of alternative splice variants of type 1 inositol 1,4,5-triphosphate receptor (Nucifora et al. 1995) (figure 3.11). Discrepancy in sample loading was controlled for by staining for neurofilament (NF-160). A low level of NF-160 expression can be seen in protein extracted using TBS, no expression is seen in TBS-Tx100 extracted protein (band in wild type TBS-Tx100 (6) might be due to spillage adjacent lane (5) TBS wild type), and high level of expression is shown in protein extracted with TBS-SDS buffer (figure 3.12). Neurofilament is known to be mostly present as insoluble protein.

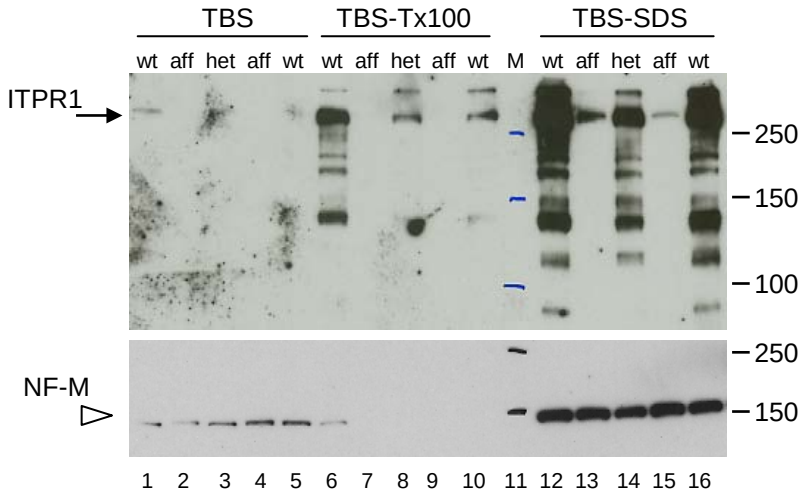

Figure 3.12. Western blot analysis of ITPR1 protein in mouse cerebellum
Three week old littermates (129x1B6; *n*=5) were used: wt, wild type, *Itpr1*$^{wt/wt}$; het, heterozygote, *Itpr1*$^{wt/\Delta 18}$; aff, affected, *Itpr1*$^{\Delta 18/\Delta 18}$ mice. **Top panel**, shows ITPR1 levels in the different cerebellar fractions (black arrow; ITPR1 314kD (1:1,000) polyclonal ITPR1 anti-rabbit antibody, Chemicon; secondary antibody, donkey anti-rabbit (1:5,000), Jackson ImmunoResearch). **Lower panel**, shows anti-neurofilament expression as loading control (arrowhead; NF-M, 160kD (1:1,000) monoclonal mouse anti-neurofilament 160, medium polypeptide, Sigma; secondary antibody, donkey anti-mouse IgG (1:5,000), Jackson ImmunoResearch). TBS (tris-buffered saline), 1xTBS; TBS-Tx100 (tritonX-100), 1xTBS-1%Triton; TBS-SDS (sodium dodecyl sulfate), 1xTBS-5%SDS; M, precision plus protein dual color standard (Biorad).

The expression patterns are different in the crude and fractioned ITPR1 extraction western blots (figure 3.10 and 3.12 respectively), this is likely due to different tissue samples (crude versus fractionated extraction, whole brain versus cerebellum), different ages of the mice (33 versus 21 days) and/or different western blot system (MOPS electrophoresis and NuPage transfer buffers versus TGS electrophoresis and CAPS transfer buffers) used.

It should be noted, the epitope of the ITPR1 antibody used consisted of the last 20 amino acids at the C-terminal end of the protein (Swiss protein number, mouse P11881). Therefore any truncated ITPR1 protein, due to the mutation, that might be present would not have been detected with these experiments. Unfortunately, no ITPR1 antibody targeted N-terminal of the 18bp deletion was commercially available.

3.4 DISCUSSION

A novel 18bp in frame deletion in exon 36 of the gene encoding inositol 1,4,5-triphosphate receptor type 1 was identified to underlie a severe young onset autosomal recessive movement disorder in mice (*Itpr1*$^{\Delta 18/\Delta 18}$). The *Itpr1*$^{\Delta 18/\Delta 18}$ phenotype was found to be indistinguishable from that of *opisthotonos* mice, which has been attributed to an in frame deletion of *Itpr1* exon 43 and 44, both are spontaneous recessive disorders (Lane 1972;Street et al. 1997). Affected mice never acquire normal locomotor activity; early in locomotor development hind limbs often slip or are dragged, as development progresses adult-like walking with lifting of hind limbs should begin and locomotor speed should increase, however mice with homozygous mutation in *Itpr1* never reach this stage. Disease onset is around P14, characterized by loss of balance, truncal torsions and ataxic-like tonic/ tonic-clonic seizures, disease is progressive and lifespan ranges from 3-4 weeks. Interestingly, based on initial observation, heterozygotes of either model do not display any of the disease-related features. *Itpr*$^{opt/\Delta 18}$ mice, generated by cross-breeding heterozygote *Itpr*$^{wt/\Delta 18}$ females with a heterozygote male *Itpr*$^{wt/opt}$, displayed a phenotype indistinguishable from homozygous *Itpr*$^{\Delta 18/\Delta 18}$ and *opt* mice as described (Street et al. 1997), indicating mutations in *Itpr*$^{\Delta 18/\Delta 18}$ and *Itpr*$^{opt/opt}$ mice are allelic. Furthermore, the above phenotype is similar, although less severe, to that described in a mouse line with targeted deletion of *Itpr1*, *tm1Tno*; where most *Itpr1*-deficient mice die *in utero*, live pups have severe ataxia and tonic/ tonic-clonic seizures and die around weaning time alike *opt* and *Itpr*$^{\Delta 18/\Delta 18}$ mice (Matsumoto et al. 1996).

ITPR1, a polypeptide of 2749 residues, contains five functionally distinct regions; an N-terminal domain which contains a suppressor region (1-225) and is capable of binding IP3 (226-576), a transmembrane channel-forming region (2277-2590) and coupling domain (2591-2749) both located to the C-terminus, and a regulatory segment connecting the two termini (577-2276) (Foskett et al. 2007) (figure 3.13). ITPR1 is coupled to Ca^{2+} channels and facilitates Ca^{2+} release from the endoplasmic reticulum after binding by the intracellular second messenger inositol 1,4,5-triphosphate (Matsumoto and Nagata 1999). The central region of ITPR1 is also referred to as the transducing domain, for being involved in transferring a signal from the N-terminal ligand-binding region to the channel portion at the C-terminus of the receptor, or as the modulatory domain, for binding numerous molecules implicated in receptor regulation. Small molecules, such as Ca^{2+} and ATP, as well as, proteins, such as CaM, FKBP12,

CARP, G*β*/Rack1 and Caspase3, have been suggested to bind to the modulatory and transducing domain. Phosphorylation sites for PKA, PKC, PKG, CaMKII have also been mapped in this region (Patterson et al. 2004). The *Itpr1*$^{\Delta 18}$ mutation (1533-1538) is located in the carbonic anhydrase-related protein (CARP)-binding site of ITPR1. CARP is a member of the carbonic anhydrase (CA) family, based on its high similarity in sequence although it lacks catalytic activity due to absence of a zinc-binding domain. The function of CARP remains unknown. Although CARP binding of ITPR1 has been shown to inhibit IP3-ligand binding, essential for channel activation, suggesting CARP to act as an ITPR1 antagonist (Hirota et al. 2003).

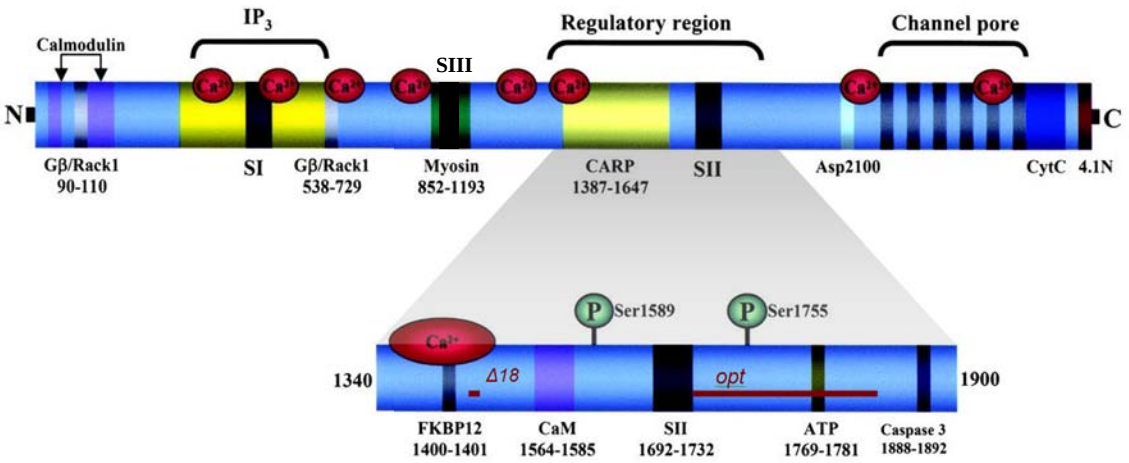

Figure 3.13. Schematic representation of the domain architecture of ITPR1

ITPR1 is structurally divided into five functionally distinct segments (Foskett et al. 2007). The N-terminal domain containing a suppressor region (aa1-225) and IP3-binding site (aa226-576), which together with the regulatory domain (aa577-2276) form the cytoplasmic protein structure (~80% of full length). The transmembrane channel forming domain (aa2277-2590; ~10% of full length protein) is located towards the C-terminus. The coupling region (aa2591-2749) makes up the C-terminal tail. In red, the *Itpr1*$^{\Delta 18}$ (*Δ18*; aa1533-1538) and *opisthotonos* (*opt*; aa1732-1839) mutations. N, amine (-NH_2) terminus; C, carboxyl (-COOH) terminus; IP3, inositol 1,4,5-triphosphate; Ca^{2+}, calcium binding site; P, phosphorylation site; SI, splicing region I (aa318-332); SII, splicing region II (aa1693-1732); SIII, splicing region III (aa903-912); aa, amino acid (numbers given); Gβ/Rack1, G*β* homologue receptor for activated C kinase-1; CARP, carbonic anhydrase-related protein; Asp, aspartic acid; CytC, cytochrome *c*; 4.1N, 4.1N protein; FKBP12, FK506-binding protein (12kDa); CaM, calmodulin, calcium modulating protein; ATP, adenosine triphosphate. Adapted from Patterson et al. (2004).

ITPR1 is the major neuronal member of the ITPR (alias IP3R, P400) family in the CNS, and is predominantly enriched in cerebellar Purkinje cells but also concentrated in neurons in the hippocampal CA1 region, caudate putamen and cerebral cortex, and hence is essential for proper brain function (Nakanishi et al. 1991). As demonstrated by immunohistochemistry and western blot analysis, ITPR1 protein levels are dramatically decreased resulting in an almost total lack of expression in *Itpr1*$^{\Delta 18/\Delta 18}$ mouse cerebellum compared to *Itpr1* wild type mice, with heterozygote *Itpr1*$^{wt/\Delta 18}$ mice showing intermediate expression. The deletion, even though in frame, might result in changes in the tertiary structure of the protein, known to be critical in ITPR functioning. Structural data suggest subtle conformational changes are sufficient in regulating channel gating (Patterson et al. 2004). Misfolded, dysfunctional protein might be subject to clearance by the molecular chaperones, ubiquitin-dependent proteasome and/or autophagy pathways (Duenas et al. 2006), subsequently resulting in the observed, dramatically reduced protein levels in *Itpr1*$^{\Delta 18}$ mice.

Despite clearly reduced ITPR1 protein levels in the cerebellum, electrophysiological studies showed a strong calcium response could still be elicited from intracellular calcium stores in Purkinje neurons from *opt* mice, however, calcium response to repeated QA (quisqualate, IP3-agonist) application showed less attenuation in homozygote *opt* mice compared to wild type littermates (Street et al. 1997). These findings and the observation that *Itpr1*$^{\Delta 18}$ and *opt* mice demonstrated an indistinguishable phenotype although caused by different mutations, deletion of amino acids 1533-1538 and 1732-1839 of the ITPR1 modulatory domain respectively, suggest alterations in the structure of ITPR1 protein to be a less likely explanation for the observed phenotype. An alternative explanation would be functional insufficiency resulting in a change in the ratio of ITPR1 and RyR (ryanodine receptor) in the Purkinje cell membranes, and possibly other proteins that regulate the calcium balance across the endoplasmic reticulum membrane, such as the calcium pump, luminal calcium-binding molecules and other luminal and cytosolic accessory proteins, thereby changing properties of release from IP3-sensitive calcium stores and eventually affecting downstream regulations. This concept is consistent with findings by Hernandez and colleagues (2007) showing the subcellular distribution of ITPR isoforms may critically determine the repertoire of spatial patterns of Ca^{2+} signals, and the observation of clearly diminished ITPR1 expression shown in the cerebellum of mice with mutation in *Itpr1* by western blot and immunohistochemistry (paragraph 3.3.5) (Street et al. 1997). Moreover, mice heterozygous for *Itrp1* mutation appear to

be functionally indistinguishable from wild type littermates even though clearly reduced ITPR1 protein expression levels have been shown in their cerebellum. Heterozygote *Itpr1*$^{\Delta 18}$ and *opt* mice displayed no obvious abnormalities in their motor behavior (Street et al. 1997;van de Leemput et al. 2007). Heterozygous *tm1Tno* mice on the other hand, have been described to demonstrate impaired motor coordination on a rotating rod at two months of age, although otherwise showing no abnormalities in spontaneous motor activity, muscle strength or walking patterns (Ogura et al. 2001).

Studying *Itpr*$^{\Delta 18}$ mice in addition to the current models *opt* and *tm1Tno*, will aid in gaining a deeper understanding of the role of ITPR1 in calcium regulation in the brain, which will eventually lead to more insight of calcium dysregulation underlying movement disorders.

3.5 CONCLUSION

A novel mutation in the gene encoding inositol 1,4,5-triphosphate receptor type 1 underlies a severe young onset autosomal recessive movement disorder in mice. The 18bp in frame deletion in *Itpr1* exon 36 was shown to be allelic to that of another model, *opisthotonos* (*opt*) which was first described in 1972 (Lane 1972) and has been attributed to an in frame deletion of both exon 43 and 44 in the *Itpr1* gene (Street et al. 1997). The *Itpr1*$^{\Delta 18}$ mutation results in a decreased to an almost complete lack of ITPR1 protein expression in heterozygote and homozygote mutant mouse cerebellum respectively.

CHAPTER 4 MOLECULAR GENETIC CHARACTERIZATION OF *SCA15* IN HUMANS

4.1 CHAPTER AIM

To identify the genetic cause of spinocerebellar ataxia (SCA) 15 in humans and characterize the disease-causing gene(s).

4.2 INTRODUCTION

Discovery that a recessive deletion in the gene encoding inositol 1,4,5-triphosphate receptor type 1 causes a severe movement disorder in mice led to a search for an equivalent disorder in humans. Literature was searched for a calcium-sensitive channelopathy associated with human 3p26, the syntenic region to 6(+) 108.2-108.5Mb of the mouse genome, but where no causal mutation had been identified. SCA15, an adult-onset autosomal dominant progressive ataxia had been linked to this region, human 3p24.2-3pter (Storey et al. 2001;Knight et al. 2003). Missense mutation of *ITPR1* had previously been ruled out (Knight et al. 2003), the mode of inheritance was inconsistent with that seen in *Itpr1*$^{\Delta 18/\Delta 18}$ and *opt* mice (Street et al. 1997) and ataxic mouse models showed no signs of cerebellar atrophy. However, the phenotypic presence of ataxia in the mice, and a correlation between mode of inheritance and disease progression led to a re-examination of this candidate gene as a possible cause of SCA15. This study was undertaken in collaboration with MA Knight and colleagues, authors of the paper describing identification of the *SCA15* locus (Knight et al. 2003).

4.3 BACKGROUND

Work described in papers on SCA15 by MA Knight and colleagues has been included for completion of this chapter and has been clearly indicated as such (Storey et al. 2001;Knight et al. 2003).

4.3.1 Phenotypic characterization SCA15

SCA15, as first described in an Australian kindred (Storey et al. 2001) (figure 4.1), is an autosomal dominant cerebellar ataxia type III (ADCA III). Ages of onset range from mid-childhood to middle age and a very slow progression of disease has been observed. The phenotype is that of a 'pure' cerebellar ataxia, characterized by a mild degree of gait ataxia, a pattern of gaze-evoked nystagmus ± rebound, and brisk lower limb reflexes (table 4.1). MRI brain scans show atrophy of the cerebellar vermis, more so superiorly and dorsally, the appearance of the brainstem remaining normal (figure 4.2).

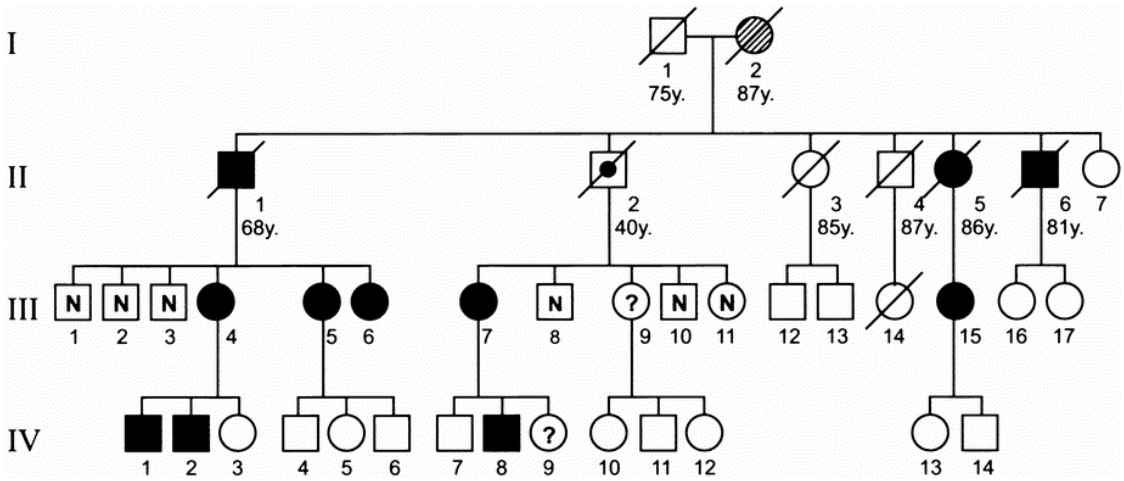

Figure 4.1. Pedigree of SCA15 kindred (AUS1)

Filled symbols denote affected individuals (based on clinical examination or unequivocal family report); open symbols unexamined, unaffected individuals by family report; bullseye symbol denotes obligate carrier, reportedly had been asymptomatic; ? if uncertain affected status; N, no symptomatology, no signs of cerebellar disease on examination; hatched, anecdotal information suggests affected; diagonal line deceased (ages at death shown); y, years of age; square, male; circle, female. No offspring are shown of those formally examined and found unaffected. None is shown of generation V, being children or young adults, and none suspected of being affected, according to family reports. No indicative history is known antecedent to I1 and I2. Reproduced from Storey et al. (2001).

clinical data	no. of affected patients (of 7)
gait ataxia	5
limb ataxia	6
dysarthria	5
dysphagia	2 (?3)
nystagmus, gaze-evoked	3
dysmetric saccades	3
VOR gain <1	3
failure to suppress VOR	4
brisk lower limb reflexes	3
titubation	2
postural tremor	1
age at onset, y, mean (range)	26 (10-50)
age at current assessment, y, mean (range)	56 (39-69)
duration of symptoms, y, mean (range)	29 (10-54)

Table 4.1. Clinical features as observed in SCA15 kindred during neurological examination

Dysarthria, difficulty in articulating words; dysphagia, difficulty in swallowing; nystagmus, a rapid, involuntary, oscillatory motion of the eyeball; saccades, a rapid intermittent eye movement, as that which occurs when the eyes fix on one point after another in the visual field; VOR, vestibulo-ocular reflex, a reflex eye movement that stabilized images on the retina during head movement; titubation, a disturbance of body equilibrium in standing or walking, resulting in an uncertain gait and trembling. ?, questionable in one subject; no, number; y, years. Adapted from Storey et al. (2001).

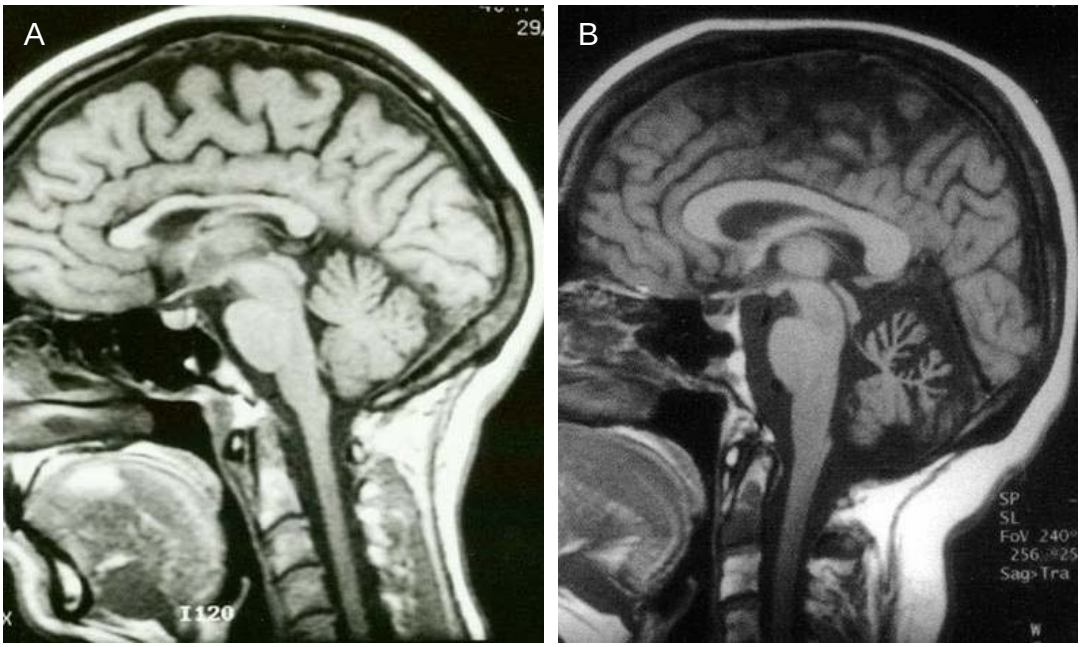

Figure 4.2. Images MRI brain scan of a healthy control and a SCA15 patient

Representation of midline sagittal MRI (magnetic resonance imaging) brain scan. **A.** Healthy control. **B.** SCA15 patient (age 62 years, subject III15, figure 4.1). The cerebellar atrophy disproportionately affects the vermis, more so superiorly and dorsally. The appearance of the brainstem is normal. (MA Knight (NINDS/NIH), personal communication).

4.3.2 Genetic characterisation SCA15

4.3.2.1 Linkage analysis SCA15

Knight and colleagues (2003) performed a genome wide linkage screen using 383 microsatellite markers from the ABI prism linkage mapping set (version 2) at a marker density of 10cM. Linkage analysis was carried out using MLINK (multi-locus linkage analysis of the LINKAGE package, version 5.1; (Lathrop et al. 1984), under the assumptions of autosomal dominant transmission of *SCA15*, 90% penetrance by age 50, disease allele frequency of 0.00002 with 0% phenocopy rate, equal marker allele frequencies, and non sex-linked. Initial genome wide analysis indicated linkage to chromosome 3p with a maximum LOD score of 2.95 at a recombination fraction (θ) of 0.00 obtained at marker D3S1304.

Fine mapping was performed by using 10 additional microsatellite markers on chromosome 3p selected through the Genome Database. Multipoint linkage analysis, using LINKMAP (LINKAGE package, version 5.1; (Lathrop et al. 1984), supported linkage of *SCA15* to 3p24.2-3pter, with a maximum LOD score of 3.54 for marker D3S1560 (figure 4.3).

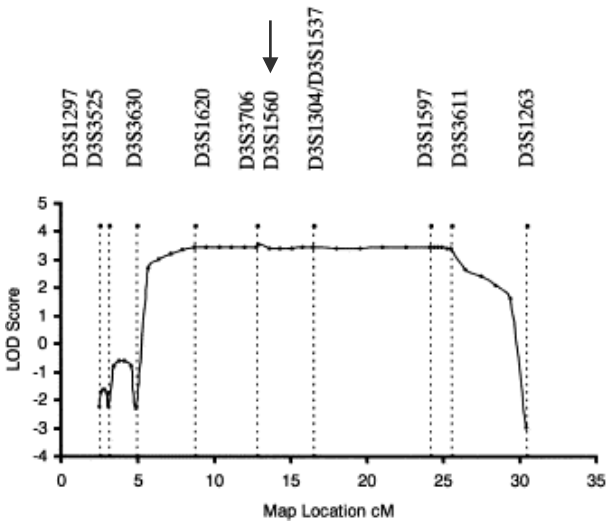

Figure 4.3. Multipoint LOD score analysis of *SCA15*

Multipoint LOD scores plotted against genetic location, defined as distance in cM from telomere of chromosome 3p. A maximum multipoint LOD score of 3.54 was obtained for D3S1560 at 12.9cM (arrow). Markers used in the multipoint analysis are indicated. Adapted from Knight et al. (2003).

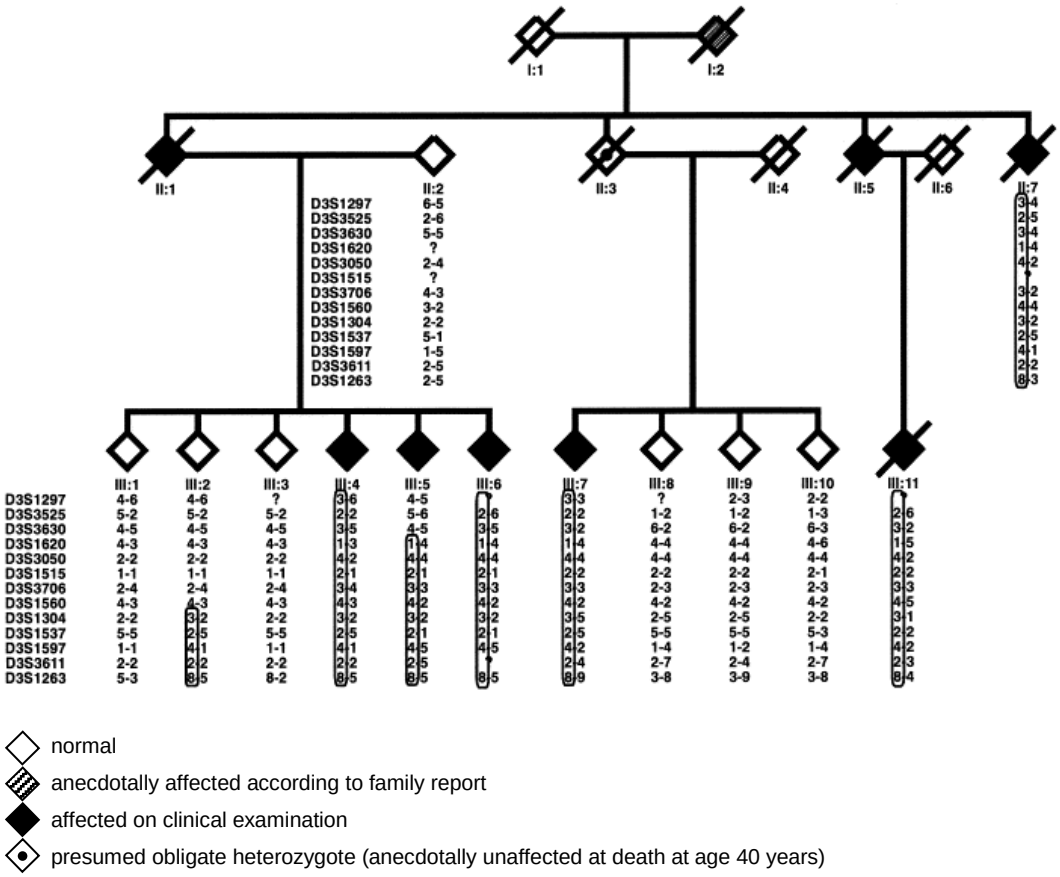

Figure 4.4. Haplotype blocks in pedigree of AUS1 *SCA15* kindred

Haplotypes for 13 microsatellite markers spanning ~30cM on chromosome 3-24.2-3pter are shown. The haplotype segregating with disease is boxed. To preserve the confidentiality of the family members, the sex of the individuals was omitted and the data from individuals in generation IV have not been published, but were included in the analysis. Adapted from Knight et al. (2003).

Haplotype analysis showed co-segregation with disease at the linked locus (figure 4.4). Informative recombination in family members III-2 and III-5 enabled narrowing down the candidate region. The distal recombination site lies between D3S3630 and D3S1620 as observed in individual III-5. Individual III-2, who at age 71 years showed no cerebellar symptoms and was normal based on focussed neurological examination, carried part of the disease haplotype with a recombination occurring between D3S1560 and D3S1304. Assuming full penetrance of the disease, the candidate region was refined to an 11.6cM interval between D3S3630 and D3S1304. The 11.6cM *SCA15* locus on 3p24.2-3pter was found to be extremely gene poor,

containing only nine known genes based on the June 2002 human genome sequence freeze (build 30 (hg12), http://genome.ucsc.edu; figure 4.5).

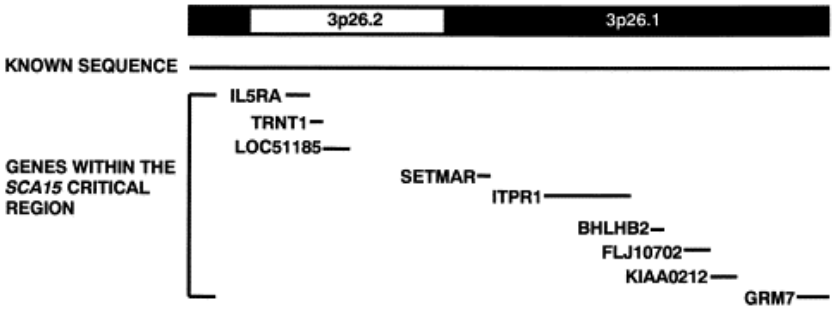

Figure 4.5. Genes mapping to the *SCA15* locus, human build 30 (hg12) June 2002
Schematic diagram adapted from the UCSC Genome Browser on Human June 2002 Freeze of chromosome 3 showing the nine know genes that map to the SCA15 critical region: *IL5RA*, *interleukin 5 receptor, alpha*; *TRNT1*, *tRNA nucleotidyl transferase, CCA-adding, 1*; LOC, hypothetical protein in which orthologs have not yet been determined; *SETMAR*, *SET domain an mariner transposase fusion gene*; SET domain, [Su(var)3-9, Enhancer-of-zeste, Trithorax] domain, a protein lysine methyltransferase enzyme; *ITPR1*, *inositol 1,4,5-triphosphate receptor 1*; *BHLHB2*, *basic helix-loop-helix domain containing, class B2*; FLJ, Japanese database Full-Length human cDNA clone; KIAA, human novel large (>4kb) cDNA identified in the Human Unidentified Gene-Encoded (HUGE) protein database (http://www.kazusa.or.jp/huge); *GRM7*, *glutamate receptor, metabotropic 7*. Reproduced from Knight et al. (2003).

4.3.2.2 Sequence analysis SCA15

Knight and colleagues (2003) suggested *inositol 1,4,5-triphosphate receptor type 1* (*ITPR1*) as a likely candidate gene based on its 3p genetic locus, predominant expression in cerebellar Purkinje cells, and the spontaneous *Itpr1* deletion (*opisthotonos*) and targeted *Itpr1* knockout (*tm1Tno*) mouse models both described to display an ataxic phenotype (Matsumoto et al. 1996;Street et al. 1997).

Knight et al. (2003) detected no aberrant RNA products caused by intron variants based on RT-PCR (reverse transcriptase – polymerase chain reaction), no mutations resulting in premature termination of protein synthesis as studied by SDS-page (sodium dodecyl sulfate - polyacrylamide gel electrophoresis) and no gross rearrangements, deletions or insertions were observed in ITPR1 from *SCA15* patient samples based on genomic Southern blots. In order to screen the promoter and entire coding region of the *ITPR1* gene for mutations, they used denaturing high performance liquid chromatography (DHPLC). Several variations were identified (table 4.2), however all were found in unrelated controls as well, suggesting the findings were polymorphic variants unrelated to *SCA15* etiology. Knight and colleagues concluded that *ITPR1* was not the causative gene underlying the *SCA15* phenotype.

***ITPR1* exon**	**nucleotide change**	**protein change**	**DHPLC temperature (°C)**
19	2218 A → G	Lys → Lys	55
22	2869 A → C	Leu → Leu	57
29	IVS29-nt57 T → G		55, 57, 59
48	6784 A → G	Thr → Thr	56, 58
54	7756 G → A	Lys → Lys	61, 63

Table 4.2. *ITPR1* variants identified using DHPLC

ITPR1 polymorphisms analysed and detected using Varian-Helix DHPLC equipment. DHPLC, denaturing high performance liquid chromatography; °C, degrees Celsius; IVS, intronic variants; nt, nucleotide. ITPR1 mRNA RefSeq NM_002222, obtained from GenBank. Adapted from Knight et al. (2003).

4.4 RESULTS

4.4.1 Genetic characterization SCA15

At the time the study described in this chapter started, 13 genes and 4 unknown transcripts had been assigned to the *SCA15* locus (build 35, human May 2004 (hg17), http://genome.ucsc.edu; table 4.3).

transcript	description
CNTN4	*contactin 4*
CHL1	*cell adhesion molecule with homology to L1CAM (close homolog of L1)*
LOC402123	
CNTN6	*contactin 6*
IL5RA	*interleukin 5 receptor, alpha*
TRNT1	*tRNA nucleotidyl transferase, CCA-adding,1*
CRBN	*cereblon (previously LOC51185)*
LOC440943	
LRRN1	*leucine rich repeat protein 1, neuronal*
SETMAR	*SET domain and mariner transposase fusion gene*
SUMF1	*sulfatase modifying factor 1*
LOC401048	
ITPR1	*inositol 1,4,5-triphosphate receptor 1*
BHLHB2	*basic helix-loop-helix domain containing, class B2*
LOC442073	
ARL10C	*ADP-ribosylation factor-like 10C (alias ARL8B, previously FLJ10702)*
EDEM1	*ER degradation enhancer, mannosidase alpha-like 1 (previously KIAA0212)*

Table 4.3. Genes mapping to the *SCA15* locus, human build 35 (hg17) May 2004

Table with the 13 known genes and 4 unknown transcripts within the SCA15 linkage region as defined by (Knight et al. 2003), based on the UCSC genome browser, build 35, human May 2004 (hg17). *L1CAM*, L1 gene family of neural Cell Adhesion Molecules; LOC, hypothetical protein in which orthologs have not yet been determined; SET domain, [Su(var)3-9, Enhancer-of-zeste, Trithorax] domain, a protein lysine methyltransferase enzyme; ADP, adenosine diphosphate; FLJ, Japanese database Full-Length human cDNA clone; ER, endoplasmic reticulum; KIAA, human novel large (>4kb) cDNA identified in the Human Unidentified Gene-Encoded (HUGE) protein database (http://www.kazusa.or.jp/huge).

4.4.1.1 Sequence analysis SCA15

In order to re-examine the *ITPR1* candidate gene as a possible cause of *SCA15*, genomic DNA from 3 affected members (III4, III5, IV8, figure 4.1) and 1 member with unknown disease status (III9, figure 4.1) from the AUS1 *SCA15* kindred were obtained. Sanger-based sequence analysis of the 58 coding exons and splice sites of *ITPR1* of two affected family members and one unrelated control, failed to show any coding alterations segregating with disease or any alterations that were inconsistent with Mendelian patterns of inheritance within the family. Several known polymorphisms were identified (table 4.4), although findings were only partly compliant with those reported by Knight et al. (2003) (table 4.2). This might be explained by study of different individuals of the *SCA15* family in both studies, unfortunately it was not possible to back track which samples were used in the original study.

nucleotide	exon	rs.no.	variant found	GT (c/a/a)	population freq.
c.6921**A**>G	48	rs13079522	p.T2191T	AA/ AA/ AG	0.350 ±0.229
c.7258C>**T***	50	rs2291862	p.L2304L	CC/ TC/ CC	0.368 ±0.221
c.7839**T**>C	54	rs711631	p.T2497T	TT/ CT/ CC	0.248 ±0.250
c.7893**G**>A	54	rs901854	p.K2515K	GG/ GG/ GA	0.469 ±0.120
	exon (UTR)				
g.4687413A>**G**	19[-1]	rs2306875	p.R669R	AA/ AA/ AG	0.496 ±0.044

Table 4.4. *ITPR1* variants identified by Sanger-based sequence analysis

ITPR1 polymorphisms analysed and detected using ABI prism 3100 genetic analyser platform, based on *ITPR1* RefSeq NM_001099952.1 obtained from GenBank. Detailed information on genetic variations from NCBI dbSNP (http://www.ncbi.nlm.nih.gov/projects/SNP), including ancestral allele, rs-number, variant found at protein level and population frequency. *A/G variant in dbSNP, A being the ancestral allele, whereas C/T variant found. rs.no, reference number; GT (c/a/a), genotype of variant (control/ affected SCA15/ affected SCA15); population freq, average population frequency heterozygote ±standard error; c, cDNA sequence; p, protein sequence; g, genomic DNA sequence; in bold, signifies ancestral allele; 19[-1], exon 19 -1 nucleotide, thus the base pair adjacent to start (5'-end) exon 19.

Miura et al. (2006) had just published work suggesting the contactin 4 (*CNTN4*) gene locus at 3p26 as a candidate gene for SCA16, based on a point mutation (4,256C→T) in the 3'UTR of the gene which co-segregated with disease but was not detected in 520 control subjects. Because the *SCA16* and *SCA15* loci overlap, sequence analysis (Sanger-based) of the 24 coding exons and splice sites of *CNTN4* was undertaken in two affected SCA15 family members and one unrelated control. Several known polymorphisms were identified, as well as an unknown non-synonymous variant in exon 12 (table 4.5), however this genotypic variant was subsequently found in neurologically normal controls (NDPT006, neurologically normal Caucasian control panel; Coriell Cell Repositories, http://ccr.coriell.org).

nucleotide	exon	rs.no.	variant found	GT (c/a/a)	population freq.
c.1463A>T	12	n/a	p.K487N	AA/ AT/ AT	n/a
c.2090T>**C**	16	rs6790908	p.N623N	CT/CT/CC	n/a
c.2132G>**A**	16	rs6803232	p.P637P	GA/GA/AA	0.489 ±0.074
c.2414**A**>T	19	rs6802588	p.R731R	AT/ (n/a)/ AA	0.485 ±0.085
	exon (UTR)				
g.3018840T>**C**	17[-23]	rs9820464	n/a	CT/ CC/ CC	0.154 ±0.231
g.3024653C>**T**	21[-8]	rs6800354	n/a	CT/ CC/ CT	0.281 ±0.248

Table 4.5. *CNTN4* variants identified by Sanger-based sequence analysis

CNTN4 polymorphisms analysed and detected using ABI prism 3100 genetic analyser platform, based on *CNTN4* RefSeq NM_175607 obtained from GenBank. Detailed information on genetic variations from NCBI dbSNP (http://www.ncbi.nlm.nih.gov/projects/SNP), including ancestral allele, rs-number, variant found at protein level and population frequency. rs.no, reference number; GT (c/a/a), genotype of variant (control/ affected SCA15/ affected SCA15); population freq, average population frequency heterozygote ±standard error; c, cDNA sequence; p, protein sequence; g, genomic DNA sequence; in bold, signifies ancestral allele; 17[-23], 23 base pairs 5' of exon 17; 21[-8], 8 base pairs 5' of exon 21.

4.4.1.2 Genome wide SNP analysis SCA15

Concurrent with sequence analysis, high density genome wide SNP genotyping (Infinium HumanHap550 genotyping chips, Illumina) was carried out. Visualization of Log R ratio, a surrogate for copy number, and B allele frequency metrics from the genome wide SNP genotyping experiments clearly showed a contiguous region of approximately 200kb long with decreased copy number and apparent homozygosity. Data were consistent with a heterozygous genomic deletion (Simon-Sanchez et al. 2007) across the first one third of *ITPR1* (inositol 1,4,5-triphosphate receptor, type 1) and the first half of a neighboring gene *SUMF1* (sulfatase modifying factor 1) (figure 4.6). This deletion was apparent in all three affected family members studied and absent from the family member with unknown disease status (AUS1 family, figure 4.1). SNP data showed a deletion between 188kb and 210kb in size; examination of SNPs at flanking unknown regions of this deletion allowed to delimit the borders of the deletion to 7.5kb on the telomeric side of the deletion (between rs12634249 and rs793396) and ~14.4kb on the centromeric side of the deletion (between rs4073665 and rs17709863).

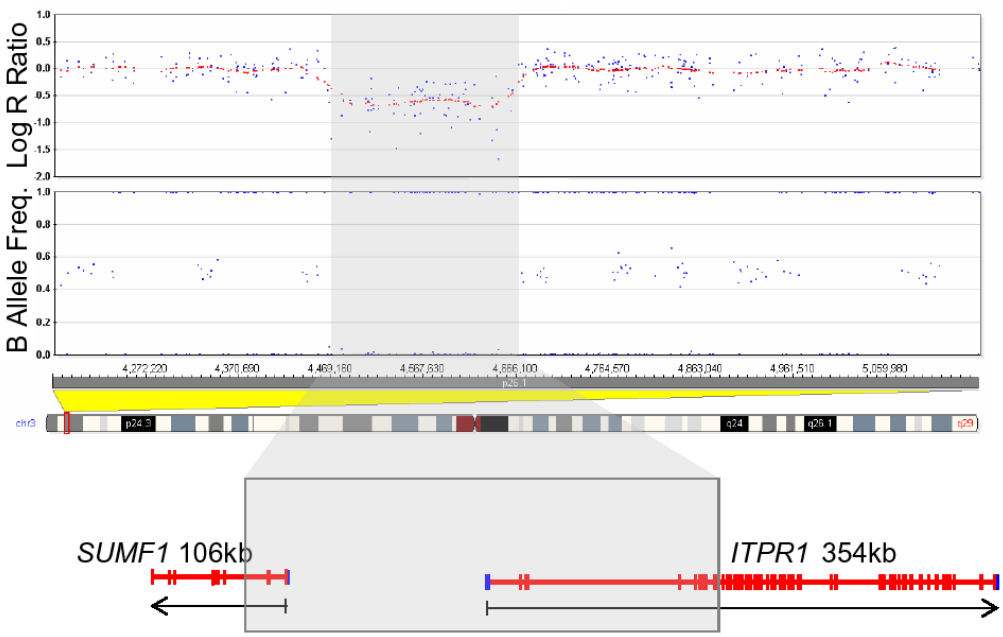

Figure 4.6. Metrics derived from analysis of DNA from affected family member III5 using Illumina Infinium HumanHap550 genotyping chips

The upper and lower plots are Log R ratio and B allele frequency respectively, at an ~800kb segment on the p arm of chromosome 3. Log R ratio, ratio of normalized, observed R to expected R for each SNP (each SNP is a blue dot) serving as a surrogate of copy number at each locus; B allele frequency, a measure of the number of times the A or B alleles are detected at each locus (each SNP is denoted by a blue dot). SNPs with a B allele frequency of 1 are apparent B/B homozygotes, SNPs with a B allele frequency of 0.5 are apparent A/B heterozygotes and those with a B allele frequency of 0 are apparent A/A homozygotes. Clearly these plots show a contiguous region ~200kb long, with decreased copy number and apparent homozygosity (bounded by a grey background). As has been demonstrated previously this is indicative of a heterozygous genomic deletion (Simon-Sanchez et al. 2007). Below these plots is a schematic of the two known genes affected by this deletion, *ITPR1* and *SUMF1*.

In an attempt to fine map the breakpoints of the disease-causing deletion, a series of experiments designed to refine the unknown intervals at the edges between definite deleted and definite diploid sequences were performed. These data narrowed the unknown borders to ~4kb on the telomeric side and ~7kb on the centromeric side. All possible combinations of forward orientation primers designed within the newly defined telomeric boundary and reverse orientation primers designed within the newly defined centromeric boundary were used in PCR assays in an attempt to amplify across the deletion in affected family members (figure 4.7). Using PCR primers T3f (telomeric 3

forward) and C11r (centromeric 11 reverse), which should be >200kb apart, a fragment 953bp in size was amplified using DNA from each of the three affected family members (III4, III5, IV8) as template. Sequencing of this fragment revealed a deletion of 201,509bp stretching between intron 3 of *SUMF1* and intron 10 of *ITPR1* (figure 4.8). This mutation removes the first 3 of 9 exons of *SUMF1* and the first 10 of 58 exons of *ITPR1*. When running the same assay to amplify the deletion specific fragment in the family member of unknown affected status, as well as, an unaffected member (III3, figure 4.7) no product was obtained.

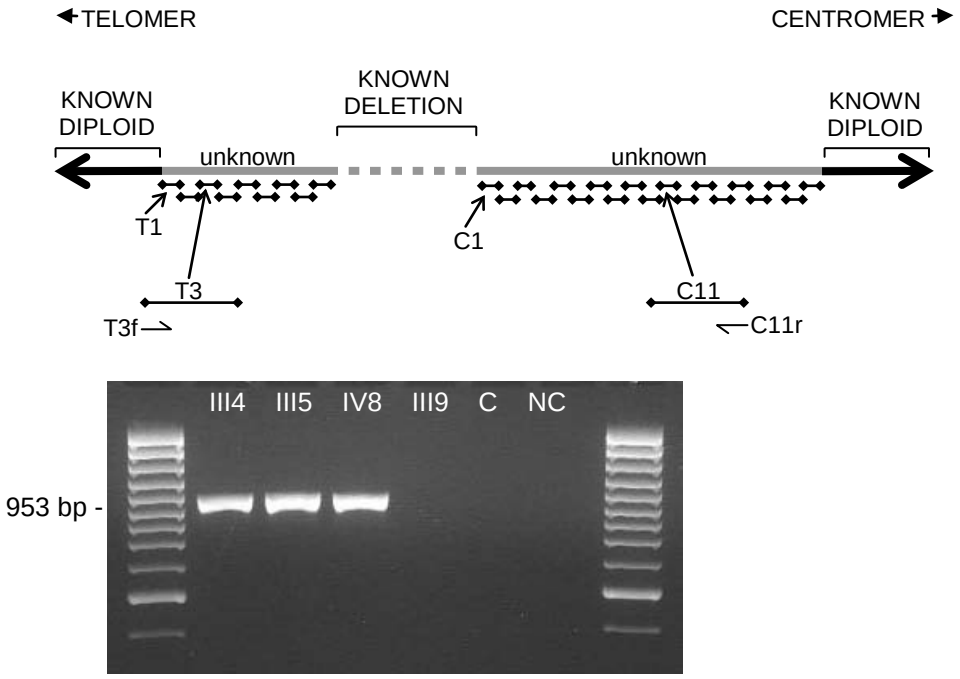

Figure 4.7. Assay to determine the deletion breakpoint of the *SCA15* locus in AUS1 family
Upper panel. Schematic of primer pairs used to narrow the unknown regions between known deleted sequence and known diploid sequence at the SCA15 locus. Nine primer pairs (T1-T9) were used to amplify across the unknown region telomeric to the known deleted region; nineteen primer pairs (C1-C19) were used to amplify across the unknown region centromeric to the known deleted region. All PCRs were carried out in the three affected family members. Analysis of these data narrowed the unknown region and ultimately enabled amplification across the deletion breakpoint in the three affected family members, using primers T3f (telomeric 3 forward) and C11r (centromeric 11 reverse), producing a fragment of 953bp in affected individuals. **Lower panel.** Gel showing amplification product using primer pair T3f and C11r from affected pedigree members III4, III5, IV8; in pedigree member III9 with unknown disease affected status; in a neurologically normal control (C); and a no template control (NC).

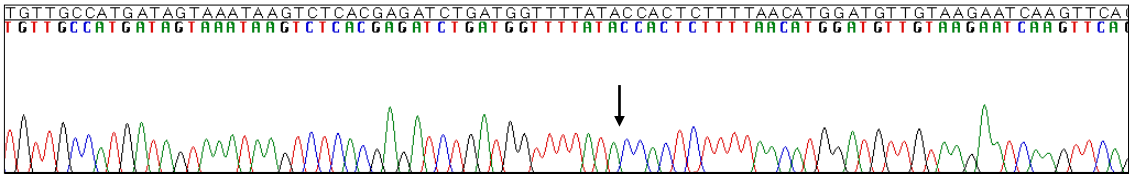

4427834	CCATCTAATATGGTTTGGCTGAGTCCCCATCCAAATCTCATCTTGAATTAT	4427884
4427885	AGCTCCAATAATCCCACCTGTCATGGGAGGGACTCAGTGGGAGGTAACTGA	4427935
4427936	ATCATGGGAGCAGGTTTTCCTGTGCTGTTGCCATGATAGTAAATAAGTCTC	4427986
4427987	ACGAGATCTGATGGTTTTATA	4428007
	\	
4629517	CCACTCTTTTAACATGGATGTTGTAAGAA	4629545
4629546	TCAAGTTCAGCCGGACATGGTGGCTCATGCCTGTAATCCCAGCACTTTGGG	4629596
4629597	AGGCCAAGGTGGGTGGATCACCTGAGGTCGGGAGTTTGAAACCAGCCTGAC	4629647
4629648	CAACATGGAGAAACCCTGTCTCTACTAAAAAATACAAAATTAGCCAAGCGT	4629698

Figure 4.8. Sequence across the deletion breakpoint of the *SCA15* locus in AUS1 family

Sequence of the flanking edges of the deletion underlying SCA15 extending through *SUMF1* and *ITPR1*. **Upper panel.** Sequence from the PCR product generated using primers T3f and C11r from genomic DNA from an affected family member. Arrow denotes location breakpoint in sequence. **Lower panel.** Sequence flanking deleted region; green font indicates nucleotides telomeric to the deletion (*SUMF1*), blue font indicates nucleotides centromeric to the deletion (*ITPR1*).

4.4.1.3 Analysis SCA15 mutation in control samples

In order to define whether the variation was a benign polymorphism, the assay used to determine the deletion breakpoint was applied to 259 neurologically normal controls (NDPT002, NDPT006, NDPT009, neurologically normal Caucasian control panel; Coriell Cell Repositories, http://ccr.coriell.org). No PCR product was obtained for any of the samples, indicating absence of the deletion (appendix VI).

In addition, genome wide SNP data at chromosome 3p26.1, the deletion locus, from 577 individuals of European descent who were either controls or individuals with an unrelated neurological disorder were analyzed (48 Caucasian controls, 269 USA ALS cases, 260 Italian controls). Data were generated using Infinium HumanHap550 genotyping chips or a combination of HumanHap300 with HumanHap240 supplement (Illumina) and were part of other studies at the Laboratory of Neurogenetics (NIA/NIH, Bethesda (MD), USA). Beadstudio metrics for one individual (ND-5029; Coriell Cell Repositories, http://ccr.coriell.org) showed homozygosity with decreased copy number, suggesting a heterozygous genomic deletion at the *ITPR1* locus (figure 4.9, A). However, since the B allele frequency calls were deviating slightly from the expected frequencies (1, B/B homozygote; 0.5, A/B heterozygote; 0, A/A homozygote) and it was previously shown that EBV (Epstein-Barr virus) immortalized lymphocyte cell lines (LCLs) can introduce structural artifacts (Simon-Sanchez et al. 2007), DNA extracted directly from blood of individual ND-5029 was analyzed. High density genotype chip data obtained from ND-5029 DNA from LCL (HumanHap300, HumanHap240) and blood (HumanHap550) were compared to confirm sample identity; genotype calls for 94 SNPs on chromosome 3 were analysed and all, except one (likely a miss-call), were found identical. Log R ratio and B allele frequency showed no evidence of a deletion at 3p26.1 in the DNA from the ND-5029 blood sample (figure 4.9, B) suggesting an LCL artifact in the initial observation. No deletion affecting the coding sequence of either gene, *ITPR1* or *SUMF1* was found in any of the remaining samples; however, a single individual (Italian control, HumanHap550) was identified with a possible heterozygous deletion approximately 6kb in size within intron 40-41 of *ITPR1*, at least 5kb away from exon 40 (figure 4.10). Given the location of this alteration it is unlikely to effect the expression or splicing of *ITPR1*. No DNA extracted directly from blood was available for this individual.

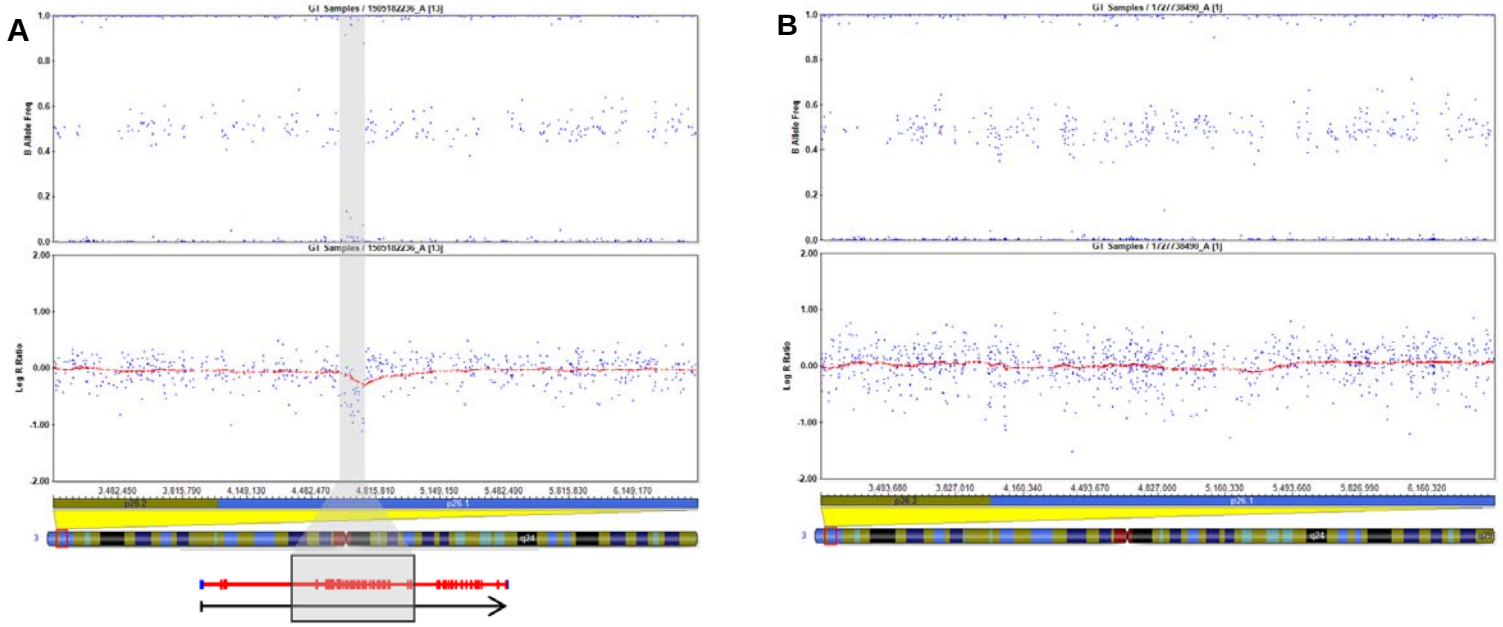

Figure 4.9. Beadstudio metrics for ND_5029 based on DNA from lymphocyte cell line or blood

The upper and lower plots are Log R ratio and B allele frequency respectively of a segment on the p arm of chromosome 3. Each SNP is denoted by a blue dot. **A.** Log R ratio and B allele frequency for ND-5029 DNA derived from LCL (lymphocyte cell line). These plots show a contiguous region ~140kb long, with decreased copy number and apparent homozygosity (bounded by a grey background), indicative of a heterozygous genomic deletion. However, note the B allele frequency calls deviation from the expected frequencies (1, B/B homozygote; 0.5, A/B heterozygote; 0, A/A homozygote) indicative of an LCL-induced structural artefact (Simon-Sanchez et al. 2007). Below these plots is a schematic of *ITPR1*, showing the exons/ introns affected by this possible deletion. Metrics generated by combining HumanHap300 and HumanHap240s genotype data (Illumina). **B.** Log R ratio and B allele frequency for ND-5029 DNA isolated from blood. No evidence of the deletion seen in DNA from LCL (A.), suggesting it was indeed a cell line induced artefact. Data were generated using HumanHap550 genotyping chip (Illumina).

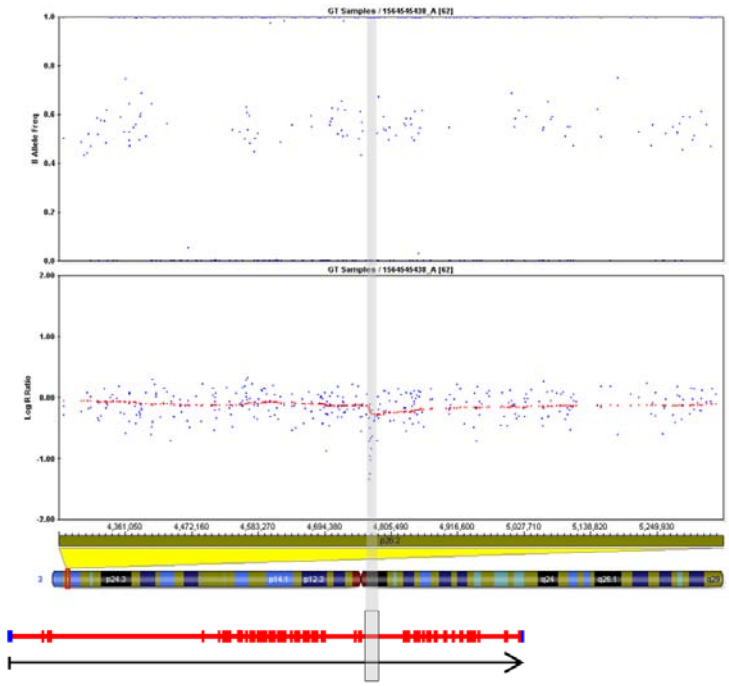

Figure 4.10. Beadstudio metrics for Italian control based on DNA from lymphocyte cell line
The upper and lower plots are Log R ratio and B allele frequency respectively of a segment on the p arm of chromosome 3. The plots show a possible heterozygous genomic deletion ~6kb in size, with decreased copy number and apparent homozygosity (bounded by a grey background). As has been previously shown, EBV immortalized lymphocyte cell lines (LCL) can induce structural artefacts (Simon-Sanchez et al. 2007); figure 4.9). No DNA extracted directly from blood was available for this individual. However, the schematic of *ITPR1* below the plots, shows this possible deletion does not affect any of the exons. And given the location of this alteration, at least 5kb 3' of exon 40, it would be unlikely to affect the expression or splicing of *ITPR1*. Data were generated using HumanHap550 genotyping chip (Illumina).

4.4.1.4 Genome wide SNP analysis additional SCA familial cases

To further establish genetic deletion at *ITPR1* as the cause of SCA15, high density genome wide SNP genotype data (HumanHap550; Illumina) from an ADCA III cohort were analysed. DNA was extracted from blood of cases with an inherited cerebellar ataxia similar to that described in the AUS1 family, ascertained through neurology clinics in London (England; *n*=43) and Cardiff (Wales; *n*=19). Genotype data from probands of two of these families (H27390, London; H3331, London) showed deletions at the *SCA15* locus from *SUMF1* through *ITPR1* (figure 4.11, 4.12). In both families, mutation was shown to segregate with disease (figure 4.11, 4.12). High density genotype chip data (HumanHap550) obtained from AUS1, H27390 and H3331 family members were compared to reveal any relatedness between the families; genotype calls for ~200 SNPs were analysed in each region flanking the deletion on chromosome 3, these data showed the AUS1, H27390 and H3331 families do not share a disease haplotype.

Family H27390 (ADCA III cohort, London)

A strategy similar to the one outlined above enabled amplification and subsequent sequence analysis across the breakpoint in family H27390 (figure 4.11). SNP genotype data narrowed the unknown intervals at the edges between definite deleted and definite diploid sequences to ~10kb on the telomeric side and ~3kb on the centromeric side. All possible combinations of forward orientation, telomeric, primers and reverse orientation, centromeric, primers, designed at 500bp intervals, were used in PCR assays. Using primers T11f (telomeric 11 forward) and C3r (centromeric 3 reverse), which should be >340kb apart, a fragment of 366bp in size was amplified using DNA from each of the two affected family members (figure 4.11). The deletion spans 344,408bp, removing exons 1-3 of *SUMF1* and 1-44 of *ITPR1*.

Family H3331 (ADCA III cohort, London)

SNP genotype data narrowed the unknown intervals at the edges between definite deleted and definite diploid sequences to ~6.5kb on the telomeric side and ~5kb on the centromeric side, in individual H3331. Primers were designed at 500bp intervals, and all possible combinations of forward orientation, telomeric, primers and reverse orientation, centromeric, primiers were used in PCR assays. However, no sequence across the breakpoint in family H3331 was obtained (figure 4.12). Therefore, all telomeric primer pairs, as well as the centromeric primer pairs were amplified using PCR and subsequently sequences were analysed (*n*=2; H3331 family member 4, 6).

Based on heterozygous calls in the sequences thus obtained, the telomeric region was narrowed to ~2.5kb and the centromeric region was further narrowed to ~3kb. These newly defined regions were used to design a second, and even a third, primer set in an attempt to generate sequence data across the breakpoint in family H3331, however thus far remaining unsuccessful. Based on the newly defined intervals, the deletion is estimated to be approximately 310kb in length, removing exons 1-3 of *SUMF1* and exons 1-40 of *ITPR1* (based on NCBI human build 36).

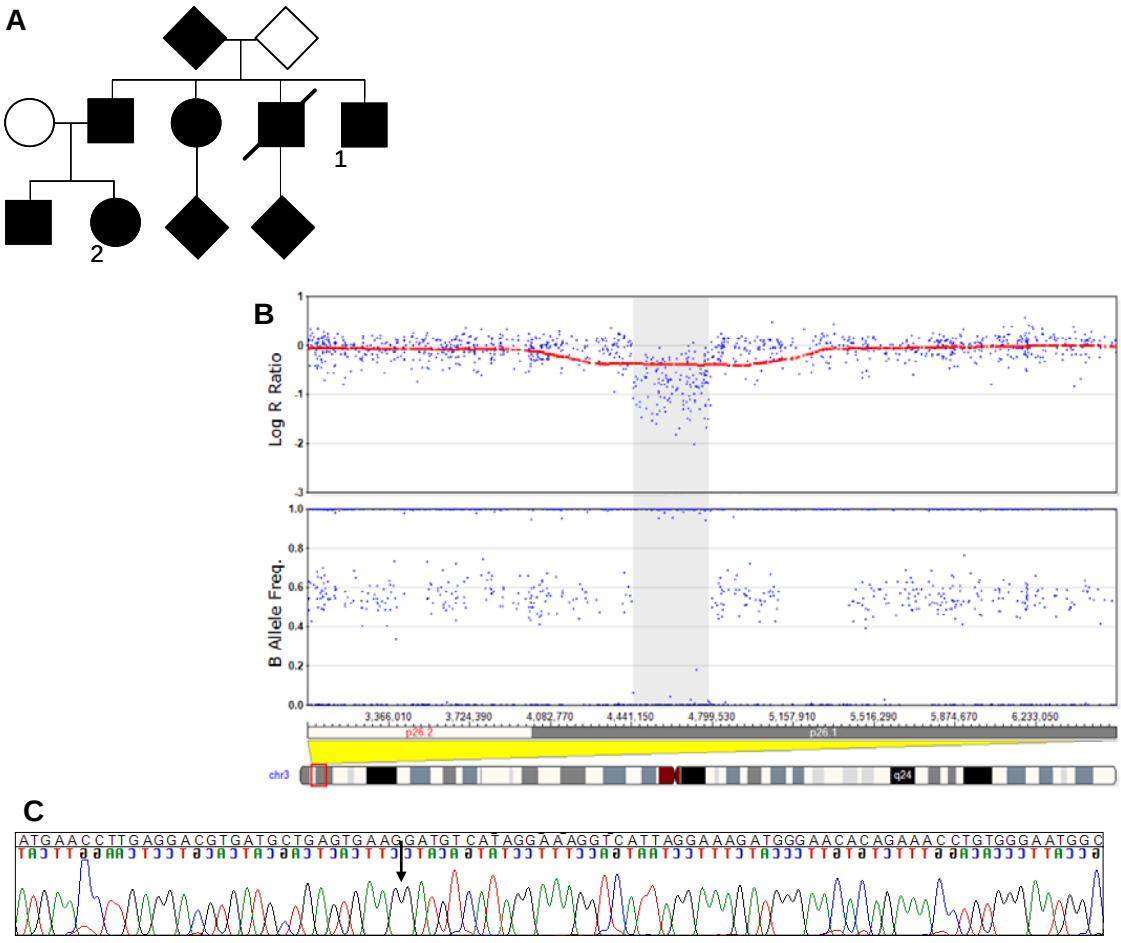


```
4415589  TGACAGGTCAAGAGATATGTCACCATACATATCCAGAACAAGTGAAAGCAG  4415639
4415640  GGGTTCGAAGGAAGGACATTCTGATACATACTACAACATGGATGAACCTTG  4415690
4415691  AGGACGTGATGCTGAGTGAAG                                4415711
                                  \
4760119                            GATGTCATAGGAAAGGTCATTAGGAAAGA  4760147
4760148  TGGGAACACAGAAACCTGTGGGAATGGCAGTTATTTTTTCTTTACTATTTA  4760198
4760199  GAACTGAGAGTCCACACTAACAGTCGATTTGGGTGTGTGGTTTAAATGGAC  4760249
```

Figure 4.11. Family H27390 (London cohort), data showing mutation at *SCA15* locus

A. Shows family pedigree; numbers indicate family members assayed, all of whom were affected and all of whom carried a deletion at this locus. Bold number indicates proband. **B.** Data were generated using HumanHap550 high density genome wide SNP chips (Illumina). The upper and lower plots are Log R ratio and B allele frequency respectively, at an ~3.5Mb segment on the p arm of chromosome 3 (each SNP is denoted by a blue dot). Closer examination of SNP data, genotype calls, enabled narrowing of the unknown intervals at the edges between definitive deleted and definitive diploid sequences to ~10kb on the telomeric side (between rs17685501 and rs11713682) and ~3kb on the centromeric side (between rs17729477 and rs17729525). **C.** Sequence flanking deleted region. Arrow denotes location breakpoint in sequence. Green font indicates nucleotides telomeric to the deletion (*SUMF1*); blue font indicates nucleotides centromeric to the deletion (*ITPR1*). The deletion is 344,408bp in length, removing exons 1-3 of *SUMF1* and exons 1-44 of *ITPR1*. Basepair positions are based on NCBI genome build 36 reference assembly.

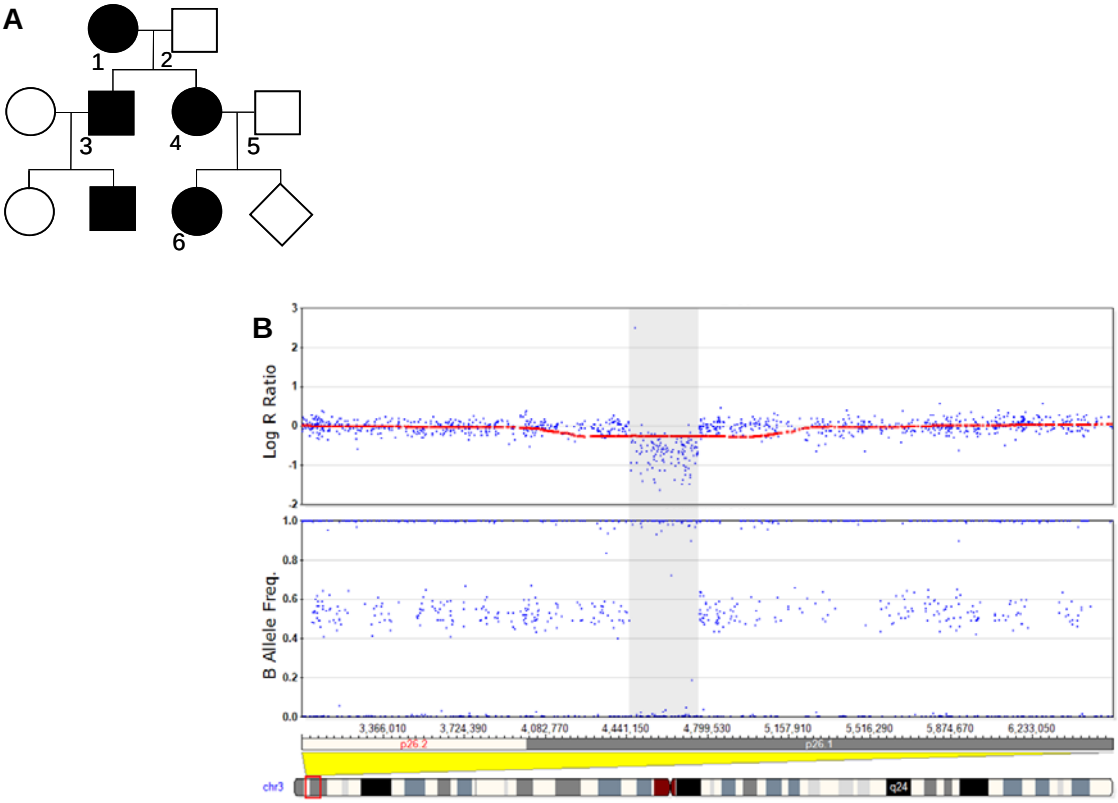

Figure 4.12. Family H3331 (London cohort), data showing mutation at *SCA15* locus

A. Shows family pedigree; numbers indicate family members assayed, all of whom were affected carried a deletion at this locus whereas all of whom were unaffected did not carry the deletion. Bold number indicates proband. **B.** Data were generated using HumanHap550 high density genome wide SNP chips (Illumina). The upper and lower plots are Log R ratio and B allele frequency respectively, at an ~3.5Mb segment on the p arm of chromosome 3 (each SNP is denoted by a blue dot). Closer examination of SNP data, genotype calls, enabled narrowing of the unknown intervals at the edges between definitive deleted and definitive diploid sequences to ~6.5kb on the telomeric side (between rs17516078 and rs12634249) and ~5kb on the centromeric side (between rs11714054 and rs4685812). Based on these findings the deletion was estimated to be approximately 310kb in length, thereby removing exons 1-3 of *SUMF1* and exons 1-39/40 of *ITPR1* (based on NCBI human build 36 reference assembly).

4.4.1.5 Sequence analysis additional SCA familial cases

In order to get more insight into the genetic mechanism underlying *ITPR1* pathology in SCA15 and to rule out the possibility that deletion of *SUMF1* causes or contributes to SCA15, although biologically unlikely, a classical sequencing approach was undertaken in a cohort of familial ADCA III cases (*n*=38; London (UK) cohort) in search for distinct *ITPR1* mutations. Sanger-based sequence analysis of the 58 coding exons and an additional 30bp of each flanking region to include splice sites identified several known polymorphisms, as well as an unknown synonymous variation in exon 26 and unknown variations in the intronic regions 5' of exon 38 and 5' of exon 44, and the 3' intronic region of exon 42 (table 4.6). The variants found in exon 26 and 5' of exon 38 were subsequently shown in neurologically normal controls (NDPT020 and NDPT023 respectively, neurologically normal Caucasian control panel; Coriell Cell Repositories, http://ccr.coriell.org). The variations identified in the intronic regions near exon 42 and 44 in SCA patients were not found in the over 400 neurologically normal controls studied (exon 42, *n*=415; exon 44, *n*=409; NDPT019, NDPT020, NDPT022, NDPT023, NDPT024, neurologically normal Caucasian control panels; Coriell Cell Repositories, http://ccr.coriell.org). More controls are needed to be conclusive, however given the location of the variations, in the intron and 18bp and 12bp away from the exon (42 and 44 respectively), they are unlikely to be disease causing.

By the time this thesis was written, Hara et al. (2008) published findings on a Japanese family with autosomal dominant SCA. They describe a missense mutation in exon 25 of *ITPR1* (AAB04947.2), the C8581→T variation resulting in substitution of leucine for proline (P1059L). This nucleotide change was absent in 234 normal chromosomes in Japanese controls. Unfortunately the control cohort was small and no further studies were published to confirm their findings, therefore these results and the pathogenicity of this variation should be considered with caution until further characterization of the mutation or additional families have been identified. To date, in five families with hereditary ataxia, four with SCA15 and one with SCA16, disease has been ascribed to deletions in *ITPR1* (van de Leemput et al. 2007;Hara et al. 2008;Iwaki et al. 2008).

nucleotide	exon	rs.no.	variant found	sample freq.	population freq.
c.2574G>A	20	rs41289636	p.A742A	GA_1, GG_{37}	n/a
c.3006A>C	22	rs58408221	p.L886L	AA_{27}, CA_9, CC_2	n/a
c.3528C>T	26	n/a	p.T1060T	CT_1, CC_{37}	n/a
c.4944C>T	35	rs34748547	p.S1532S	CT_1, CC_{37}	0.028 ±0.115
c.5469C>T	39	rs61757111	p.N1707N	CT_1, CC_{37}	n/a
c.6315**C**>T	43	rs6442905	p.N1989N	CT_2, CC_{36}	0.031 ±0.120
c.6900A>G	48	rs34491089	p.K2184K	AG_1, AA_{37}	0.025 ±0.110
c.6921**A**>G	48	rs13079522	p.T2191T	AA_{22}, AG_{12}, GG_4	0.350 ±0.229
c.7258C>**T***	50	rs2291862	p.L2304L	CC_{18}, CT_{16}, TT_4	0.368 ±0.221
c.7839C>T	54	rs711631	p.T2497T	CC_{26}, CT_5, TT_7	0.248 ±0.250
c.7893A>**G**	54	rs901854	p.K2515K	AA_{18}, AG_{12}, GG_8	0.469 ±0.120
	exon (UTR)				
g.4687413A>**G**	19[-1]	rs2306875	p.R669R	AA_{16}, AG_{19}, GG_3	0.496 ±0.044
g.4700239G>A	26[+4]	rs2306878	n/a	GA_1, GG_{37}	n/a
n/a, C>T	38[-21]	n/a	n/a	CT_1, CC_{37}	n/a
n/a, G>A	42[+18]	n/a	n/a	GA_1, GG_{37}	n/a
n/a, G>T	44[-12]	n/a	n/a	GT_1, GG_{37}	n/a

Table 4.6. *ITPR1* variants identified in ADCA III cohort (London)

ITPR1 polymorphisms analysed and detected in an ADCA III cohort (London, UK; *n*=38) using the ABI prism 3730 genetic analyser platform. Data based on *ITPR1* RefSeq NM_001099952.1, NP_001093422, obtained from GenBank. Detailed information on genetic variations from NCBI dbSNP (http://www.ncbi.nlm.nih.gov/projects/SNP), including ancestral allele, rs-number, variant found at protein level and population frequency. *A/G variant in dbSNP, A being the ancestral allele, whereas C/T variant found. Nucleotide, in bold signifies ancestral allele; rs.no, reference number; sample frequency, genotype with in subscript number of samples in which genotype found; population freq, average population frequency heterozygote ±standard error; c, cDNA; p, protein; g, genomic DNA.

4.4.1.6 ITPR1 dosage alteration analysis in a French ADCA III cohort

To study the prevalence of genetic dosage alteration of *ITPR1* in spinocerebellar ataxia, quantitative duplex PCR was carried out for $ITPR1_{exon10}$ (figure 4.13; appendix VII). Genomic DNA from samples of the Paris (French) ADCA III cohort (*n*=267) were used. Dosage data for control samples III5 and III4 (AUS1 family, figure 4.1), known to carry a deletion in *ITPR1* including exon 10 (figure 4.7), indicated heterozygous deletion of $ITPR1_{exon10}$ ($2^{-\Delta\Delta Ct}$ between 0.4 and 0.6) as expected. Whereas samples H3332 (H3331 family, figure 4.12) and III9 (AUS1 family, figure 4.1), known to have two full length copies of *ITPR1*, showed dosage values within the normal range ($2^{-\Delta\Delta Ct}$ between 0.8 and 1.2). The no template control (NC) resulted in absence of a signal for both the *hemoglobin* and the *ITPR1* probe. Measurements for three of the samples failed to meet the quality requirements; signal was obtained for both *hemoglobin* and *ITPR1* suggesting the quality of the DNA was insufficient.

Dosage data for three samples suggested duplication of $ITPR1_{exon10}$ ($2^{-\Delta\Delta Ct}$ greater than or equal to 1.3; AAD4-2G, AAD1-6E, AAD1-10D; figure 4.14; appendix VII). High density genome wide SNP data (HumanHap610-Quad) for two of these samples showed no evidence for dosage alteration in *ITPR1* (figure 4.14). However, the high density assay SNP might miss smaller deletions, even several exons in size, due to insufficient resolution (SNP density). Indeed the 610-Quad high density SNP chip used, did not contain SNPs within exon 10 of *ITPR1* ($ITPR1_{exon10}$ chromosome position 4662265-4662412: nearest 610-Quad SNPs: rs4594601 (intron 8) position 4661814, rs4685793 (intron 10) position 4668087). The quantity of the third sample was insufficient to carry out the assay. The *ITPR1* dosage data for these samples remain inconclusive based on the data presented. Southern blot analysis would be an alternative technique to estimate gene dosage levels and thus validate the data. Gene dosage data for two of the samples indicated heterozygous deletion of *ITPR1* exon 10 ($2^{-\Delta\Delta Ct}$ between 0.4 and 0.6; AAD1-3A, AAD4-8H; figure 4.13; appendix VII). Findings in both samples were subsequently confirmed by high density genome wide SNP data (HumanHap610-Quad). Log R ratio and B allele frequency plots for both samples showed decreased copy number and apparent homozygosity, indicative of a heterozygous genomic deletion (figure 4.15). Based on the BeadStudio metrics the entire *ITPR1* gene appears to be deleted in AAD1-3A, whereas in AAD4-8H *ITPR1* and *SUMF1* both seem to be partly deleted including the first exons. Taken together the $ITPR1_{exon10}$ dosage data suggest <1% (2/263) of spinocerebellar ataxia cases are caused by deletion at *ITPR1*.

Figure 4.13. Gene dosage analysis of *ITPR1*$_{exon10}$ from a French ADCA III cohort

Each bar denotes the mean of six replicates (unless indicated otherwise; •, 5 replicates; ••, 4 replicates) for one sample, expressed as $2^{-\Delta\Delta Ct}$ ±SD (standard deviation). **A, B, C, D, E, F, G.** Each graph displays data for all samples assayed on the sample 384-well plate, for which Ct (cycle threshold) 23-30, with SD ≤0.16 of dosage relative to *hemoglobin* (ΔCt), and normalized to control DNA (average ΔCt of unaffected controls). Samples French ADCA III cohort in light grey (↑**,** gene dosage indicates deletion); affected controls (**a.** III5, **c.** III4 AUS1 family, figure 4.1) in blue; unaffected controls (**b.** H3332, H3331 family, figure 4.12; **d.** III9, AUS1 family, figure 4.1) in dark grey; no template control (**e.** water). The $2^{-\Delta\Delta Ct}$ value was considered a heterozygous deletion between 0.4 and 0.6, normal between 0.8 and 1.2, and duplication at a value greater than or equal to 1.3. Assays were carried out on an ABI Prism 7900HT Sequence Detection System (Applied Biosystems) and data were analyzed using SDS software (Sequence Detection System, version 2.2.2; Applied Biosystems) and excel (2003; Microsoft). **(figure 4.13, *on next page*)**

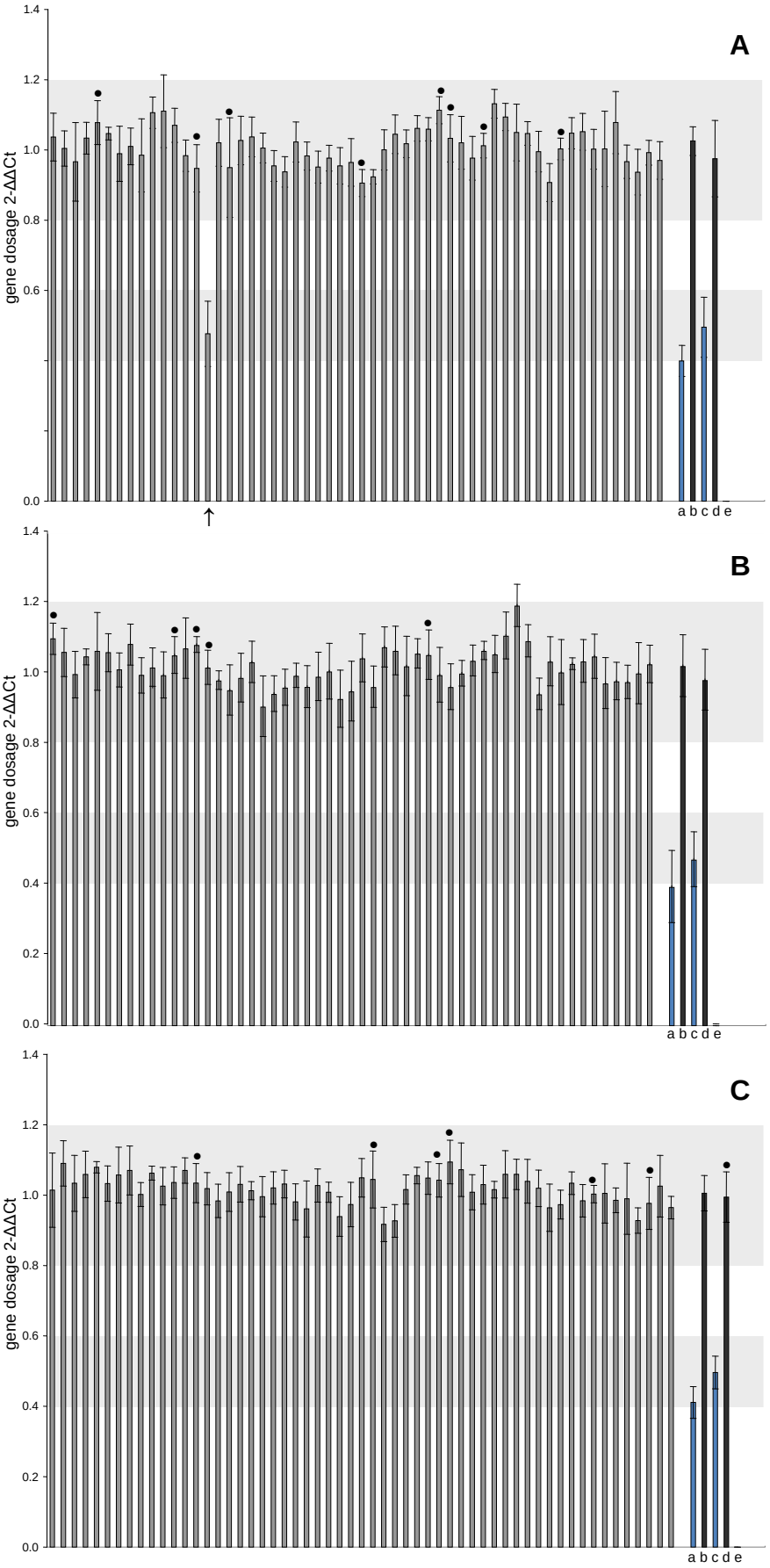

(figure 4.13, *continued on next page*)

(figure 4.13, *continued from previous page*)

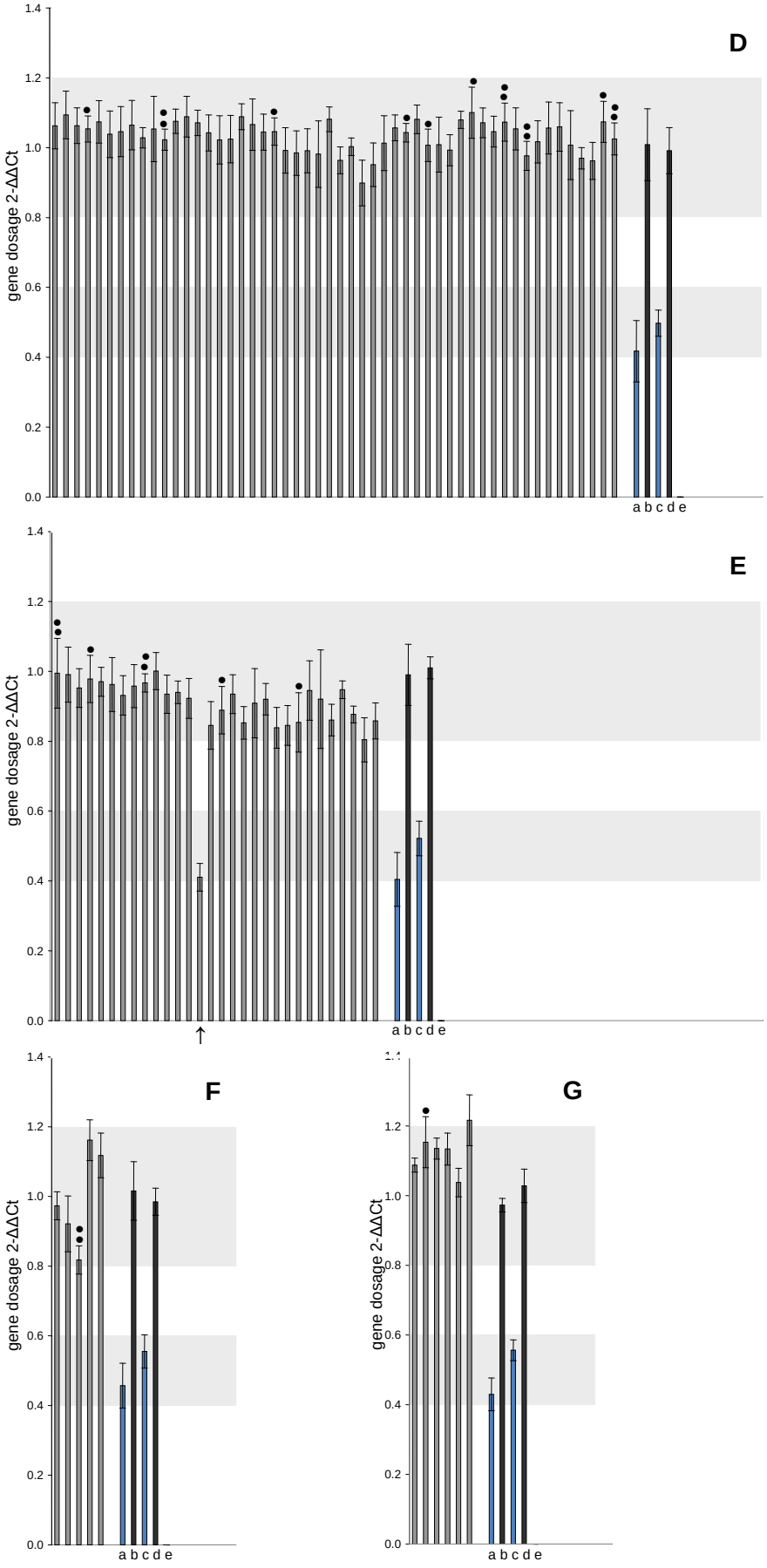

Figure 4.14. Gene dosage analysis; duplication

Gene dosage assay data for *ITPR1*$_{exon10}$ are shown for samples that repeatedly showed increased dosage (AAD4-2G (**A.**), AAD1-6E (**B, C.**), AAD1-10D (**D, E.**); appendix VII). Corresponding structural genome analysis data (HumanHap610-Quad) demonstrated no evidence for genetic dosage alteration in *ITPR1*. **A, B, D. *gene dosage assay*** Data representative for the three assay repeats, carried out independently, are shown; sample data with corresponding controls. Each bar denotes the mean of six replicates (unless indicated otherwise; ••, 4 replicates) for one sample, expressed as $2^{-\Delta\Delta Ct}$ ±SD ($2^{-\Delta\Delta Ct}$, ITPR1$_{exon10}$ dosage relative to *hemoglobin* and normalized to control DNA; SD, standard deviation). Accepted data displayed Ct (cycle threshold) values between 23 and 30, $SD_{\Delta Ct}$ ≤0.16 (ΔCt, dosage relative to *hemoglobin*). Sample in light grey (**s**); affected controls in blue (**a.** III5, **c.** III4 AUS1 family, figure 4.1); unaffected controls in dark grey (**b.** H3332, H3331 family, figure 4.12; **d.** III9, AUS1 family, figure 4.1); no template control (**e.** water). The $2^{-\Delta\Delta Ct}$ value was considered a heterozygous deletion between 0.4 and 0.6, normal between 0.8 and 1.2, and duplication at a value greater than or equal to 1.3. Assays were carried out on an ABI Prism 7900HT Sequence Detection System (Applied Biosystems) and data were analyzed using SDS software (Sequence Detection System, version 2.2.2; Applied Biosystems) and excel (2003; Microsoft). **C, E. *HumanHap610-Quad*** BeadStudio metrics derived from analysis of genomic DNA using Illumina Infinium HumanHap610-Quad high density whole genome SNP genotyping chips. The upper and lower plots are Log R ratio and B allele frequency respectively, at an ~10Mb segment on the p arm of chromosome 3 that contains *ITPR1*. Log R ratio, ratio of normalized, observed R to expected R for each SNP (each SNP is a blue dot) serving as a surrogate of copy number at each locus; B allele frequency, a measure of the number of times the A or B alleles are detected at each locus (each SNP is denoted by a blue dot). SNPs with a B allele frequency of 1 are apparent B/B homozygotes, SNPs with a B allele frequency of 0.5 are apparent A/B heterozygotes and those with a B allele frequency of 0 are apparent A/A homozygotes. Assays were carried out on the Illumina Infinium platform (Illumina) and data were analyzed using BeadStudio software (genotyping module, v2.3.25; Illumina). **(figure 4.14, *on next page*)**

(figure 4.14, *continued from previous page*)

AAD4-2G **A.**

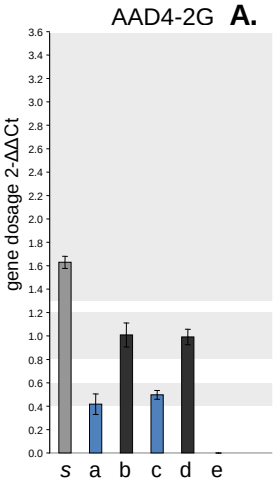

AAD1-6E **B.**

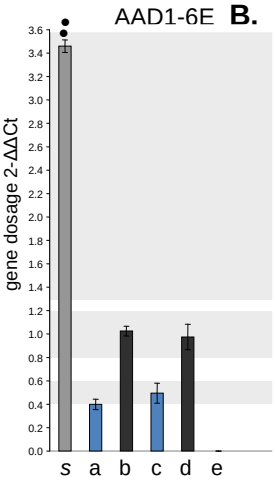

AAD1-6E **C.**

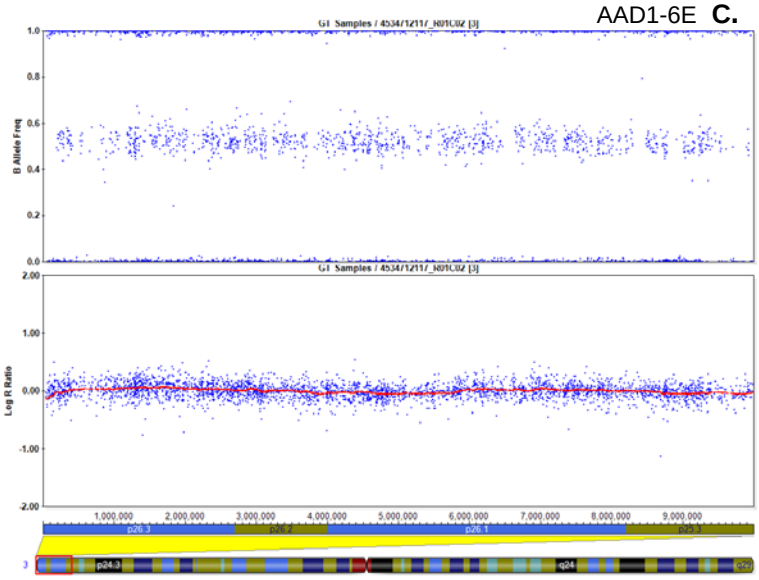

AAD1-10D **D.**

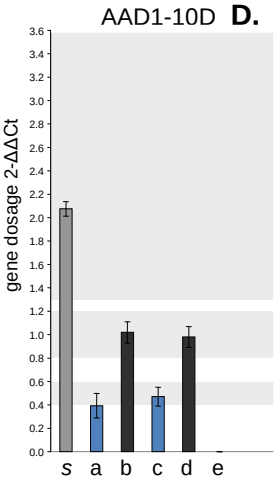

AAD1-10D **E.**

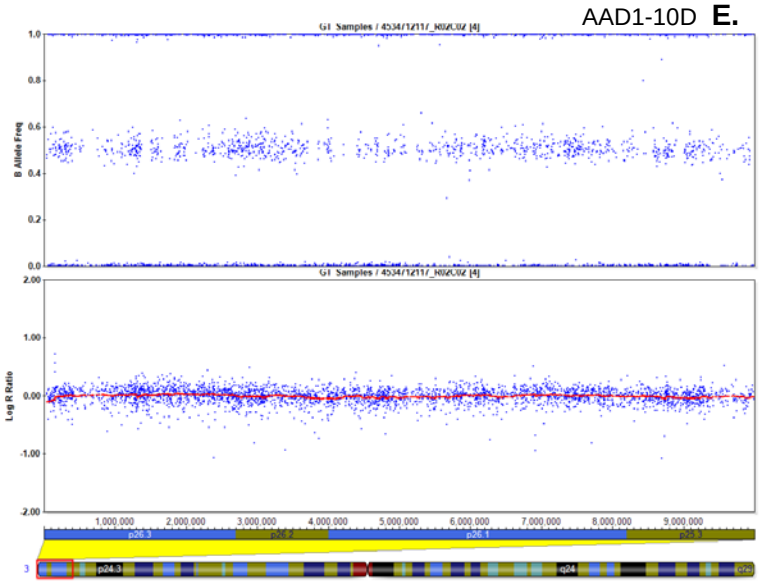

Figure 4.15. Gene dosage analysis; heterozygous deletion

Gene dosage assay data for *ITPR1*$_{exon10}$ are shown for samples that repeatedly showed decreased dosage (AAD1-3A (**A, B.**), AAD4-8H (**C, D.**); appendix VII), with corresponding structural genome analysis data (HumanHap610-Quad) confirming heterozygous deletion in *ITPR1*. **A, C. *gene dosage assay*** Data representative for both the assay repeats, carried out independently, are shown; sample data with corresponding controls. Each bar denotes the mean of six replicates for one sample, expressed as $2^{-\Delta\Delta Ct}$ ±SD ($2^{-\Delta\Delta Ct}$, ITPR1$_{exon10}$ dosage relative to *hemoglobin* and normalized to control DNA; SD, standard deviation). Accepted data displayed Ct (cycle threshold) values between 23 and 30, $SD_{\Delta Ct}$ ≤0.16 (ΔCt, dosage relative to *hemoglobin*). Sample in light grey (***s***); affected controls in blue (**a.** III5, **c.** III4 AUS1 family, figure 4.1); unaffected controls in dark grey (**b.** H3332, H3331 family, figure 4.12; **d.** III9, AUS1 family, figure 4.1); no template control (**e.** water). The $2^{-\Delta\Delta Ct}$ value was considered a heterozygous deletion between 0.4 and 0.6, normal between 0.8 and 1.2, and duplication at a value greater than or equal to 1.3. Assays were carried out on an ABI Prism 7900HT Sequence Detection System (Applied Biosystems) and data were analyzed using SDS software (Sequence Detection System, version 2.2.2; Applied Biosystems) and excel (2003; Microsoft). **B, D. *HumanHap610-Quad*** BeadStudio metrics derived from analysis of genomic DNA using Illumina Infinium HumanHap610-Quad high density whole genome SNP genotyping chips. The upper and lower plots are Log R ratio and B allele frequency respectively, at an ~10Mb segment on the p arm of chromosome 3 that contains *ITPR1*. Log R ratio, ratio of normalized, observed R to expected R for each SNP (each SNP is a blue dot) serving as a surrogate of copy number at each locus; B allele frequency, a measure of the number of times the A or B alleles are detected at each locus (each SNP is denoted by a blue dot). SNPs with a B allele frequency of 1 are apparent B/B homozygotes, SNPs with a B allele frequency of 0.5 are apparent A/B heterozygotes and those with a B allele frequency of 0 are apparent A/A homozygotes. A contiguous region with decreased copy number and apparent homozygosity (bounded by a grey background), is indicative of a heterozygous genomic deletion (Simon-Sanchez et al. 2007). Assays were carried out on the Illumina Infinium platform (Illumina) and data were analyzed using BeadStudio software (genotyping module, v2.3.25; Illumina). **(figure 4.15, *on next page*)**

(figure 4.15, *continued from previous page*)

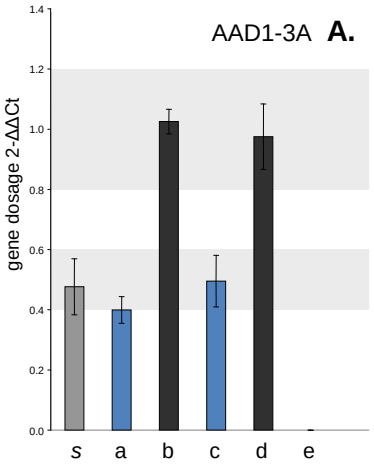

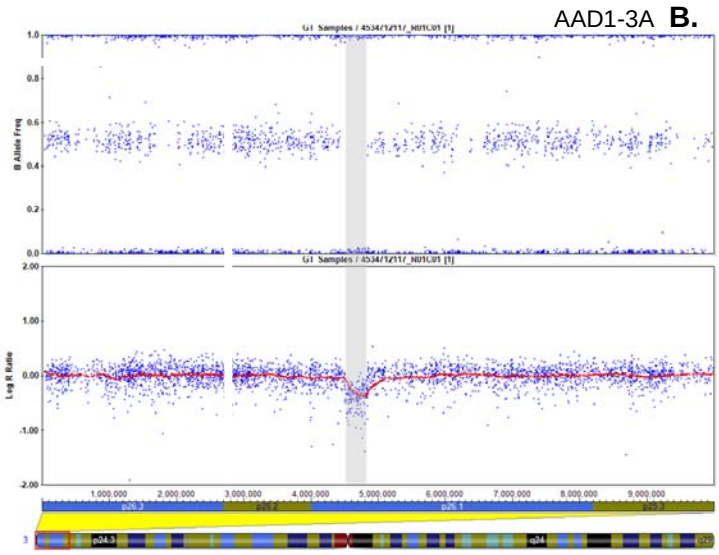

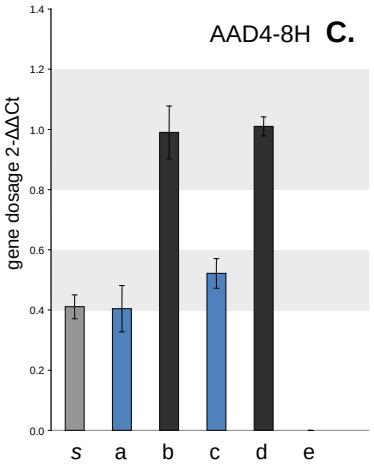

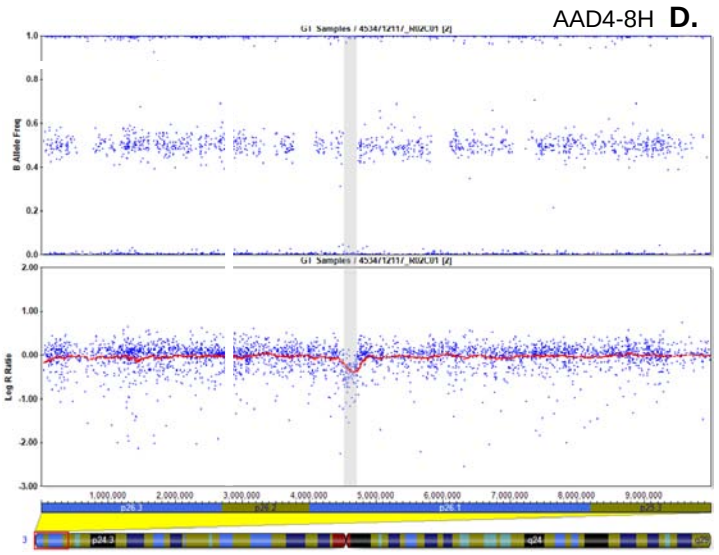

4.4.2 Molecular characterization SCA15

4.4.2.1 Characterization ITPR1 protein levels SCA15

To study the effects of the *ITPR1* deletion on protein expression, western blot analysis was undertaken. In further support of a major role for ITPR1 in SCA15 etiology, study of protein levels of ITPR1 in Epstein-Barr virus (EBV) immortalized lymphocytes from affected and unaffected AUS1 family members revealed that all affected members showed a dramatic decrease in ITPR1 levels when compared with the family member without the deletion (figure 4.16).

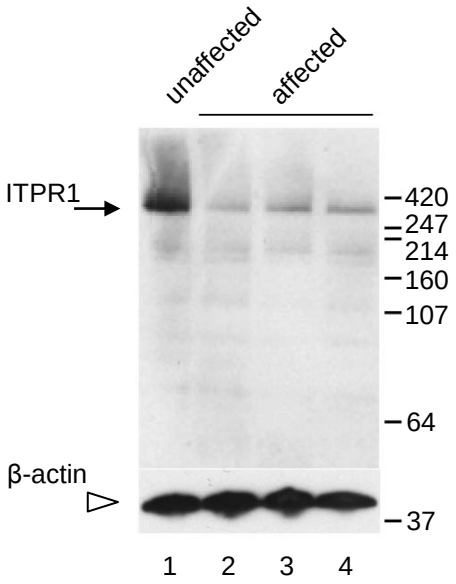

Figure 4.16. Western blot analysis of ITPR1 protein levels in EBV immortalized lymphocytes from AUS1 family members

Western blot performed to examine ITPR1 levels in EBV immortalized lymphocytes from AUS1 affected family members carrying the *ITPR1* deletion and from an AUS1 family member of unknown disease status who does not carry the deletion. Notably the samples from patients with *ITPR1* deletion show a dramatic decrease in ITPR1 levels (arrow; ITPR1, 314kD). To demonstrate equal loading, samples were diluted one in five and western blot was repeated using an antibody against beta-actin (arrowhead; beta-actin, 42kD).

4.5 DISCUSSION

4.5.1 Characterization SCA15

4.5.1.1 Spinocerebellar ataxia type 15 (SCA15)

Spinocerebellar ataxia (SCA) 15 was first described in an Australian family, AUS1 (Storey et al. 2001). Clinical presentation was an autosomal dominantly inherited 'pure' cerebellar ataxia, onset ranged from mid-childhood to middle age, characterized by slow progression, mild degree of gait ataxia, dysarthria, gaze evoked nystagmus with ± rebound and brisk lower limb reflexes, in some patients head and/or action tremor were noted. MRI showed prominent cerebellar atrophy with sparing of the brainstem (Storey et al. 2001). The SCA15 locus had been previously mapped to 3p24.2-3pter (Knight et al. 2003). Data presented in this thesis show deletions in the gene encoding inositol 1,4,5-triphosphate receptor type 1, *ITPR1*, to underlie SCA15 in humans (van de Leemput et al. 2007). Initially, a deletion was identified at the p arm of chromosome 3 in the original SCA15 family (AUS1) that comprised *ITPR1* exons 1-10 of 58 and *SUMF1* (sulfatase modifying factor 1) exons 1-3 of 9, as was shown by structural analysis based on high density genome wide genotyping (Illumina). Pathogenicity of the genetic deletion at *ITPR1* as the cause of the ataxic phenotype in SCA15 was further established by findings in two additional families with inherited cerebellar ataxia, phenotypically highly similar to that described in AUS1; deletion of exons 1-44 of *ITPR1* and 1-3 of *SUMF1* in family H27390, and deletion of exons 1-40 of *ITPR1* and 1-3 of *SUMF1* in family H3331. No structural changes were found in *ITPR1* and/or *SUMF1* studied in 836 control subjects (paragraph 4.4.1.3), except a single individual with a possible heterozygous deletion within intron 40 of *ITPR1*, at least 5kb away from the nearest exon, exon 40 (figure 4.10). In further support, western blot analysis of ITPR1 protein levels in EBV immortalized lymphocytes showed a dramatic decrease in ITPR1 levels in affected AUS1 individuals compared to a family member without the deletion.

4.5.1.2 Sulfatase modifying factor 1 (SUMF1)

Although the possibility that deletion of *SUMF1*, encoding sulfatase modifying factor 1, causes or contributes to SCA15 can not be ruled out based on these results, biologically this seems unlikely. Homozygous mutation of *SUMF1* results in autosomal recessive multiple sulfatase deficiency (MSD; OMIM ID 607939), a metabolic disorder characterized by hepatosplenomegaly, deafness and developmental delay (Cosma et al. 2003;Dierks et al. 2003;Cosma et al. 2004). To date no dominant MSD cases,

heterozygous mutation in *SUMF1*, have been described in the literature. Northern blot analysis has demonstrated *SUMF1* mRNA expression in several bodily tissues, with higher abundance in kidney and liver whereas expression in brain tissue was very low (Cosma et al. 2003). Contrary, analysis of *Sumf1*$^{-/-}$ mice tissue sections demonstrated massive and generalized cell vacuolization, particularly in macrophages suggesting the presence of active phagocytosis, with microglia becoming the predominant cell type in the Purkinje cell layer (Settembre et al. 2007). However, no co-occurrence of ataxia has been described in parents of patients with multiple sulfatase deficiency.

4.5.1.3 SCA15, SCA16 as described

Since publication of these data (van de Leemput et al. 2007), additional families have been described in which *ITPR1* mutations were shown to segregate with an ataxic phenotype similar to SCA15 (table 4.7). SCA16 was first described in a Japanese family as an autosomal dominant cerebellar ataxia. Characterized by slow progression, initial symptom is nystagmus, followed by ataxic gait and/or dysarthria, some patients presented with head tremor. Interestingly, mild mental dysfunction was described in two patients. MRI showed cerebellar atrophy without brainstem involvement (Miyoshi et al. 2001). *SCA16* was recently mapped to 3p26.2-pter, partly overlapping the *SCA15* locus (Miura et al. 2006). Based on quantitative real time PCR data of a SCA16 patient and his unaffected brother, heterozygous deletion of exons 1-48 of *ITPR1*, but not *SUMF1*, was identified as the genetic cause of SCA16. Deletion specific PCR showed the deletion was present in all affected SCA16 individuals but not unaffected family members studied (Iwaki et al. 2008).

Two additional Japanese SCA families presented with a slow progressive, autosomal dominant cerebellar ataxia in which postural and action tremor were more prominent than described in AUS1, SCA15 (Gardner et al. 2005) and SCA16 families (Miyoshi et al. 2001). Initial presentation in family A was ataxic gait, dysarthria and nystagmus, in some cases tremor of neck and/or hand was noted. In family B, tremor of trunk and upper extremities preceded ataxic symptoms, no nystagmus was described in any of the patients. In both families cerebellar atrophy without brainstem involvement was found (Hara et al. 2004). Linkage was found on chromosomal region 3p26.1-25.3, a locus overlapping with *SCA15*. It should be noted family A mainly contributed to this result, the multipoint LOD score obtained from family B did not reach significance (Hara et al. 2004). In family A, deletion of the entire *ITPR1* gene and exon 1 of *SUMF1* was initially detected based on decreased $\log_2$ R ratios obtained by high density

oligonucleotide array-based comparative genomic hybridization (aCGH), and confirmed using quantitative real time PCR which showed gene expression levels of *ITPR1* and *SUMF1* exons studied were reduced by half in affected individuals compared to unaffected family members. In addition, mRNA expression analysis showed SUMF1 and ITPR1 levels were reduced by half in an affected family member compared to the normal control levels (Hara et al. 2008). In family B, a missense mutation in exon 25 of *ITPR1* (AAB04947.2) was found in affected, but not unaffected, individuals using sequence analysis. The C8581→T variation results in substitution of leucine for proline (P1059L). This nucleotide change was absent in 234 normal chromosomes in Japanese controls (Hara et al. 2008). Unfortunately the control cohort was small (*n*=234) and no further studies, such as protein expression analysis, were published to confirm their findings, therefore these results and the pathogenicity of this variation should be considered with caution until further characterization of the mutation or additional families have been identified.

SCA families	***SUMF1* (9)**	***ITPR1* (58)**	**references**
AUS1, SCA15	1-3	1-10	van de Leemput et al. (2007)
H27390	1-3	1-44	van de Leemput et al. (2007)
H3331	1-3	1-40	van de Leemput et al. (2007)
SCA16		1-48	Iwaki et al. (2008)
Japanese A	1	1-58	Hara et al. (2008)
Japanese B*		25; C8581T	Hara et al. (2008)

Table 4.7. Genetic alterations found in SCA15 (SCA16) families

Genetic alteration found in spinocerebellar ataxia type 15 (16) published to data; the original SCA15 family (AUS1) and two London (UK) SCA families (H27390, H3331) from this study, and three Japanese families as described in literature (SCA16, Japanese A, Japanese B families). For both genes, *SUMF1* and *ITPR1*, the exons within the deleted region are given as described for each family, as well as the missense mutation in *ITPR1* exon 25 found in Japanese family B. *, note NCBI accession number AAB04947.2 (*Homo sapiens*, *ITPR1*) was given as source in the paper by (Hara et al. 2008), however in this thesis *ITPR1* accession number NM_001099952.1 (*Homo sapiens*; RefSeq) has been used throughout which would place the missense mutation in family Japanese B in exon 26 of *ITPR1*. SCA, spinocerebellar ataxia; *SUMF1* (9), sulfatase modifying factor 1 (9 exons); *ITPR1* (58), inositol 1,4,5-triphosphate receptor type 1 (58 exons).

4.5.1.4 Inositol 1,4,5-triphosphate receptor type 1 (ITPR1)

The data provide compelling evidence that deletion in the gene encoding inositol 1,4,5-triphosphate receptor type 1, *ITPR1*, underlies SCA15 and SCA16 in humans; raising the question whether the SCA16 family should be regarded as having SCA15 (Gardner 2008). Mutation at *ITPR1* is biologically plausible as a cause of ataxia since the protein is highly expressed in Purkinje cells, mice with mutation at this locus present with ataxia (chapter 3), and perturbed Ca^{2+} signaling has previously been implicated in the etiology of ataxia, notably in episodic ataxia type 2 and SCA6 (Zhuchenko et al. 1997). Given that autosomal dominant congenital non-progressive ataxia (NPCA) has been mapped to the chromosome 3pter region thereby overlapping the SCA15 locus (Dudding et al. 2004), *ITPR1* is clearly a gene of importance for screening in these families.

Haploinsufficiency at *ITPR1* would be the potential pathogenic mechanism underlying SCA15. This concept is consistent with the observation that heterozygous deletion leads to a later onset disorder in humans, whereas homozygous deletion in mice leads to an early onset disorder, able to be expressed within the much shorter life span of the mouse (chapter 3). The alternative, existence of an alternate start site for *ITPR1* that may result in a pathogenic gain of function, seems unlikely as the deletions in *ITPR1* described in Japanese families with an ataxic movement disorder phenotypic similar to SCA15, have different deletion breakpoints compared to those found in this study (table 4.7) (Hara et al. 2008;Iwaki et al. 2008).

Following the finding of a genetic deletion at *ITPR1* as the cause of SCA15, a total of 325 additional cases with an inherited cerebellar ataxia similar to that described in the AUS1 family were screened for alterations in *ITPR1* (HumanHap550, London cohort (*n*=43), Cardiff cohort (*n*=19); gene dosage assay, French cohort (*n*=263)). High density genome wide SNP genotype data (HumanHap550) resulted in de identification of two families with deletion at the SCA15 locus from *SUMF1* through *ITPR1* (paragraph 4.3.2.5), in addition, the assay for genetic dosage alteration in $ITPR1_{exon10}$ lead to the identification of two cases with heterozygous deletion in *ITPR1* (paragraph 4.4.1.6). Taken together these data suggest genetic alterations at *ITPR1* underlie approximately over 1% of autosomal dominant SCA type III (ADCA III) cases for which currently no genetic cause has been identified. Hara et al. (2008) screened 54 autosomal dominant SCA families in addition to Japanese A and Japanese B, although no deviating gene copy numbers were found. Regarding the small number of samples

screened thus far, this estimate has to be considered with caution. Further studies based on larger cohorts are required, not only looking at *ITPR1* gene dosage levels but also screening for missense mutations.

4.5.2 Genetic mutational mechanism underlying SCA15

4.5.2.1 Mechanisms underlying chromosomal rearrangements; NAHR, NHEJ

Genomic disorders have been defined as disorders in which the clinical phenotype is caused by abnormal dosage of a gene or genes located within a rearranged segment of the genome. These rearrangements include deletions, duplications, inversions and translocations. Whereas the point mutations in conventional Mendelian disease usually result from DNA replication or repair errors, the rearrangements in genomic disorders are initiated by double strand breaks (DSBs) and occur via recombination mechanisms. Two competing repair processes target DSBs; non-allelic homologous recombination (NAHR) and non-homologous end joining (NHEJ) (figure 4.17; 4.18).

Non-allelic homologous recombination (NAHR) is the most common mechanism underlying disease-associated genome rearrangements. NAHR uses a sister chromatid or homologue to connect the two strands and repair the genomic break, often using LCRs (low copy repeats) as substrates. LCRs, also known as segemental duplications or duplicons, are usually 10-500kb in size and >95% identical (Shaw and Lupski 2004). They are the product of segmental duplications of the genome and may represent genes, pseudogenes, gene fragments, repeat gene clusters and other chromosomal segments. The genome wide frequency of LCRs has been estimated at 5-10%, and although they are distributed unevenly with clustering in pericentromeric and subtelomeric areas, LCR mediated NAHR results in a clustering of rearrangement breakpoints (Shaw and Lupski 2004). NAHR between LCRs in direct orientation on the same chromosome results in reciprocal deletions and duplications, whereas NAHR between LCRs in inverted orientation on the same chromosome results in inversions. NAHR can also occur between LCRs located on different chromosomes, resulting in reciprocal translocations (Shaw and Lupski 2004).

Non-homologous end joining (NHEJ) is another repair mechanism underlying chromosomal rearrangements. Presence of LINE (long interspersed nuclear element) sequences, increased density of *Alu* elements (SINE, short interspersed nuclear element), and AT-rich palindromes have been observed at some of the NHEJ breakpoints but not all, suggesting that genome architecture (presence of abundant repetitive elements) may stimulate although not necessarily mediate these non-recurrent rearrangements (J Duckworth (LNG/NIA/NIH), personal communication). NHEJ is less accurate than NAHR because it simply joins DNA ends together, often resulting in a scattering of breakpoints (Shaw and Lupski 2004). Despite the

inaccuracy of NHEJ, it is still a widely used repair mechanism in mammals, possibly explained by the many repeat sequences present in their genomes complicating sequence alignment, a requirement for NAHR (Shaw and Lupski 2004). Several genomic disorders have been associated with NHEJ with rearrangement breakpoints located within apparently unique sequence, such as the deletion formation in the *dystrophin* gene associated with Duchenne muscular dystrophy (DMD) (Shaw and Lupski 2004).

Regardless of recombination mechanism, NAHR or NHEJ, genomic architectural features have been associated with many rearrangement breakpoints. This suggests that chromosomal rearrangements are not random events, but result from predisposition to rearrangement due to the existence of complex genomic architecture that may create instability in the genome.

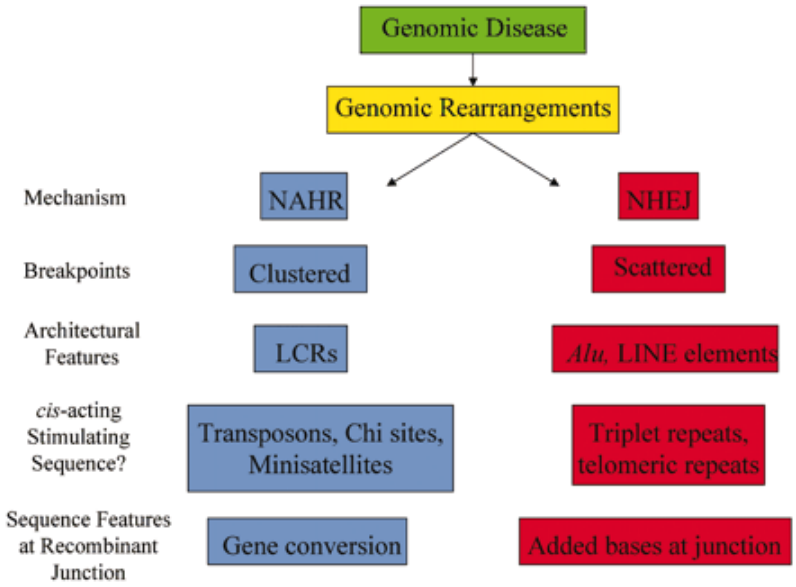

Figure 4.17. Mechanisms of genomic rearrangements

Features associated with each of the two major recombination mechanisms are shown; NAHR, non-allelic homologous recombination (blue), and NHEJ, non-homologous end joining (red). LCR, low copy repeat, also known as segmental duplication or duplicon; *Alu* element, short DNA sequence originally characterized by the action of the *Alu* restriction endonuclease, and at about 300bp in length it is classified as a short interspersed nuclear element (SINE); LINE, long interspersed nuclear element, a retrotransposon (transposon via RNA intermediates), a genetic element that moves by copying itself. Reproduced from Shaw and Lupski (2004).

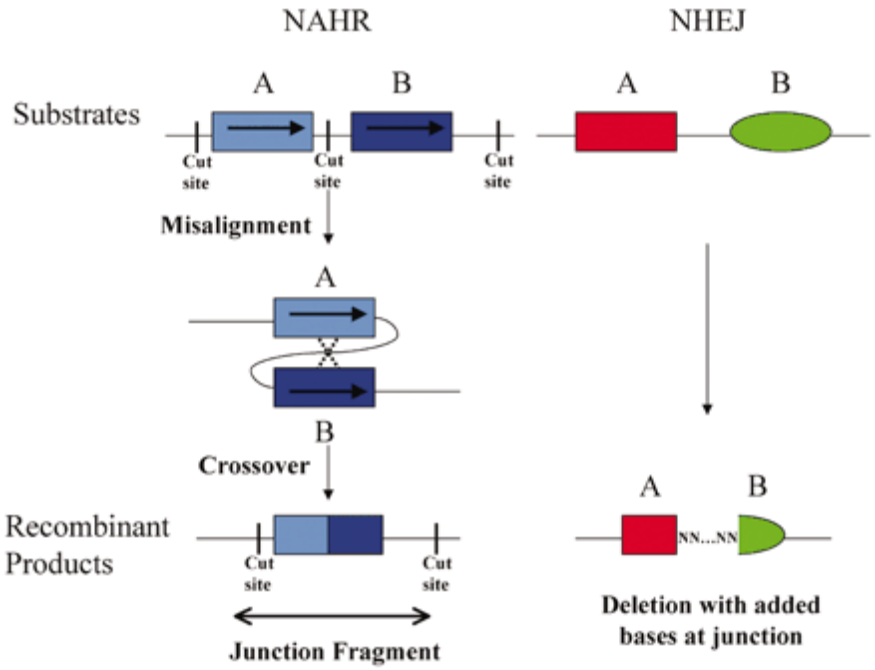

Figure 4.18. Generation of deletion rearrangement by NAHR and NHEJ

The substrates and products of recombination are shown. **Left.** NAHR utilizes two non-allelic LCRs (A and B) as substrates for recombination. The LCRs are depicted as blue rectangles due to high homology, but are different shades of blue signifying the few *cis*-morphisms or paralogous sequence variants that distinguish them. LCRs A and B, directly oriented (shown by arrows) misalign and subsequent homologous recombination results in a deletion with a single recombinant LCR, shown as a two-tone blue rectangle. Restriction enzyme consensus sequences (cut sites) are depicted as vertical lines on either side of the recombinant LCR with deletion of the consensus sequence between the two substrate LCRs. Digestion using this enzyme results in the isolation of a recombination-specific junction fragment, shown below. **Right.** NHEJ utilizes two non-homologous sequences as substrates for recombination; red rectangle (A), and green oval (B). The two sequences are joined via NHEJ, with deletion of the intervening fragment. Additional bases (NN…NN) are added at the deletion junction. Reproduced from Shaw and Lupski (2004).

4.5.2.2 Chromosomal rearrangements in SCA15, SCA16

Chromosome rearrangement breakpoints have been located throughout the genome. However, they predominate in the pericentromeric and subtelomeric regions, particularly in intervals containing complex genomic architecture such as low copy repeats (LCRs) or AT-rich palindromes (Shaw and Lupski 2004). Indeed, the *SCA15* locus is located in the telomeric region of the short arm (p arm) of chromosome 3 (figure 4.6) (Knight et al. 2003).

For NAHR, two large, highly homologous repeats, albeit low copy repeats (LCRs) or common repeats (like AT-rich palindromes), have to be present at the breakpoints for recombination to occur often leading to a clustering of breakpoints across families. Using PipMaker, Hara et al. (2008) compared the 1Mb genomic sequence surrounding *SUMF1* and *ITPR1* against itself. Sequence analysis of the breakpoint junction of all reported SCA15 (SCA16) cases showed that distal breakpoints were scattered within a ~65kb region and proximal breakpoints within a ~223kb region. Moreover, in none of the SCA15 (SCA16) families described to date has significant homology been observed when comparing the reference sequence at the distal and proximal breakpoints. However overlap of two to five nucleotides between distal and proximal junction sequences have been identified in each family (table 4.8).

SCA families	**breakpoint sequence**	**architectural feature(s)**	
		distal	***proximal***
AUS1, SCA15	TA	L1/LINE, LTR	within L1/LINE, followed by *AluSp*
H27390	TGAAG	L1/LINE	no repeats within ±200bp window
H3331	n/a	n/a	n/a
SCA16	TA	AT-rich region	AT-rich region, end of SINE repeat at -90bp
Japanese A	AT	within AT-repeat	near *Alu*Sx

Table 4.8. Genetic elements present near breakpoints SCA15 (SCA16)

LINE, long interspersed nuclear element, a retrotransposon (transposon via RNA intermediates), a genetic element that moves by copying itself; *Alu* element, short DNA sequence originally characterized by the action of the *Alu* restriction endonuclease, and at about 300bp in length it is classified as a short interspersed nuclear element (SINE); LTR, long terminal repeat, retrotransposons (genetic elements transposed by reverse transcription of RNA) with direct LTRs that range from ~100bp to over 5kb in size. Data based on Human assembly March 2006 (NCBI build 36.1 (hg18)) (J Duckworth (LNG/NIA/NIH), personal communication; Hara et al. 2008;Iwaki et al. 2008).

NHEJ usually involves tandem repeats, such as $(AT)_n$, and often at least one breakpoint is situated near or in a repeat (SINE, LINE) (J Duckworth (LNG/NIA/NIH), personal communication). Even though, breakpoints are scattered, sequence analysis has shown breakpoints in all families are near or in AT-rich regions or retrotransposons (LINE, SINE; table 4.8). Both distal and proximal breakpoints in the AUS1 family were found to be near or in a LINE retrotransposon (table 4.8; appendix VIII). In the H27390 family, the distal breakpoint is in proximity of a LINE retrotransposon, whereas sequence searches failed to identify any genomic elements that might have mediated the proximal breakpoint (table 4.8; appendix VIII). Iwaki et al. (2008) described both telomeric and centromeric breakpoints in the SCA16 family are located within AT-rich regions without presence of any repetitive elements (although J Duckworth (LNG/NIA/NIH) did identify a SINE repeat near the proximal breakpoint). Hara et al. (2008) used RepeatMasker software to identify any genomic elements, and found the distal breakpoint was embedded within an AT-dinucleotide repeat and the proximal breakpoint to be located just before an *AluSx* element.

Although no predictors of NHEJ are currently known, the presence of AT-repeats and LINE and SINE (*Alu*) genetic elements together with scattered breakpoints, suggest NHEJ to be the mechanism underlying the structural chromosome rearrangements found in SCA15 (SCA16).

4.6 CONCLUSION

Data presented, show the utility of investigating spontaneous mouse mutations in understanding human disease. *Itpr1*$^{\Delta 18}$ mice are of interest as a potential model of SCA15, and have not only aided in getting insight in disease etiology but also in discovery of the genetic cause. With three spinocerebellar ataxia families segregating a *SUMF1-ITPR1* deletion, two additional families identified, and this deletion not observed in a control population, the data provide compelling evidence that the association is causal and that heterozygous deletion in *ITPR1* is indeed the genetic basis of the disease, with SCA15 the diagnosis in the two British and two French families as well as the original Australian family (AUS1). Standard sequencing approaches alone can be insufficient to confidently rule out a candidate disease gene as was shown, a comprehensive gene dosage approach is also required. As demonstrated, high density genome wide SNP analysis can facilitate rapid detection of these structural genomic mutations that may underlie disease. Data add weight to a role for aberrant intracellular Ca^{2+} signaling in Purkinje cells in the pathogenesis of spinocerebellar ataxia.

CHAPTER 5 GENERAL DISCUSSION AND RECOMMENDATION FOR FUTURE WORK

5.1 DISCUSSION

5.1.1 On the pathogenesis of a mutation

The positional gene discovery approach has proven an effective method for identifying disease genes in an unbiased manner, evident from research in Huntington's disease (The Huntington's Disease Collaborative Research Group 1993), cystic fibrosis (Riordan et al. 1989), breast cancer (Miki et al. 1994;Wooster et al. 1995) and many other disorders. Not every variant found is causative, so how does one determine whether a newly found variant is indeed the underlying genetic cause of the disease.

Confidence in the pathogenicity of a novel variant increases based on findings of segregation in the family; i.e. presence of the mutation in affected members and absence in unaffected family members. It should be noted that interpretation of pedigree data for evidence of segregation might be complicated by incomplete penetrance, age-dependent penetrance and/or phenotypic variation within the family. In addition, absence of the variant in a large cohort (*n* ≥1000) of matched controls known to be normal in reference to the disease under investigation, without family history and with matched ethnicity compared to the original family would suggest the finding not to be a rare polymorphism. An additional gold standard for proving pathogenicity is identification of additional families with a highly similar phenotype, symptoms and disease progression, with segregation of an independent mutation in the gene under investigation. A single nucleotide change resulting in a premature stop increases likelihood of pathogenicity as this leads to truncation of the protein and may effectively result in a null-allele. Functional studies, for example RNA and protein data, from cell and/or animal models are also of great value by providing insight into the effect of the mutation at the molecular level, for example by studying expression and interactions.

Data presented in this thesis, show how a forward genetics approach led to the identification of an 18bp deletion at *Itpr1* to underlie a severe spontaneous movement disorder in mice. The *Itpr1*$^{\Delta 18}$ mice enabled the subsequent finding of deletion at *ITPR1*

to be the underlying genetic cause of SCA15 in humans. Five spinocerebellar ataxia families are described, segregating a *SUMF1-ITPR1* deletion, resulting in dramatically reduced protein expression. Deletions in *ITPR1* were not observed in a large control population (*n*=836). Western blot and immunohistochemistry data of *Itpr1*$^{\Delta 18}$ mice brain or cerebellar tissue show an almost complete lack of ITPR1 protein expression in homozygote mutant mice compared to wild type littermates, with heterozygote mice showing intermediate ITPR1 expression levels (figures 3.9, 3.10 and 3.12). Similar, western blot data in Epstein-Barr virus (EBV) immortalized lymphocytes from affected and unaffected AUS1 family members revealed that all affected members showed a dramatic decrease in ITPR1 levels when compared with the family member without the deletion (figure 4.16). Interestingly, the decrease in ITPR1 protein expression in heterozygote humans seems more pronounced than that observed in heterozygote *Itpr1*$^{\Delta 18}$ mice. This might be due to brain or cerebellar tissue studied in mice versus the lymphocytes studied in human. Unfortunately, the search for brain tissue from SCA15 patients has so far been unsuccessful. Another explanation might be a dominant negative effect of the mutation on ITPR1 protein expression, present and observed in humans but not in the mice possibly caused by interspecies differences (such as protein expression, distribution, interactions, modifications). Nonetheless, in addition to aiding in disease gene discovery, *Itpr1*$^{\Delta 18}$ mice are of great interest as a potential model for SCA15 in future studies. Taken together, the data provide compelling evidence that the association is causal and that heterozygous deletion in *ITPR1* is indeed the genetic basis of the disease, with SCA15 the diagnosis in the two British and two French families as well as the original Australian family (AUS1).

5.1.2 Aberrant calcium homeostasis in disease

A study of current literature revealed several different disorders in humans associated with various calcium-sensitive channelopathies. Changes in calcium homeostasis have been widely implicated in the pathophysiology of epilepsies, and calcium channels are one of the major targets of antiepileptic drugs (Trasande and Ramirez 2007;Landmark 2007). Paroxysmal dyskinesias, increasingly recognized to coexist with epilepsy, have also been associated with alterations in calcium regulation (Du et al. 2005). Changes in mitochondrial calcium transport, resulting in oxidative stress, are a major cause of a wide variety of cardiovascular conditions including hypoxia and arrhythmias (Shimoda et al. 2006;Sobie et al. 2006). Perturbed calcium signalling has previously been implicated in the etiology of ataxia, notably in episodic ataxia type 2 and several spinocerebellar ataxias, changes in calcium levels in the brain resulted either directly from channel mutation, or indirectly by alteration of calcium modulators (Zhuchenko et al. 1997;Zecevic et al. 1999;Lin et al. 2000).

Purkinje cell degeneration in SCA6 has been associated with polyglutamine expansions in the *CACNA1A* gene, encoding a major pore forming subunit of the Ca(v)2.1 voltage-dependent P/Q-type calcium channel (Zhuchenko et al. 1997). P/Q-type calcium channels have been shown to be highly expressed in granule cells and Purkinje cells of the cerebellar cortex, and have been suggested to play a major role in synaptic transmission (Ishikawa et al. 1999). Missense mutation in *CACNA1A* leads to episodic ataxia type 2 (EA2) (Zhuchenko et al. 1997). Moreover, KLHL1, the actin-organizing protein associated with SCA8, has been shown to interact with and modulate voltage-gated calcium channels, in particular the alpha (1A) subunit of P/Q-type channels (Aromolaran et al. 2007). Recently, SCA15 and SCA16 have been attributed to deletions in the *ITPR1* (*inositol 1,4,5-triphosphate receptor, type 1*) gene (van de Leemput et al. 2007;Iwaki et al. 2008). *ITPR1* encodes an IP3(inositol 1,4,5-triphosphate)-gated calcium-release channel located in the endoplasmic reticulum membrane, thereby controlling Ca^{2+} release from the major cellular calcium store and playing a critical role in maintaining intracellular calcium homeostasis. Interestingly, mutations in PRKCG have been identified in SCA14 pathology. PKC (protein kinase C) is another major player in the IP3-pathway (Chen et al. 2003). PPP2R2B, implicated in SCA12, has been shown to interact with PKC (Holmes et al. 1999;Price and Mumby 1999). These findings suggest a role for aberrant calcium signaling in the pathogenesis of spinocerebellar ataxia.

5.1.3 Effect mutation in *ITPR1* on calcium homeostasis

A detailed description of the complex dynamics of calcium homeostasis and signaling is beyond the scope of this thesis; a comprehensive review has been published by Berridge and colleagues (2003). Based on relevance to data presented, the role of inositol 1,4,5-triphosphate receptors (ITPRs) in calcium processes will be the focus of this discussion.

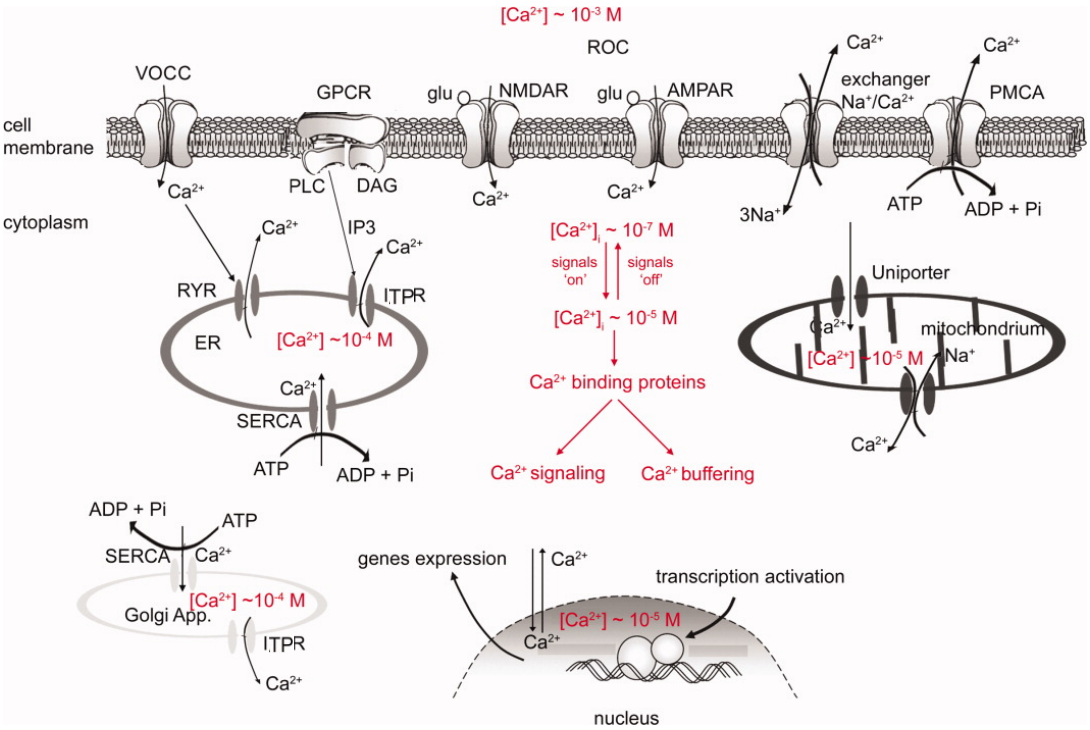

Figure 5.1 Calcium homeostasis regulation in neurons

In healthy neurons, calcium (Ca^{2+}) signals in the cytoplasm are induced by the calcium influx from the outside or by the calcium mobilization from the intracellular calcium stores such as the endoplasmic reticulum (ER) or the Golgi apparatus. Calcium enters the neuron through voltage-operated calcium channels (VOCCs), and through some glutamate (glu)-activated receptor-operated channels (ROCs); the N-methyl-D-aspartate (NMDA) receptors and some α-amino-3-hydroxy-5-methyl-4-isoxazole propionate (AMPA) receptors. Activation of some G-protein-coupled receptors (GPCRs) mobilizes calcium from the ER via inositol 1,4,5-triphosphate (IP3) receptors (ITPRs) and calcium-activated ryanodine receptors (RyRs). Calcium signals are transmitted to cellular effectors by calcium-binding protein sensors. Some of the calcium signals affect gene transcription in the nucleus. Calcium clearance mechanisms restoring its basal level during the recovery phase comprise calcium-binding protein buffers, plasma membrane calcium ATPase (PMCA), Na^{+}/Ca^{2+}-exchanger, and sarco-endoplasmatic reticulum calcium ATPase (SERCA). During the recovery, mitochondria sequester calcium through a uniporter. The calcium concentration in the nucleus is also controlled. $[Ca^{2+}]_i$, calcium concentration in the cytoplasm. Ca^{2+}, calcium ions; DAG, diacylglycerol; Golgi app, Golgi apparatus; M, molar (mole of solute per liter of solution); Na^{+}, sodium ions; Pi, inorganic phosphate; PLC, phospholipase C. Adapted from Wojda et al. (2008).

5.1.3.1 Role of ITPR1 in calcium signaling

Calcium homeostasis, is maintained by a highly complex network thereby providing a precise way to control the intracellular calcium concentration ($[Ca^{2+}]_i$). Tight regulation of calcium homeostasis allows generation of a variety of calcium signals, presented as repetitive intracellular calcium rises, which can be distinguished by distinct spatial dimensions (from nano-domains up to gradients in the whole cell body), temporal dimension, amplitude, frequency of oscillations, and localization in the neuron (Wojda et al. 2008). These properties allow various calcium transients to regulate a diverse range of essential generic (cell survival; proliferation, differentiation, apoptosis and gene transcription) and cell type specific (in neurons calcium regulates plasticity and synaptic transmission) processes, even within one cell (Wojda et al. 2008). The essential role of calcium signaling in cell regulation and survival, suggests any major changes to the complex calcium balance would not be compatible with life.

Calcium ions needed to control the activity of the cell can be supplied to the cytosol from the extracellular space or from intracellular calcium stores (figure 5.1). To maintain equilibrium the influx of extracellular calcium must be balanced by calcium extrusion, at the same time intracellular calcium stores must reaccumulate the same amount of calcium as they release (Missiaen et al. 2000). ITPRs and ryanodine receptors (RyRs) form the Ca^{2+}-release channels responsible for the calcium flow from the endoplasmic reticulum, the major intracellular calcium store in neuronal cells, into the cytoplasm (Bardo et al. 2006). IP3, released into the cytoplasm when cells are activated by external stimuli, activates the ITPR. Released calcium then exerts a positive feedback on its own release, known as the calcium-induced calcium release (CICR). Subsequent inhibition of calcium release is then caused by the decreasing luminal calcium concentration and by the increase in the concentration of the cytoplasmic Ca^{2+}/calmodulin-complex (Missiaen et al. 2000).

Calcium homeostasis does not refer to a cell acting as a uniform excitable medium. In order to decode extracellular stimuli into repetitive changes in $[Ca^{2+}]_i$, calcium compartmentalization is essential. A hierarchical organization of discontinuous calcium release events allows $[Ca^{2+}]_i$ increases to remain highly localized through involvement of single channels (‘blips’), to recruit multiple neighboring Ca^{2+}-permeable channels clustered in functional units (‘puffs’), or to generate a global $[Ca^{2+}]_i$ rise that propagates through the rest of the cell as a calcium wave (Parker et al. 1996) (figure 5.2).

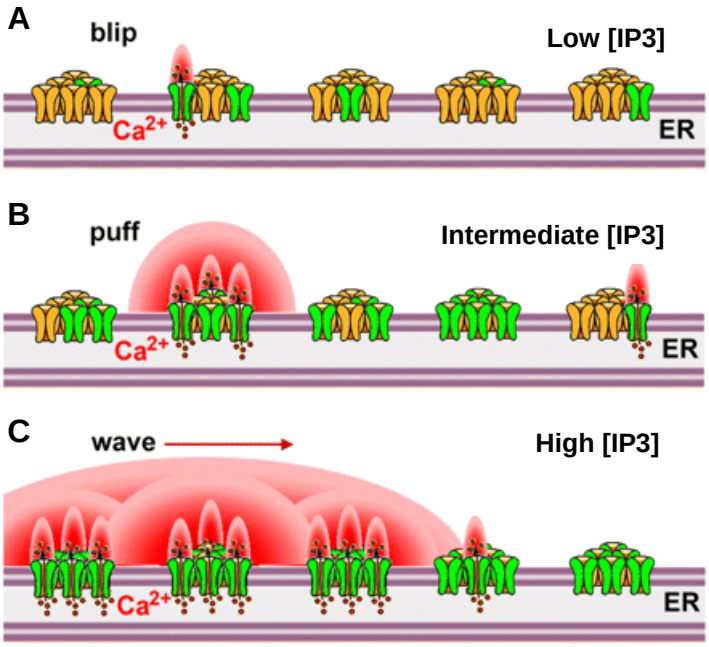

Figure 5.2 ITPR regulated calcium signaling; blips, puffs and waves

Schematic illustrating putative activity of inositol 1,4,5-triphosphate (IP3) receptor/channels in the presence of increasing concentrations of IP3. ITPRs are shown arranged in clusters that form discrete release sites within the continuous endoplasmic reticulum (ER). **A.** At low [IP3] during weak agonist stimulation, few receptors (in green) bind IP3. Others (in yellow) are not IP3 ligand-bound and therefore not activated. Consequently, highly localized small calcium (Ca^{2+}) signals ('blips') are generated by calcium released through a single or few ITPR channels rising cytoplasmic calcium concentration (shown in red). **B.** At higher levels of [IP3], coordinated opening of several channels (IP3 ligand-bound) within a cluster is triggered by calcium release from one channel acting as an activating ligand to stimulate gating of nearby channels ('puffs') through a process of Ca^{2+}-induced Ca^{2+} release (CICR). **C.** Even higher [IP3] evokes global propagating calcium signals (waves). Calcium released at one cluster can trigger calcium release at adjacent clusters by CICR, leading to the generation of calcium waves that propagate by successive cycles of calcium release, diffusion, and CICR. Adapted from Foskett et al. (2007).

The characteristics of calcium wave propagation, even whether a wave can propagate at all, depend upon spatial factors including the separation between release sites and the diffusivity of Ca^{2+} ions, as well as on the properties of the IP3 receptors themselves. The significance of absolute channel density and the spatial distribution of the channels have been shown by a near lack of correlation between 'puffs' arising from sites spaced several micrometers (μm) apart, indicating that different sites can

function autonomously. Occurrence of puffs at more closely adjacent sites can be highly correlated, although the distances between sites are sufficiently great to preclude this happening in most instances (Parker et al. 1996). Moreover, although Ca^{2+} ions diffusing from a 'puff' are able to trigger calcium release from a closely adjacent site (1-2μm distance) this often results in only small calcium activity, suggesting more than passive diffusion is required for signal propagation (Parker et al. 1996). An explanation would be the complexity of ITPR regulation. Gating of the ITPR channel involves channel activation, inhibition, inactivation, stochastic attrition and sequestration. These processes in turn are complex functions of ligand (Ca^{2+}, IP3, ATP) sensitivities and concentration, interactions with proteins, phosphorylation state, and more. The processes and interactions are further complicated by the context of complex cellular machinery, such as pumps and buffers, which participate in regulating cytoplasmic calcium concentration (Foskett et al. 2007) (figure 5.1).

5.1.3.2 Effect ITPR1 mutation on calcium signaling

As described, calcium homeostasis and signaling are highly complex processes. Even at the level of a single receptor/channel, like ITPR1, many pathways are in place to regulate channel functioning. Subtle changes lead to different signaling messages. Data shown demonstrate deletion in ITPR1 in SCA15 patients leads to dramatically decreased ITPR1 protein levels (van de Leemput et al. 2007) (figure 4.16). In normal cells, activation of G-protein-coupled receptors (GPCRs) by external stimuli, binding of presynaptic neurotransmitters, induces calcium release from the endoplasmic reticulum via ITPR1. The decreased ITPR1 levels found in SCA15 might result in reduced intracellular calcium release. This would not necessarily lessen the intensity of the calcium signal, but likely alter its features, such as propagation and shape. Highly simplified; in normal neurons IP3 ligand-binding regulates signal propagation whereas CICR (calcium-induced calcium release) modifies its shape (oscillation) (Wojda et al. 2008) (figure 5.1). In neurons with reduced ITPR1 levels, relatively more IP3 ligand would be available to switch the receptor/channels to their active state in favor of signal propagation. On the other hand, this effect would likely be counteracted by the increased distance between clusters and decreased channel density within each cluster, as channels would be expected to be more dispersed across the membrane resulting from decreased ITPR1 expression. The alterations in ITPR1 cluster patterns might evoke irregular abortive calcium waves or transient calcium puffs which remain localized, within a μm of their origin.

In this hypothesis calcium signaling could still be induced, possibly by being partly restored by other calcium signaling modulators (for example ryanodine receptors which are functionally similar to ITPR), however signaling characteristics would be altered and information on localization of the intracellular calcium rise and/or spatial properties might subsequently be misinterpreted at the molecular level. This, in turn would lead to changes in downstream signaling, such as changes in the amount of neurotransmitters released in transduction of the signals to neighboring cells (also a calcium-dependent process) or which genes to transcribe for normal cell functioning. This hypothesis is supported by electrophysiological studies in cerebellar slice preparations from *Itpr1*-deficient and *Itpr1*^{opt} mice that have shown that calcium signaling in Purkinje cells is not severely impaired in these models, although attenuation following (repeated) stimulation is decreased due to absence of long-term depression (LTD) (Matsumoto et al. 1996;Street et al. 1997;Inoue et al. 1998;Tu et al. 2002).

SCA15 is a slowly progressive disease; the slow progression might be explained by a process similar to the aging hypothesis describing how subtle changes in calcium homeostasis might control cognitive decline in normal aging (Toescu and Verkhratsky 2007). Dysregulation of calcium homeostasis, observed in physiological aging, is suggested to not be just a global excess of calcium ions in the neuron but a complex spatiotemporal dynamic process, gradually impairing neuronal mitochondria, the endoplasmic reticulum, the plasma membrane and signal transduction processes. Disease progression in SCA15 brains might be explained by similar processes of gradual impairment although more pronounced, possibly altering a more generalized response than in normal aging, and with the important difference of eventually leading to neuronal cell death. The already impaired calcium homeostasis and signaling systems in SCA15 neurons are no longer able to provide significant compensatory potential to protect neurons against persistent cellular stress conditions, calcium toxicity, associated with normal aging. Alteration of calcium homeostasis plays a central role in apoptosis, and perturbation of intracellular calcium compartmentalization has long been recognized to be potentially cytotoxic (Orrenius et al. 2003). The aging hypothesis also points to the interplay between calcium homeostasis, signaling and other signal transduction networks. Diversity of molecules involved in calcium homeostasis and signaling appears to underlie distinct responses in various neurons to the same stimuli, which might explain the impairment of only one specific type of neuron or region of the brain in physiological aging or neurodegeneration. For

example, the Purkinje cell specific neurodegeneration observed in SCA15. Subtle differences in molecular networks and therefore in the effect of deletion in ITPR1 on these networks, combined with the functional somatotopic organization of the cerebellar vermis (figure 5.3), the region most affected by neuronal atrophy in SCA15 brains, might explain the differences in phenotype observed between the different SCA15 (SCA16) families (van de Leemput et al. 2007;Hara et al. 2008;Iwaki et al. 2008) (chapter 4.5.1).

All of the SCA cases with a mutation in ITPR1 currently identified show a dominant inheritance pattern (van de Leemput et al. 2007;Hara et al. 2008;Iwaki et al. 2008). Regarding the essential role of calcium signaling in cell regulation and survival, it is likely any major changes to the complex calcium balance would not be compatible with life, suggesting homozygosity for deletion at *ITPR1* in humans might result in prenatal lethality. This concept is supported by the observation that most *Itpr1*-deficient mice, *tm1Tno*, die *in utero* (Matsumoto et al. 1996). *Itpr1*-deficient mice that survive birth display severe ataxia and tonic or tonic-clonic seizures, and die at weaning time at three weeks of age.

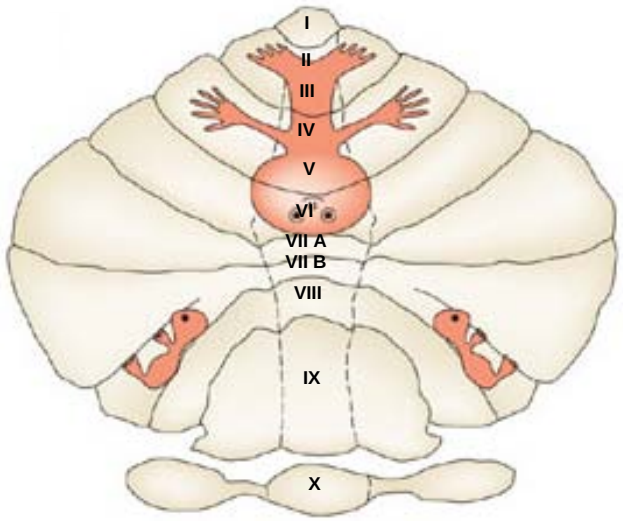

Figure 5.3 Functional somatotopic organization of the cerebellum
Sketched representation of the human body on an unfolded view of the cerebellar cortex. Cerebellar coding of motor behavior of different body parts is more complex than simple topic representation, containing local, modular repeats of small segments of receptor locations, with a global topography that includes splits, disproportions and other transformations. In general, neuroimaging studies have confirmed the classical view of representation in the cerebellum, characterized by the existence of two homunculi, one in the anterior lobe and one in the posterior lobe. I-X, denote the different hemispherical lobules of the cerebellum; I-V, anterior lobe; VI-IX, posterior lobe; X, flocculonodular lobe. Adapted from Manni and Petrosini (2004).

5.1.4 Therapeutic strategies for *ITPR1* deficiency

Data presented herein suggest that therapeutic approaches that stabilize neuronal calcium homeostasis may be able to slow down or possibly even prevent cerebellar degeneration thereby relieving associated symptoms. SCA15 is characterized by a dramatic decrease in ITPR1 protein expression (figure 4.16) (van de Leemput et al. 2007) which has been suggested to result in a decrease in calcium release, leading to altered calcium homeostasis and ultimately resulting in dysfunctional calcium signaling. Evidence for this hypothesis comes from a study of treatment of *Itpr1*-deficient mice with calcium-antagonists, anticonvulsants such as pentobarbital or diazepam; when *tm1Tno* mice were treated with either one of these drugs ataxic movements became more prominent (Matsumoto et al. 1996). Even though a strong calcium release from intracellular calcium stores can still be elicited in Purkinje neurons from *opt* mice, the calcium response to repeated QA (quisqualate, IP_3-agonist) application shows less attenuation in homozygote *opt* mice compared to wild type littermates (Street et al. 1997). These data suggest therapeutic strategies aimed at enhancing endogenous calcium release and buffering mechanisms might be beneficial in the treatment of SCA15.

Acetazolamide (Diamox), has several pharmacological characteristics that might be potentially beneficial in the treatment of SCA15. The major pharmacological action of acetazolamide is noncompetitive, reversible, inhibition of carbonic anhydrase. Even though carbonic anhydrase is found in many sites throughout the body, its anticonvulsant effect is specifically related to inhibition of the enzyme in the CNS (Rogawski and Porter 1990). Interestingly, Carbonic anhydrase-related protein (CARP) is highly concentrated in cerebellar Purkinje cells. CARP is a member of the carbonic anhydrase family based on its high similarity in sequence, although it lacks catalytic activity due to absence of a zinc-binding domain, and has been shown to bind the ITPR modulatory domain thereby inhibiting IP3 binding, an ITPR ligand essential for channel activation (Patterson et al. 2004). Inhibition of CARP by acetazolamide would facilitate IP3-ligand binding to ITPR1, thereby inducing ITPR1 channel activation (open state), increasing channel function and possibly restoring ITPR1 calcium signaling function in SCA15 patients. Acetazolamide has previously been shown to be effective against various types of seizure, including generalize tonic-clonic, myoclonic and atonic seizures, attributed to its inhibitory effect on carbonic anhydrase (Rogawski and Porter 1990). Initial trials in SCA6 and episodic ataxia type 2 have suggested acetazolamide can temporarily reduce the severity of symptoms (Melberg et al.

1997;Yabe et al. 2001;Strupp et al. 2007). Despite high initial efficacy, acetazolamide has been found to have limited usefulness in chronic treatment due to rapid development of tolerance, possibly caused by an increase in carbonic anhydrase activity by activation of existing enzyme molecules and *de novo* synthesis of the enzyme (Rogawski and Porter 1990). Development of tolerance may be delayed or prevented by using acetazolamide as an adjunct to other (antiepileptic) drugs.

Any potential drug should meet several criteria, including specificity for the disease target within the complexity of calcium homeostasis regulatory pathways and effectiveness across the blood-brain barrier. Target specificity is of great importance not only to reduce side effects, but also because ITPR subtypes play major roles in calcium signaling in several tissues and cells types, and as such are also essential in functioning of the heart (Kockskamper et al. 2008). Therefore efficacy at neuroprotective concentrations without severe side effects will have to be unequivocally demonstrated in animal models before any compound can be qualified for clinical trials. The current existing heterozygous ITPR1 mouse models (>1 year of age) would be beneficial in these initial studies (Matsumoto et al. 1996;Street et al. 1997;van de Leemput et al. 2007). Although the underlying cellular and molecular mechanisms are unclear, implementation of preventative changes in diet (reduction in dietary energy intake; coffee consumption, as caffeine is a phosphodiesterase inhibitor thereby preventing inactivation of the intracellular second messengers cAMP and cGMP) and lifestyle (exercise and cognitive stimulation) might enhance the ability of neurons to control calcium fluxes over time.

The search for treatment of cerebellar symptoms is encouraged by the high degree of plasticity in the cerebellum. As has been shown over the decades, symptoms of cerebellar disease in younger individuals, for example following tumor resection, tend to improve gradually with time if the underlying disease process does not itself progress (Konczak et al. 2005). It has been suggested that affected cerebellar functions are possibly compensated for by other parts of the brain. The lesion site has been shown to be critical for any motor recovery, as lesions affecting the deep cerebellar nuclei are not well compensated (Konczak et al. 2005). As described in the original Australian SCA15 family, MRI scans show cerebellar atrophy of the vermis, more so superiorly and dorsally, with substantial sparing of the tonsils and hemispheres (Storey et al. 2001), suggesting that if a treatment is to be found that would stop disease progression, cerebellar function might recover to some extent, especially in younger onset cases.

5.2 ONGOING AND FUTURE WORK

Data presented implicate a major role for aberrant calcium homeostasis in SCA etiology. To gain insight into the effect of SCA15 *ITPR1* mutation at the molecular level, electron microscopy studies of the spatial distribution of ITPR channels would be of great value as changes in the distribution of individual channels and channel density in clusters are expected to affect calcium signal propagation. In addition electrophysiology, studying the mechanisms underlying neuronal calcium signaling directly, would provide insight in the effects of ITPR1 mutation on signal propagation and would reveal any subtle changes. Despite a dramatic reduction in ITPR1 protein levels in Purkinje cells of SCA15 patients the disease phenotype is relatively mild, suggesting other proteins involved in maintaining calcium homeostasis and signaling might, partially, avert the effects of ITPR1 deficiency. Therefore it would be interesting to study changes in expression levels of other calcium modulators in SCA15. Unfortunately, the search for brain tissue of SCA15 patients has so far been unsuccessful. Findings suggest mutation in *ITPR1* (SCA15) to be a relatively common cause of autosomal dominant SCA in families of European descent, further studies are needed to confirm these initial findings and to determine whether this holds true for populations worldwide. Identification of non-deletion mutations, such as a point mutation or duplication, would provide insight into SCA15 and genotype-phenotype causation. In addition, it would be interesting to search for *ITPR1* mutations in other diseases, for example epilepsy, as different mutations might lead to an alternate phenotype or disease, similar to mutations described in CACNA1A, which have been associated with SCA6, EA2 and migraine (Ophoff et al. 1996;Zhuchenko et al. 1997).

Screening for mutations in ryanodine receptors (RyRs), specifically RyR type 3 the subtype mostly expressed in the brain, in autosomal dominant spinocerebellar ataxia cases might be insightful into SCA etiology based on functional similarities with ITPRs, both function as intracellular calcium release channels activated by many different extracellular stimuli (Bardo et al. 2006). Ongoing studies include efforts to identify novel ataxia disease genes by structural analysis based on high density genome wide SNP data (Infinium, Illumina) obtained from familial SCA cohorts, similar to the approach taken in this project. A promising example of which is association of duplication at chromosome 11q12.2-11q12.3 with SCA20 (Knight et al. 2008). Future plans include study of copy number variation (CNV), autozygosity and homozygosity in a large cohort of spinocerebellar ataxia cases, using high density genome wide SNP data.

5.3 CONCLUSIONS

A novel mutation in the gene encoding inositol 1,4,5-triphosphate receptor type 1 underlies a severe young onset autosomal recessive movement disorder in mice.

Data presented, show the utility of investigating spontaneous mouse mutations in understanding human disease. *Itpr1*$^{\Delta 18}$ mice are of interest as a potential model of SCA15, and have not only aided in getting insight in disease etiology but also in discovery of the genetic cause.

Data provide compelling evidence heterozygous deletion in *ITPR1* is the genetic basis of SCA15.

Standard sequencing approaches alone can be insufficient to confidently rule out a candidate disease gene as was shown, a comprehensive gene dosage approach is also required. As demonstrated, high density genome wide SNP analysis can facilitate rapid detection of these structural genomic mutations that may underlie disease.

Data add weight to a role for aberrant intracellular Ca^{2+} signaling in Purkinje cells in the pathogenesis of spinocerebellar ataxia.

REFERENCES

PERSONAL COMMUNICATION

Chandran J., Laboratory of Neurogenetics, National Institute on Aging, National Institutes on Health (Bethesda, MD, USA)

Cookson M.R., Laboratory of Neurogenetics, National Institute on Aging, National Institutes on Health (Bethesda, MD, USA)

Duckworth J., Laboratory of Neurogenetics, National Institute on Aging, National Institutes on Health (Bethesda, MD, USA)

Eppig J.T., Induced Mutant Research, The Jackson Laboratory (Bar Harbor, ME, USA)

Gwinn-Hardy K., National Institute of Neurological Disorders and Stroke, National Institutes on Health (Bethesda, MD, USA)

Holtzclaw L., Laboratory of Cellular and Synaptic Neurophysiology, National Institute on Child Health and Development, National Institutes of Health (Bethesda, MD, USA)

Houlden H., Institute of Neurology, University College London (London, UK) and National Hospital for Neurology and Neurosurgery (London, UK)

Knight M.A., National Institute of Neurological Disorders and Stroke, National Institutes of Health (Bethesda, MD, USA)

Paridiadou L., Laboratory of Neurogenetics, National Institute on Aging, National Institutes on Health (Bethesda, MD, USA)

Xie C., Laboratory of Neurogenetics, National Institute on Aging, National Institutes on Health (Bethesda, MD, USA)

PUBLICATIONS

Acevedo-Arozena A., Wells S., Potter P., Kelly M., Cox R. D., and Brown S. D. (2008) ENU mutagenesis, a way forward to understand gene function. *Annu Rev Genomics Hum Genet* **9,** 49-69.

Altschul S. F., Gish W., Miller W., Myers E. W., and Lipman D. J. (1990) Basic local alignment search tool. *J Mol Biol* **215,** 403-410.

Aromolaran K. A., Benzow K. A., Koob M. D., and Piedras-Renteria E. S. (2007) The Kelch-like protein 1 modulates P/Q-type calcium current density. *Neuroscience* **145,** 841-850.

Austin C. P., Battey J. F., Bradley A., Bucan M., Capecchi M., Collins F. S., Dove W. F., Duyk G., Dymecki S., Eppig J. T., Grieder F. B., Heintz N., Hicks G., Insel T. R., Joyner A., Koller B. H., Lloyd K. C., Magnuson T., Moore M. W., Nagy A., Pollock J. D., Roses A. D., Sands A. T., Seed B., Skarnes W. C., Snoddy J., Soriano P., Stewart D. J., Stewart F., Stillman B., Varmus H., Varticovski L., Verma I. M., Vogt T. F., von Melchner H., Witkowski J., Woychik R. P., Wurst

W., Yancopoulos G. D., Young S. G., and Zambrowicz B. (2004) The knockout mouse project. *Nat Genet* **36,** 921-924.

Baker D. J., Chen J., and van Deursen J. M. (2005) The mitotic checkpoint in cancer and aging: what have mice taught us? *Curr Opin Cell Biol* **17,** 583-589.

Balling R. (2001) ENU mutagenesis: analyzing gene function in mice. *Annu Rev Genomics Hum Genet* **2,** 463-492.

Bardo S., Cavazzini M. G., and Emptage N. (2006) The role of the endoplasmic reticulum Ca2+ store in the plasticity of central neurons. *Trends Pharmacol Sci* **27,** 78-84.

Bergami M., Rimondini R., Santi S., Blum R., Gotz M., and Canossa M. (2008) Deletion of TrkB in adult progenitors alters newborn neuron integration into hippocampal circuits and increases anxiety-like behavior. *Proc Natl Acad Sci U S A* **105,** 15570-15575.

Berridge M. J., Bootman M. D., and Roderick H. L. (2003) Calcium signalling: dynamics, homeostasis and remodelling. *Nat Rev Mol Cell Biol* **4,** 517-529.

Bininda-Emonds O. R., Cardillo M., Jones K. E., MacPhee R. D., Beck R. M., Grenyer R., Price S. A., Vos R. A., Gittleman J. L., and Purvis A. (2007) The delayed rise of present-day mammals. *Nature* **446,** 507-512.

Brignolio F., Leone M., Tribolo A., Rosso M. G., Meineri P., and Schiffer D. (1986) Prevalence of hereditary ataxias and paraplegias in the province of Torino, Italy. *Ital J Neurol Sci* **7,** 431-435.

Burright E. N., Clark H. B., Servadio A., Matilla T., Feddersen R. M., Yunis W. S., Duvick L. A., Zoghbi H. Y., and Orr H. T. (1995) SCA1 transgenic mice: a model for neurodegeneration caused by an expanded CAG trinucleotide repeat. *Cell* **82,** 937-948.

Cagnoli C., Mariotti C., Taroni F., Seri M., Brussino A., Michielotto C., Grisoli M., Di Bella D., Migone N., Gellera C., Di Donato S., and Brusco A. (2006) SCA28, a novel form of autosomal dominant cerebellar ataxia on chromosome 18p11.22-q11.2. *Brain* **129,** 235-242.

Camargos S., Scholz S., Simon-Sanchez J., Paisan-Ruiz C., Lewis P., Hernandez D., Ding J., Gibbs J. R., Cookson M. R., Bras J., Guerreiro R., Oliveira C. R., Lees A., Hardy J., Cardoso F., and Singleton A. B. (2008) DYT16, a novel young-onset dystonia-parkinsonism disorder: identification of a segregating mutation in the stress-response protein PRKRA. *Lancet Neurol* **7,** 207-215.

Chandran J. S., Lin X., Zapata A., Hoke A., Shimoji M., Moore S. O., Galloway M. P., Laird F. M., Wong P. C., Price D. L., Bailey K. R., Crawley J. N., Shippenberg T., and Cai H. (2008) Progressive behavioral deficits in DJ-1-deficient mice are associated with normal nigrostriatal function. *Neurobiol Dis* **29,** 505-514.

Chen D. H., Brkanac Z., Verlinde C. L., Tan X. J., Bylenok L., Nochlin D., Matsushita M., Lipe H., Wolff J., Fernandez M., Cimino P. J., Bird T. D., and Raskind W. H. (2003) Missense mutations in the regulatory domain of PKC gamma: a new mechanism for dominant nonepisodic cerebellar ataxia. *Am J Hum Genet* **72,** 839-849.

Chen W. L., Lin J. W., Huang H. J., Wang S. M., Su M. T., Lee-Chen G. J., Chen C. M., and Hsieh-Li H. M. (2008) SCA8 mRNA expression suggests an antisense regulation of KLHL1 and correlates to SCA8 pathology. *Brain Res* **1233,** 176-184.

Chung M. Y., Lu Y. C., Cheng N. C., and Soong B. W. (2003) A novel autosomal dominant spinocerebellar ataxia (SCA22) linked to chromosome 1p21-q23. *Brain* **126,** 1293-1299.

Chung M. Y. and Soong B. W. (2004) Reply to: SCA-19 and SCA-22: evidence for one locus with a worldwide distribution. *Brain* **127,** E7.

Copeland N. G., Jenkins N. A., Gilbert D. J., Eppig J. T., Maltais L. J., Miller J. C., Dietrich W. F., Weaver A., Lincoln S. E., Steen R. G., Stein L. D., Nadeau J. H., and Lander E. S. (1993) A genetic linkage map of the mouse: current applications and future prospects. *Science* **262,** 57-66.

Cosma M. P., Pepe S., Annunziata I., Newbold R. F., Grompe M., Parenti G., and Ballabio A. (2003) The multiple sulfatase deficiency gene encodes an essential and limiting factor for the activity of sulfatases. *Cell* **113,** 445-456.

Cosma M. P., Pepe S., Parenti G., Settembre C., Annunziata I., Wade-Martins R., Di Domenico C., Di Natale P., Mankad A., Cox B., Uziel G., Mancini G. M., Zammarchi E., Donati M. A., Kleijer W. J., Filocamo M., Carrozzo R., Carella M., and Ballabio A. (2004) Molecular and functional analysis of SUMF1 mutations in multiple sulfatase deficiency. *Hum Mutat* **23,** 576-581.

Craddock N., O'Donovan M. C., and Owen M. J. (2008) Genome-wide association studies in psychiatry: lessons from early studies of non-psychiatric and psychiatric phenotypes. *Mol Psychiatry* **13,** 649-653.

David G., Abbas N., Stevanin G., Durr A., Yvert G., Cancel G., Weber C., Imbert G., Saudou F., Antoniou E., Drabkin H., Gemmill R., Giunti P., Benomar A., Wood N., Ruberg M., Agid Y., Mandel J. L., and Brice A. (1997) Cloning of the SCA7 gene reveals a highly unstable CAG repeat expansion. *Nat Genet* **17,** 65-70.

Devos D., Schraen-Maschke S., Vuillaume I., Dujardin K., Naze P., Willoteaux C., Destee A., and Sablonniere B. (2001) Clinical features and genetic analysis of a new form of spinocerebellar ataxia. *Neurology* **56,** 234-238.

Dierks T., Schmidt B., Borissenko L. V., Peng J., Preusser A., Mariappan M., and von Figura K. (2003) Multiple sulfatase deficiency is caused by mutations in the gene encoding the human C(alpha)-formylglycine generating enzyme. *Cell* **113,** 435-444.

Doyle J., Ren X., Lennon G., and Stubbs L. (1997) Mutations in the Cacnl1a4 calcium channel gene are associated with seizures, cerebellar degeneration, and ataxia in tottering and leaner mutant mice. *Mamm Genome* **8,** 113-120.

Du W., Bautista J. F., Yang H., Diez-Sampedro A., You S. A., Wang L., Kotagal P., Luders H. O., Shi J., Cui J., Richerson G. B., and Wang Q. K. (2005) Calcium-sensitive potassium channelopathy in human epilepsy and paroxysmal movement disorder. *Nat Genet* **37,** 733-738.

Dudding T. E., Friend K., Schofield P. W., Lee S., Wilkinson I. A., and Richards R. I. (2004) Autosomal dominant congenital non-progressive ataxia overlaps with the SCA15 locus. *Neurology* **63,** 2288-2292.

Duenas A. M., Goold R., and Giunti P. (2006) Molecular pathogenesis of spinocerebellar ataxias. *Brain* **129,** 1357-1370.

Everett C. M. and Wood N. W. (2004) Trinucleotide repeats and neurodegenerative disease. *Brain* **127,** 2385-2405.

Fillon G. and Kahle P. J. (2005) Alpha-synuclein transgenic mice: relevance to multiple system atrophy. *Mov Disord* **20 Suppl 12,** S64-S66.

Flanigan K., Gardner K., Alderson K., Galster B., Otterud B., Leppert M. F., Kaplan C., and Ptacek L. J. (1996) Autosomal dominant spinocerebellar ataxia with sensory axonal neuropathy (SCA4): clinical description and genetic localization to chromosome 16q22.1. *Am J Hum Genet* **59,** 392-399.

Fletcher C. F., Lutz C. M., O'Sullivan T. N., Shaughnessy J. D., Jr., Hawkes R., Frankel W. N., Copeland N. G., and Jenkins N. A. (1996) Absence epilepsy in tottering mutant mice is associated with calcium channel defects. *Cell* **87,** 607-617.

Foskett J. K., White C., Cheung K. H., and Mak D. O. (2007) Inositol trisphosphate receptor Ca2+ release channels. *Physiol Rev* **87,** 593-658.

Gao H., Boustany R. M., Espinola J. A., Cotman S. L., Srinidhi L., Antonellis K. A., Gillis T., Qin X., Liu S., Donahue L. R., Bronson R. T., Faust J. R., Stout D., Haines J. L., Lerner T. J., and MacDonald M. E. (2002) Mutations in a novel CLN6-encoded transmembrane protein cause variant neuronal ceroid lipofuscinosis in man and mouse. *Am J Hum Genet* **70,** 324-335.

Gardner R. J. (2008) "SCA16" is really SCA15. *J Med Genet* **45,** 192.

Gardner R. J., Knight M. A., Hara K., Tsuji S., Forrest S. M., and Storey E. (2005) Spinocerebellar ataxia type 15. *Cerebellum* **4,** 47-50.

Gidalevitz T., Ben Zvi A., Ho K. H., Brignull H. R., and Morimoto R. I. (2006) Progressive disruption of cellular protein folding in models of polyglutamine diseases. *Science* **311,** 1471-1474.

Guenet J. L. (2005) The mouse genome. *Genome Res* **15,** 1729-1740.

Haberhausen G., Damian M. S., Leweke F., and Muller U. (1995) Spinocerebellar ataxia, type 3 (SCA3) is genetically identical to Machado-Joseph disease (MJD). *J Neurol Sci* **132,** 71-75.

Hara K., Fukushima T., Suzuki T., Shimohata T., Oyake M., Ishiguro H., Hirota K., Miyashita A., Kuwano R., Kurisaki H., Yomono H., Goto J., Kanazawa I., and Tsuji S. (2004) Japanese SCA families with an unusual phenotype linked to a locus overlapping with SCA15 locus. *Neurology* **62,** 648-651.

Hara K., Shiga A., Nozaki H., Mitsui J., Takahashi Y., Ishiguro H., Yomono H., Kurisaki H., Goto J., Ikeuchi T., Tsuji S., Nishizawa M., and Onodera O. (2008) Total deletion and a missense mutation of ITPR1 in Japanese SCA15 families. *Neurology* **71,** 547-551.

Harding A. E. (1983) Classification of the hereditary ataxias and paraplegias. *Lancet* **1,** 1151-1155.

Harding A. E. (1993) Clinical features and classification of inherited ataxias. *Adv Neurol* **61,** 1-14.

Hellenbroich Y., Bernard V., and Zuhlke C. (2008) Spinocerebellar ataxia type 4 and 16q22.1-linked Japanese ataxia are not allelic. *J Neurol* **255,** 612-613.

Hellenbroich Y., Gierga K., Reusche E., Schwinger E., Deller T., de Vos R. A., Zuhlke C., and Rub U. (2006) Spinocerebellar ataxia type 4 (SCA4): Initial pathoanatomical study reveals widespread cerebellar and brainstem degeneration. *J Neural Transm* **113,** 829-843.

Hernandez E., Leite M. F., Guerra M. T., Kruglov E. A., Bruna-Romero O., Rodrigues M. A., Gomes D. A., Giordano F. J., Dranoff J. A., and Nathanson M. H. (2007) The spatial distribution of inositol 1,4,5-trisphosphate receptor isoforms shapes Ca2+ waves. *J Biol Chem* **282,** 10057-10067.

Hirota J., Ando H., Hamada K., and Mikoshiba K. (2003) Carbonic anhydrase-related protein is a novel binding protein for inositol 1,4,5-trisphosphate receptor type 1. *Biochem J* **372,** 435-441.

Holmes S. E., O'Hearn E. E., McInnis M. G., Gorelick-Feldman D. A., Kleiderlein J. J., Callahan C., Kwak N. G., Ingersoll-Ashworth R. G., Sherr M., Sumner A. J., Sharp A. H., Ananth U., Seltzer W. K., Boss M. A., Vieria-Saecker A. M., Epplen J. T., Riess O., Ross C. A., and

Margolis R. L. (1999) Expansion of a novel CAG trinucleotide repeat in the 5' region of PPP2R2B is associated with SCA12. *Nat Genet* **23,** 391-392.

Houlden H., Johnson J., Gardner-Thorpe C., Lashley T., Hernandez D., Worth P., Singleton A. B., Hilton D. A., Holton J., Revesz T., Davis M. B., Giunti P., and Wood N. W. (2007) Mutations in TTBK2, encoding a kinase implicated in tau phosphorylation, segregate with spinocerebellar ataxia type 11. *Nat Genet* **39,** 1434-1436.

Ikeda Y., Dick K. A., Weatherspoon M. R., Gincel D., Armbrust K. R., Dalton J. C., Stevanin G., Durr A., Zuhlke C., Burk K., Clark H. B., Brice A., Rothstein J. D., Schut L. J., Day J. W., and Ranum L. P. (2006) Spectrin mutations cause spinocerebellar ataxia type 5. *Nat Genet* **38,** 184-190.

Imbert G., Saudou F., Yvert G., Devys D., Trottier Y., Garnier J. M., Weber C., Mandel J. L., Cancel G., Abbas N., Durr A., Didierjean O., Stevanin G., Agid Y., and Brice A. (1996) Cloning of the gene for spinocerebellar ataxia 2 reveals a locus with high sensitivity to expanded CAG/glutamine repeats. *Nat Genet* **14,** 285-291.

Inoue T., Kato K., Kohda K., and Mikoshiba K. (1998) Type 1 inositol 1,4,5-trisphosphate receptor is required for induction of long-term depression in cerebellar Purkinje neurons. *J Neurosci* **18,** 5366-5373.

Ishikawa K., Fujigasaki H., Saegusa H., Ohwada K., Fujita T., Iwamoto H., Komatsuzaki Y., Toru S., Toriyama H., Watanabe M., Ohkoshi N., Shoji S., Kanazawa I., Tanabe T., and Mizusawa H. (1999) Abundant expression and cytoplasmic aggregations of [alpha]1A voltage-dependent calcium channel protein associated with neurodegeneration in spinocerebellar ataxia type 6. *Hum Mol Genet* **8,** 1185-1193.

Ishikawa K., Toru S., Tsunemi T., Li M., Kobayashi K., Yokota T., Amino T., Owada K., Fujigasaki H., Sakamoto M., Tomimitsu H., Takashima M., Kumagai J., Noguchi Y., Kawashima Y., Ohkoshi N., Ishida G., Gomyoda M., Yoshida M., Hashizume Y., Saito Y., Murayama S., Yamanouchi H., Mizutani T., Kondo I., Toda T., and Mizusawa H. (2005) An autosomal dominant cerebellar ataxia linked to chromosome 16q22.1 is associated with a single-nucleotide substitution in the 5' untranslated region of the gene encoding a protein with spectrin repeat and Rho guanine-nucleotide exchange-factor domains. *Am J Hum Genet* **77,** 280-296.

Iwaki A., Kawano Y., Miura S., Shibata H., Matsuse D., Li W., Furuya H., Ohyagi Y., Taniwaki T., Kira J., and Fukumaki Y. (2008) Heterozygous deletion of ITPR1, but not SUMF1, in spinocerebellar ataxia type 16. *J Med Genet* **45,** 32-35.

Jakobsson M., Scholz S. W., Scheet P., Gibbs J. R., VanLiere J. M., Fung H. C., Szpiech Z. A., Degnan J. H., Wang K., Guerreiro R., Bras J. M., Schymick J. C., Hernandez D. G., Traynor B. J., Simon-Sanchez J., Matarin M., Britton A., van de Leemput J., Rafferty I., Bucan M., Cann H. M., Hardy J. A., Rosenberg N. A., and Singleton A. B. (2008) Genotype, haplotype and copy-number variation in worldwide human populations. *Nature* **451,** 998-1003.

Jensen-Seaman M. I., Furey T. S., Payseur B. A., Lu Y., Roskin K. M., Chen C. F., Thomas M. A., Haussler D., and Jacob H. J. (2004) Comparative recombination rates in the rat, mouse, and human genomes. *Genome Res* **14,** 528-538.

Johnson K. R., Sweet H. O., Donahue L. R., Ward-Bailey P., Bronson R. T., and Davisson M. T. (1998) A new spontaneous mouse mutation of Hoxd13 with a polyalanine expansion and phenotype similar to human synpolydactyly. *Hum Mol Genet* **7,** 1033-1038.

Kawaguchi Y., Okamoto T., Taniwaki M., Aizawa M., Inoue M., Katayama S., Kawakami H., Nakamura S., Nishimura M., Akiguchi I., Kimura J., Narumiya S., and Kakizuka A. (1994) CAG expansions in a novel gene for Machado-Joseph disease at chromosome 14q32.1. *Nat Genet* **8,** 221-228.

Knight M. A., Gardner R. J., Bahlo M., Matsuura T., Dixon J. A., Forrest S. M., and Storey E. (2004) Dominantly inherited ataxia and dysphonia with dentate calcification: spinocerebellar ataxia type 20. *Brain* **127,** 1172-1181.

Knight M. A., Hernandez D., Diede S. J., Dauwerse H. G., Rafferty I., van de Leemput J., Forrest S. M., Gardner R. J., Storey E., van Ommen G. J., Tapscott S. J., Fischbeck K. H., and Singleton A. B. (2008) A duplication at chromosome 11q12.2-11q12.3 is associated with spinocerebellar ataxia type 20. *Hum Mol Genet* **17,** 3847-3853.

Knight M. A., Kennerson M. L., Anney R. J., Matsuura T., Nicholson G. A., Salimi-Tari P., Gardner R. J., Storey E., and Forrest S. M. (2003) Spinocerebellar ataxia type 15 (sca15) maps to 3p24.2-3pter: exclusion of the ITPR1 gene, the human orthologue of an ataxic mouse mutant. *Neurobiol Dis* **13,** 147-157.

Kockskamper J., Zima A. V., Roderick H. L., Pieske B., Blatter L. A., and Bootman M. D. (2008) Emerging roles of inositol 1,4,5-trisphosphate signaling in cardiac myocytes. *J Mol Cell Cardiol* **45,** 128-147.

Koeppen A. H., Hans M. B., Shepherd D. I., and Best P. V. (1977) Adult-onset hereditary ataxia in Scotland. *Arch Neurol* **34,** 611-618.

Koide R., Ikeuchi T., Onodera O., Tanaka H., Igarashi S., Endo K., Takahashi H., Kondo R., Ishikawa A., Hayashi T., Saito M., Tomoda A., Miike T., Naito H., Ikuta F., and Tsuji S. (1994) Unstable expansion of CAG repeat in hereditary dentatorubral-pallidoluysian atrophy (DRPLA). *Nat Genet* **6,** 9-13.

Konczak J., Schoch B., Dimitrova A., Gizewski E., and Timmann D. (2005) Functional recovery of children and adolescents after cerebellar tumour resection. *Brain* **128,** 1428-1441.

Koob M. D., Moseley M. L., Schut L. J., Benzow K. A., Bird T. D., Day J. W., and Ranum L. P. (1999) An untranslated CTG expansion causes a novel form of spinocerebellar ataxia (SCA8). *Nat Genet* **21,** 379-384.

Lalonde R. and Strazielle C. (2007) Spontaneous and induced mouse mutations with cerebellar dysfunctions: behavior and neurochemistry. *Brain Res* **1140,** 51-74.

Lalouette A., Guenet J. L., and Vriz S. (1998) Hotfoot mouse mutations affect the delta 2 glutamate receptor gene and are allelic to lurcher. *Genomics* **50,** 9-13.

Lander E. S., Linton L. M., Birren B., Nusbaum C., Zody M. C., Baldwin J., Devon K., Dewar K., Doyle M., FitzHugh W., Funke R., Gage D., Harris K., Heaford A., Howland J., Kann L., Lehoczky J., LeVine R., McEwan P., McKernan K., Meldrim J., Mesirov J. P., Miranda C., Morris W., Naylor J., Raymond C., Rosetti M., Santos R., Sheridan A., Sougnez C., Stange-Thomann N., Stojanovic N., Subramanian A., Wyman D., Rogers J., Sulston J., Ainscough R., Beck S., Bentley D., Burton J., Clee C., Carter N., Coulson A., Deadman R., Deloukas P., Dunham A., Dunham I., Durbin R., French L., Grafham D., Gregory S., Hubbard T., Humphray S., Hunt A., Jones M., Lloyd C., McMurray A., Matthews L., Mercer S., Milne S., Mullikin J. C., Mungall A., Plumb R., Ross M., Shownkeen R., Sims S., Waterston R. H., Wilson R. K., Hillier L. W., McPherson J. D., Marra M. A., Mardis E. R., Fulton L. A., Chinwalla A. T., Pepin K. H., Gish W. R., Chissoe S. L., Wendl M. C., Delehaunty K. D., Miner T. L., Delehaunty A., Kramer J. B., Cook L. L., Fulton R. S., Johnson D. L., Minx P. J., Clifton S. W., Hawkins T., Branscomb E., Predki P., Richardson P., Wenning S., Slezak T., Doggett N., Cheng J. F., Olsen A., Lucas S., Elkin C., Uberbacher E., Frazier M., Gibbs R. A., Muzny D. M., Scherer S. E., Bouck J. B., Sodergren E. J., Worley K. C., Rives C. M., Gorrell J. H., Metzker M. L., Naylor S. L., Kucherlapati R. S., Nelson D. L., Weinstock G. M., Sakaki Y., Fujiyama A., Hattori M., Yada T., Toyoda A., Itoh T., Kawagoe C., Watanabe H., Totoki Y., Taylor T., Weissenbach J., Heilig R., Saurin W., Artiguenave F., Brottier P., Bruls T., Pelletier E., Robert C., Wincker P., Smith D. R., Doucette-Stamm L., Rubenfield M., Weinstock K., Lee H. M., Dubois J., Rosenthal A., Platzer M., Nyakatura G., Taudien S., Rump A., Yang H., Yu J., Wang J., Huang G., Gu J., Hood L., Rowen L., Madan A., Qin S., Davis R. W., Federspiel N. A., Abola A. P., Proctor M. J., Myers

R. M., Schmutz J., Dickson M., Grimwood J., Cox D. R., Olson M. V., Kaul R., Raymond C., Shimizu N., Kawasaki K., Minoshima S., Evans G. A., Athanasiou M., Schultz R., Roe B. A., Chen F., Pan H., Ramser J., Lehrach H., Reinhardt R., McCombie W. R., de la B. M., Dedhia N., Blocker H., Hornischer K., Nordsiek G., Agarwala R., Aravind L., Bailey J. A., Bateman A., Batzoglou S., Birney E., Bork P., Brown D. G., Burge C. B., Cerutti L., Chen H. C., Church D., Clamp M., Copley R. R., Doerks T., Eddy S. R., Eichler E. E., Furey T. S., Galagan J., Gilbert J. G., Harmon C., Hayashizaki Y., Haussler D., Hermjakob H., Hokamp K., Jang W., Johnson L. S., Jones T. A., Kasif S., Kaspryzk A., Kennedy S., Kent W. J., Kitts P., Koonin E. V., Korf I., Kulp D., Lancet D., Lowe T. M., McLysaght A., Mikkelsen T., Moran J. V., Mulder N., Pollara V. J., Ponting C. P., Schuler G., Schultz J., Slater G., Smit A. F., Stupka E., Szustakowski J., Thierry-Mieg D., Thierry-Mieg J., Wagner L., Wallis J., Wheeler R., Williams A., Wolf Y. I., Wolfe K. H., Yang S. P., Yeh R. F., Collins F., Guyer M. S., Peterson J., Felsenfeld A., Wetterstrand K. A., Patrinos A., Morgan M. J., de Jong P., Catanese J. J., Osoegawa K., Shizuya H., Choi S., and Chen Y. J. (2001) Initial sequencing and analysis of the human genome. *Nature* **409,** 860-921.

Landmark C. J. (2007) Targets for antiepileptic drugs in the synapse. *Med Sci Monit* **13,** RA1-RA7.

Lane P. W. (1972) New mutants and linkages: opisthotonos (opt). *Mouse News Lett* **47,** 36.

Lathrop G. M., Lalouel J. M., Julier C., and Ott J. (1984) Strategies for multilocus linkage analysis in humans. *Proc Natl Acad Sci U S A* **81,** 3443-3446.

Leone M., Bottacchi E., D'Alessandro G., and Kustermann S. (1995) Hereditary ataxias and paraplegias in Valle d'Aosta, Italy: a study of prevalence and disability. *Acta Neurol Scand* **91,** 183-187.

Lin X., Antalffy B., Kang D., Orr H. T., and Zoghbi H. Y. (2000) Polyglutamine expansion down-regulates specific neuronal genes before pathologic changes in SCA1. *Nat Neurosci* **3,** 157-163.

Lindblad-Toh K., Winchester E., Daly M. J., Wang D. G., Hirschhorn J. N., Laviolette J. P., Ardlie K., Reich D. E., Robinson E., Sklar P., Shah N., Thomas D., Fan J. B., Gingeras T., Warrington J., Patil N., Hudson T. J., and Lander E. S. (2000) Large-scale discovery and genotyping of single-nucleotide polymorphisms in the mouse. *Nat Genet* **24,** 381-386.

Manni E. and Petrosini L. (2004) A century of cerebellar somatotopy: a debated representation. *Nat Rev Neurosci* **5,** 241-249.

Mariotti C., Brusco A., Di Bella D., Cagnoli C., Seri M., Gellera C., Di Donato S., and Taroni F. (2008) Spinocerebellar ataxia type 28: A novel autosomal dominant cerebellar ataxia characterized by slow progression and ophthalmoparesis. *Cerebellum* **7,** 184-188.

Matsumoto M. and Nagata E. (1999) Type 1 inositol 1,4,5-trisphosphate receptor knock-out mice: their phenotypes and their meaning in neuroscience and clinical practice. *J Mol Med* **77,** 406-411.

Matsumoto M., Nakagawa T., Inoue T., Nagata E., Tanaka K., Takano H., Minowa O., Kuno J., Sakakibara S., Yamada M., Yoneshima H., Miyawaki A., Fukuuchi Y., Furuichi T., Okano H., Mikoshiba K., and Noda T. (1996) Ataxia and epileptic seizures in mice lacking type 1 inositol 1,4,5-trisphosphate receptor. *Nature* **379,** 168-171.

Matsuura T., Yamagata T., Burgess D. L., Rasmussen A., Grewal R. P., Watase K., Khajavi M., McCall A. E., Davis C. F., Zu L., Achari M., Pulst S. M., Alonso E., Noebels J. L., Nelson D. L., Zoghbi H. Y., and Ashizawa T. (2000) Large expansion of the ATTCT pentanucleotide repeat in spinocerebellar ataxia type 10. *Nat Genet* **26,** 191-194.

Meisler M. H. (1992) Insertional mutation of 'classical' and novel genes in transgenic mice. *Trends Genet* **8,** 341-344.

Melberg A., Mattsson P., and Westerberg C. E. (1997) Loss of control after a cup of coffee. *Lancet* **350,** 1220.

Miki Y., Swensen J., Shattuck-Eidens D., Futreal P. A., Harshman K., Tavtigian S., Liu Q., Cochran C., Bennett L. M., Ding W., Bell R., Rosenthal J., Hussey C., Tran T., McClure M., Frye C., Hattier T., Phelps R., Haugen-Strano A., Katcher H., Yakumo K., Gholami Z., Schaffer D., Stone S., Bayer S., Wray C., Bogden R., Dayananth P., Ward J., Tonin P., Narod S., Bristow P. K., Norris F. H., Helvering L., Morrison P., Rosteck P., Lai M., Barrett J. C., Lewis C., Neuhausen S., Cannon-Albright L., Goldgar D., Wiseman R., Kamb A., and Skolnick M. H. (1994) A strong candidate for the breast and ovarian cancer susceptibility gene BRCA1. *Science* **266,** 66-71.

Missiaen L., Robberecht W., van den B. L., Callewaert G., Parys J. B., Wuytack F., Raeymaekers L., Nilius B., Eggermont J., and De Smedt H. (2000) Abnormal intracellular ca(2+)homeostasis and disease. *Cell Calcium* **28,** 1-21.

Miura S., Shibata H., Furuya H., Ohyagi Y., Osoegawa M., Miyoshi Y., Matsunaga H., Shibata A., Matsumoto N., Iwaki A., Taniwaki T., Kikuchi H., Kira J., and Fukumaki Y. (2006) The contactin 4 gene locus at 3p26 is a candidate gene of SCA16. *Neurology* **67,** 1236-1241.

Miyoshi Y., Yamada T., Tanimura M., Taniwaki T., Arakawa K., Ohyagi Y., Furuya H., Yamamoto K., Sakai K., Sasazuki T., and Kira J. (2001) A novel autosomal dominant spinocerebellar ataxia (SCA16) linked to chromosome 8q22.1-24.1. *Neurology* **57,** 96-100.

Morrison P. J., Johnston W. P., and Nevin N. C. (1995) The epidemiology of Huntington's disease in Northern Ireland. *J Med Genet* **32,** 524-530.

Moseley M. L., Schut L. J., Bird T. D., Day J. W., and Ranum L. P. (2000) Reply- *Nat Genet* **24,** 215.

Nagafuchi S., Yanagisawa H., Ohsaki E., Shirayama T., Tadokoro K., Inoue T., and Yamada M. (1994a) Structure and expression of the gene responsible for the triplet repeat disorder, dentatorubral and pallidoluysian atrophy (DRPLA). *Nat Genet* **8,** 177-182.

Nagafuchi S., Yanagisawa H., Sato K., Shirayama T., Ohsaki E., Bundo M., Takeda T., Tadokoro K., Kondo I., Murayama N., Tanaka Y., Kikushima H., Umino K., Kurosawa H., Furukawa T., Nihei K., Inoue T., Sano A., Komure O., Takahashi M., Yoshizawa T., Kanazawa I., and Yamada M. (1994b) Dentatorubral and pallidoluysian atrophy expansion of an unstable CAG trinucleotide on chromosome 12p. *Nat Genet* **6,** 14-18.

Nakamura K., Jeong S. Y., Uchihara T., Anno M., Nagashima K., Nagashima T., Ikeda S., Tsuji S., and Kanazawa I. (2001) SCA17, a novel autosomal dominant cerebellar ataxia caused by an expanded polyglutamine in TATA-binding protein. *Hum Mol Genet* **10,** 1441-1448.

Nakanishi S., Maeda N., and Mikoshiba K. (1991) Immunohistochemical localization of an inositol 1,4,5-trisphosphate receptor, P400, in neural tissue: studies in developing and adult mouse brain. *J Neurosci* **11,** 2075-2086.

Nemes J. P., Benzow K. A., Moseley M. L., Ranum L. P., and Koob M. D. (2000) The SCA8 transcript is an antisense RNA to a brain-specific transcript encoding a novel actin-binding protein (KLHL1). *Hum Mol Genet* **9,** 1543-1551.

Nucifora F. C. Jr., Li S. H., Danoff S., Ullrich A., and Ross C. A. (1995) Molecular cloning of a cDNA for the human inositol 1,4,5-trisphosphate receptor type 1, and the identification of a third alternatively spliced variant. *Brain Res Mol Brain Res* **32,** 291-296.

Ogura H., Matsumoto M., and Mikoshiba K. (2001) Motor discoordination in mutant mice heterozygous for the type 1 inositol 1,4,5-trisphosphate receptor. *Behav Brain Res* **122,** 215-219.

Ohata T., Yoshida K., Sakai H., Hamanoue H., Mizuguchi T., Shimizu Y., Okano T., Takada F., Ishikawa K., Mizusawa H., Yoshiura K., Fukushima Y., Ikeda S., and Matsumoto N. (2006) A -16C>T substitution in the 5' UTR of the puratrophin-1 gene is prevalent in autosomal dominant cerebellar ataxia in Nagano. *J Hum Genet* **51,** 461-466.

Ophoff R. A., Terwindt G. M., Vergouwe M. N., van Eijk R., Oefner P. J., Hoffman S. M., Lamerdin J. E., Mohrenweiser H. W., Bulman D. E., Ferrari M., Haan J., Lindhout D., van Ommen G. J., Hofker M. H., Ferrari M. D., and Frants R. R. (1996) Familial hemiplegic migraine and episodic ataxia type-2 are caused by mutations in the Ca2+ channel gene CACNL1A4. *Cell* **87,** 543-552.

Orr H. T., Chung M. Y., Banfi S., Kwiatkowski T. J., Jr., Servadio A., Beaudet A. L., McCall A. E., Duvick L. A., Ranum L. P., and Zoghbi H. Y. (1993) Expansion of an unstable trinucleotide CAG repeat in spinocerebellar ataxia type 1. *Nat Genet* **4,** 221-226.

Orrenius S., Zhivotovsky B., and Nicotera P. (2003) Regulation of cell death: the calcium-apoptosis link. *Nat Rev Mol Cell Biol* **4,** 552-565.

Osborne R. J. and Thornton C. A. (2006) RNA-dominant diseases. *Hum Mol Genet* **15 Spec No 2,** R162-R169.

Parker I., Choi J., and Yao Y. (1996) Elementary events of InsP3-induced Ca2+ liberation in Xenopus oocytes: hot spots, puffs and blips. *Cell Calcium* **20,** 105-121.

Patterson R. L., Boehning D., and Snyder S. H. (2004) Inositol 1,4,5-trisphosphate receptors as signal integrators. *Annu Rev Biochem* **73,** 437-465.

Perutz M. F. (1996) Glutamine repeats and inherited neurodegenerative diseases: molecular aspects. *Curr Opin Struct Biol* **6,** 848-858.

Polo J. M., Calleja J., Combarros O., and Berciano J. (1991) Hereditary ataxias and paraplegias in Cantabria, Spain. An epidemiological and clinical study. *Brain* **114 (Pt 2),** 855-866.

Price N. E. and Mumby M. C. (1999) Brain protein serine/threonine phosphatases. *Curr Opin Neurobiol* **9,** 336-342.

Pulst S. M., Nechiporuk A., Nechiporuk T., Gispert S., Chen X. N., Lopes-Cendes I., Pearlman S., Starkman S., Orozco-Diaz G., Lunkes A., DeJong P., Rouleau G. A., Auburger G., Korenberg J. R., Figueroa C., and Sahba S. (1996) Moderate expansion of a normally biallelic trinucleotide repeat in spinocerebellar ataxia type 2. *Nat Genet* **14,** 269-276.

Rijkers T., Peetz A., and Ruther U. (1994) Insertional mutagenesis in transgenic mice. *Transgenic Res* **3,** 203-215.

Riordan J. R., Rommens J. M., Kerem B., Alon N., Rozmahel R., Grzelczak Z., Zielenski J., Lok S., Plavsic N., Chou J. L., Drumm M. L., Iannuzzi M. C., Collins F. S., and Tsui L-C. (1989) Identification of the cystic fibrosis gene: cloning and characterization of complementary DNA. *Science* **245,** 1066-1073.

Rogawski M. A. and Porter R. J. (1990) Antiepileptic drugs: pharmacological mechanisms and clinical efficacy with consideration of promising developmental stage compounds. *Pharmacol Rev* **42,** 223-286.

Sachidanandam R., Weissman D., Schmidt S. C., Kakol J. M., Stein L. D., Marth G., Sherry S., Mullikin J. C., Mortimore B. J., Willey D. L., Hunt S. E., Cole C. G., Coggill P. C., Rice C. M., Ning Z., Rogers J., Bentley D. R., Kwok P. Y., Mardis E. R., Yeh R. T., Schultz B., Cook L., Davenport R., Dante M., Fulton L., Hillier L., Waterston R. H., McPherson J. D., Gilman B., Schaffner S., Van Etten W. J., Reich D., Higgins J., Daly M. J., Blumenstiel B., Baldwin J., Stange-Thomann N., Zody M. C., Linton L., Lander E. S., and Altshuler D. (2001) A map of

human genome sequence variation containing 1.42 million single nucleotide polymorphisms. *Nature* **409,** 928-933.

Sanpei K., Takano H., Igarashi S., Sato T., Oyake M., Sasaki H., Wakisaka A., Tashiro K., Ishida Y., Ikeuchi T., Koide R., Saito M., Sato A., Tanaka T., Hanyu S., Takiyama Y., Nishizawa M., Shimizu N., Nomura Y., Segawa M., Iwabuchi K., Eguchi I., Tanaka H., Takahashi H., and Tsuji S. (1996) Identification of the spinocerebellar ataxia type 2 gene using a direct identification of repeat expansion and cloning technique, DIRECT. *Nat Genet* **14,** 277-284.

Schelhaas H. J., Verbeek D. S., van de Warrenburg B. P., and Sinke R. J. (2004) SCA19 and SCA22: evidence for one locus with a worldwide distribution. *Brain* **127,** E6.

Schoenberg B. S. (1978) Epidemiology of the inherited ataxias. *Adv Neurol* **21,** 15-32.

Schols L., Bauer P., Schmidt T., Schulte T., and Riess O. (2004) Autosomal dominant cerebellar ataxias: clinical features, genetics, and pathogenesis. *Lancet Neurol* **3,** 291-304.

Settembre C., Annunziata I., Spampanato C., Zarcone D., Cobellis G., Nusco E., Zito E., Tacchetti C., Cosma M. P., and Ballabio A. (2007) Systemic inflammation and neurodegeneration in a mouse model of multiple sulfatase deficiency. *Proc Natl Acad Sci U S A* **104,** 4506-4511.

Shaw C. J. and Lupski J. R. (2004) Implications of human genome architecture for rearrangement-based disorders: the genomic basis of disease. *Hum Mol Genet* **13,** R57-R64.

Shimoda L. A., Wang J., and Sylvester J. T. (2006) Ca2+ channels and chronic hypoxia. *Microcirculation* **13,** 657-670.

Silva M. C., Coutinho P., Pinheiro C. D., Neves J. M., and Serrano P. (1997) Hereditary ataxias and spastic paraplegias: methodological aspects of a prevalence study in Portugal. *J Clin Epidemiol* **50,** 1377-1384.

Simon-Sanchez J., Scholz S., Fung H. C., Matarin M., Hernandez D., Gibbs J. R., Britton A., De Vrieze F. W., Peckham E., Gwinn-Hardy K., Crawley A., Keen J. C., Nash J., Borgaonkar D., Hardy J., and Singleton A. (2007) Genome-wide SNP assay reveals structural genomic variation, extended homozygosity and cell-line induced alterations in normal individuals. *Hum Mol Genet* **16,** 1-14.

Sobie E. A., Song L. S., and Lederer W. J. (2006) Restitution of Ca(2+) release and vulnerability to arrhythmias. *J Cardiovasc Electrophysiol* **17 Suppl 1,** S64-S70.

Soong B. W. and Paulson H. L. (2007) Spinocerebellar ataxias: an update. *Curr Opin Neurol* **20,** 438-446.

Stevanin G., Bouslam N., Thobois S., Azzedine H., Ravaux L., Boland A., Schalling M., Broussolle E., Durr A., and Brice A. (2004) Spinocerebellar ataxia with sensory neuropathy (SCA25) maps to chromosome 2p. *Ann Neurol* **55,** 97-104.

Stevanin G., Herman A., Durr A., Jodice C., Frontali M., Agid Y., and Brice A. (2000) Are (CTG)n expansions at the SCA8 locus rare polymorphisms? *Nat Genet* **24,** 213.

Storey E., Gardner R. J., Knight M. A., Kennerson M. L., Tuck R. R., Forrest S. M., and Nicholson G. A. (2001) A new autosomal dominant pure cerebellar ataxia. *Neurology* **57,** 1913-1915.

Street V. A., Bosma M. M., Demas V. P., Regan M. R., Lin D. D., Robinson L. C., Agnew W. S., and Tempel B. L. (1997) The type 1 inositol 1,4,5-trisphosphate receptor gene is altered in the opisthotonos mouse. *J Neurosci* **17,** 635-645.

Strupp M., Zwergal A., and Brandt T. (2007) Episodic ataxia type 2. *Neurotherapeutics* **4,** 267-273.

Subramanian S., Mishra R. K., and Singh L. (2003) Genome-wide analysis of microsatellite repeats in humans: their abundance and density in specific genomic regions. *Genome Biol* **4,** R13.

Taguchi A., Wanaka A., Mori T., Matsumoto K., Imai Y., Tagaki T., and Tohyama M. (1996) Molecular cloning of novel leucine-rich repeat proteins and their expression in the developing mouse nervous system. *Brain Res Mol Brain Res* **35,** 31-40.

The Huntington's Disease Collaborative Research Group (1993) A novel gene containing a trinucleotide repeat that is expanded and unstable on Huntington's disease chromosomes. *Cell* **72,** 971-983.

Toescu E. C. and Verkhratsky A. (2007) The importance of being subtle: small changes in calcium homeostasis control cognitive decline in normal aging. *Aging Cell* **6,** 267-273.

Trasande C. A. and Ramirez J. M. (2007) Activity deprivation leads to seizures in hippocampal slice cultures: is epilepsy the consequence of homeostatic plasticity? *J Clin Neurophysiol* **24,** 154-164.

Traynor B. J., Codd M. B., Corr B., Forde C., Frost E., and Hardiman O. (1999) Incidence and prevalence of ALS in Ireland, 1995-1997: a population-based study. *Neurology* **52,** 504-509.

Truant R., Atwal R. S., Desmond C., Munsie L., and Tran T. (2008) Huntington's disease: revisiting the aggregation hypothesis in polyglutamine neurodegenerative diseases. *FEBS J* **275,** 4252-4262.

Tu H., Miyakawa T., Wang Z., Glouchankova L., Iino M., and Bezprozvanny I. (2002) Functional characterization of the type 1 inositol 1,4,5-trisphosphate receptor coupling domain SII(+/-) splice variants and the Opisthotonos mutant form. *Biophys J* **82,** 1995-2004.

van de Leemput J., Chandran J., Knight M. A., Holtzclaw L. A., Scholz S., Cookson M. R., Houlden H., Gwinn-Hardy K., Fung H. C., Lin X., Hernandez D., Simon-Sanchez J., Wood N. W., Giunti P., Rafferty I., Hardy J., Storey E., Gardner R. J., Forrest S. M., Fisher E. M., Russell J. T., Cai H., and Singleton A. B. (2007) Deletion at ITPR1 underlies ataxia in mice and spinocerebellar ataxia 15 in humans. *PLoS Genet* **3,** e108.

van de Warrenburg B. P., Sinke R. J., Verschuuren-Bemelmans C. C., Scheffer H., Brunt E. R., Ippel P. F., Maat-Kievit J. A., Dooijes D., Notermans N. C., Lindhout D., Knoers N. V., and Kremer H. P. (2002) Spinocerebellar ataxias in the Netherlands: prevalence and age at onset variance analysis. *Neurology* **58,** 702-708.

van Swieten J. C., Brusse E., de Graaf B. M., Krieger E., van de G. R., de K., I, Maat-Kievit A., Leegwater P., Dooijes D., Oostra B. A., and Heutink P. (2003) A mutation in the fibroblast growth factor 14 gene is associated with autosomal dominant cerebellar ataxia [corrected]. *Am J Hum Genet* **72,** 191-199.

Venter J. C., Adams M. D., Myers E. W., Li P. W., Mural R. J., Sutton G. G., Smith H. O., Yandell M., Evans C. A., Holt R. A., Gocayne J. D., Amanatides P., Ballew R. M., Huson D. H., Wortman J. R., Zhang Q., Kodira C. D., Zheng X. H., Chen L., Skupski M., Subramanian G., Thomas P. D., Zhang J., Gabor Miklos G. L., Nelson C., Broder S., Clark A. G., Nadeau J., McKusick V. A., Zinder N., Levine A. J., Roberts R. J., Simon M., Slayman C., Hunkapiller M., Bolanos R., Delcher A., Dew I., Fasulo D., Flanigan M., Florea L., Halpern A., Hannenhalli S., Kravitz S., Levy S., Mobarry C., Reinert K., Remington K., Abu-Threideh J., Beasley E., Biddick K., Bonazzi V., Brandon R., Cargill M., Chandramouliswaran I., Charlab R., Chaturvedi K., Deng Z., Di F., V, Dunn P., Eilbeck K., Evangelista C., Gabrielian A. E., Gan W., Ge W., Gong F., Gu Z., Guan P., Heiman T. J., Higgins M. E., Ji R. R., Ke Z., Ketchum K. A., Lai Z., Lei Y., Li Z., Li J., Liang Y., Lin X., Lu F., Merkulov G. V., Milshina N., Moore H. M., Naik A. K., Narayan

V. A., Neelam B., Nusskern D., Rusch D. B., Salzberg S., Shao W., Shue B., Sun J., Wang Z., Wang A., Wang X., Wang J., Wei M., Wides R., Xiao C., Yan C., Yao A., Ye J., Zhan M., Zhang W., Zhang H., Zhao Q., Zheng L., Zhong F., Zhong W., Zhu S., Zhao S., Gilbert D., Baumhueter S., Spier G., Carter C., Cravchik A., Woodage T., Ali F., An H., Awe A., Baldwin D., Baden H., Barnstead M., Barrow I., Beeson K., Busam D., Carver A., Center A., Cheng M. L., Curry L., Danaher S., Davenport L., Desilets R., Dietz S., Dodson K., Doup L., Ferriera S., Garg N., Gluecksmann A., Hart B., Haynes J., Haynes C., Heiner C., Hladun S., Hostin D., Houck J., Howland T., Ibegwam C., Johnson J., Kalush F., Kline L., Koduru S., Love A., Mann F., May D., McCawley S., McIntosh T., McMullen I., Moy M., Moy L., Murphy B., Nelson K., Pfannkoch C., Pratts E., Puri V., Qureshi H., Reardon M., Rodriguez R., Rogers Y. H., Romblad D., Ruhfel B., Scott R., Sitter C., Smallwood M., Stewart E., Strong R., Suh E., Thomas R., Tint N. N., Tse S., Vech C., Wang G., Wetter J., Williams S., Williams M., Windsor S., Winn-Deen E., Wolfe K., Zaveri J., Zaveri K., Abril J. F., Guigo R., Campbell M. J., Sjolander K. V., Karlak B., Kejariwal A., Mi H., Lazareva B., Hatton T., Narechania A., Diemer K., Muruganujan A., Guo N., Sato S., Bafna V., Istrail S., Lippert R., Schwartz R., Walenz B., Yooseph S., Allen D., Basu A., Baxendale J., Blick L., Caminha M., Carnes-Stine J., Caulk P., Chiang Y. H., Coyne M., Dahlke C., Mays A., Dombroski M., Donnelly M., Ely D., Esparham S., Fosler C., Gire H., Glanowski S., Glasser K., Glodek A., Gorokhov M., Graham K., Gropman B., Harris M., Heil J., Henderson S., Hoover J., Jennings D., Jordan C., Jordan J., Kasha J., Kagan L., Kraft C., Levitsky A., Lewis M., Liu X., Lopez J., Ma D., Majoros W., McDaniel J., Murphy S., Newman M., Nguyen T., Nguyen N., and Nodell M. (2001) The sequence of the human genome. *Science* **291,** 1304-1351.

Verbeek D. S., Schelhaas J. H., Ippel E. F., Beemer F. A., Pearson P. L., and Sinke R. J. (2002) Identification of a novel SCA locus (SCA19) in a Dutch autosomal dominant cerebellar ataxia family on chromosome region 1p21-q21. *Hum Genet* **111,** 388-393.

Verbeek D. S., van de Warrenburg B. P., Wesseling P., Pearson P. L., Kremer H. P., and Sinke R. J. (2004) Mapping of the SCA23 locus involved in autosomal dominant cerebellar ataxia to chromosome region 20p13-12.3. *Brain* **127,** 2551-2557.

Vuillaume I., Devos D., Schraen-Maschke S., Dina C., Lemainque A., Vasseur F., Bocquillon G., Devos P., Kocinski C., Marzys C., Destee A., and Sablonniere B. (2002) A new locus for spinocerebellar ataxia (SCA21) maps to chromosome 7p21.3-p15.1. *Ann Neurol* **52,** 666-670.

Wang T. and Morgan J. I. (2007) The Purkinje cell degeneration (pcd) mouse: an unexpected molecular link between neuronal degeneration and regeneration. *Brain Res* **1140,** 26-40.

Waters M. F., Minassian N. A., Stevanin G., Figueroa K. P., Bannister J. P., Nolte D., Mock A. F., Evidente V. G., Fee D. B., Muller U., Durr A., Brice A., Papazian D. M., and Pulst S. M. (2006) Mutations in voltage-gated potassium channel KCNC3 cause degenerative and developmental central nervous system phenotypes. *Nat Genet* **38,** 447-451.

Wheeler R. B., Sharp J. D., Schultz R. A., Joslin J. M., Williams R. E., and Mole S. E. (2002) The gene mutated in variant late-infantile neuronal ceroid lipofuscinosis (CLN6) and in nclf mutant mice encodes a novel predicted transmembrane protein. *Am J Hum Genet* **70,** 537-542.

Wojda U., Salinska E., and Kuznicki J. (2008) Calcium ions in neuronal degeneration. *IUBMB Life* **60,** 575-590.

Wooster R., Bignell G., Lancaster J., Swift S., Seal S., Mangion J., Collins N., Gregory S., Gumbs C., and Micklem G. (1995) Identification of the breast cancer susceptibility gene BRCA2. *Nature* **378,** 789-792.

Worth P. F., Houlden H., Giunti P., Davis M. B., and Wood N. W. (2000) Large, expanded repeats in SCA8 are not confined to patients with cerebellar ataxia. *Nat Genet* **24,** 214-215.

Woychik R. P. and Alagramam K. (1998) Insertional mutagenesis in transgenic mice generated by the pronuclear microinjection procedure. *Int J Dev Biol* **42,** 1009-1017.

Xie G., Clapcote S. J., Nieman B. J., Tallerico T., Huang Y., Vukobradovic I., Cordes S. P., Osborne L. R., Rossant J., Sled J. G., Henderson J. T., and Roder J. C. (2007) Forward genetic screen of mouse reveals dominant missense mutation in the P/Q-type voltage-dependent calcium channel, CACNA1A. *Genes Brain Behav* **6,** 717-727.

Yabe I., Sasaki H., Yamashita I., Takei A., and Tashiro K. (2001) Clinical trial of acetazolamide in SCA6, with assessment using the Ataxia Rating Scale and body stabilometry. *Acta Neurol Scand* **104,** 44-47.

Yamada M., Sato T., Tsuji S., and Takahashi H. (2008) CAG repeat disorder models and human neuropathology: similarities and differences. *Acta Neuropathol* **115,** 71-86.

Young N. D. and Tanksley S. D. (1989) Restriction fragment length polymorphism maps and the concept of graphical genotypes. *Theor Appl Genet* **77,** 95-101.

Yu G. Y., Howell M. J., Roller M. J., Xie T. D., and Gomez C. M. (2005) Spinocerebellar ataxia type 26 maps to chromosome 19p13.3 adjacent to SCA6. *Ann Neurol* **57,** 349-354.

Zecevic N., Milosevic A., and Ehrlich B. E. (1999) Calcium signaling molecules in human cerebellum at midgestation and in ataxia. *Early Hum Dev* **54,** 103-116.

Zhuchenko O., Bailey J., Bonnen P., Ashizawa T., Stockton D. W., Amos C., Dobyns W. B., Subramony S. H., Zoghbi H. Y., and Lee C. C. (1997) Autosomal dominant cerebellar ataxia (SCA6) associated with small polyglutamine expansions in the alpha 1A-voltage-dependent calcium channel. *Nat Genet* **15,** 62-69.

Zoghbi H. Y. (2000) Spinocerebellar ataxias. *Neurobiol Dis* **7,** 523-527.

APPENDIX I.

AMPLIFICATION PROGRAMS

Phases; Di, initial denaturation; D, denaturation; A, annealing; E, extension; Ef, final extension.

Temp, temperature in degrees Celsius. Duration in ’ minutes; ’’ seconds.

PCR amplification

57-to-52

		15 cycles			16 cycles			14 cycles				
phase	Di	D	A	E	D	A	E	D	A	E	Ef	
temp.	94°C	94°C	57°C	72°C	94°C	57°C	72°C	94°C	52°C	72°C	72°C	4°C
duration	3’	30”	30”	30”	30”	30”	30”	30”	30”	30”	5’	hold

65-to-55

		8 cycles			16 cycles			16 cycles				
phase	Di	D	A	E	D	A	E	D	A	E	Ef	
temp.	94°C	94°C	65°C	72°C	94°C	65°C	72°C	94°C	55°C	72°C	72°C	4°C
duration	3’	20”	20”	30”	20”	20”	1’	30”	20”	30”	5’	hold

60-to-50

		8 cycles			16 cycles			16 cycles				
phase	Di	D	A	E	D	A	E	D	A	E	Ef	
temp.	94°C	94°C	60°C	72°C	94°C	60°C	72°C	94°C	50°C	72°C	72°C	4°C
duration	4’	20”	20”	30”	20”	20”	1’	20”	20”	30”	5’	hold

62-to-52

		8 cycles			16 cycles			16 cycles				
phase	Di	D	A	E	D	A	E	D	A	E	Ef	
temp.	94°C	94°C	62°C	72°C	94°C	62°C	72°C	94°C	52°C	72°C	72°C	4°C
duration	4’	20”	20”	30”	20”	20”	1’	20”	20”	30”	5’	hold

Sequence amplification

sequencing (mouse)

	25 cycles			
phase	D	A	E	
temp.	96°C	50°C	60°C	4°C
duration	30”	15”	3’	hold

sequencing (human)

		30 cycles			
phase	Di	D	A	E	
temp.	96°C	96°C	50°C	60°C	4°C
duration	1’	10”	5”	4’	hold

Genotype amplification

genotyping (using microsatellites)

		30 cycles				
phase	Di	D	A	E	Ef	
temp.	95°C	94°C	55°C	72°C	72°C	4°C
duration	12’	15”	15”	30”	10’	hold

PRIMERS

Sq f, forward primer sequence; sq r, reverse primer sequence; amplicon (bp), lengt in base pairs of amplicon; pcr, polymerase chain reaction. Mg^{2+}, magnesium (25mM); DMSO, dimethyl sulfoxide.

Table I.1 Primers used for genome wide linkage in mouse

exon	primer	sq f	sq r	amplicon (bp)	pcr program
1	MHAP35FRA8	TGTAGCTGAACCAGTGTGCC	CATCCATGTTTCCGTGTGAG	163	57-to-52
1	MHAP61FRC7	TGTCAAGGAGGATGTTTGGA	GGACCTAATTGGTTTGAATGGA	171	57-to-52
1	MHAP84FLD1	TTTTACTTGGGCTCCACACC	TTTCCACCTTGATCCAAAAA	157	57-to-52
1	MHAP31FLD3	TCCCCATCTCCACAGAAACT	ATAGGAGACCAGGGAGCCAT	163	57-to-52
1	MHAP37FRD9	AGCATTGCTGAAACAGCTCC	TAATTGGTGTGTGTGTGGGG	168	57-to-52
1	MHAP84FRF7	TGTTTTTGTTTTGGCTTGGA	ACCATCAGGCTGGTGAGAAT	168	57-to-52
1	MHAP46FRF9	CCAATCGTCACAAGTCAGTGAT	AAGAGATCATTGCCATACAGGAA	104	57-to-52
1	MHAP29FRH9	TCTGCCTTGTTGATGCTTTG	TCTCCATTCCTTGAGGGTCA	194	57-to-52
1	MHAP87FRH9	GAGCACCAAGCACACACG	CTCAGGTCATCCTCAGCCTT	172	57-to-52
1	MHAP86FRB10	AGGCTGAGCTTCAAAGTTGG	TGTCAAGGGCATCAAGAAGTC	158	57-to-52
1	MHAP15FLB5	TTCTCCACTGTGGCTGTTTG	GAGCCTGTTTGTAGACTGGAAGA	156	57-to-52
1	MHAP17FRC10	TCACTTGGTTCATCAGTTCAGG	GCCAGGGATTTATCAGAGCTT	195	57-to-52
1	MHAP57FLC4	CACTCTGGGATACCCTGCAT	TTCACAGGGGGAATCTTCTG	172	57-to-52
1	MHAP26FRG10	CCGGTGGAGATGTTCCTTTA	ATCTGCTGGATCCTCACAGG	175	57-to-52
1	MHAP82FLH4	TGGTTCTTGACTGTTGACGC	GGTCTTCCAGAACCTGACCA	158	57-to-52
2	MHAP87FRD8	TAAGTCTTCTCCCATTGCCC	CAGATAACATCTGAGGCCTTG	152	57-to-52
2	MHAP61FRE7	TTCATTTCTAAAACCCAGTTTTTCT	AATCAGGGGCCCAGTTTG	154	57-to-52
2	MHAP71FRF8	CCTGAGGACAACTCTGGAGC	AGCTGCAGAAGCATAGAGGG	163	57-to-52
2	MHAP59FLA6	CTTCCCCCACACCTGACTAC	GGATTTTGGGAAGGAGAGGT	181	57-to-52
2	MHAP64FRC10	GGGGGACACACACCATGT	TTCCTGTACAACTGGTTGCTTG	151	57-to-52
2	MHAP4FLC5	CCCTGGACCCCTTTTCTCTA	AGCCTGGGTACTCACCACAC	195	57-to-52
2	MHAP46FRD10	TGCTCTGCATTTTGATTTGG	GACTGCATGTGGGGAGAGAT	194	57-to-52

2	MHAP33FRE11	GAGCCACCCATAGCTGAGAG	CACTCCGTCCAGTCAATGC	151	57-to-52	
2	MHAP45FRF11	CCAGATGGATTTCCATGGTC	AGGGCTTGCTCTCACAGGTA	174	57-to-52	
2	MHAP59FLH4	CCCTGAGTTACATCCCCAAG	CAGGACAAACAGCACTTCCA	280	57-to-52	
3	MHAP11FLD2	CAGGAAACCATTTCTTTCTGGA	TTTGAATGTGCCAACTCTTTTT	189	57-to-52	
3	MHAP9FLH3	CTCAGGGTCCTTAGCACTGG	CACACAGGCGACTTCGTTTA	161	57-to-52	
3	MHAP59FLD5	TTCATGGGTGAACAAGAGCA	ACAATCAAAGCTGGCTCCAT	151	57-to-52	
4	MHAP71FRA7	TAGAAAATCTGGGCTGGGAA	CTTTCAAGTCAGGGCAAAGC	186	57-to-52	
4	MHAP37FRC9	AGCGGTTCTCAACCTTGTGT	TTGCTCACATTGTGGTGACA	177	60-to-50	
4	MHAP91FLF2	GGGGTAGGGAGTGGGTACAT	GTACCCAGGGTCCAGCATAA	158	57-to-52	
4	MHAP82FLF3	GTAGTGTGGGGGAGGTGCTA	ACGGGATCTTGCCATGTAAC	155	57-to-52	
4	MHAP7FRA12	GCAAACATTTCCATTCTCAGC	CACATTCACGCTTATTCATACACC	107	57-to-52	
4	MHAP11FLC5	ATGTGGTCTTGTTGGGGATG	TCCAGCCTTTATCTGACCAGT	170	57-to-52	
4	MHAP33FRE10	ATGGTAGAGCCACTGCCAAG	GGTTAGGTGCTTTTGGTTGC	151	57-to-52	
4	MHAP88FRE10	CTGACAAGCTGACAATGACGA	TTTTCTAATGGCAGGGATGG	160	57-to-52	
4	MHAP34FLE5	TGTGGAAAGCTGATCGTGAA	TTGGTTGGGTTTTTGTCTTTG	185	60-to-50	Mg^{2+}
5	MHAP95FRA9	CATGATGAGCCCAGGAAGAT	CCAACCATTTGGAAGCCTTA	186	57-to-52	
5	MHAP59FRC8	ACCAACAGACAAAACTGCCC	AGTGATGACCCTGTGGTGTG	165	57-to-52	
5	MHAP20FRD8	GCAAGCCCCAAAGAATTGTA	AAGAACAGCACGTTGGGTTT	174	57-to-52	
5	MHAP36FRF7	CCAAACTGTTGCAAGGACAA	GACATAGACACAGACACCCCC	168	57-to-52	
5	MHAP91FLH1	TGAGGTCTGTGTTTCCACCA	CCTTGCCCTTTACACTCAGC	151	57-to-52	
5	MHAP35FLB5	CTCAGAGGCAATGGGAAGAG	AGCTGATGTTGGCTAAGGTTG	177	57-to-52	
6	MHAP84FRB9	TTCTCGGGGCATAATAGTGG	GCCAGCAAGAAACACACTCA	193	57-to-52	
6	MHAP34FLD3	TTACCTGATGTCCTTGTGCG	GGGGAAACTGGAAGTTCCTT	168	57-to-52	
6	MHAP67FLF1	TGAGTGATCACGTGGACAGG	CCTTCTATTGCCTATCCCAGC	152	57-to-52	
6	MHAP85FLG2	GGATCCTTATTCTCCTCACTGC	ACATGGGGTGGTGTTCTGTT	161	57-to-52	
6	MHAP25FRB12	CCAAACTGGAAAAAGGCATC	CTGAGACCTGTGGGTGGTTT	187	57-to-52	
6	MHAP17FRE10	CCAGAGATTCCGCTGTCTGT	TTGAGGTGCTTCGTGTTAAAAA	178	57-to-52	
6	MHAP27FRG11	GAAAAACCCTGCCAGAATCA	AGCTGCCTGACATGGGTACT	159	57-to-52	
6	MHAP85FLG5	TGGATTATAGTAAGGTCTCTTTGGA	GCCAAAAAGAATGCCTGATT	166	57-to-52	
6	MHAP94FRG12	CTCTGTTGTTTTGGAAGCACA	TTTGCTTGTTAAATGCCCCT	153	57-to-52	

6	MHAP28FRH10	CCAGTCCCTCTGAAGATGCT	CAGACCTAGGGACACCCTGA	158	57-to-52	
7	MHAP71FRB7	TCTGGAACTGACCTGAAGGC	GTGAATGCCAACACTGCATC	176	57-to-52	
7	MHAP85FRC7	CTAACAGGGAACAGGCAAGG	GCTGTAGCCTGGTTCAAGGT	174	57-to-52	
7	MHAP22FRE8	GAAGTCAGAGTGGCCTCACC	TGACCCACAAAGCCTCTTTT	155	57-to-52	
7	MHAP34FLE3	TTTTTGAGGCGGAGTCTAGC	TGGCTAAAGTTGCCAATCAA	155	57-to-52	
7	MHAP44FLF2	ACTCTGGGGTCAGTGAGAGG	TTATTCCGGGCTACAGATGG	155	57-to-52	
7	MHAP4FRG8	GCAGAAGGGAAGACAGTTGC	AGCCGTGAAGAGAGGCATAA	154	57-to-52	
7	MHAP7FLG2	AGCTGGGCTTCACCTGAGTA	CTCATGGCTTGACTCTGGAAG	157	57-to-52	
7	MHAP6FLG3	GCTGGGCTTTCACTGATTTC	CGCAGGGGCAAATATAGAAG	162	57-to-52	
7	MHAP64FLH2	ATGGGAGTTTCCATGCAGTT	TATGCAGCAGACTGGGTAGC	177	57-to-52	
7	MHAP57FLA5	AGCAAGACAAAAAGGTCCCC	TGGCTTAAAATTGCATCATCA	155	57-to-52	
7	MHAP26FRC10	CGGGTGTCCTGGATGTTTAG	CACTAGGCTTTCTTGCCAGC	182	57-to-52	
7	MHAP27FRC12	TTGGCAGAGTAGTCCAAGCA	ACCGTCACTCTCATCGGAAC	156	57-to-52	
7	MHAP5FLC6	GGTCTTCCTGTGTAATTTTGGG	TTTGGGGCTAGTTGTCATCA	170	57-to-52	
7	MHAP70FLD6	ATGTGCACACACACCAGACA	CCTCCAGACAAGGTCTCCTG	153	57-to-52	
7	MHAP64FLF5	TCCCCCTGGATCTTCTCTTT	GGGATGTGGACTCTGAAGAAA	165	57-to-52	
7	MHAP57FLH4	TGGAGCATTTACACCTGCTG	TTTCCAGCCTTTCCTCTGAA	185	57-to-52	
8	MHAP58FLA1	CACGGTTGTGACATTTGAGG	GAAGGCACATAAACGGATGG	193	57-to-52	
8	MHAP87FLD2	CAATGCACAAGTCAGCATCA	GATGAGGCCTGACAAAGCTC	108	57-to-52	
8	MHAP80FLE1	TAAAGCCCACACTCACCACA	GAGGGAAAAATGGGGTCTTC	196	57-to-52	
8	MHAP27FRE8	AGCTGAACCCTGAAAACAGC	GCCCAGACATTCCCATGTTA	188	57-to-52	
8	MHAP82FLE3	GGCAGCCTCACACTAGGAAG	TCCTGTTGACCTGTGGTTCC	178	57-to-52	
8	MHAP88FRG8	CCCTCCACAATGAAGGCTAC	GGGCAATCTGTGAAGGTTTT	186	57-to-52	
8	MHAP27FRH8	TGGAGGGAGACATTGAGAGG	GGTCCTTGGGAGGTGCTTAT	177	57-to-52	
8	MHAP34FLH3	AATGAATCAGAAGCCGGCTG	TTCTGGTGGCAGATAATGTC	203	65-to-55	
8	MHAP45FLB4	TTTCTTTGAGTCATTTTTGTTGTTG	GGTTTCCTCTCCCTCAGTCTC	170	60-to-50	Mg^{2+}
8	MHAP86FLD4	GGGAACAGGCTCACAAAGTC	CCCAAGGCACAGCTTAGTTC	182	57-to-52	
8	MHAP16FLE5	CCTGGTTGGCAAAATGAGTT	CCCTCAGTGTTTTTGGATGT	198	57-to-52	
8	MHAP30FLG5	TTTGAGTTGCAGGGTTTTCC	AATGCTAATGAGCCAGGCAG	154	60-to-50	
9	MHAP84FRA11	GATGACGCTGGTGGAGACTT	AGTGAGCCGTCTAGCACCAT	200	57-to-52	

9	MHAP56FRB10	TACCTGACCTAGGGTTCGGA	TGGTGGAGGCTGATTTTCTT	180	57-to-52
9	MHAP63FLC5	TTGGTGTGCATGGGAACTTA	TGCTGTTGGACACACCATTT	175	57-to-52
9	MHAP28FLG6	GAAAGCGTTCATTAGCAGGC	AGGTAGGTGGTCACAGACGC	161	57-to-52
10	MHAP61FLE2	GAGGCTAGTCGGCAACTGAC	TCATGTACCAACTCCCACCA	194	57-to-52
10	MHAP91FLG3	CCCAAGTGGTGAAAGCAAAG	CCATGCCTTGAGGTTTTGAT	188	57-to-52
10	MHAP15FLB4	GGAAACAGCAGTAAGGAGAACG	TGAGTTCTTCCTCCCCTGAA	200	57-to-52
10	MHAP61FRF11	AAAAACAGAAAAAGGCAGTGACA	AACAGGGCACCATAGAAACAA	151	57-to-52
10	MHAP61FRG10	GCATGTGAGAGGGCTGAAAT	CCCAGCTTTTCTGCAGTGAT	152	57-to-52
10	MHAP7FRH11	ATTGGCAGTGATGTGGCATA	ATTGCATCTAACAGGGAGCG	183	57-to-52
11	MHAP90FLA2	CTCTGTGCCCTTTTGACCTT	AGAGACAGACGCCTCTGGAA	155	57-to-52
11	MHAP28FRA9	TCACAGTAACATGGGAGCCA	TGTGATACAAAGCCAGCCAG	151	57-to-52
11	MHAP89FLE3	TCCAGAGTCACACCAAGATCA	TATCTGTGCTGGGACCATCC	189	57-to-52
11	MHAP86FRF9	CAGTGAGATGGGAGAGACGTG	CCTGATTCCTTGAAGTAAGGC	152	60-to-50
11	MHAP66FLG3	CCTCCTGTCTAAATGAGAAGGTGTA	AGGTGTCCCCTGTCATTGTC	160	57-to-52
11	MHAP12FRH7	TAGGGAACTGTCCCTGCCTA	ACTCCTGTTCCCTTCTGGCT	159	57-to-52
11	MHAP48FLH3	TAGGAGGAAGTCTCCACCCC	ATCCCATCAAGCACAGCTTC	152	57-to-52
11	MHAP26FRC11	CCAAGGACCCTGCAATTCTA	ATCGCAGCTGGCTAAAATGT	178	60-to-50
11	MHAP9FLC5	TTGATGACTTCTTGGAGCTGAA	CCTTTGAGGGGACTCCAGTA	178	57-to-52
12	MHAP34FLD1	ACAGCTTCGTGTGAGCTGTG	GGCAGAACCTGACCTTAGCA	165	57-to-52
12	MHAP91FLD3	CGACACCCCCACTCTTAATG	ATTCAAGGAATGCTGCCACT	168	57-to-52
12	MHAP22FRE7	ATGCTGTCAGGCTTGTGTTG	CGCATTCCTGAGCTGAATTT	174	57-to-52
12	MHAP86FLE2	CCACTATAATATCCATGCTGTGTT	CAGACAGGGAAGGAGGGAG	173	57-to-52
12	MHAP46FRF7	GGAGCCTGGTGTTCACTGAT	AATGCCTGGCAAAGAAACAC	174	57-to-52
12	MHAP42FLF3	GTAAGACGCTTGGGCAAAAA	GAAGCCTTCTCACCTTCCCT	181	57-to-52
12	MHAP70FRD12	CTAGAACTTACCTTGCCCTGGA	TCCGAAGACACTCGTAGGCT	151	57-to-52
12	MHAP28FLH4	TAAGGGGACCCTCAGTTGAA	TTGCCACAATGCTTTGGATA	163	57-to-52
12	MHAP44FLH5	TGGGTATCTCACAACCAAACC	TCAAGCTAAAGTCTCCACTCCA	155	57-to-52
13	MHAP22FRG8	CCATGAGCCTTGAAGAAGGA	TGTACACATGAGACTCCGGC	168	57-to-52
13	MHAP70FLA5	CCAGCCTAGGATGTGTTCAA	TACCCTTCACCACCACACAA	179	57-to-52
13	MHAP28FLB6	AACTGACAGGGTGGTTGGTC	CATTTTGGAAATGTCGGCTT	170	57-to-52

13	MHAP76FRC10	TGGGAACAGGGCAAGAATTA	GGATCACACTGACTGCCTGA	194	57-to-52	
13	MHAP35FRD10	GGTAACCAACAGCATCAGCA	TTACCTTATATCAGCATGGCAA	153	57-to-52	
13	MHAP5FRG12	TGCAGTGAAAGCATGAGGAC	TTCACTGGTCTGGAACTCTCC	160	57-to-52	
14	MHAP59FLB3	CCTCTGAATGCCTAAGCAGG	TGCTTGACACAAGGCTATGC	187	57-to-52	
14	MHAP88FRB12	GGGAGACACACACACACAGG	ATGTTCCTCCAAGCATCAGG	187	65-to-55	
14	MHAP64FLE4	AAAATGGTTGGGCAAAAATG	GAGCTATGGTCCCAAATAGCC	151	57-to-52	
14	MHAP31FLF5	TCACTCTGGGAAGCCATTTC	TCTGAATACAAAGCAGCCCC	159	57-to-52	
15	MHAP64FRA8	CCAGGGCTTGAGTTTGGATA	CCCCACACACTGTGACAATC	157	57-to-52	
15	MHAP86FRA8	AGCCTCTCCTGCTGTTTCC	TCTGCATCACTGTTAAGTTC	217	60-to-50	
15	MHAP94FLA2	TTGCAGGTGTCTTTTATCTTCC	GACAGAGACTTTGGGGATGC	181	60-to-50	
15	MHAP35FRA9	GATTTGTCCCAGTTGTGCCT	CCTCACAGGGTCTCCTCTTG	152	57-to-52	
15	MHAP9FLB1	CCGTGATTACATCCCTTGGT	TGACTTCACAGCAACATGGA	162	57-to-52	
15	MHAP30FLD1	GTGGCTAGTGCCTCTCACAA	TACTGGGTGAGTCTGTGGGC	169	60-to-50	
15	MHAP75FRD10	TTTCCATTCAATCAACACCATC	TTTCCAGTGTTGCTCAGATTG	161	57-to-52	Mg^{2+}
15	MHAP59FLF6	CACTGTTGCGAACTGCTCAT	GCACAGTCTGAGAACTCCCC	159	57-to-52	DMSO
15	MHAP33FLG6	CACTACCGGTGTGTGTCACC	TGTTGGGTTGATGACTGGAA	167	57-to-52	
16	MHAP44FLE5	GGGGTCTGTTCGTCTCAAAA	ATAGAGTCAAAGGGGTGGGG	195	57-to-52	
17	MHAP54FLE3	CCATGCTGTCCTCAAACTCA	GCAGAAAGAGGGGAACTGTG	191	57-to-52	
17	MHAP66FLB6	CATGTGGTGCTCTTGTTTGG	TGGTTCATTAGAGGAGCCTTTT	165	57-to-52	
18	MHAP9FRE8	TTTGATTACCCTCCGGAACA	ATTTCCCACTCAGCAGCCTA	153	57-to-52	
18	MHAP54FLG3	CCAAAAGCTTTGAGGGGAAT	GAAATCAGAATGCTGGAGGC	155	57-to-52	
18	MHAP7FRB10	TTCGGTTACCACACACCATT	AGCCATGCTGGTATTTCCTG	166	57-to-52	
18	MHAP11FRF10	CCTCTGGACACATTCTTCTCG	CCCAGTCTCCACTGTAAAGCA	151	57-to-52	
19	MHAP17FRC8	CCCTAAACCCTAGCCCTGAC	GAAATTGATGGGTGGCATCT	187	57-to-52	
19	MHAP5FLH5	CGTAGAACCAGGCGCTTTAG	GCAGCACATGGCATAGAGAA	158	57-to-52	
x	12_5_11_6	GATGGCTAATTCCAGGCCTAC	CAACAGCAGAGCTGTACCCA	152	57-to-52	
x	MHAP94FLC5	CATGGTCACCTGGCAACA	TCTGGTGCAATTCTACAACCC	154	57-to-52	
x	MHAP28FLD4	GGAATGGGAAAAGAATGCAA	TGAGGTGCGTACCAAAAGAA	193	57-to-52	

MHAP35FLE5, MHAP45FLB4 4 mg Mg^{2+}; MHAP75FRD10 3 mg Mg^{2+}; MHAP59FLF6 2% DMSO.

Primer sequences obtained from Lindblad-Toh et al. (2000).

Table I.2 Primers used for finemapping of mouse chromosome 6

uniSTS	primer	sq f	sq r	amplicon (bp)	pcr program	
186271	MHAP58FLC3	CCCTGGAGAAATCTGAAACC	CTAATGGTTGCATTTTGGGG	174	57-to-52	
125213	MHAa54c9	AGATTCCAGGCAGACAGCAT	GCAAACCACCTCCAAACCTA	155	57-to-52	
125903	X99043	CTGAGAAGCCATTAGCCCAG	GGTGGCAACACAAGGAAAAG	198	57-to-52	
n/a	D6Mit337.3	TGTCTGTCTATCATCTGTCTGTCTG	TCAAGTTGACAGCATTAACTACCAC	111	57-to-52	
130759	D6Mit214	TGTAGGCAGTCCGTGTACATG	AATTAGAGATATAGAGAGGGGTTTTGA	303-332	60-to-50	
130777	D6Mit230	TTCAGGTTCAGTGACAGACCC	TTCAGGTACCTACCCATGAATG	124-139	57-to-52	
130734	D6Mit192	TTTATCCCAAATCATTTCTGCA	TTTGCATTTTATAAACTTTTGGAGG	192-221	57-to-52	
130950	D6Mit44	CCCGTGTCCAGGGTACTG	GCATGGTACCCCAGCTTCTA	143-148	57-to-52	
130648	D6Mit104	CTCCAAATGCATGTGGACAC	CATCCCTCATGCCTCTGC	144-152	57-to-52	
130950	D6Mit44	[6~FAM]CCCGTGTCCAGGGTACTG	GCATGGTACCCCAGCTTCTA	143-148	GT	
130924	D6Mit37	[5HEX]AAAGAATTGCACATCCACTGG	TGCCCAGGATGTTTAAGAGG	250	GT	
130833	D6Mit286	[6~FAM]GCCTCCACAAGCACCACTAT	TGCTATTACAGTGTCTTTAAAAAAAAA	118	GT	
130900	D6Mit35	[5HEX]AATGCAACTCTGATCAATCGG	ATCTGGATTCATTGTAGACACCTG	222	GT	
6292642	rs6292642	CAGGGAATGTAGTAAAGTTAAC	GGGAAGATTTAACTACATTG	192	57-to-52	
13478948	rs13478948	ACAACCAAGAACATCACAGGAC	GAATGAATGGCCACGGAG	207	57-to-52	
13478949	rs13478949	ATTCATTTGTCTTAGTCTGC	CTTCAGGGAGCAGTATTAG	137	57-to-52	Mg2+
13478950	rs13478950	AATGTAGCAGAAGGTTGGTC	GATAATATAAGGGAAGCCATTG	279	57-to-52	
13478951	rs13478951	GAAACAAATCACATACCACAAG	TTCAGGAGTTTCATGTATTGTG	194	57-to-52	
6344812	rs6344812	AATTTAACCCTGTAGCAAGTGC	CTCAGTGGCTCAGACATCCC	271	57-to-52	
4226165	rs4226165	TTGTGCTGAGACTCTTGCC	ATTTACTGACCTGGGTGAAG	248	57-to-52	Mg2+
13478958	rs13478958	GCTCCTCTTGGCTGTCAGTC	AGCCAAGGGTTCCAGGATC	169	57-to-52	
13478959	rs13478959	CCGCTCATATCTCATTCTCTTG	CTTTCCAGGGTCAGCTCTAC	217	57-to-52	
13478961	rs13478961	TGCAAGTAGTATTTAGCCACAG	TTAGAACTCAGGTCCTTGTATG	257	57-to-52	
13478963	rs13478963	TTGCAGGCTGTGGATTCTC	AGGACAATCAGGAAAGAAGGAC	158	57-to-52	Mg2+

n/a, not available; GT, genotype amplification for microsatellites; uniSTS, refSNP; source rs#, NCBI SNP (www.ncbi.nlm.nih.gov/SNP/MouseSNP.cgi), build 34.1.

Table I.3 Primers used for sequencing mouse Itpr1

exon	primer	sq f	sq r	amplicon (bp)	pcr program	
1	m_ITPR1 exon1	ACTACATTGCCCAGGGAGC	AGAACTCCCGGTGATCAGG	402	57-to-52	
2	ITPR1 exon2	AGATCCCTCCGACTTAGCTG	GCCATGCTTCACTTCTGAG	416	57-to-52	
3	itpr1exon3	TGCAGATGTCCTCACTTGGC	GAAGTGACTAACGCAGGATTTG	423	57-to-52	
4	ITPR1 exon4	TGGGTTACGATTATTTCACTCC	TCACAGGCACAGCAACACC	337	57-to-52	
5	m_ITPR1 exon5	AACACCTTAGTAAAACTGGAAAGC	CACCGTCAGCCACCATTC	278	57-to-52	
6	itpr1exon6	GCCCTGAAAGCTGAGTCCAAG	GACCCAATAGCATGACCAAGTG	447	57-to-52	
7	m_ITPR1 exon7	TTTACTTGACAAAGAGAGCTATGG	GGCTTCAATTCTAAACCTTTCC	323	57-to-52	
8	ITPR1 exon8	CAGAACCGTGGAGCAGTACC	CCAACCCTCACCCATATACC	203	57-to-52	
9+10	itpr1exon9.10	TCCACCTCAATGCCTTTCACTC	ACGGTGTGCTTGCTTCCCTG	824	57-to-52	
11	ITPR1 exon11	CAGTTCAGTGGCATTTCATTG	AGAAGGGCAGACGAGGAAG	297	57-to-52	
12	m_ITPR1 exon12	GGATGACTGCAGGTATTGACG	TTTCTTAAATGCGGCTCCAG	215	57-to-52	
13	m_ITPR1 exon13	TCCTGTGGACTGGACAGATG	GCTTCGGTTAAAGTCCATGC	316	57-to-52	
14	itpr1exon14	GAGCCACTGATTCCCAAG	GCTTCACCCAGATCCTCAG	368	57-to-52	
15	m_ITPR1 exon15	TGCCCAATATCCTGTAAAGAAAG	CTGCCCCTCTCGCACAC	331	57-to-52	
16	ITPR1 exon16	CGGGCAGCTTCAATTTATG	ATCCCACAGGCTTCTCACAG	411	57-to-52	
17	itpr1exon17	TGGTGCACGCCTTTGATTC	CAGCACGTCATAGCCAATCTG	516	57-to-52	
18	ITPR1 exon18	TGCTCCTTTCAGACATATTTGC	CACCAGGGACAGCTACAGTTC	433	60-to-50	
19	m_ITPR1 exon19	CTTGTGTACTTGAGGAAGTCAGG	GAGGAGCTAGGTTTATTCCCC	285	57-to-52	
20	m_ITPR1 exon20	TTCTGTGTGTCTCTGGGCTG	CACTAATGCCTTAGAGTGACCAAC	356	57-to-52	
21	ITPR1 exon21	GCTGACCCTTACTCTGGCATAC	CCTATGTGGCTTCTCTGCG	534	57-to-52	
22	m_ITPR1 exon22	GTCTTTGCAGGCTAAGCAGC	TTCAAAACGATAGCATTGTGATAC	335	60-to-50	
23	itpr1exon23	GGTGGGTGTGCAAGCTTTC	AGAACGGACGAGGACAGGAC	489	57-to-52	
24	ITPR1 exon24	CTTTCTGGGTTCCTTGGGTC	GGAAAGGTAGGAGATGGC	502	57-to-52	
25	m_ITPR1 exon25	GGCTTGGCAAAGTGTTAAAG	TGAAATCTTCTCTCTTTGAGCC	292	57-to-52	
26	m_ITPR1 exon26	TGCTTTTGAAGCAGATTAGGC	AAACCCTGGGCAAATTACAG	220	57-to-52	
27	m_ITPR1 exon27	AATTGTCGTTCAGCTCTGCC	GAGAGAGACATAATCCTTTCATTGC	332	57-to-52	
28	ITPR1 exon28	GGTCCTTCAGGCCTTCAAAC	AGCAACCATCCTATCATCTACG	451	57-to-52	
29	ITPR1 exon29	GTGAACATCTTGGGCTGCCTG	TGTGCCTTCAACTCGTCGATC	268	60-to-50	Mg^{2+}

30	itpr1exon30	AGTACACTGGCCATTGAAAC	ACGTGGACTTGCTTTAGG	448	57-to-52	
31	m_ITPR1 exon31	TCCCACCTTAGTAGAGGGTATTAGC	TTCTAACAAGGTCAAGAATACACAAC	293	57-to-52	
32	ITPR1 exon32	AGGACTTTGCTGGCTAATGG	TGCCAGATCACACAGAGAAGAC	436	57-to-52	
33	ITPR1 exon33	AGAAAGTGTGGTTGGTCAGTCC	AAGGGCCTGAAATCTGCG	493	57-to-52	
34	ITPR1 exon34	TCTTGCCAACAGGAACAGTG	GTGGTTGCTTGTGTAAATCTCC	348	57-to-52	
35	ITPR1 exon35	TCTTTACTTCTGTCCCGTGAGG	ACAGGTACTATGGGCAACTTCC	384	57-to-52	
36	ITPR1 exon36	TTGACCCTTCTGGAATCCTC	GTTTCTCACTGTGCTGGCTTG	399	57-to-52	
37	m_ITPR1 exon37	CTAGTGGGCCATGAGGATTC	CCTCTTCTGTGTAGCGGAGC	349	57-to-52	
38	ITPR1 exon38	GGATTGGGAGGCGATGCTTC	CGGAGCGGGAAGTGTCAGTAAC	531	60-to-50	
39	m_ITPR1 exon39	GACTAGTTAGATCAGAATACTTGTGGC	TAAGGGGCTTCCACACACTC	270	57-to-52	
40	m_ITPR1 exon40	CAACTTTCTAACATTTACACTCTTGTG	CCAGAGAACACGGTACAAGG	202	57-to-52	
41	ITPR1 exon41	TGTCAACAGCCCAGTCCCATG	CAAAGCAGCAGCAGATCAGTCC	352	60-to-50	
42	m_ITPR1 exon42	TTGTTTGTGACTGATGCTGAAG	TCGTAGTTGTGTGGCTGAGG	197	57-to-52	
43	m_ITPR1 exon43	CCTGAATATCCTGTGTATGTGTG	AAGCAAAAGCAGACAGCTCC	313	60-to-50	
44	m_ITPR1 exon44	GAGCATTAAAGGTTGGCACTTAG	GTCTCCCTCCTGAGACCAAG	361	60-to-50	Mg^{2+}
45	itpr1exon45	CAGGCACTAATAAGCAGAATGG	CCTGTTGGAACCTGGAAGC	393	57-to-52	
46	itpr1exon46	GCAAGGCTGGGCTCTACATTC	TCCTGGAGGTCTCTGGGTTC	590	57-to-52	
47	ITPR1 exon47	CAAAGTAGCAGCATGGATGACC	AAGTGGCACGGAAATGTCTC	413	60-to-50	
48	m_ITPR1 exon48	CCTGTTAGCCTTTGACGTCTG	TGTCACATGCCAGGTAAAGC	256	57-to-52	
49	ITPR1 exon49	CCTCTGTCCGTATGCTTCTAAG	AGTTCCGTGGTGCTCCTGTC	288	57-to-52	
50	m_ITPR1 exon50	TGTCTAAGCTATAGATGCCAGTCC	AGTCAGTCTCAGGGTGCCTC	270	57-to-52	
51	m_ITPR1 exon51	CATGAGAAAGAAAGAAACCTGG	AACATGCCAACCCTGGTATAG	274	57-to-52	
52	m_ITPR1 exon52	AGTTCACTGCCAATAGCAAAG	GTGCACGCACTCCCCTG	351	57-to-52	
53	itpr1exon53	ATGAGTTCTCCAATGACCTG	ATGACAGCAATAGAAACCATAG	486	57-to-52	
54	m_ITPR1 exon54	CATTAGACCTGTCTTACTCTGTCACC	TTGAAAACCAAAGTCAAGATGC	345	57-to-52	
55	itpr1exon55	ACTCGGTGCTAAGGCTCCTC	AAGATCGGATGCAGTTGGAG	373	57-to-52	
56	m_ITPR1 exon56	GTTTCCAAGAGAGTAAATGATGC	AGACACAGTTGCCTGCTAAGG	360	57-to-52	
57	m_ITPR1 exon57	ATCAGCCGTGAACTAGGGAC	CTTCCAATACCACCTGCCTC	252	57-to-52	
58	ITPR1 exon58	CACATATCTGACTCGTAACGGC	TCCCAGCTCATGTTCCAGAC	396	60-to-50	
59	itpr1exon59	AGGAGACTTGGTTGGGAG	TACCCACTCCATTGCCAC	392	57-to-52	

60	ITPR1 exon60	GCCCTCCTACCATGATGAAAG	TGAACCAGGAAGGCAGAGC	363	60-to-50
61	itpr1exon61	TTTGGGCCAGTCAGTAGTACC	CATTACCGCAGCGTGAGTG	442	57-to-52
62	itpr1exon62	TGACGCACAGGAAGTGTC	TCACCATGCCAACAGAGC	339	57-to-52

Mg^{2+}, 1µl MgCl (25mM)/10µl reaction.

Table I.4 Primers used for sequencing human ITPR1 (AUS1 family)

primer	sq f	sq r	amplicon (bp)	pcr program	
hIP3R1_1*	TAACCATGTGGATGTGCTGCTG	CTGCCCGCAGTAAAGGAACC	395	57-to-52	
hIP3R1_2	GTTAGAGCTCATCTTCCGCG	ACTCATTATTGACTACAGCA	172	60-to-50	
hIP3R1_3	CTAAGCCAACTCTTAGTGACTT	TAAGCTGATGTTATGATGTC	249	60-to-50	
hIP3R1_4	TCATACACTTGACAGAGCAT	TTCAAGTGAGTCAAGGTGAC	155	60-to-50	
hIP3R1_5	TCTCTATACACCCTCAATGGC	CACCATTACACCCAGATACC	219	60-to-50	
hIP3R1_6	GTATGAACTGGCGACATTTG	CCTCAGCTGCATTCTTTGTAAC	237	60-to-50	
hIP3R1_7	GTATGATTGAGAGAAGGAATG	CATGCTTGGAAGCATGGCACG	286	57-to-52	
hIP3R1_8	CAGTGGTCAATCCGCAGTCC	CAGACCCGCTCCTGCAGGATAAC	216	60-to-50	
hIP3R1_9*	TTCCAAACTCTGCCAGCAGG	CCACGTCACCCTGACAGTCAAC	387	57-to-52	
hIP3R1_10*	TCTGTGTTTCAGGTCAATTCCG	GGCTGATATCCTCTAAACCCAG	402	57-to-52	
hIP3R1_11	CTCCTGAACTATGACTTGTG	GGCTACAGGCGAATGAGGAA	222	60-to-50	Mg^{2+}
hIP3R1_12	TGTAGAAAGTGAAGGCTTTGGC	CTACACCAGGCCTGATTCTT	261	60-to-50	
hIP3R1_13	GCTATAGAGTAAACCTCAAT	GATCTGTCCTCAAAGGAGCCCT	230	60-to-50	
hIP3R1_14	GTTTGATTAAAGTCTTATCCTTC	CATGGATGTCAGAAACTCTCAG	288	60-to-50	
hIP3R1_15*	ATTCGTCCAGAAGGCTTCCAAG	GCTCACTGCAACCTCCATTTCC	371	57-to-52	DMSO
hIP3R1_16	TTGAAGCCCTAAGTGATTGC	CTCAGGAGGAAAGTTCACAA	277	60-to-50	
hIP3R1_17	CTACGCTTAACCATATTGTC	CTGCATCTTACAGGCAGAGAC	288	60-to-50	Mg^{2+}
hIP3R1_18	GTATGTTGGACCTGTGCACT	CCTCATGAGCACCAACACTG	279	60-to-50	
hIP3R1_19	AGTGTCTTTCCATGTGTCTT	CAAATTCCTAAGTGCCACTG	355	57-to-52	
hIP3R1_20	CATTCATCCTGAATGATTTCT	CTACTGCCGCACAGAATAATG	360	57-to-52	
hIP3R1_21	GACCCAGGAAGACCTCTCTG	ATGACCACTGAGAGGCAGAT	259	60-to-50	Mg^{2+}
hIP3R1_22	CATCAAATGGAATTGAAGGG	GGGCATCTCTCAGATGTATG	288	57-to-52	
hIP3R1_23	TGACATATGCCTCTGAGCAT	ATCTGAATGGCGCCTCTGTG	309	60-to-50	
hIP3R1_24	GCAGAGTCAAGATGGTATGT	ATTTTCCTTAGAGCCAGGTC	257	60-to-50	
hIP3R1_25	GCAGACCTTCCTGCATCTGA	CTCTGAGAGCTCTGGAAGAG	157	60-to-50	
hIP3R1_26-27*	AGGCATTTGTCATTCATTTGGC	GTTTCGAGAAGCCCATCCATCC	513	57-to-52	
hIP3R1_28	CTGACAGTAGCCCAAGAGTT	AGCTCCTTAGAGAATTCATA	176	60-to-50	
hIP3R1_29	CGCCACCACCCTCTGCAATC	CAATATCCAGATGTGAAGAGT	296	60-to-50	Mg^{2+}

hIP3R1_30	TGGCCCAGGAATCAGTGCTT	AGCCAAAGAACAAGCTGTTC	248	60-to-50	
hIP3R1_31	TTAATCTGTTCTGTCAGCTT	TTCTACAGAACACCAGATGG	309	57-to-52	
hIP3R1_32	CCTGCAAGCTTGTAATCTAA	ACAGCACACACCACATAGCA	348	60-to-50	Mg^{2+}
hIP3R1_33	CAGCTAATGAGTTCCATACA	CACTCTCCAACTCTGCCTCC	227	60-to-50	
hIP3R1_34	GAGTCGCAGATTTCTTAATG	GGTGTATCGTGAACATTCTG	240	60-to-50	
hIP3R1_35	GGATCATCAGTAGTCTACAA	GCAGCCTTACTACTGTCAGAC	249	60-to-50	
hIP3R1_36	GTTGTAGGCTCACGACTCAT	CTGTGTGTGGCAATCACGTG	281	60-to-50	
hIP3R1_37	GTCAGCGTCTGCCTGAGCCG	CAAGGTTCTGGCAAATGAAC	240	60-to-50	
hIP3R1_38	AATTAGCTTCAAGGAAGTAA	TCAGTAATGCCTGAGCTAAG	248	60-to-50	Mg^{2+}
hIP3R1_39	CCTCGGTGATGCATTAAATG	CACTTGATTCACACACGAAG	229	60-to-50	
hIP3R1_40	CATTAGCTGTTCTGATTGTG	GACTCTCCTCCTGCTCAGCA	296	60-to-50	
hIP3R1_41	GTCAGTTACAGTGTTCACAA	TAACAAGGACTCTTCTGGTG	280	60-to-50	
hIP3R1_42	CATGAGGACTCTGCAGCCTT	CTGAACCATCAGAGGAAGGCA	373	57-to-52	
hIP3R1_43	GCTATCAGAATGGCAGGATG	TGAACTAGTCTCTATCAACAT	354	57-to-52	
hIP3R1_44	CTGTTGGCCTTTGACGTCTG	CCATGTGCATGTGCCAAGGCA	255	60-to-50	
hIP3R1_45	CAGTTGGCACCTGCATTCAG	ATATCGTCGCAATGCTCCTTG	223	60-to-50	
hIP3R1_46	GCTGTCCATCCAGTCCTGTGT	GACCTGTAGGGAGGCAGCATC	238	60-to-50	
hIP3R1_47	TCTGTGTTCCTGTTGTTGTTGTGAAGAG	TGCACACTAATGGCCTCAACA	217	60-to-50	Mg^{2+}
hIP3R1_48	CAGTAGCAAATAGTCTTAGT	CCAGAACTGTGTCTCTCTGTG	308	60-to-50	
hIP3R1_49	CCACATTGCATTCCTGGCGT	CTAGCCTTCCTGCTGCTTCTA	244	60-to-50	
hIP3R1_50	CTGTACTCAGTGAAGGCACA	AGGCATTCCTATTAATCTGCA	285	60-to-50	
hIP3R1_51	GCTCTCATGAAGAGTTTGGCA	GAGAGAGGACATAGGACACTC	291	60-to-50	
hIP3R1_52	TGTACATCTAACATCAAGGC	GGAGATATCTGCATTACTAA	346	57-to-52	
hIP3R1_53	CATATGCTGCCAGATTGTTCA	GCATCAGCTAAGCCTCTGGAG	203	60-to-50	
hIP3R1_54	CTCACGTTTTCTCTCTGTTGT	TACACTCAACACCGCTGCATG	262	60-to-50	
hIP3R1_55	CAGGCTCCGCAGACCAAAGGG	CCACATGCCTCTGCCACGCTG	290	60-to-50	
hIP3R1_56	CTACTGACAGTTCTGTTATTG	CTGTTGTGCAGCTCCCCGATG	335	60-to-50	
hIP3R1_57	TACCTCTAGAAGTGACTCAGT	CTAGATGAAGCACTACTGAT	327	57-to-52	
hIP3R1_58	TGACGTACAGGAAGTATCTGG	ATCAGAACTCATTAGCCATAC	211	60-to-50	

Primer sequences were obtained from Knight et al. (2003). * exons 1, 9, 10, 15 and 26-27 were designed using Gene Runner (v3.05; Hastings software).

Table I.5 Primers used for sequencing human CNTN4

primer	sq f	sq r	amplicon (bp)	pcr program
hCNTN4_1	GTTGCCTATGAGCAGGTCC	TGATCCTTAGCAATCTTACCTACTCC	264	65-to-55
hCNTN4_2	TGATTTAATTTTAGACCGGGAAG	TCTGTAAGGGAAGGTTTTCAATG	259	65-to-55
hCNTN4_3	CCCTCCAATGGTACTTTCCC	GCGATTTTATCATTGCCGTC	361	65-to-55
hCNTN4_4(a)	ACAAAAGGGATACGGGAAGC	TATGCATGGAAACACATGCT	504	62-to-52
hCNTN4_4(b)	ACAGCCATCCACAATGACAG	TATGCATGGAAACACATGCT	528	62-to-52
hCNTN4_5	GATGTCACCATTGCTGGGTAG	AAAATCTAGTCTCTAAAATGAAACTGC	439	65-to-55
hCNTN4_6	GTGCTACCAACGCAGTTTTG	AAATGACACTGTGCACTCAGC	308	65-to-55
hCNTN4_7	GATTACTTCCTATCTGTATTTAGTGGG	ACAACAAAGCTTCATGTGCC	437	65-to-55
hCNTN4_8	GAGCCACAATTCATGACTGC	AGGGGCAGAATCCAAGATG	424	65-to-55
hCNTN4_9	AGTTTGCAAAACACCCAACC	CACCATCTCTCCCAAAATGC	399	65-to-55
hCNTN4_10	CTGAATGTCTCCCCAGTCTTG	AACAATTCACCATTCTCCCG	376	65-to-55
hCNTN4_11	ATGATGGCTGTTTTCTTCCC	TTTCTTGGATTGAACATTTATGC	337	65-to-55
hCNTN4_12	AGCCAAGATTGCACCACTG	CATCCTTCCAAAGCTTCTGTTC	426	60-to-50
hCNTN4_13	AATGTAGCAATGATTTATGGTTTG	GATGAATTAATTTAGCAATACAGTGG	364	65-to-55
hCNTN4_14	TTAGTATTTCATCCTGCTCTTGG	GAGCAGGAATTAACCAAGAGTTTC	402	65-to-55
hCNTN4_15	AATGCTTTCATCAGCCAGTG	CAATGTTCAGCTTCTGCCTG	359	65-to-55
hCNTN4_16(i)	TGGCTCCTTTACTTGGGTG	TTAGACGTTCCTTGCCACAG	300	62-to-52
hCNTN4_17	TGAGGATGGATGGATGTTCC	TAACACAGAGCCGCATGAGC	350	65-to-55
hCNTN4_18	CAATGCTGTTGCTGATCTCC	AGAGGAGGAAACTTCCCAGC	306	65-to-55
hCNTN4_19	AACGCCAAATAAGATGGGTG	TGTACCATGCGAAATTGATTG	449	65-to-55
hCNTN4_20	TCTGCAAAATGAGGGTTTGG	GTGGGAATGTGGGTCTCTTC	350	65-to-55
hCNTN4_21	AACTCCATCATAAGAATCTGCG	GCTGAGGGAAATTTGAATCC	413	65-to-55
hCNTN4_22	TAGCCCATTAAATTGCCTCC	ACCAGGGAAACTGACAATGC	319	65-to-55
hCNTN4_23	GGCAGCCAGACAACCTCTAC	GCTTTTGCAGGCTGAATGTC	390	65-to-55
hCNTN4_24	ATCCATGCAGTTCTGCTGTTTC	TGTCTTCAGTGCATTGCAGAG	418	60-to-50

Table I.6 Primers used in assay to determine breakpoint AUS1 family

forward	sq f	reverse	sq r
itpr1 fr1 2f	CAATGGTCAGCTTTCTAGTTGTG	itpr1 fr1 2r	CATTGTTGCAGGTCATACAGG
itpr1 fr1 3f	**TGAATGCTCAATTTTCCAGC**	itpr1 fr1 3r	ATTTTGCTGAATGCCCTGTC
itpr1 fr1 4f	CTCATGGGGAAAGAACCCAC	itpr1 fr1 4r	GAAAGAAAGACCTGAATCTTGC
itpr1 fr1 5f	GACACTTCCAAGGCCTCTTC	itpr1 fr1 5r	TTCACAGCTTTCTTTGCTCC
itpr1 fr1 6f	CAAGCTGCTGGCTAATCAAC	itpr1 fr1 6r	AAATGGAGGTGGTGAACTGG
itpr1 fr1 7f	CCACCGTTTGTTTCCATGTC	itpr1 fr1 7r	TTTCTGAGTCCTCTGGGAAGTC
itpr1 fr1 8f	TCTCAGCCTATAAGGAAGGTAGG	itpr1 fr1 8r	CAGACTCCTTGACCTCACCC
itpr1 fr1 9f	AGTGGCTCTCAGGCTTTGTG	itpr1 fr1 9r	CCACCTCAAGAACTTGGC
itpr1 fr1 10f	CAAGAATGAGAAGGAGCCAAC	itpr1 fr1 10r	TAAGCAGAATTTGGGGCATC
itpr1 fr2 2f	TGTTGAGTTGGGAAGCCTTG	itpr1 fr2 2r	GCTGGTGAAGCCAGAGAATC
itpr1 fr2 3f	ACATCCATCTTGTCCAAGGC	itpr1 fr2 3r	CGACACAGCAACAAATGAGG
itpr1 fr2 4f	GTCCCTGTCATTCCAGATCC	itpr1 fr2 4r	CCAAAGGATGTGCTGAAAATG
itpr1 fr2 5f	CCAAAAGTGTTGGATTTATTGAATG	itpr1 fr2 5r	TCTGTGCTGAAGAAGGCAAG
itpr1 fr2 6f	AGCCTTGTAAACATGACCC	itpr1 fr2 6r	CCCACATCTATCCCACTGAAG
itpr1 fr2 7f	CCTGCAAGAGTGATAGCTTG	itpr1 fr2 7r	CATGAAAAGGACTATTTTCCAGC
itpr1 fr2 8f	TGGATGACACAGTTGTTGTGAG	itpr1 fr2 8r	CACCTGGTTAAATATTGTTGTGATAG
itpr1 fr2 9f	GCAGAAGGAAAGAATAAGTACTTTGG	itpr1 fr2 9r	TGCTGCAATTACACAGAAAGG
itpr1 fr2 10f	TGCAGGACAAAGAAGGAAATG	itpr1 fr2 10r	GAATATATACCATGCCATACCATACC
itpr1 fr2 11f	GAGTTGTTCCCAACTTCTGG	**itpr1 fr2 11r**	**GGGAAAATGGATAGAGGGTG**
itpr1 fr2 12f	AGGTTGTGGTAAGCCGAGAG	itpr1 fr2 12r	GCACAGTCAATGCAAATTTAGAG
itpr1 fr2 13f	GCTTTCCAGCTTGGGTGAC	itpr1 fr2 13r	TCAGCACTGGCAAATCTACAG
itpr1 fr2 14f	TGTCTGTAGCTTATTGATCACCC	itpr1 fr2 14r	CCAGAAGTCTGCTCCCAAG
itpr1 fr2 15f	TGTTTTCACATTTTGGCTCC	itpr1 fr2 15r	CAAAGGGATCCACAGGTCAC
itpr1 fr2 16f	TGCGTTCATGGGTCACG	itpr1 fr2 16r	GTTGGTGCCATAAACAATTAGAC
itpr1 fr2 17f	TGTGAACACAGTTGTTTGGG	itpr1 fr2 17r	AGGAGGAAAAGCAAGGTGAC
itpr1 fr2 18f	GCATTACTTGGCAGCAGAGG	itpr1 fr2 18r	CCTCCTGTCCTTCAGCATTG
itpr1 fr2 19f	CTTGGGAGGGTGAAGCAG	itpr1 fr2 19r	GCATGCCACGACAATGATAC
itpr1 fr2 20f	AGTGAATTCATTGTCTTCCTCTG	itpr1 fr2 20r	AAGCCTATTTCTGACCTTGCAG

(table I.6, *continued from previous page*)

Primers were run using both 60-to-50 and 65-to-55 programs. In bold, telomeric forward (T3f) and centromeric reverse (C11r) primers which were used in the PCR-based assay for detection of the SCA15 deletion in *ITPR1* in the AUS1 family.

Table I.7 Primers used in assay to determine breakpoint H27390 family

forward	sq f	reverse	sq r
H27390 frag1 1F	CATCCAAACTCACTAGACG	H27390 frag1 1R	TACTACAAGTCTGGTTATGTCC
H27390 frag1 2F	GCAAAGACATGTTTCCCACC	H27390 frag1 2R	TGTCACATTGCTTTCAAGATAGG
H27390 frag1 3F	AGGAGTGGAAATTCTAGGCAG	H27390 frag1 3R	TTCAATGTAAAATTAAGTCTTAGCTCC
H27390 frag1 4F	AATCCTCCCAACTCAGCCTC	H27390 frag1 4R	GTGTGTGGGAGAATTTCCTG
H27390 frag1 5F	TCCACTTAGGTTCCTTACATTGC	H27390 frag1 5R	TTGAGTAACCCAGTGCTTTCC
H27390 frag1 6F	CCAGGAAAATAACCCACGG	H27390 frag1 6R	GACACTATAGAGGGGATGCTTTTAG
H27390 frag1 7F	AGTAAGGCAGGGCAGGAGTG	H27390 frag1 7R	CTTGCCCCACCTTGGTC
H27390 frag1 8F	TGAGACAAGAGCTTGGGACC	H27390 frag1 8R	GGGTCAGGGTTAGGTTGGAG
H27390 frag1 9F	CAAAACCCCATACAGAACCAG	H27390 frag1 9R	TTTGAAATACCTGTTTAATGTGACC
H27390 frag1 10F	CATCCCTCAGCATGACTCTC	H27390 frag1 10R	AAGTGGAATCCTTGTCCTTTTG
H27390 frag1 11F	**GACCTCAAGAAGGCATGAATAC**	H27390 frag1 11R	AAATCAACCTGGTTAGGAACAGAC
H27390 frag1 12F	TCTTTGTAACAGCTCTATGGGG	H27390 frag1 12R	TGGGGTTTCTTGAGATTCTTG
H27390 frag1 13F	AAGGTCTAACATTTATGCAC	H27390 frag1 13R	CTGCTGGGATTATCGATG
H27390 frag2 1F	GGCCCTTCATTCAGAGGAG	H27390 frag2 1R	ATCAGGGCTGTGATGATGTC
H27390 frag2 2F	ACTGGGAGTGGTAAGCATTG	H27390 frag2 2R	ACACAATACAGAGAAACTCAGCAG
H27390 frag2 3F	AAGGGCCGGTTGAAGAATAG	**H27390 frag2 3R**	**ATGGTGGCCAGGTACACAAG**
H27390 frag2 4F	CATTAGGAAAGATGGGAACACAG	H27390 frag2 4R	ACGTGGGTGCTTACGGATAC

Primers were run using 60-to-50 program. In bold, telomeric forward (T11f) and centromeric reverse (C3r) primers which were used in the PCR-based assay for detection of the H27390 family deletion in *ITPR1*.

Table I.8 Primers used in assay to determine breakpoint H3331 family

Table I.8(a)

forward	sq f	reverse	sq r
H3331 frag1 1F	AGCTCATCTCTGCATTGTC	H3331 frag1 1R	ATTTGGTCCTGAGATCTAAC
H3331 frag1 2F	TCATAAGGGCCACATTCTCTG	H3331 frag1 2R	GCAACACCATCTTGAAAACTTC
H3331 frag1 3F	GATGAGCTTTCAGTATGTCTCAAAC	H3331 frag1 3R	CCTTGACAAATGAGAGGAGTAGG
H3331 frag1 4F	CGGGTCAGACTGCATTATTC	H3331 frag1 4R	TTTCCTCGGATGTGGGG
H3331 frag1 5F	GGGATCTGGGTTGCTGG	H3331 frag1 5R	GTGTTGGGCGCCTGTAGTC
H3331 frag1 6F	TGACAACAGTAGCTCACACTGG	H3331 frag1 6R	GACAGGGTTTTGTCATGTTGC
H3331 frag1 7F	CCTTATGAATAACAAATGCAGTCAG	H3331 frag1 7R	GGGTAGAAGCTTTCAATATCTAGTTTC
H3331 frag1 8F	GTGTGACACAGCAAGACC	H3331 frag1 8R	TCCCAGGTTACATACACAG
H3331 frag2 1F	GCAGGGAAGTCAGGAATGAGTC	H3331 frag2 1R	TGGGATGAGTGAGGTGGAC
H3331 frag2 2F	TTCTGTGGTGTGGGTACAGC	H3331 frag2 2R	AATCCTCAAGGACTCCTGTTC
H3331 frag2 3F	TTGTGGTTTGAAGTGCTCCC	H3331 frag2 3R	CTGGAGCTCAAGACCAGC
H3331 frag2 4F	TCACTATGTCACCCAAGCTG	H3331 frag2 4R	AAAATTGCCATACCAGGGG
H3331 frag2 5F	GTTTACCATTTGGCCCTTTG	H3331 frag2 5R	GGAAAACGTTTGTAGGAGGC
H3331 frag2 6F	GACAAAGCAGGACATTCCTTAG	H3331 frag2 6R	TGAGGGTTCCATTTGGGG
H3331 frag2 7F	GCAGCGGTTTGAAACTAG	H3331 frag2 7R	TTTGGATGAGCTGTTACG

None of the initial primer combinations (table I.8(a)) allowed to obtain sequence across the breakpoint in the H3331 family. However, sequences acquired with fragment 1 (*SUMF1*) primer pair 6 and fragment 2 (*ITPR1*) primer pair 4 showed heterozygous calls within the sequence thereby narrowing the breakpoint region. Based on this newly defined region new sets of primers was designed, see table I.8(b) and I.8(c). Although, the exact breakpoint in the H3331 family remains unknown as no sequence across the breakpoint has been obtained.

Table I.8(b)

forward	sq f	reverse	sq r
H3331_frag1new_1F	CTGGATTTCTTCCCCTCCTC	H3331_frag1new_1R	CCTGTGAAAAGGAAAATCCC
H3331_frag1new_2F	CTCCACCTACTGGGCTCAAG	H3331_frag1new_2R	TCCAGAATAGAGCCTCACACC
H3331_frag1new_3F	AAGTGATGCTCCCACCTCAG	H3331_frag1new_3R	AGCAACATGACAAAACCCTG
H3331_frag1new_4F	TGGATATGAAATCTTTGGTTCAC	H3331_frag1new_4R	AGCCTGGGCAAAATAGTGAG
H3331_frag1new_5F	CTTCCACAGCAGGAATACTGG	H3331_frag1new_5R	AAATCGTTGGGTATTCAGGC
H3331_frag2new_1F	CCCACTGAATCCTCAACAGG	H3331_frag2new_1R	CCTGTTTCCCTGAATTCCC
H3331_frag2new_2F	TTTGTTTGTTTGTTTGAGACGG	H3331_frag2new_2R	AGGCATCTCACACTCGGAAG
H3331_frag2new_3F	AAGATGGCAGTTCCCACAAC	H3331_frag2new_3R	GGGCACCTGTAGTCCCAG
H3331_frag2new_4F	TGGGAAATTTCATTGCCTTG	H3331_frag2new_4R	TCTTGCAGTAATTTCTTGCCC
H3331_frag2new_5F	ATAGGATGGTGACGGTTCCC	H3331_frag2new_5R	GCTTCATCCCAGAATGTCTCTC
H3331_frag2new_6F	CTCCTTTGAGAAATGGTGGC	H3331_frag2new_6R	CTCAGCAACATAGCAAGACCC
H3331_frag2new_7F	GACACGTTGGTTGGGCTATC	H3331_frag2new_7R	GACAAACCCCAAGGTCACTG

Table I.8(c)

forward	sq f	reverse	sq r
H3331(F)F1c	AAAGCAACAGGAAATCAGACC	H3331(F)R1c	CTTGGTGTGAGGCTCTATTCTG
H3331(F)F2b	TCTCCTGACCTCGTGATCCG	H3331(F)R2b	ACCTACTGGGCTCAAGCAATTC
H3331(F)F3b	AGACCAGTCTGAGCAACATGAC	H3331(F)R3b	TGCTGTGTCACACTGGCTG
H3331(F)F4a	AAAGAAGAGGCCAGGCATG	H3331(F)R4a	AGTGGCCATGGGAACAATATG
H3331(F)F5a	AAATCGTTGGGTATTCAGGC	H3331(F)R5a	TCCCAGGTTACATACACAGTGG
H3331(R)F1a	TTCTGGTCTAGCAAGAGGTCTG	H3331(R)R1a	CCCTGAATTCCCATTTATTAGC
H3331(R)F2a	TGTCACCCAAGCTGGAGTG	H3331(R)R2a	CAGGAAAGCAGTTAGGACAATC
H3331(R)F3a	TAGCGCAGCTCTCTGAGTGACG	H3331(R)R3a	ACCAGCCTGGCCAACATGTAG
H3331(R)F4a	AATTGACCCAAGTCCTTCTGAC	H3331(R)R4a	TGAATGATGCTGACAAGTCTTG
H3331(R)F5a	AACATGAGGGTAAAGTGTGTGG	H3331(R)R5a	GCTTCATCCCAGAATGTCTCTC
H3331(R)F6a	AATGGAAGGCCAGTTTGTGAG	H3331(R)R6a	GAGTCCTGAGGTGGGCATATAG

Table I.9 Primers used for sequencing human ITPR1 (London cohort)

primer	sq f	sq r	amplicon (bp)	pcr program
h.ITPR1 1	TAACCATGTGGATGTGCTGCTG	CTGCCCGCAGTAAAGGAACC	395	60-to-50
h.ITPR1 2	TTGTAATTTGGAGCATTTCTGTTAG	CCTCCTTGGCGGTTTAGATAG	238	60-to-50
h.ITPR1 3	TAAGGCGCTTTGGAAAATTG	AGCCAAGTAAAACGGTGACG	317	60-to-50
hITPR1_4	CATGCATAGGAAGCCTCTAGTG	CACACCAACAACACACTTCAAG	298	60-to-50
hITPR1_5	AGCTCTGCTACCAAGTGGTTC	CACCATTACACCCAGATACCAC	430	60-to-50
h.ITPR1 6	CATTTGTTCTGCGTCACTGC	TCCAAACCCTGTCTTAGGTG	250	60-to-50
h.ITPR1 7	GGTATGATTGAGAGAAGGAATGG	TCCAACTTTCAACGTCTCCTCC	327	60-to-50
h.ITPR1 8	ACTGCCCAGTGGTCAATCC	AAGTCACTCTCAGCACACGC	258	60-to-50
h.ITPR1 9.10	CTAGGCTGCGGTGAGAAGTC	AAGGTGGGTATAAGTACTTGTTTGTG	629	60-to-50
h.ITPR1 11	CCCTCCTGAACTATGACTTGTG	TACAGGCGAATGAGGAAAGG	258	60-to-50
h.ITPR1 12	TTTCTTCTCCGTTCCTGTGG	GGATTCCAAGAAACCTGGTC	321	60-to-50
h.ITPR1 13	TGCAGTAGGAAACCACTTTGC	AAAGCAACAAATCTCCACGC	319	60-to-50
h.ITPR1 14	TTGGGATCAGCCAGTGTCTC	ACTCCACCCCATGGATGTC	328	60-to-50
hITPR1_15	CTGTTTAACTGGCTCATTCGTC	ACTGCAACCTCCATTTCCTG	382	60-to-50
h.ITPR1 16	ATGTAATCCAGCCACCCTTG	CACTGAACTATTCTGCATCCATTC	379	60-to-50
h.ITPR1 17	GGAAACATTGCTGCTTTCTTTAG	AAGCACCAGCTAAGTCCCTG	329	60-to-50
h.ITPR1 18	AAGGAAGAATTGGGGTCCAG	AAATGATAGGGCTAGGTTTTATTCC	281	60-to-50
h.ITPR1 19	TGTGTCTTTATGCTGAAAGTAAAGC	AAACGAGCAACAAATTCCTAAG	353	60-to-50
h.ITPR1 20	CCCAGACGACCCTTCATTC	TGAGACCATATGGGGCTATC	393	60-to-50
h.ITPR1 21	CTTTTGAAGCTGAGTGACCC	TCACATATTTTCTATTTGCCCC	304	60-to-50
h.ITPR1 22	CAAGTCTGTCATTTCTAAACTGGTC	AAGGCTGGAGGGCATCTC	324	60-to-50
h.ITPR1 23	TTTCTCTCAAAGAGCCCCTG	CATCAGAACAGAGGGACTGG	354	60-to-50
h.ITPR1 24	CAGTGTGTGGTGGCTTGG	TGTTTGCTCTCCCCATTTTC	288	60-to-50
h.ITPR1_25	ACTCAACAGCTTTACCCTGC	CAAAACAACCTAAGCCCAGAG	265	62-to-52
h.ITPR1 26.27	TAGGTTAGGTGCATCTGGGC	ACCAGAAGAGGATGCTCCC	571	60-to-50
h.ITPR1 28	CCCTTTCTTTCCTAAAGGTCG	GCTCAAATGTGTGTACCTTCAAC	255	60-to-50
h.ITPR1 29	CCACCACCCTCTGCAATC	GTGAAGAGTTTGGGGAAACC	282	60-to-50
h.ITPR1 30	ACGTTAGCAGGAGGTGTTGG	AACAAGCTGTTCCTCCTCCC	281	60-to-50

h.ITPR1 31	CATGGGTTTAAATGCTTCCC	CCTGAAGAGGGTGCAAGTTC	416	60-to-50
h.ITPR1 32	GAACCTCTCTCTTCCTCTGTGAATAG	ACCACCATGTCTCCCAGTG	422	60-to-50
h.ITPR1 33	TTGCTGTGAAGTTGAGGCAG	TGCAGCTGTTTTCTTCATGTG	321	60-to-50
h.ITPR1_33p	ATAGAAGTAAGACTTGGCAGTG	ACTCTGCCTCCTCAGTTC	286	60-to-50
h.ITPR1 34	AGGAGGGAGTCGCAGATTTC	TCCCAAATTCACATCAAGCC	277	60-to-50
h.ITPR1 35	ATCTGGGGTCCAGTGGTTC	GCTCAATAAATGGCAGCCTTAC	304	60-to-50
h.ITPR1 36	CTAGGGCATTACGTCCATCTG	AGATGCTCTGTGGCTCAAGG	349	60-to-50
h.ITPR1 37	GGGCAGAAATCAATGTCCTC	GACAACGTCTCCTTCTTCGG	314	60-to-50
h.ITPR1 38	TGCCCTGAAGTATCTTTAACCTG	AGGTGGGTTTTGAAAGGTCC	326	60-to-50
h.ITPR1 39	CTGAGTACCCCTGTGTGTTTTG	TGTTAGGAGGAAACATGCAGC	294	60-to-50
h.ITPR1 40	GTGCATAAAGTGTTGGTGCG	CCCAGACATCTGGCTCCC	358	60-to-50
h.ITPR1 41	GTTTTGGTGTCATGAGTGGG	TGAAAACAATGAAGGATAACAAGG	328	60-to-50
h.ITPR1 42	GAGTGTCACCTTTGGAGTGG	GCTGAACCATCAGAGGAAGG	405	60-to-50
h.ITPR1 43	TGGCAGGATGAATAACGTTTC	CACAGGCTTCGTGATTTCTG	362	60-to-50
h.ITPR1 44	TAGCAGTTCAGCCTGTTGGC	ATGTGCCAAGGCAAAACAC	259	60-to-50
h.ITPR1 45	GTCTGTTTAGCCGGGATGC	AAGCTCCAGGAAGCAGATCC	288	60-to-50
h.ITPR1 46	CATGCTGTCCATCCAGTCC	AAGGAAAAGCAAGACTGGGG	284	60-to-50
h.ITPR1 47	AATACCCAACATGAGAAAGGAG	TGAATGAATGCACGCCAG	275	60-to-50
h.ITPR1 48	ACCACCGAGTCTACCACCAG	AAATGAACGCACCATCAAGC	361	60-to-50
h.ITPR1 49	GAAGGGCCACATTGCATTC	ACTGCACCAATACATCCAGG	292	60-to-50
h.ITPR1 50	TGCATGTTTTAGGTCTGTCCC	AAAGCACAGGCCAGGATTC	341	60-to-50
h.ITPR1 51	GTGTGAGATGCTCTCGTTGC	AGGGTCTGTGATGAGAGAGAGG	323	60-to-50
h.ITPR1 52	AAACCAAGTTTGCATTATGGG	CGTGTTAGGGAGATACAATGGG	395	60-to-50
h.ITPR1 53	TTAATCAGCCGTGAATTGGG	TCTTCTTCCAACATCACCTGC	260	60-to-50
h.ITPR1 54	GATGGCATTCAGGAAACAGG	CTGCATGGTGCTCCCAC	296	60-to-50
h.ITPR1 55	GTCTCACTTGAGCTGTGCCC	ATCACACCCTCGCAGTATCC	328	60-to-50
h.ITPR1 56	ACAGGAGTGAAACCACAGCC	ATCCGTGAGAAGGGCTCAG	401	60-to-50
itpr1_57_Txii	AGATCAGAGCAGCAGTGGCAG	CCTGATCCTTTAATTCCGACAG	465	62-to-52
ITPR1_57(a)	AGGAAACATGGCACGGTAAG	AGCACCATGGCTTTATCCTG	467	62-to-52
hITPR1_58	ATGGTTCAGTATGCGATTTGAC	GCACAAATGAAATGTCATCATG	368	62-to-52

APPENDIX II.

SUPLEMENTARY VIDEO - SEVERE MOVEMENT DISORDER IN MICE

A CD-rom containing a video of affected and unaffected mice has been attached to the back cover of this thesis.

A, B. Affected mice (first two mice shown). Phenotype is characterized by altered muscle tone, splayed hindlimbs, dragging of the hind limbs and apparently touch-induced seizures, marked by severe truncal, upper and lower limb contractions into unusual, twisting postures.

C. Unaffected littermate (third mouse shown).

APPENDIX III.

RAW DATA - LENGTH AND WEIGHT MEASUREMENTS

Length and weight measurements of the mice were carried out by L Parisiadou (LNG/NIA/NIH). Length, (cm; ruler, Origene), from nose to base of tail, and weight (g; balance, Ohaus Scout II 1200x0.1g), SRA210) measurements of 3 week old mice were taken.

cage 556404 (♀F119x♂F116)
pups born 10 Dec.2007
measurements taken 30 Dec.2007

	sex	genotype	length (cm)	weight (g)
1	M	wt	5.5	7.7
2	M	wt	5.3	5.9
3	M	het	5.6	7.7
4	M	wt	4.5-5.0*	5.6
5	F	wt	5.4	7.7
6	F	het	5.0	7.3
7	M	het	5.1	6.8
8	F	het	4.7	5.8
9	M	het	4.5	4.0
10	M	homo	4.7 (4.5-<5.0)**	4.8
11	M	homo	4.5	5.3

Table III.1 Length and weight measurements (litter A)

* 4.8 was used for statistical analysis; ** 4.7 was used for statistical analysis.

cage 556394 (♀F114x♂F116)
pups born 11 Dec.2007
measurements taken 30 Dec.2007

	sex	genotype	length (cm)	weight (g)
1	M	het	5.5	10.5
2	F	het	5.5	8.5
3	F	wt	5.5	8.3
4	F	wt	5.0	6.2
5	F	wt	5.5	9.1
6	F	het	5.4	9.1
7	M	het	5.4	8.4
8	M	homo	5.0	4.9

Table III.2 Length and weight measurements (litter B)

Dec, December; cm, centimeter; g, gram; M, male; F, female; wt, wild type; het, heterozygote for *Itpr1*$^{\Delta 18}$; homo, homozygote, for *Itpr1*$^{\Delta 18}$.

APPENDIX IV.

DATA - LINKAGE ANALYSIS MICE

A crude genome wide linkage strategy was carried out to map the location of the genetic cause of the severe movement disorder in mice (paragraph 3.3.3). Genotypes of 18 mice (unaffected mice, *n*=7; affected mice *n*=11) were obtained for 120 fragments, each containing one or more C57BL/6J-129x1/SvJ strain specific SNPs (Lindblad-Toh et al. 2000). LOD (logarithm of odds) scores for each SNP were determined using MLINK (version 5.1) (Lathrop et al. 1984). A region of high linkage was assigned to chromosome 6, (+)108.2-108.5Mb, on the 129x1/SvJ background. Theta denotes the recombination fraction; max, maximum.

Chromosome 1

Locus	Theta 0.01	Theta 0.05	Theta 0.10	Theta 0.20	Theta 0.30	Theta Max	Max LOD Score
35fra8(1)	-4.61	-1.99	-1.02	-0.26	-0.01	0.38	0.03
35fra8(4)	-4.61	-1.99	-1.02	-0.26	-0.01	0.38	0.03
61frc7(1)	-4.60	-1.97	-0.97	-0.21	0.03	0.35	0.05
84fld1(1)	-4.90	-2.23	-1.20	-0.37	-0.07	0.41	0.01
31fld3(2)	-3.01	-3.00	-2.15	-0.94	-0.37	0.50	0.00
37frd9(1)	-0.92	0.27	0.60	0.63	0.39	0.15	0.67
37frd9(3)	-0.62	0.55	0.85	0.81	0.50	0.14	0.89
37frd9(4)	-1.80	-0.52	-0.08	0.18	0.17	0.24	0.20
46frf9(1)	-3.88	-1.87	-1.07	-0.39	-0.11	0.49	0.00
29frh9(1)	0.06	0.05	0.04	0.03	0.01	0.00	0.07
86frb10(2)	-5.71	-2.43	-1.20	-0.26	0.02	0.36	0.05
15flb5(1)	-5.71	-2.43	-1.20	-0.26	0.02	0.36	0.05
17frc10(1)	-3.26	-1.33	-0.62	-0.10	0.03	0.34	0.04
17frc10(2)	-4.61	-1.99	-1.02	-0.26	-0.01	0.38	0.03
57flc4(1)	-0.62	0.55	0.85	0.81	0.50	0.14	0.89
82flh4(2)	-7.35	-3.82	-2.22	-0.85	-0.27	0.50	0.00

Processed on Tue May 24 09:23:08 2005

Chromosome 2

Locus	Theta 0.01	Theta 0.05	Theta 0.10	Theta 0.20	Theta 0.30	Theta Max	Max LOD Score
87frd8(1)	-3.85	-1.30	-0.42	0.08	0.08	0.24	0.11
61fre7(1)	-3.50	-1.53	-0.79	-0.22	-0.03	0.41	0.01
71frf8(1)	-0.99	-0.36	-0.15	-0.01	0.01	0.30	0.01
71frf8(2)	0.06	0.05	0.04	0.03	0.01	0.00	0.07
71frf8(3)	0.00	0.00	0.00	0.00	0.00	0.50	0.00
71frf8(4)	0.00	0.00	0.00	0.00	0.00	0.50	0.00
59fla6(1)	-6.42	-3.06	-1.73	-0.62	-0.17	0.47	0.00
59fla6(2)	-6.42	-3.06	-1.73	-0.62	-0.17	0.47	0.00
64frc10(1)	0.06	0.05	0.04	0.03	0.01	0.00	0.07
4flc5(1)	-5.20	-2.53	-1.48	-0.60	-0.22	0.50	0.00
46frd10(1)	-6.42	-3.06	-1.74	-0.64	-0.20	0.50	0.00
33fre11(1)	-4.44	-1.86	-0.92	-0.26	-0.07	0.50	0.00
45frf11(1)	-5.20	-2.53	-1.48	-0.60	-0.22	0.50	0.00
59flh4(2)	-3.85	-1.30	-0.42	0.08	0.08	0.24	0.11

Processed on Tue May 24 09:29:45 2005

Chromosome 3

Locus	Theta 0.01	Theta 0.05	Theta 0.10	Theta 0.20	Theta 0.30	Theta Max	Max LOD Score
11fld2(1)	0.00	0.00	0.00	0.00	0.00	0.50	0.00
9flh3(1)	-2.62	-0.73	-0.11	0.21	0.16	0.22	0.22
59fld5(2)	-4.60	-1.97	-0.98	-0.22	0.01	0.35	0.03

Processed on Tue May 24 09:34:24 2005

Chromosome 4

No data available.

Chromosome 5

Locus	Theta 0.01	Theta 0.05	Theta 0.10	Theta 0.20	Theta 0.30	Theta Max	Max LOD Score
95fra9(1)	-11.61	-5.85	-3.45	-1.39	-0.49	0.50	0.00
59frc8(1)	-7.10	-2.60	-0.97	0.18	0.41	0.29	0.41
20frd8(1)	-7.52	-2.99	-1.32	-0.08	0.23	0.32	0.23
36frf7(1)	-1.81	-0.57	-0.16	0.06	0.06	0.24	0.07
36frf7(2)	-2.01	-0.13	0.48	0.71	0.49	0.18	0.71
91flh1(1)	-12.99	-6.34	-3.72	-1.46	-0.49	0.50	0.00
35flb5(3)	-3.89	-1.33	-0.42	0.16	0.20	0.27	0.22

Processed on Thu Jun 2 12:09:27 2005

Chromosome 6

Locus	Theta 0.01	Theta 0.05	Theta 0.10	Theta 0.20	Theta 0.30	Theta Max	Max LOD Score
84frb9(1)	-2.92	-1.06	-0.41	0.03	0.11	0.29	0.11
34fld3 (1)	-8.26	-3.61	-1.85	-0.51	-0.09	0.44	0.00
85flg2(3)	4.88	5.10	4.78	3.75	2.49	0.04	5.13
25frb12(1)	-6.28	-2.39	-0.98	-0.02	0.14	0.29	0.14
25frb12(2)	-11.08	-5.10	-2.80	-0.97	-0.31	0.50	0.00
27frg11(1)	-12.86	-6.92	-4.01	-1.52	-0.49	0.50	0.00
85flg5(1)	4.26	3.92	3.48	2.53	1.49	0.00	4.34
85flg5(2)	4.26	3.92	3.48	2.53	1.49	0.00	4.34
94frg12(1)	0.06	0.05	0.04	0.03	0.01	0.00	0.07
94frg12(2)	0.06	0.05	0.04	0.03	0.01	0.00	0.07
94frg12(3)	0.06	0.05	0.04	0.03	0.01	0.00	0.07
28frh10(2)	-11.70	-5.90	-3.50	-1.42	-0.51	0.50	0.00

Processed on Tue May 31 10:51:52 2005

Chromosome 7

Locus	Theta 0.01	Theta 0.05	Theta 0.10	Theta 0.20	Theta 0.30	Theta Max	Max LOD Score
71frb7(2)	0.06	0.05	0.04	0.03	0.01	0.00	0.07
71frb7(3)	0.06	0.05	0.04	0.03	0.01	0.00	0.07
71frb7(4)	0.06	0.05	0.04	0.03	0.01	0.00	0.07
85frc7(1)	0.00	0.00	0.00	0.00	0.00	0.50	0.00
85frc7(2)	-11.59	-5.99	-3.56	-1.44	-0.50	0.50	0.00
22fre8(2)	0.06	0.05	0.04	0.03	0.01	0.00	0.07
34fle3(1)	-0.88	-0.30	-0.14	-0.07	-0.04	0.50	0.00
34fle3(2)	-4.47	-1.81	-0.80	-0.03	0.17	0.32	0.17
34fle3(3)	-3.49	-1.49	-0.71	-0.11	0.06	0.34	0.07
44flf2(1)	-7.42	-3.45	-1.94	-0.73	-0.27	0.50	0.00
44flf2(3)	-9.61	-4.51	-2.50	-0.90	-0.31	0.50	0.00
4frg8(1)	0.06	0.05	0.04	0.03	0.01	0.00	0.07
4frg8(3)	0.06	0.05	0.04	0.03	0.01	0.00	0.07
4frg8(4)	0.06	0.05	0.04	0.03	0.01	0.00	0.07
7flg2(1)	0.06	0.05	0.04	0.03	0.01	0.00	0.07
6flg3(1)	-11.46	-6.44	-3.83	-1.56	-0.57	0.50	0.00
64flh2(1)	0.06	0.05	0.04	0.03	0.01	0.00	0.07
64flh2(5)	0.06	0.05	0.04	0.03	0.01	0.00	0.07
57fla5(1)	0.06	0.05	0.04	0.03	0.01	0.00	0.07
26frc10(1)	-9.61	-4.51	-2.50	-0.90	-0.31	0.50	0.00
26frc10(2)	-9.61	-4.51	-2.50	-0.90	-0.31	0.50	0.00
27frc12(1)	-6.39	-4.55	-3.11	-1.19	-0.38	0.50	0.00
5flc6(1)	-8.64	-4.95	-2.85	-1.06	-0.32	0.50	0.00
70fld6(1)	0.00	0.00	0.00	0.00	0.00	0.50	0.00
70fld6(2)	0.00	0.00	0.00	0.00	0.00	0.50	0.00
64flf5(1)	-6.40	-2.51	-1.10	-0.12	0.07	0.30	0.07
64flf5(2)	-8.40	-3.79	-2.05	-0.71	-0.23	0.50	0.00
57flh4(1)	-9.75	-5.21	-2.94	-1.09	-0.39	0.50	0.00
57flh4(2)	-9.75	-5.21	-2.94	-1.09	-0.39	0.50	0.00

Processed on Thu Jun 2 12:11:28 2005

Chromosome 8

Locus	Theta 0.01	Theta 0.05	Theta 0.10	Theta 0.20	Theta 0.30	Theta Max	Max LOD Score
58fla1(1)	-11.37	-5.39	-3.07	-1.16	-0.41	0.50	0.00
87fld2(1)	-8.50	-4.42	-2.59	-1.04	-0.38	0.50	0.00
80fle1(1)	-7.56	-4.11	-2.50	-1.07	-0.41	0.50	0.00
27fre8(1)	-7.50	-2.91	-1.20	0.07	0.38	0.31	0.39
27fre8(2)	-7.50	-2.91	-1.20	0.07	0.38	0.31	0.39
27fre8(4)	-7.50	-2.91	-1.20	0.07	0.38	0.31	0.39
27fre8(5)	-7.50	-2.91	-1.20	0.07	0.38	0.31	0.39
82fle3(1)	-6.23	-3.78	-2.25	-0.94	-0.36	0.50	0.00
88frg8(2)	-8.66	-5.93	-3.97	-1.74	-0.67	0.50	0.00
88frg8(3)	-7.26	-5.10	-3.28	-1.41	-0.54	0.50	0.00
88frg8(4)	-5.86	-4.49	-3.08	-1.35	-0.52	0.50	0.00
27frh8(1)	0.00	0.00	0.00	0.00	0.00	0.50	0.00
27frh8(2)	0.00	0.00	0.00	0.00	0.00	0.50	0.00
34flh3(1)	0.00	0.00	0.00	0.00	0.00	0.50	0.00
45flb4(1)	-3.88	-1.90	-1.11	-0.44	-0.16	0.50	0.00
45flb4(2)	-3.88	-1.90	-1.11	-0.44	-0.16	0.50	0.00
86fld4(1)	0.00	0.00	0.00	0.00	0.00	0.50	0.00
16fle5(1)	-4.25	-2.20	-1.36	-0.60	-0.24	0.50	0.00
30flg5(1)	-4.73	-2.09	-1.10	-0.34	-0.10	0.50	0.00
30flg5(2)	-4.73	-2.09	-1.10	-0.34	-0.10	0.50	0.00
30flg5(3)	-4.73	-2.09	-1.10	-0.34	-0.10	0.50	0.00

Processed on Thu Jun 2 12:13:22 2005

Chromosome 9

Locus	Theta 0.01	Theta 0.05	Theta 0.10	Theta 0.20	Theta 0.30	Theta Max	Max LOD Score
84fra11(1)	-8.37	-5.74	-3.96	-1.68	-0.64	0.50	0.00
84fra11(2)	-6.96	-4.52	-2.62	-0.97	-0.34	0.50	0.00
56frb10(2)	-7.64	-3.13	-1.45	-0.24	0.06	0.33	0.07
56frb10(3)	-8.33	-4.10	-2.11	-0.57	-0.08	0.40	0.01
63flc5(2)	-7.97	-3.35	-1.59	-0.23	0.18	0.34	0.20
28flg6(1)	-7.24	-3.93	-2.18	-0.78	-0.26	0.50	0.00

Processed on Thu Jun 2 12:14:51 2005

Chromosome 10

Locus	Theta 0.01	Theta 0.05	Theta 0.10	Theta 0.20	Theta 0.30	Theta Max	Max LOD Score
61fle2(1)	-5.39	-2.71	-1.65	-0.70	-0.25	0.50	0.00
91flg3(1)	0.06	0.05	0.04	0.03	0.01	0.00	0.07
15flb4(1)	0.06	0.05	0.04	0.03	0.01	0.00	0.07
61frf11(1)	-7.45	-3.42	-1.84	-0.54	-0.07	0.40	0.04
61frg10(2)	0.06	0.05	0.04	0.03	0.01	0.00	0.07
7frh11(1)	0.06	0.05	0.04	0.03	0.01	0.00	0.07

Processed on Thu Jun 2 12:15:51 2005

Chromosome 11

Locus	Theta 0.01	Theta 0.05	Theta 0.10	Theta 0.20	Theta 0.30	Theta Max	Max LOD Score
90fla2(1)	-9.24	-5.51	-3.36	-1.44	-0.55	0.50	0.00
90fla2(2)	-9.07	-5.59	-3.44	-1.48	-0.57	0.50	0.00
28fra9(1)	0.06	0.05	0.04	0.03	0.01	0.00	0.07
89fle3(1)	-10.67	-5.10	-2.81	-0.97	-0.29	0.50	0.00
86frf9(1)	0.06	0.05	0.04	0.03	0.01	0.00	0.07
66flg3(1)	-10.67	-5.10	-2.81	-0.97	-0.29	0.50	0.00
12frh7(1)	-9.48	-6.28	-4.64	-2.05	-0.78	0.50	0.00
48flh3(1)	-10.88	-6.24	-3.64	-1.35	-0.39	0.47	0.00
48flh3(2)	-11.05	-5.59	-3.20	-1.16	-0.32	0.45	0.01
26frc11(1)	-4.61	-2.61	-1.55	-0.63	-0.23	0.50	0.00
9flc5(1)	-11.70	-5.92	-3.53	-1.47	-0.56	0.50	0.00
9flc5(2)	-10.36	-5.27	-3.12	-1.26	-0.44	0.50	0.00
9flc5(3)	-11.70	-5.92	-3.53	-1.47	-0.56	0.50	0.00

Processed on Thu Jun 2 12:17:01 2005

Chromosome 12

Locus	Theta 0.01	Theta 0.05	Theta 0.10	Theta 0.20	Theta 0.30	Theta Max	Max LOD Score
34fld1(1)	-6.52	-2.59	-1.12	-0.05	0.18	0.30	0.18
91fld3(1)	-6.38	-4.55	-3.36	-1.36	-0.46	0.50	0.00
22fre7(1)	-5.71	-2.40	-1.14	-0.17	0.11	0.34	0.12
22fre7(2)	-7.29	-3.32	-1.80	-0.58	-0.15	0.50	0.00
86fle2(1)	-9.96	-4.65	-2.58	-0.90	-0.25	0.50	0.00
46frf7(1)	-5.49	-2.78	-1.69	-0.72	-0.27	0.50	0.00
46frf7(2)	-8.91	-3.66	-1.69	-0.23	0.14	0.32	0.15
46frf7(3)	-8.91	-3.66	-1.69	-0.23	0.14	0.32	0.15
46frf7(4)	-4.61	-1.98	-0.99	-0.25	-0.02	0.38	0.01
42flf3(1)	0.00	0.00	0.00	0.00	0.00	0.50	0.00
70frd12(5)	-7.21	-2.65	-0.97	0.21	0.41	0.28	0.42
28flh4(1)	0.00	0.00	0.00	0.00	0.00	0.50	0.00
44flh5(1)	-8.90	-3.64	-1.65	-0.17	0.20	0.32	0.21
44flh5(2)	-9.19	-4.19	-2.16	-0.58	-0.07	0.39	0.01

Processed on Thu Jun 2 12:22:13 2005

Chromosome 13

Locus	Theta 0.01	Theta 0.05	Theta 0.10	Theta 0.20	Theta 0.30	Theta Max	Max LOD Score
22frg8(1)	-10.49	-4.55	-2.31	-0.60	-0.10	0.50	0.00
22frg8(2)	-10.49	-4.55	-2.31	-0.60	-0.10	0.50	0.00
70fla5(1)	-11.47	-6.68	-4.04	-1.70	-0.65	0.50	0.00
28flb6(1)	-13.15	-7.28	-4.32	-1.74	-0.61	0.50	0.00
76frc10(3)	-6.31	-2.41	-0.99	0.00	0.20	0.30	0.20
35frd10(2)	-14.21	-7.07	-4.14	-1.63	-0.56	0.50	0.00
5frg12(1)	-4.33	-1.73	-0.78	-0.11	0.05	0.33	0.05

Processed on Thu Jun 2 12:19:05 2005

Chromosome 14

Locus	Theta 0.01	Theta 0.05	Theta 0.10	Theta 0.20	Theta 0.30	Theta Max	Max LOD Score
59flb3(1)	-6.57	-3.23	-1.89	-0.74	-0.25	0.50	0.00
88frb12(1)	-6.00	-3.28	-1.96	-0.81	-0.30	0.50	0.00
64fle4(1)	-6.01	-3.33	-1.99	-0.82	-0.31	0.50	0.00
64fle4(2)	-6.01	-3.33	-1.99	-0.82	-0.31	0.50	0.00
31flf5(1)	0.00	0.00	0.00	0.00	0.00	0.50	0.00
31flf5(2)	0.00	0.00	0.00	0.00	0.00	0.50	0.00
31flf5(3)	0.00	0.00	0.00	0.00	0.00	0.50	0.00

Processed on Tue May 24 09:44:51 2005

Chromosome 15

No data available.

Chromosome 16

Locus	Theta 0.01	Theta 0.05	Theta 0.10	Theta 0.20	Theta 0.30	Theta Max	Max LOD Score
44fle5(1)	0.06	0.05	0.04	0.03	0.01	0.00	0.07
44fle5(2)	0.06	0.05	0.04	0.03	0.01	0.00	0.07
44fle5(3)	0.06	0.05	0.04	0.03	0.01	0.00	0.07

Processed on Wed May 11 09:54:02 2005

Chromosome 17

Locus	Theta 0.01	Theta 0.05	Theta 0.10	Theta 0.20	Theta 0.30	Theta Max	Max LOD Score
54fle3(2)	-4.61	-2.61	-1.55	-0.63	-0.23	0.50	0.00
66flb6(3)	-2.47	-1.20	-0.72	-0.32	-0.13	0.50	0.00

Processed on Wed May 11 10:01:25 2005

Chromosome 18

Locus	Theta 0.01	Theta 0.05	Theta 0.10	Theta 0.20	Theta 0.30	Theta Max	Max LOD Score
9fre8(1)	0.00	0.00	0.00	0.00	0.00	0.50	0.00
9fre8(2)	0.00	0.00	0.00	0.00	0.00	0.50	0.00
9fre8(3)	0.00	0.00	0.00	0.00	0.00	0.50	0.00
9fre8(4)	0.00	0.00	0.00	0.00	0.00	0.50	0.00
9fre8(5)	0.06	0.05	0.04	0.03	0.01	0.00	0.07
54flg3(1)	0.06	0.05	0.04	0.03	0.01	0.00	0.07
7frb10(1)	-2.62	-0.73	-0.11	0.21	0.16	0.22	0.22
11frf10(1)	0.06	0.05	0.04	0.03	0.01	0.00	0.07

Processed on Tue May 24 10:50:46 2005

Chromosome 19

Locus	Theta 0.01	Theta 0.05	Theta 0.10	Theta 0.20	Theta 0.30	Theta Max	Max LOD Score
17frc8(1)	-6.01	-3.25	-1.88	-0.71	-0.23	0.50	0.00
5flh5(1)	-4.61	-1.99	-1.02	-0.26	-0.01	0.38	0.03

Processed on Wed May 11 13:10:51 2005

Chromosome X

Locus	Theta 0.01	Theta 0.05	Theta 0.10	Theta 0.20	Theta 0.30	Theta Max	Max LOD Score
12_5_11_6(1)	-1.34	-0.14	0.21	0.34	0.23	0.18	0.34
94flc5(1)	-4.61	-2.61	-1.56	-0.64	-0.23	0.50	0.00
28fld4(1)	0.00	0.00	0.00	0.00	0.00	0.50	0.00

Processed on Tue May 24 13:41:40 2005

APPENDIX V.

IMMUNOHISTOCHEMISTRY - EXPERIMENTAL CONTROLS

To determine antibody specificity and levels of background fluorescence, experimental control data were obtained based on the wild type tissue (129x1B6, wild type for the *Itpr1* 18bp deletion, three weeks of age). Antibody dilutions used are the same as in the data presented in figure 3.9. Detailed description of the methods has been given in section 2.3.4.3.

Secondary controls were used to determine secondary antibody specificity by incubation of the tissue without primary antibody. For both secondary controls (Alexa Fluor 555, Alexa Fluor 488) no signal was obtained. Images are undistinguishable from the blank control, in which no primary or secondary antibodies were used, that shows only autofluorescence. The secondary antibodies demonstrate specific binding at the concentrations used. In addition, peptide competition was carried out to study the specificity of the ITPR1 primary antibody. Prior to section incubation, anti-ITPR1 primary and corresponding peptide (10:1) were incubated overnight. In images thus obtained, ITPR1 staining of the dendrites was reduced to background levels (similar to secondary and blank controls), whereas signal intensity of the Purkinje cell bodies was clearly reduced. Indicating ITPR1 antibody binding was specific for the Purkinje cells in the cerebellum.

Figure V.1 Immunohistochemistry, experimental controls

Immunohistochemmistry of cerebellum from three week old (129x1B6) animal, wild type for the *Itpr1* 18bp deletion. Experimental controls for polyclonal ITPR1 anti-rabbit (**A, B, C, D**) and monoclonal calbindin anti-mouse (**E, F, G**) antibodies. Images show Purkinje cells of the cerebellum. **A.** Primary ITPR1 antibody (1:2000, Chemicon), secondary Alexa Fluor 555 antibody (1:2000, Invitrogen). **B.** Secondary control; no primary antibody, secondary Alexa Fluor 555 antibody (1:2000, Invitrogen). **C.** Blank; no primary antibody, no secondary antibody. **D.** Peptide competition; Primary ITPR1 antibody (1:2000, Chemicon) pre-incubated with peptide (ITPR1 antigen, 1:20,000, Chemicon), secondary Alexa Fluor 555 antibody (1:2000, Invitrogen). **E.** Primary calbindin antibody (1:6000, Sigma), secondary Alexa Fluor 488 antibody (1:3000, Invitrogen). **F.** Secondary control; no primary antibody, secondary Alexa Fluor 488 antibody (1:3000, Invitrogen). **G.** Blank; no primary antibody, no secondary antibody. (Achroplan 63x/0.9 W; Carl Zeiss) Scale bars denote 20µm. **(figure V.1, *on next page*)**

(figure V.1, *continued from previous page*)

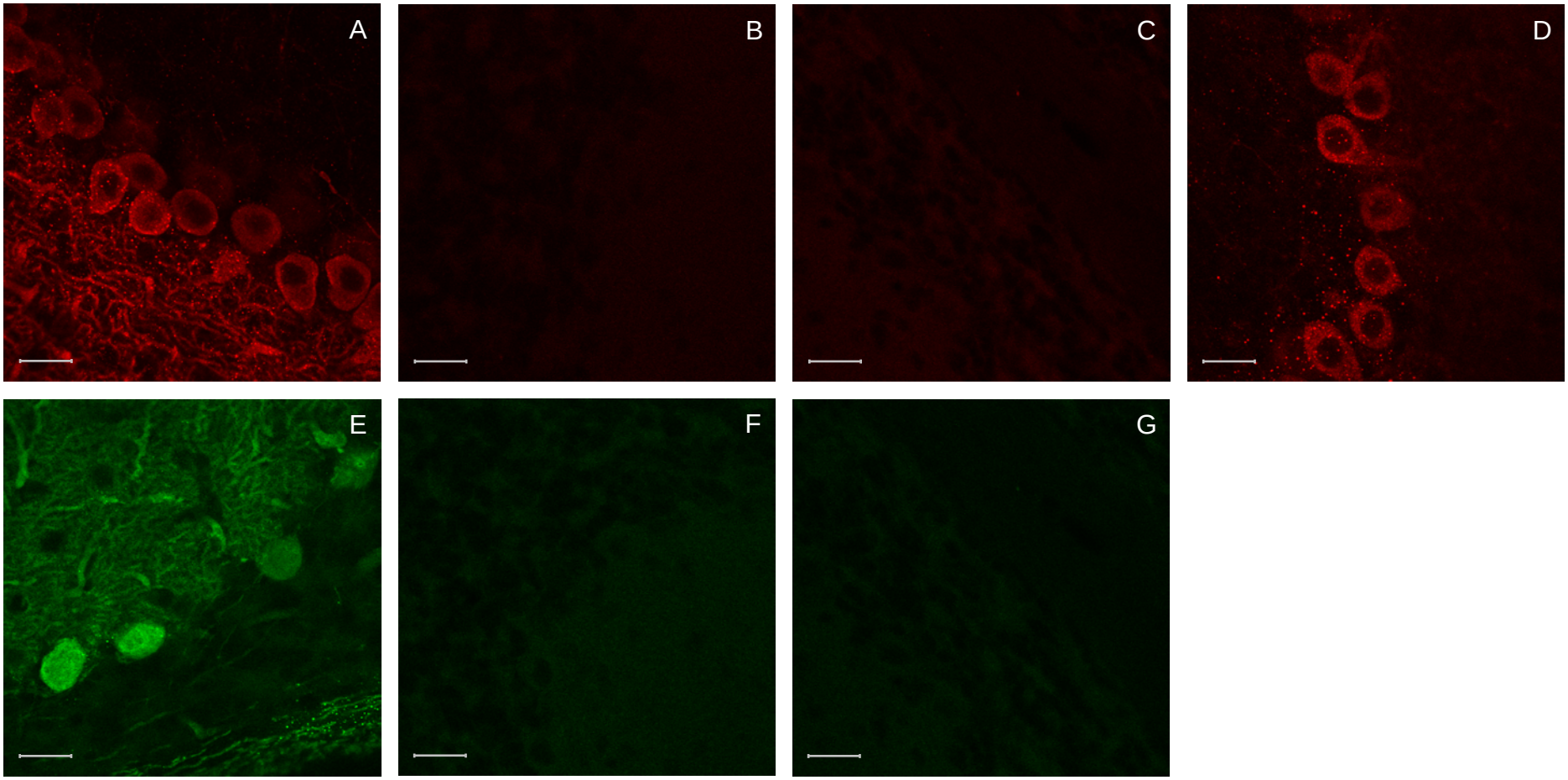

APPENDIX VI.

ASSAY BREAKPOINT AUS1 (T3F, C11R) IN CONTROLS

The T3f and C11r primers, from the assay used to define the deletion breakpoint spanning *SUMF1* and *ITPR1* in the AUS1 (SCA15) kindred, were used to screen 259 neurologically normal controls for the deletion. Controls were obtained from Coriell Cell Repositories (neurologically normal Caucasian controls panel; NDPT002, NDPT006, NDPT009; http://ccr.coriell.org).

PCR based assay was carried out as described in paragraph 4.4.1.2 using the 60-to-50 amplification program (appendix I). Each control plate included a positive control (affected individual III5 of the AUS1 kindred (figure 4.1), 953bp band (figure 4.7)) and a no template control (NC). Either 6µl PCR product with 3µl orangeG or 5µl size reference (L; GeneRuler 100bp DNA ladder plus (0.1µg/µl, ready to use), Fermentas) were loaded on a 2% agarose gel in 1xTBE with ethidium bromide, at 120V for approximately 45 minutes.

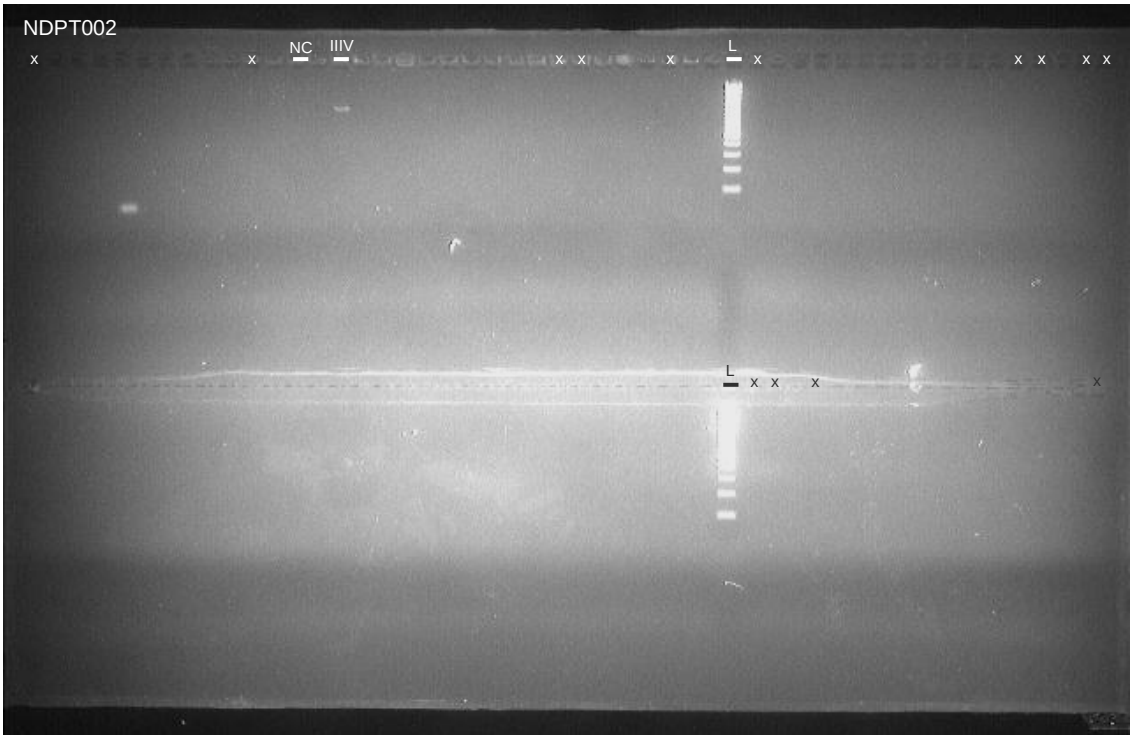

Figure VI.1 NDPT002; gel assay T3f, C11r

No PCR product was obtained for any of the NDPT002 samples (*n*=75), indicating absence of the deletion. Positive control (III5) gave 953bp product; NC, no product; x, empty lanes.

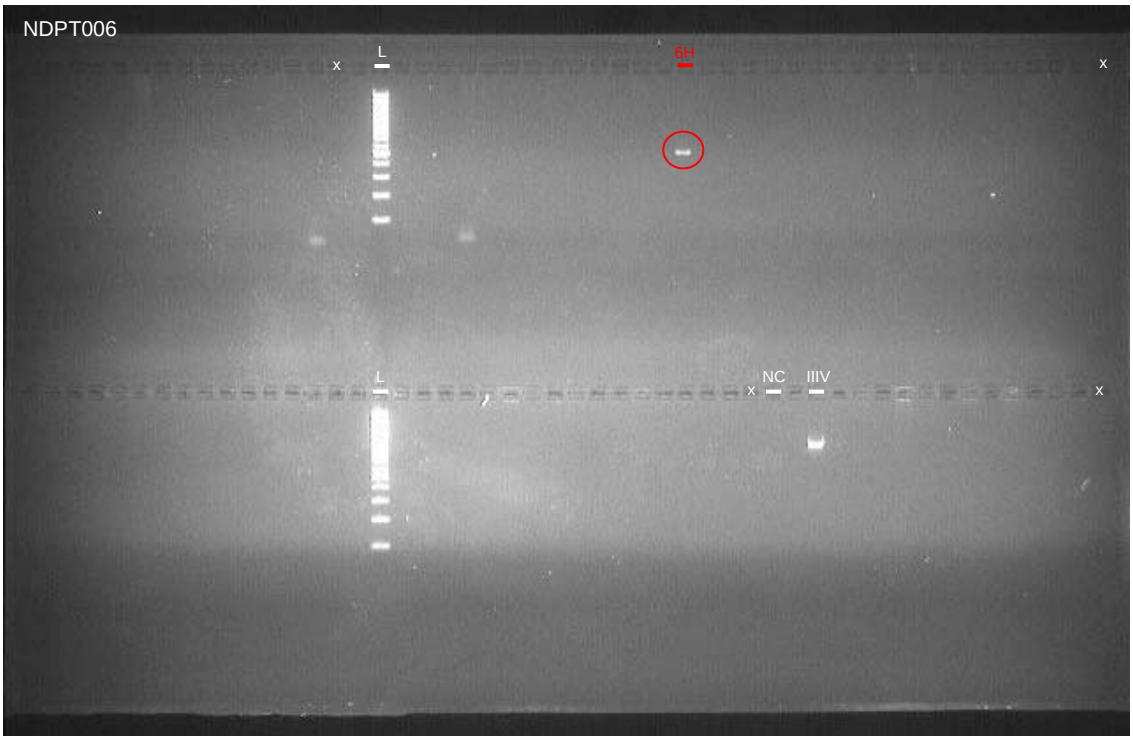

Figure VI.2 NDPT006; gel assay T3f, C11r

With the exception of well 6H, no PCR product was obtained for any of the NDPT006 samples (*n*=92), indicating absence of the deletion. Assay for NDPT006, 6H was repeated, see figure VI.4 for results. Positive control (III5) gave 953bp product; NC, no product; x, empty lanes.

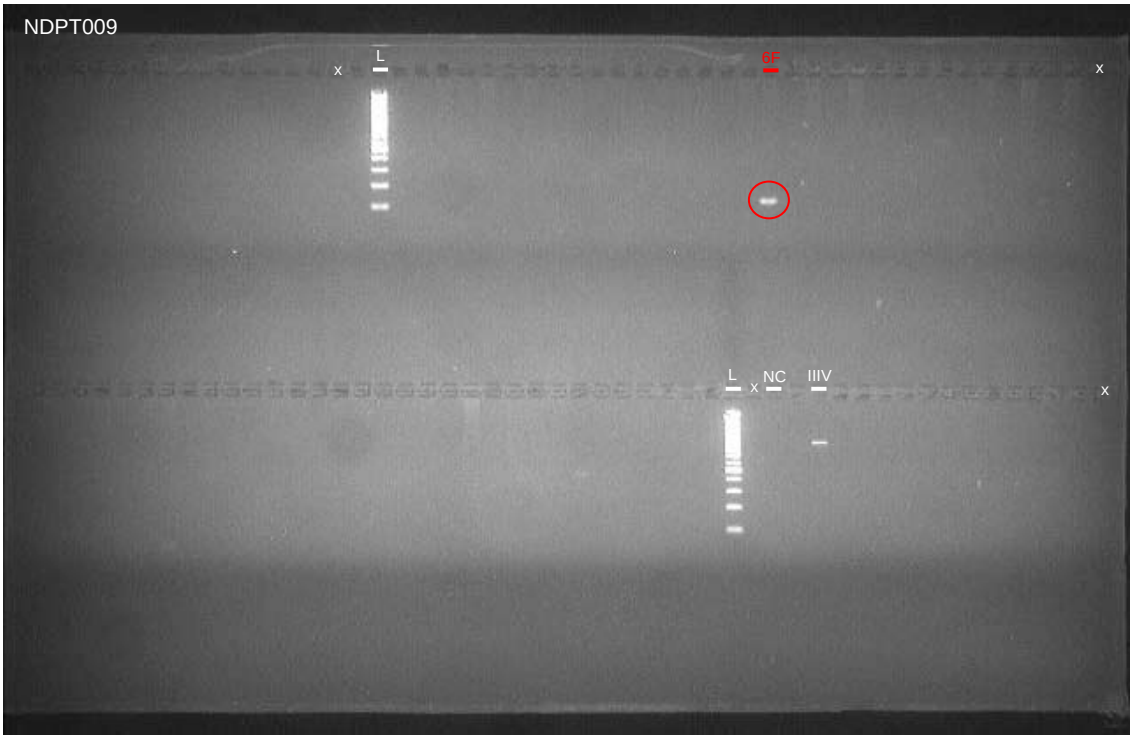

Figure VI.3 NDPT009; gel assay T3f, C11r

With the exception of well 6F, no PCR product was obtained for any of the NDPT009 samples (*n*=92), indicating absence of the deletion. Assay for NDPT009, 6F was repeated, see figure VI.4 for results. Positive control (III5) gave 953bp product; NC, no product; x, empty lanes.

Figure VI.4 Repeat NDPT006 (6H), NDPT009 (6F); gel assay T3f, C11r

Samples were amplified in duplicates. No PCR product was obtained for either NDPT006 (6H) or NDPT009 (6F) samples, indicating absence of the deletion. Positive control (III5) gave 953bp product; NC, no product.

APPENDIX VII.

DATA - GENE DOSAGE ANALYSIS *ITPR1*$_{EXON10}$

Study of *ITPR1* gene dosage was carried out by quantitative duplex PCR. Samples were assayed on an ABI Prism 7900HT Sequence Detection System (Applied Biosystems) and data were analyzed using the $2^{-\Delta\Delta Ct}$ method (SDS software (Sequence Detection System, version 2.2.2; Applied Biosystems) and excel (2003; Microsoft)).

$\Delta Ct = Ct_{ITPR1exon10} - Ct_{hemoglobin}$

SD = SD ΔCt

$2^{-\Delta\Delta Ct}$ = 2^-(avg.ΔCt - avg.$\Delta Ct_{controls}$)

Accepted sample data required 4-6 replicates, Ct (23-30), SD≤0.16 . Gene dosage, $2^{-\Delta\Delta Ct}$ values (0.4-0.6) indicated heterozygous deletion; $2^{-\Delta\Delta Ct}$ (0.8-1.2) indicated normal dosage; $2^{-\Delta\Delta Ct}$ ≥1.3 was considered a duplication. Ct, cycle threshold; SD, standard deviation; controls, normal dosage (H3332 (H3331 family), figure 4.12; III9 (AUS1 family), figure 4.1). In addition, deletion controls (III5, III4 (AUS1 family), figure 4.1) and a no template control (water) were included on each assay. Genomic DNA from samples of a French ADCA III cohort (*n*=267) were assayed. Data given in this appendix are the $2^{-\Delta\Delta Ct}$ and SD, used to generate the graphs in paragraph 4.4.1.6.

VII.1 Gene dosage data; graph A (figure 4.13)

SD	$2^{-\Delta\Delta Ct}$		SD	$2^{-\Delta\Delta Ct}$		SD	$2^{-\Delta\Delta Ct}$		SD	$2^{-\Delta\Delta Ct}$	
0.07	1.04	**1A**				0.09	0.48	**3A**	0.06	1.02	**4A**
0.05	1.00	**1B**	0.10	0.98	**2B**	0.07	1.02	**3B**	0.04	0.98	**4B**
0.11	0.97	**1C**				0.14	0.95	**3C**	0.05	0.95	**4C**
0.05	1.03	**1D**	0.04	1.11	**2D**	0.07	1.03	**3D**	0.04	0.98	**4D**
0.06	1.08	**1E**	0.10	1.11	**2E**	0.06	1.04	**3E**	0.05	0.95	**4E**
0.02	1.05	**1F**	0.05	1.07	**2F**	0.04	1.01	**3F**	0.07	0.96	**4F**
0.08	0.99	**1G**	0.04	0.98	**2G**	0.04	0.95	**3G**	0.04	0.91	**4G**
0.05	1.01	**1H**	0.07	0.95	**2H**	0.04	0.94	**3H**	0.02	0.92	**4H**
SD	$2^{-\Delta\Delta Ct}$		**SD**	$2^{-\Delta\Delta Ct}$		**SD**	$2^{-\Delta\Delta Ct}$		**SD**	$2^{-\Delta\Delta Ct}$	
0.06	1.00	**5A**	0.06	0.98	**6A**	0.05	0.91	**7A**	0.06	0.94	**8A**
0.06	1.04	**5B**	0.04	1.01	**6B**	0.03	1.00	**7B**	0.04	0.99	**8B**
0.04	1.02	**5C**	0.04	1.13	**6C**	0.04	1.05	**7C**	0.05	0.97	**8C**
0.04	1.06	**5D**	0.04	1.09	**6D**	0.05	1.05	**7D**	0.04	0.40	**III5 - 8D**
0.03	1.06	**5E**				0.06	1.00	**7E**	0.04	1.03	**H3332 - 8E**
0.04	1.11	**5F**	0.08	1.05	**6F**	0.11	1.00	**7F**	0.09	0.50	**III4 - 8F**
0.07	1.03	**5G**	0.03	1.05	**6G**	0.09	1.08	**7G**	0.11	0.98	**III9 - 8G**
0.08	1.02	**5H**	0.06	1.00	**6H**	0.05	0.97	**7H**	#VALUE!	#VALUE!	**NC 8H**

VII.2 Gene dosage data; graph B (figure 4.13)

SD	$2^{-\Delta\Delta Ct}$		SD	$2^{-\Delta\Delta Ct}$		SD	$2^{-\Delta\Delta Ct}$		SD	$2^{-\Delta\Delta Ct}$	
0.04	1.10	**1A**	0.05	1.00	**2A**				0.05	0.96	**4A**
0.07	1.06	**1B**	0.06	1.02	**2B**	0.03	0.98	**3B**	0.04	0.99	**4B**
0.07	1.00	**1C**	0.07	0.99	**2C**	0.07	0.95	**3C**	0.06	0.96	**4C**
0.02	1.05	**1D**	0.05	1.05	**2D**	0.07	0.99	**3D**	0.07	0.99	**4D**
0.11	1.06	**1E**	0.09	1.07	**2E**	0.06	1.03	**3E**	0.08	1.00	**4E**
0.05	1.06	**1F**							0.08	0.93	**4F**
0.05	1.01	**1G**	0.03	1.08	**2G**	0.09	0.90	**3G**	0.09	0.95	**4G**
0.06	1.08	**1H**	0.05	1.02	**2H**	0.05	0.94	**3H**	0.07	1.04	**4H**
SD	$2^{-\Delta\Delta Ct}$		**SD**	$2^{-\Delta\Delta Ct}$		**SD**	$2^{-\Delta\Delta Ct}$		**SD**	$2^{-\Delta\Delta Ct}$	
0.06	0.96	**5A**	0.07	0.96	**6A**	0.05	0.94	**7A**	0.05	0.97	**8A**
0.06	1.07	**5B**	0.04	1.00	**6B**	0.07	1.03	**7B**	0.09	1.00	**8B**
0.07	1.06	**5C**	0.05	1.04	**6C**	0.09	1.00	**7C**	0.06	1.03	**8C**
0.09	1.02	**5D**	0.03	1.06	**6D**	0.02	1.03	**7D**	0.11	0.39	**III5 - 8D**
0.04	1.06	**5E**	0.06	1.05	**6E**	0.06	1.03	**7E**	0.09	1.02	**H3332 - 8E**
0.07	1.05	**5F**	0.07	1.11	**6F**	0.07	1.05	**7F**	0.08	0.47	**III4 - 8F**
			0.06	1.19	**6G**	0.07	0.97	**7G**	0.09	0.98	**III9 - 8G**
0.08	0.99	**5H**	0.05	1.09	**6H**	0.06	0.98	**7H**	#VALUE!	#VALUE!	**NC 8H**

VII.3 Gene dosage data; graph C (figure 4.13)

SD	$2^{-\Delta\Delta Ct}$		SD	$2^{-\Delta\Delta Ct}$		SD	$2^{-\Delta\Delta Ct}$		SD	$2^{-\Delta\Delta Ct}$	
0.11	1.01	**1A**	0.03	1.00	**2A**	0.05	1.01	**3A**	0.05	1.03	**4A**
0.06	1.09	**1B**	0.02	1.06	**2B**	0.05	1.03	**3B**	0.03	1.01	**4B**
0.08	1.03	**1C**	0.05	1.03	**2C**	0.03	1.01	**3C**	0.06	0.94	**4C**
0.07	1.06	**1D**	0.04	1.04	**2D**	0.06	1.00	**3D**	0.06	0.97	**4D**
0.02	1.08	**1E**	0.04	1.07	**2E**	0.05	1.02	**3E**	0.05	1.05	**4E**
0.05	1.03	**1F**	0.06	1.03	**2F**	0.04	1.03	**3F**	0.08	1.04	**4F**
0.08	1.06	**1G**	0.05	1.02	**2G**	0.05	0.98	**3G**	0.05	0.92	**4G**
0.07	1.07	**1H**	0.05	0.98	**2H**	0.08	0.96	**3H**	0.05	0.93	**4H**
SD	$2^{-\Delta\Delta Ct}$		**SD**	$2^{-\Delta\Delta Ct}$		**SD**	$2^{-\Delta\Delta Ct}$		**SD**	$2^{-\Delta\Delta Ct}$	
0.04	1.02	**5A**	0.05	1.01	**6A**	0.04	0.97	**7A**	0.07	0.98	**8A**
0.02	1.06	**5B**	0.06	1.03	**6B**	0.03	1.03	**7B**	0.09	1.03	**8B**
0.05	1.05	**5C**	0.02	1.02	**6C**	0.05	0.98	**7C**	0.03	0.96	**8C**
			0.07	1.06	**6D**	0.02	1.00	**7D**	0.05	0.41	**III5 - 8D**
			0.04	1.06	**6E**	0.08	1.00	**7E**	0.05	1.01	**H3332 - 8E**
0.05	1.04	**5F**	0.06	1.04	**6F**	0.04	0.99	**7F**	0.05	0.50	**III4 - 8F**
0.06	1.09	**5G**	0.05	1.02	**6G**	0.10	0.99	**7G**	0.07	0.99	**III9 - 8G**
0.08	1.07	**5H**	0.07	0.96	**6H**	0.04	0.93	**7H**	#VALUE!	#VALUE!	**NC 8H**

VII.4 Gene dosage data; graph D (figure 4.13)

SD	$2^{-\Delta\Delta Ct}$		SD	$2^{-\Delta\Delta Ct}$		SD	$2^{-\Delta\Delta Ct}$		SD	$2^{-\Delta\Delta Ct}$	
0.07	1.06	**1A**	0.03	1.03	**2A**	0.07	1.02	**3A**	0.09	0.98	**4A**
0.07	1.09	**1B**	0.09	1.05	**2B**	0.04	1.09	**3B**	0.04	1.08	**4B**
0.05	1.06	**1C**	0.03	1.02	**2C**	0.07	1.07	**3C**	0.04	0.96	**4C**
0.04	1.05	**1D**	0.03	1.08	**2D**	0.05	1.04	**3D**			
0.06	1.07	**1E**	0.06	1.09	**2E**	0.04	1.05	**3E**	0.03	1.00	**4E**
0.07	1.04	**1F**	0.04	1.07	**2F**	0.06	0.99	**3F**			
0.07	1.05	**1G**	0.05	1.04	**2G**	0.06	0.98	**3G**	0.07	0.90	**4G**
0.07	1.06	**1H**	0.07	1.02	**2H**	0.06	0.99	**3H**	0.06	0.95	**4H**
SD	$2^{-\Delta\Delta Ct}$		**SD**	$2^{-\Delta\Delta Ct}$		**SD**	$2^{-\Delta\Delta Ct}$		**SD**	$2^{-\Delta\Delta Ct}$	
0.08	1.01	**5A**	0.04	0.99	**6A**	0.06	1.02	**7A**	0.05	0.96	**8A**
0.04	1.06	**5B**	0.02	1.08	**6B**	0.07	1.06	**7B**	0.06	1.07	**8B**
0.03	1.04	**5C**	0.07	1.10	**6C**				0.05	1.03	**8C**
0.04	1.08	**5D**	0.04	1.07	**6D**				0.09	0.42	**III5 - 8D**
0.05	1.01	**5E**	0.04	1.05	**6E**				0.10	1.01	**H3332 - 8E**
			0.05	1.07	**6F**	0.07	1.06	**7F**	0.04	0.50	**III4 - 8F**
			0.06	1.05	**6G**	0.10	1.01	**7G**	0.07	0.99	**III9 - 8G**
0.08	1.01	**5H**	0.04	0.98	**6H**	0.03	0.97	**7H**	#VALUE!	#VALUE!	**NC 8H**

VII.5 Gene dosage data; graph E (figure 4.13)

SD	$2^{-\Delta\Delta Ct}$		SD	$2^{-\Delta\Delta Ct}$		SD	$2^{-\Delta\Delta Ct}$		SD	$2^{-\Delta\Delta Ct}$	
0.10	0.99	**1A**	0.03	0.97	**2A**	0.07	0.89	**3A**	0.09	0.95	**4A**
0.08	0.99	**1B**	0.05	1.00	**2B**	0.06	0.93	**3B**	0.14	0.92	**4B**
0.06	0.95	**1C**	0.05	0.93	**2C**	0.05	0.85	**3C**	0.05	0.86	**4C**
0.07	0.98	**1D**	0.03	0.94	**2D**	0.10	0.91	**3D**	0.03	0.95	**4D**
0.04	0.97	**1E**				0.05	0.92	**3E**			
0.08	0.96	**1F**	0.06	0.92	**2F**	0.06	0.84	**3F**	0.02	0.88	**4F**
0.06	0.93	**1G**	0.04	0.41	**2G**	0.06	0.85	**3G**	0.06	0.80	**4G**
0.06	0.96	**1H**	0.07	0.85	**2H**	0.08	0.85	**3H**	0.05	0.86	**4H**

SD	$2^{-\Delta\Delta Ct}$	
0.08	0.40	**III5 - 8D**
0.09	0.99	**H3332 - 8E**
0.05	0.52	**III4 - 8F**
0.03	1.01	**III9 - 8G**
#VALUE!	#VALUE!	**NC 8H**

VII.6 Gene dosage data; graph F (figure 4.13), graph G (figure 4.13)

graph F

SD	$2^{-\Delta\Delta Ct}$	
0.04	0.97	**2A**
0.08	0.92	**2H**
0.04	0.82	**4C**
0.06	1.16	**4F**
0.06	1.12	**4G**

SD	$2^{-\Delta\Delta Ct}$	
0.06	0.46	**III5 - 8D**
0.08	1.02	**H3332 - 8E**
0.05	0.56	**III4 - 8F**
0.04	0.98	**III9 - 8G**
#VALUE!	#VALUE!	**NC 8H**

graph G

SD	$2^{-\Delta\Delta Ct}$	
0.02	1.09	**1B**
0.07	1.15	**2C**
0.03	1.14	**2E**
0.05	1.13	**2G**
0.04	1.04	**3C**
0.07	1.22	**3H**

SD	$2^{-\Delta\Delta Ct}$	
0.05	0.43	**III5 - 8D**
0.02	0.97	**H3332 - 8E**
0.03	0.56	**III4 - 8F**
0.05	1.03	**III9 - 8G**
#VALUE!	#VALUE!	**NC 8H**

VII.7 Gene dosage data; figure 4.14 (AAD4-2G, AAD1-6E, AAD1-10D)

AAD4-2G

SD	$2^{-\Delta\Delta Ct}$	
0.05	1.63	**4D-E**
0.09	0.42	**III5 - 8D**
0.10	1.01	**H3332 - 8E**
0.04	0.50	**III4 - 8F**
0.07	0.99	**III9 - 8G**
#VALUE!	#VALUE!	**NC 8H**
SD	$2^{-\Delta\Delta Ct}$	
0.07	1.46	**3G-r1**
0.06	0.46	**III5 - 8D**
0.08	1.02	**H3332 - 8E**
0.05	0.56	**III4 - 8F**
0.04	0.98	**III9 - 8G**
#VALUE!	#VALUE!	**NC 8H**
SD	$2^{-\Delta\Delta Ct}$	
0.07	1.36	**3A-r2**
0.05	0.43	**III5 - 8D**
0.02	0.97	**H3332 - 8E**
0.03	0.56	**III4 - 8F**
0.05	1.03	**III9 - 8G**
#VALUE!	#VALUE!	**NC 8H**

AAD1-6E

SD	$2^{-\Delta\Delta Ct}$	
0.05	3.46	**6E-B**
0.04	0.40	**III5 - 8D**
0.04	1.03	**H3332 - 8E**
0.09	0.50	**III4 - 8F**
0.11	0.98	**III9 - 8G**
#VALUE!	#VALUE!	**NC 8H**
SD	$2^{-\Delta\Delta Ct}$	
0.08	1.85	**1G-r1**
0.06	0.46	**III5 - 8D**
0.08	1.02	**H3332 - 8E**
0.05	0.56	**III4 - 8F**
0.04	0.98	**III9 - 8G**
#VALUE!	#VALUE!	**NC 8H**
SD	$2^{-\Delta\Delta Ct}$	
0.06	2.12	**1F-r2**
0.05	0.43	**III5 - 8D**
0.02	0.97	**H3332 - 8E**
0.03	0.56	**III4 - 8F**
0.05	1.03	**III9 - 8G**
#VALUE!	#VALUE!	**NC 8H**

AAD1-10D

SD	$2^{-\Delta\Delta Ct}$	
0.06	2.07	**3A-C**
0.11	0.39	**III5 - 8D**
0.09	1.02	**H3332 - 8E**
0.08	0.47	**III4 - 8F**
0.09	0.98	**III9 - 8G**
#VALUE!	#VALUE	**NC 8H**
SD	$2^{-\Delta\Delta Ct}$	
0.02	1.82	**2C-r1**
0.06	0.46	**III5 - 8D**
0.08	1.02	**H3332 - 8E**
0.05	0.56	**III4 - 8F**
0.04	0.98	**III9 - 8G**
#VALUE!	#VALUE!	**NC 8H**
SD	$2^{-\Delta\Delta Ct}$	
0.08	2.18	**2B-r2**
0.05	0.43	**III5 - 8D**
0.02	0.97	**H3332 - 8E**
0.03	0.56	**III4 - 8F**
0.05	1.03	**III9 - 8G**
#VALUE!	#VALUE!	**NC 8H**

VII.8 Gene dosage data; figure 4.15 (AAD1-3A, AAD4-8H)

AAD1-3A

SD	$2^{-\Delta\Delta Ct}$	
0.09	0.48	**B-3A**
0.04	0.40	**III5 - 8D**
0.04	1.03	**H3332 - 8E**
0.09	0.50	**III4 - 8F**
0.11	0.98	**III9 - 8G**
#VALUE!	#VALUE!	**NC 8H**
SD	$2^{-\Delta\Delta Ct}$	
0.04	0.53	**1B**
0.06	0.46	**III5 - 8D**
0.08	1.02	**H3332 - 8E**
0.05	0.56	**III4 - 8F**
0.04	0.98	**III9 - 8G**
#VALUE!	#VALUE!	**NC 8H**

AAD4-8H

SD	$2^{-\Delta\Delta Ct}$	
0.04	0.41	**F-2G**
0.08	0.40	**III5 - 8D**
0.09	0.99	**H3332 - 8E**
0.05	0.52	**III4 - 8F**
0.03	1.01	**III9 - 8G**
#VALUE!	#VALUE!	**NC 8H**
SD	$2^{-\Delta\Delta Ct}$	
0.07	0.49	**5E**
0.06	0.46	**III5 - 8D**
0.08	1.02	**H3332 - 8E**
0.05	0.56	**III4 - 8F**
0.04	0.98	**III9 - 8G**
#VALUE!	#VALUE!	**NC 8H**

APPENDIX VIII.

GENETIC ELEMENTS NEAR BREAKPOINTS SCA15

Analysis of genetic elements near the deletion breakpoint in the AUS1 and H27390 families (SCA15) were carried out by J Duckworth (LNG/NIA/NIH). At least 200bp 5' and 3p flanking the breakpoint were studied using RepeatMasker and Simple Repeats functions from the UCSC Genome Browser (http://genome.ucsc.edu). Data based on Human assembly March 2006 (NCBI build 36.1 (hg18)).

AUS1, SCA15

distal breakpoint (SUMF1)

#genoName	genoStart	genoEnd	strand	repName	repClass	repFamily
chr3	4462647	4462838	+	L1MC5	LINE	L1
chr3	4462838	4463201	+	THE1B	LTR	MaLR
chr3	4463201	4463583	+	L1MC5	LINE	L1

proximal breakpoint (ITPR1)

#genoName	genoStart	genoEnd	strand	repName	repClass	repFamily
chr3	4664175	4664546	-	L1ME1	LINE	L1
chr3	4664553	4664847	+	*AluSp*	SINE	*Alu*

Table VIII.1 Genetic elements present near breakpoints AUS1 (SCA15) family

H27390 (London)

distal breakpoint (SUMF1)

#genoName	genoStart	genoEnd	strand	repName	repClass	repFamily
chr3	4450646	4450979	+	L1MB4	LINE	L1

proximal breakpoint (ITPR1)

#genoName	genoStart	genoEnd	strand	repName	repClass	repFamily
none						

Table VIII.2 Genetic elements present near breakpoints H27390 family

AUS1, Australian kindred, original SCA15 family (Storey et al. 2001); H27390, family of the London ADCAIII cohort; *SUMF1*, *sulfatase modifying factor 1*; *ITPR1*, *inositol 1,4,5-triphosphate receptor, type 1*; geno__, prefix, related to genome; chr, chromosome; rep__, prefix, referring to repeat; LINE, long interspersed nuclear element, a retrotransposon (transposon via RNA intermediates), a genetic element that moves by copying itself; *Alu* element, short DNA sequence originally characterized by the action of the *Alu* restriction endonuclease, and at about 300bp in length it is classified as a short interspersed nuclear element (SINE); LTR, long terminal repeat, retrotransposons (genetic elements transposed by reverse transcription of RNA) with direct LTRs that range from ~100bp to over 5kb in size.

YES, THAT SEQUENCE OF WORDS I SAID MADE PERFECT SENSE.

-- THE PROFESSOR, FUTURAMA